Major and Minor Element Systematics in the Lherzolite System: A Petrological and Experimental Study

By

AI, YANG
B.Sc (Chang-chun), M.Sc (Tas)

Sumitted in fulfilment of the requirements for the degree of

Doctor of Philosophy

University of Tasmania

April 1992

This thesis contains no material which has been accepted for the award of any other degree or diploma in any university and, to the best of my knowledge and belief, contains no copy or paraphrase of material previously published or written by another person, except where due reference is made in the text of this thesis.

Ai, Yang

April, 1992

All that is visible, clings to the invisible,
the audible, to the inaudible,
the tangible, to the intangible:
perhaps the thinkable, to the unthinkable.

——— **Novalis**

Everything happening at the surface of the Earth, including such diverse phenomena as the building of the mountain ranges, the formation of ocean basins, volcanic activity, and even change in sedimentation (with their attendant rise or decline of faunal and floral populations) is a response to events taking place within the upper mantle.

——— **J B Dawson** (1980)

CONTENTS

List of Figures

List of Plates

List of Tables

Thesis Summary

This thesis is composed of two parts (six chapters). The first part (first two chapters) details a petrologic study of a suite of spinel ± garnet lherzolite xenoliths from Ming-xi, Fu-jian Province, southeastern China. The second part deals with experimental studies of systematic variations in compositions of lherzolite minerals with pressure and temperature in (complex) model lherzolite systems.

The lherzolite xenoliths from Ming-xi are the anhydrous Cr-diopside group I peridotites (Wilshire & Shervais, 1975; Frey & Prinz, 1978), enclosed in basanitic basalts of Neogene age. Petrography and composition relations between minerals reveal recrystallization of these xenoliths at 20.5 (± 0.5) kbar [estimated from the Nickel & Green (1985) barometer for the garnet-bearing samples] and 1050° - 1100°C (± 50°C) [average of temperature estimates for all samples by the two-pyroxene thermometers, the Fe^{2+}/Mg exchange thermometers, and the spinel-orthopyroxene-olivine equilibria thermometers]. The oxygen fugacity recorded by these xenoliths is - 0.5 (± 0.5) log unit relative to the FMQ buffer according to the empirical oxygen sensor of Ballhaus et al. (1991). These PT fo_2 ranges probably represent the typical mantle thermal conditions underneath the sampling region. Presence of a thin phlogopite vein in a spinel lherzolite sample implies operation of a small scale, late-stage modal metasomatism because the phlogopite is rich in TiO_2 and Cr_2O_3 and thus is probably of secondary origin according to Carswell (1975) and Dawson & Smith (1975). Two types of glasses (Na-rich and K-rich) are detected in some kelyphite rims of garnet and in at least one garnet-free sample. They have similar compositions to the feldspar microlites in the matrix of the host basalts, which are presumably the devitrification products of alkali-rich glasses in the basalts. The similarity suggests that the alkali-rich glasses in the xenoliths originated from the host basalts, and that they represent a late stage local penetration of mobile residual melt from the cooling and crystallizing host basalts.

Compositions of individual mineral phases in these xenoliths show systematic variation and are positively related to whole-rock compositions. These composition variation trends are best interpreted as a partial melting trend (e.g. Berg & O'Hara, 1973). Accepting this interpretation, it follows that the individual samples are related to each other through a partial melting process prior to recrystallization under the ambient mantle conditions. An empirical method has been developed to estimate the composition of the partial melt in equilibrium with each individual xenolith on this partial melting trend. This method is different from previous empirical methods (e.g. O'Hara et al., 1975; Nickel & Green, 1984; Frey et al., 1985) and the mineral/melt equilibria method (e.g. Hansen & Langmuir, 1978) in that it is based on the assumption that the most primitive sample in the suite of xenoliths represents the source composition and each one of all the other samples

is a residue after variable melt extraction from this source, in addition to the constraint imposed by the olivine-melt Fe^{2+}/Mg partition coefficient. Results from these calculations for the Ming-xi samples (taking sample 76222 as the source) indicate that the melt compositions are broadly picritic, with MgO ranging from 17% to 20%, and the extent of melt extraction ranges from 11% to 29%. This melt extraction model is consistent with the batch melting model. The calculated melt compositions are similar to estimates made for ultramafic rock suites by other methods (e.g. Frey et al., 1985; Francis, 1987) and experimentally-determined melt compositions from high-pressure peridotite melting studies (e.g. Falloon & Green, 1988; Falloon et al., 1988). The latter comparison allows an estimation of the melting (or melt segregation) PT conditions to be 25 - 30 kbar, 1500° - 1550°C in an anhydrous environment. Similar results are obtained for the Ronda peridotites (data from Frey et al., 1985), and for the xenolith suite from Mongolia (data from Preß et al., 1986).

In order to better understand the recrystallization process, an experimental study has been undertaken to investigate the systematic changes in composition of individual minerals with pressure and temperature in a model lherzolite system. The starting composition is the Tinaquillo lherzolite composition of Green (1963) with 40% olivine of $Fo_{91.9}$ removed to ease identification of minor phases (such as spinel and clinopyroxene) in the charges. Experiments were carried out in the pressure range of 20 - 35 kbar, temperature range of 1200° - 1500°C; with the graphite capsules as the sample container and without deliberate inclusion of any buffering or fluid-generating material. Run products were simple four- or five-phase lherzolites, and were analyzed by a Cameca SX50 microprobe in the WDS mode. Reversal experiments and homogeneity of the run products support attainment of equilibrium in most runs.

Composition of olivine does not change greatly with pressure and temperature, except that its CaO increases with rising temperature and falling pressure. Orthopyroxene composition shows small but significant variations with pressure and temperature. Both SiO_2 and Na_2O increase with increasing pressure; Al_2O_3, Cr_2O_3 and CaO increase with increasing temperature; Al_2O_3 increases with decreasing pressure; and TiO_2, MgO, FeO decrease with increasing temperature. For clinopyroxene, its CaO and Na_2O decrease sensitively with rising temperature and increase very little with increasing pressure. Both FeO and MgO increase with increasing temperature, opposite to their behaviour in orthopyroxene. SiO_2, TiO_2 and Al_2O_3 in clinopyroxene show the same responses to pressure and temperature changes as they do in orthopyroxene. FeO and MgO in garnet behave differently in response to temperature changes. With increasing temperature, FeO decreases but MgO increases, MnO decreases slightly, and both TiO_2 and Cr_2O_3 show small increases. CaO tends to decrease with increase in both temperature and pressure. In spinel, FeO and MgO show the same behaviour as they do in garnet: FeO decreases and

MgO increases with increasing temperature; Al_2O_3 decreases with increasing pressure and decreasing temperature, whereas Cr_2O_3 is the opposite. TiO_2 in spinel increases sensitively with increasing pressure.

The overall changes in mineral composition in response to temperature and pressure variation are governed by subsolidus reactions between minerals. The two most important types are: (1) the pressure-dependent reactions that involve formation of garnet at the expense of spinel and orthopyroxene with increasing pressure; and (2) temperature-dependent reactions that concern growth of clinopyroxene at the expense of spinel, orthopyroxene, and garnet with increasing temperature. Some of these reactions have been calibrated as useful mineral barometers (e.g. "the Al_2O_3 solubility in orthopyroxene coexisting with garnet" barometer of Nickel & Green, 1985) and thermometers (e.g. the "two-pyroxene" thermometers of Wells, 1977; Kretz, 1982; Bertrand & Mercier, 1985). Some are potentially useful barometers and thermometers.

In Chapter Four, the growth of garnet has been studied in great detail and a barometer based on the transition from spinel lherzolite to garnet lherzolite has been formulated. Two reactions are recognised in controlling garnet growth in the lherzolite system:

(1) $MgAl_2SiO_6 + Mg_2Si_2O_6 = Mg_3Al_2Si_3O_{12}$ (garnet growth from orthopyroxene)

(2) $MgAl_2O_4 + 2\ Mg_2Si_2O_6 = Mg_3Al_2Si_3O_{12} + Mg_2SiO_4$ (garnet growth from spinel and orthopyroxene).

They can be combined to form one reaction:

(3) $MgAl_2O_4 + 3\ Mg_2Si_2O_6 + MgAl_2SiO_6 = Mg_2SiO_4 + 2\ Mg_3Al_2Si_3O_{12}$.

With the help of the summary data of Newton (1989) in the MAS (MgO-Al_2O_3-SiO_2) system and the thermodynamic model and parameters of Gasparik & Newton (1984), a thermodynamic expression is established for this reaction, which takes the form of a barometer:

$$P^{MAS} = \frac{[0.1103(T-298)-1651] + \sqrt{\{[0.1103(T-298)-1651]^2+6.1416C\}}}{3.0708} \text{ (kbar)},$$

where $C = 0.0682T^2 - 383.68T\ln T + 3449.51T - 35674\sqrt{T} - \frac{6988632}{T} + 272223 - 8.314T\{\ln X_{Al}^{M1} + 3\ln(1 - X_{Al}^{M1})\}$, T in K, and orthopyroxene is treated as an ideal solid solution between $Mg_2Si_2O_6$ and $MgAl_2SiO_6$.

Corrections should be made for the effects of other components if this barometer is to be applied to natural mineral assemblages. Previous studies (e.g. Green & Ringwood, 1967a; O'Neill, 1981; Nickel, 1986) recognise the importance of $\Sigma R_2O_3/Px$ (Px = sum of normative pyroxenes in wt%) and Cr# ($= \frac{100Cr}{Al+Cr}$) of the whole rock in influencing the appearance of garnet. In order to quantify these effects, a detailed

experimental study was carried out with three bulk compositions of different ΣR_2O_3/Px and Cr#. The garnet-in boundary in each composition was well defined and the compositions of coexisting garnet, spinel, two pyroxenes, and olivine were analysed by the CAMECA SX50 microprobe in the WDS system. The data set is fitted to an empirical expression:

$$P^{complex} = a + bP^{MAS} + cT\ln X_{Mg}^{ol} + dT\ln X_{Mg}^{opx} + eT\ln X_{Mg}^{Gt} + fT\ln X_{Mg}^{Sp} + gT\ln X_{Cr}^{opx} + hT\ln X_{Cr}^{Gt} + iT\ln(X_{Cr}^{Sp} + X_{Fe^{3+}}^{Sp}) + jT\ln X_{Ca}^{Gt}.$$

Analysis of the data by the method of multiple linear regression produces the following constants: a = 14.52, b = 0.79, c = -0.0033, d = 0.0948, e = -0.0151, f = -0.0031, g = -0.0003, h = 0.0019, i = - 0.0003, j = - 0.0031 (r^2 = 0.9326). However, only X_{Mg}^{opx} and X_{Cr}^{Gt} are significant among all these composition terms. Assuming all variation is attributable to P^{MAS}, X_{Mg}^{opx} and X_{Cr}^{Gt}, then the empirical barometer can be simplified to:

$$P^{complex} = 19.2 + 0.95P^{MAS} + T\{0.0626\ln X_{Mg}^{opx} + 0.0014\ln X_{Cr}^{Gt}\} \quad (r^2 = 0.9285);$$

which reproduces the experimental pressures within ± 2 kbar. Application of this barometer to a number of natural garnet + spinel lherzolite xenoliths gives a range of pressure from 23.5 to 28 kbar for the xenoliths in alkali-basalts, and from 30 to 49 kbar for the xenoliths in kimberlites. The spinel + garnet lherzolite samples from Ming-xi have an equilibrium pressure of 27 (± 1) kbar at 1050°C according to this barometer, which is much higher than the estimates by the Nickel & Green (1985) barometer (20.5 ± 0.5 kbar). Reasons for this discrepancy remain a problem for future investigation.

Two by-products from the above two main experimental studies are an attempt to formulate empirical barometers and thermometers for spinel lherzolites, and a revision of the garnet - clinopyroxene Fe^{2+}/Mg exchange thermometer. The experimental data show that with increasing pressure, Ti in spinel increases and in pyroxenes decreases slightly; and that the Fe^{2+}/Mg partitioning between silicate minerals and spinel is sensitive to temperature change. Although the experiments were not specifically designed to formulate barometers and thermometers for spinel lherzolites, the data available are sufficient to demonstrate the empirical approach. Regression analyses of the experimental data yield two barometers for Ti-partitioning between spinel and orthopyroxene, and between spinel and clinopyroxene respectively:

$$P_{1(kbar)} = 0.0115(\ln K_d{}^1 - 1.1116)T - 0.044[Mg\#^{(Sp)}]^2 + 30.73[Mg\#^{(Sp)}] - 3.33[Mg\#^{(Opx)}], \quad (r^2 = 0.8067);$$

$P_{3(kbar)} = 0.0167(\ln K_d^3 - 2.3316)T - 0.008[Mg\#^{(Sp)}]^2 + 1.89[Mg\#^{(Sp)}] - 0.46[Cr\#^{(Sp)}] - 303[X_{Ti}^{Sp}]$, $(r^2 = 0.8877)$;

where $K_d^1 = \frac{Ti^{Sp}}{Ti^{Opx}}$ and $K_d^3 = \frac{Ti^{Sp}}{Ti^{Cpx}}$, T in K. Because Al in spinel decreases with increasing pressure, the ratio Ti/Al should be more sensitive to pressure change than Ti alone. Fitting the same experimental data against Ti/Al K_ds, another two empirical barometers are obtained:

$P_{2(kbar)} = 0.0111(\ln K_d^2 - 0.2188)T - 0.001[Mg\#^{(Sp)}]^2 + 0.68[Mg\#^{(Sp)}] - 0.28[Cr\#^{(Sp)}]$, $(r^2 = 0.8238)$;

$P_{4(kbar)} = 0.0203(\ln K_d^4 - 0.6546)T + 0.031[Mg\#^{(Sp)}]^2 + 295.4 + 4.56[Mg\#^{(Sp)}] - 0.91[Cr\#^{(Sp)}] - 649[X_{Ti}^{Sp}]$, $(r^2 = 0.9158)$;

where $K_d^2 = \frac{(Ti/Al)^{Sp}}{(Ti/Al)^{Opx}}$ and $K_d^4 = \frac{(Ti/Al)^{Sp}}{(Ti/Al)^{Cpx}}$. Similarly, for the Fe^{2+}/Mg partitioning between silicate minerals and spinel, four empirical thermometers are extracted for the olivine - spinel pair (K_d^5), the orthopyroxene - spinel pair (K_d^6), the clinopyroxene - spinel pair (K_d^7), and the garnet - spinel pair (K_d^8) [$K_d = \frac{(Fe^{2+}/Mg)^{Spinel}}{(Fe^{2+}/Mg)^{Silicate}}$]:

$$T_{1(K)} = \frac{1.15[Mg\#^{(ol)}]^2 - 70.4[Mg\#^{(ol)}] + 0.28[Mg\#^{(sp)}]^2 - 93.5[Mg\#^{(sp)}] + 7.06[Cr\#^{(sp)}] + 1024[X_{Ti}^{sp}] + 2844}{\ln K_d^5 - 0.655}$$

$(r^2 = 0.9448)$;

$$T_{2(K)} = \frac{3.83[Mg\#^{(Opx)}]^2 - 515.7[Mg\#^{(Opx)}] - 69.6[Mg\#^{(Sp)}] - 0.06[Cr\#^{(Sp)}]^2 + 9.2[Cr\#^{(Sp)}] + 20133}{\ln K_d^6 - 1.2034}$$

$(r^2 = 0.9791)$;

$$T_{3(K)} = \frac{156.4[Mg\#^{(Cpx)}] - 1.9[Mg\#^{(Sp)}]^2 + 195.1[Mg\#^{(Sp)}] + 0.12[Cr\#^{(Sp)}]^2 - 9.2[Cr\#^{(Sp)}] - 17728}{\ln K_d^7 - 1.004}$$

$(r^2 = 0.9982)$

$$T_{4(K)} = \frac{117[Mg\#^{(Gt)}] - 1.72[Mg\#^{(Sp)}]^2 + 166.6[Mg\#^{(Sp)}] + 0.1[Cr\#^{(Sp)}]^2 - 8.2[Cr\#^{(Sp)}] - 12564}{\ln K_d^8 - 0.5989}$$

$(r^2 = 0.9988)$.

The practical applications of these barometers and thermometers are limited by their large uncertainties (pressures ±10 kbar, temperatures ± 200°C). Nevertheless, they open up new possibilities and expose the likely difficulties that may be encountered in seeking mineral barometers and thermometers for spinel lherzolites.

Rocks of various bulk compositions with coexisting garnet and clinopyroxene occur over a wide range of pressures and temperatures in the lower crust and the upper mantle. The equilibrium temperatures of these rocks can be estimated by the garnet - clinopyroxene Fe^{2+}/Mg exchange thermometer, first developed by Råheim & Green (1974a), modified by Ellis & Green (1979), with further improvement by Krogh (1988). These thermometers, however, tend to overestimate temperatures for rocks equilibrated at relatively low pressures (e.g. amphibolites and granulites, Green & Adam, 1991). One of

the reasons is that they do not take into account the effect of Mg# of garnet on the K_d, which is found to be significant (particularly for rocks with low Mg#) by Pattison & Newton (1989). Based on the experimental data reported in this study and in the literature (total 380 pairs of coexisting garnet - clinopyroxene, covering 10 - 60 kbar, 600° - 1500°C, and a wide range of bulk compositions), a revised garnet - clinopyroxene Fe^{2+}/Mg exchange thermometer is formulated:

$$T(K)=\frac{-1523[X_{Ca}^{Gt}]^2 + 2759[X_{Ca}^{Gt}] - 8.9[Mg\#^{(Gt)}] + 1974 + 17.35P(kbar)}{\ln(K_d) + 0.849} \quad (r^2 = 0.926);$$

where $K_d=\frac{(Fe^{2+}/Mg)^{Gt}}{(Fe^{2+}/Mg)^{Cpx}}$, $X_{Ca}^{Gt}=\frac{Ca}{Ca + Mg + Fe^{2+} + Mn}$, $Mg\#^{(Gt)}=\frac{100Mg}{Mg + Fe^{2+}}$.

Application of this thermometer to rocks from the lower crust (garnet amphibolites, granulites and crustal eclogites) and the upper mantle (xenoliths in kimberlites and mineral-inclusions in diamonds) yields reasonable temperature estimates, which are consistent with estimates from other constraints (e.g. phase relations imposed by the metamorphic grade, and estimates by other thermometers that are based on different reaction schemes such as the two-pyroxene thermometer), provided that the equilibrium pressure is known and that the garnet - clinopyroxene pair in question is in mutual chemical equilibrium.

In conclusion, this study emphasizes systematic changes exhibited in mineral and whole-rock compositions and the causes of these changes, and demonstrates some possible ways of predicting these changes. Mantle processes are complicated, but in recognizing the three major processes (partial melting, recrystallization, and metasomatism), which are the main causes of the changes in mineral and whole-rock compositions, and in scrutinizing them, they can be comprehended. This idea is manifested in, among others, the detailed modelling of the partial melting process experienced by the Ming-xi lherzolite suite, the development of various mineral barometers and thermometers, and the realization of the two important types of subsolidus mineral reactions in the lherzolite system.

Acknowledgements

This project was initiated through a discussion between Prof. DH Green and Prof. XM Zhou (Nan-jing University) when Prof. Zhou visited Tasmania in November 1985. During the course of this study, Prof. Green has provided constant support, encouragement, advice and friendship, which are best shown in his careful and constructive review and correction of my thesis drafts. Prof. Zhou has been very helpful in advising relevant Chinese literature and in assisting my sample collection in China. Their guidance and supervision ensured the completion of this project and the production of this thesis.

Many people have contributed to this work in one way or another. Among them I thank:

——— Prof. S Banno of Kyoto University for his encouragement and support of this project, and advice on careful thinking of ideas.

——— Tony Crawford, Rick Varne, Keith Harris, Geoff Nichols, Chris Ballhaus, Wayne Taylor, Ron Berry, Ray Binns, and Yadong Chen for their reading of and comments on parts of this thesis; and for valuable suggestions and discussions.

——— Kiyo Niida, Trevor Falloon, Steve Eggins, Greg Yaxley, Alex Sobolev, Leonid Danyushevsky, Yuri Babich for discussions on petrogenesis of basalts and ultramafic xenoliths.

——— Keith Harris for his help and support in the high-pressure laboratory.

——— Wislaw Jablonski, Ross Lincolne, Paul Waller for their assistance with microprobe analysis.

——— Phil Robinson for his dedication toward maintaining the analytical facilities and help with the x-ray fluorescence analyses reported in Chapter Two.

——— Simon Stephens for help in the preparation of microprobe mounts and thin sections.

——— ZM Lai, WH Sun, BC Wang, YH Zheng, and JP Wang for their assistance in sampling the Ming-xi xenoliths, and for their hospitality and friendship.

——— Zhenjie Lin of Geography Department, Tony Grainger, Michael Henry, Steve Andrawartha of Computing Centre for their advice and help in solving computing problems.

——— Glen McPherson and Fiona Shelly of Mathematics Department for help in using the regression program in SAS.

——— Many friends in and outside the Geology Department, including Steve Eggins, Garry Davidson, Khin Zaw, Russell Sweeney, Mike Seitz, Memet Hermanto, Dwipa, Thanis Wongwanich, Yuenyong Panjasawatwong, Pol Chaodumrong, Aung Pwa, Soetijoso, Udi Hartono, Sampan Singharajaarapan, Michael Roach, Joe Stolz, David Huston, Massimo Gasparon, Ingvar Sigurdsson, Ruth Lanyon, Peter & Joan Fuglsang, Meave Parker, Robin Bowden, Helen Green, Leo Gunther, Peter Serov, Tony Wang, Charles Pitt, Ge Wang, Duo Li, Qu Qi, Xi-sheng Xu, Jin-jiang Huang, Yi Jiang for their invaluable help and friendship.

——— Members of Geology Department not mentioned above for the enjoyable study environment they help to create.

——— My kung-fu teacher Zhi-ji Hutuktu for his spiritual, intellectual, and physical guidance; fellow students Philip Temple, Hua Fei for their support, encouragement and friendship.

——— My parents for their understanding and spiritual as well as material support.

Chapter One

Petrography and Mineral Chemistry of a Suite of Lherzolite Xenoliths from Fu-jian, Southeastern China

Chapter One

Petrography and Mineral Chemistry of a Suite of Lherzolite Xenoliths from Fu-jian, Southeastern China

1.1 Introduction

Study of mantle-derived xenoliths has been a major subject in modern petrologic research. Because of their direct mantle origin this group of rocks provides first-hand information about the petrology and composition of the upper mantle. For this reason ultramafic xenoliths from many parts of the world have been the subject of extensive investigation since the initiation of the Upper-Mantle Project in the early 1960s. However, studies of mantle xenoliths from eastern Asia, especially China, are less reported in English literature. Only recently have a few summary papers appeared (e.g. Cao & Zhu, 1987; Fan & Hooper, 1989). Although xenoliths from China are similar to those occurring elsewhere in the world, some examples have peculiar features that deserve detailed study. These include the coexistence of spinel and garnet in lherzolite xenoliths from Ming-xi, the coexistence of lherzolite and rare eclogite from Ming-xi, the large outcrop of basalts with abundant spinel peridotites from Damaping, and the association of large amount of spinel peridotite, garnet websterite and amphibole eclogite nodules from Qi-ling (see brief descriptions by Cao & Zhu, 1987).

One of the conclusions from studies of natural xenoliths and from high-pressure experimental investigations of ultramafic systems is that the upper-mantle is layered, with garnet lherzolite occurring beneath spinel lherzolite, which in turn occurs below plagioclase lherzolite. Spinel lherzolite is the most abundant xenolith type found in alkali basalts, whereas garnet lherzolite is dominant in inclusions in kimberlites (e.g. Ringwood, 1975). There are very few localities in the world where garnet lherzolites are found in alkali basalts (Sutherland et al., 1984). Occasionally, lherzolites with garnet and spinel are found, but in most cases the two aluminous phases are in reaction relationship (e.g. Reid & Dawson, 1972; Lock & Dawson, 1980; Neal & Nixon, 1985). Very rarely, garnet and spinel are found in equilibrium relation in lherzolite inclusions in alkali basalts (e.g. Berger, 1979; Skewes & Stern, 1979). One such occurrence has been found in Da-Yang-Ke, Ming-xi county, Fu-jian Province, southeastern China. The locality is at 117°10'E, 26°54'N, the location number six of Cao & Zhu (1987). This occurrence (Fig.1.1) was first reported in Chinese literature by Sun & Lai (1980), and later studied by other Chinese geologists including Zhang (1982, M.Sc thesis). These studies are very brief and informative, but lack systematic and detailed analyses of whole-rock and mineral compositions.

Coexistence of garnet and spinel or the presence of one and not the other phase in a lherzolite may be due to (1) chemical differences in bulk rock composition such that at the same pressure and temperature, rocks with high Cr/Cr+Al and/or low ΣR_2O_3/Px (Px = sum of normative pyroxenes in wt%) will have no garnet whereas rocks with low Cr/Cr+Al and high/or ΣR_2O_3/Px will contain garnet (± spinel); (2) pressure, temperature differences such that assemblages at similar temperature will contain garnet at high pressure, and spinel at low pressure. Samples which have undergone decompression may thus show a growth of spinel + pyroxenes at the expense of garnet and olivine.

In this chapter detailed petrography and systematic mineral chemistry of a suite of lherzolite xenoliths from Ming-xi are presented. They are analyzed to understand the major mantle processes that these xenoliths have experienced, to infer the thermal conditions of the mantle underneath the sampling region, and to use petrography, mineral chemistry and P,T-sensitive chemical partitioning relationships to determine reasons for coexistence of garnet and spinel.

1.2 The Host Basalts

Cenozoic basalts occur predominantly in the eastern part of China. Three groups have been classified on the basis of their age (Wu et al., 1985): Paleogene (71.5 - 28.5 Ma), Neogene (23.8 - 2.6 Ma); and Quaternary (1.48 - 0 Ma). Their distribution is shown in Figure 1.1. Quaternary basalts mainly occur in northern China and are believed to be associated with continental rifting. Neogene basalts are usually located at the margins of the two main tectonic blocks in China, the North China Platform and the Yangtze Platform, and are considered to be related to deep faults. Paleogene basalts are normally found within the two platforms.

The host basalts of this suite of xenoliths are Neogene in age, based on fossils present in the sedimentary layers interbeded within the basalt layers (Sun & Lai, 1980). Texturally these basalts are weakly vesicular and porphyritic, with olivine and Ti-augite as the phenocryst phases (≤ 20 modal%), and olivine, Ti-augite, ilmenite, and alkali-rich glasses as matrix. Occasionally corundum is also observed both as a phenocryst phase and in the matrix. Four typical compositions of the host basalts are given in Table 1.1. They are broadly basanitic, characterised by low-SiO_2, high MgO, Al_2O_3, CaO, P_2O_5. The total alkali content ranges from 2 to 4 wt%. They probably represent near-primary mantle melts (Irving & Green, 1976), since they have Mg# in excess of 68.

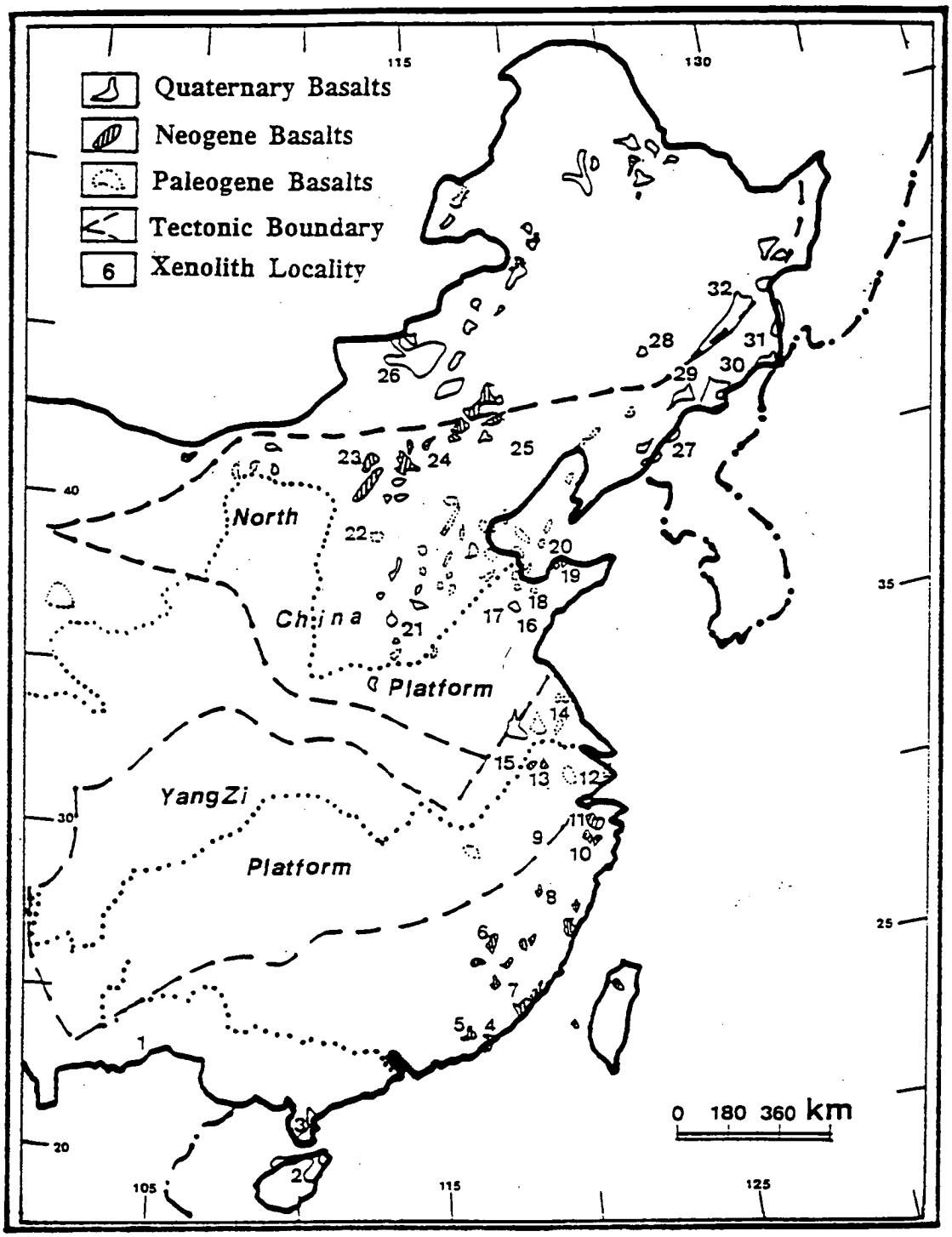

Figure 1.1. Distribution of Cenozoic basalts and xenolith localities in eastern China. Broken lines enclose the two main tectonic blocks (i.e. the North China Platform and the Yangtze Platform); Dotted lines represent the three major rivers (i.e. from north to south: the Yellow River, the Yangtze River, and the Pearl River). Ming-xi lherzolites come from xenolith locality number 6. (data source: basalt distribution - Wu et al., 1985; xenolith localities - Cao & Zhu, 1987).

Table 1.1 Microprobe Analyses of the Host Basalts

Sample #	76229	76569	76213	76568
SiO2	42.34	43.07	41.32	41.67
TiO2	2.95	3.22	2.74	3.03
Al2O3	11.61	10.57	12.06	12.56
Fe2O3	1.41	1.4	1.48	1.47
FeO	11.45	11.3	11.98	11.88
MnO	0.08	0.03	0.12	0.04
MgO	15.53	14.13	15.58	14.29
CaO	11.48	12.55	9.88	10.76
Na2O	1.11	1.32	2.83	2.4
K2O	0.68	1.17	0.73	0.59
P2O5	1.5	1.4	1.39	1.4
Sum	100.14	100.16	100.11	100.09
	CIPW NORMS			
Or	4.04	6.95	4.34	3.51
Ab	9.45	6.43	6.12	8.47
An	24.85	19.57	18.16	21.90
Ne		2.60	9.73	6.48
Di	13.57	20.12	12.96	13.20
Hd	4.63	7.14	4.80	5.07
En	0.82			
Fs	0.32			
Fo	22.30	18.27	23.15	20.82
Fa	9.62	8.20	10.83	10.10
Mt	2.06	2.04	2.16	2.15
Il	5.64	6.15	5.24	5.79
Ap	2.70	2.52	2.50	2.52
Sum	100.00	99.99	99.99	100.01
Mg#	70.74	69.03	69.86	68.20

*). Analyses were carried out on rock powders melted on an Ir strip heater.

1.3 Petrography of the Xenoliths

Twenty individual xenolith samples were selected for this study. These include one garnet lherzolite (76222), one phlogopite-bearing spinel lherzolite (76209), nine spinel lherzolites and nine spinel-bearing garnet lherzolites. Sample size ranges from 3 to 7 cm. Most show granoblastic texture (Harte,1977) and clear foliation. In terms of the textural classification of Mercier & Nicolas (1975), they vary from protogranular to tabular, often with a few large olivine and orthopyroxene porphyroblasts. Mineral grain size ranges from < 0.5 mm to 5 mm, mostly in the 1 - 2 mm range. Spinel crystals are the smallest and orthopyroxene and garnet are the largest among these minerals. Large olivine crystals often show kink bands but pyroxenes are free from exolution lamellae. Crystal boundaries are generally straight and clean, but interfacial angles at triple junctions appear to be variable from < 20° to >70° (Plate 1a & 1b).

Individual mineral grains are homogeneous without detectable chemical zoning. There is no difference (within analytical error) in chemical composition from grain to grain for all the minerals except spinels in the garnet-bearing samples. Most garnet crystals are anhedral and always have kelyphite rims, in which secondary spinel, orthopyroxene ± clinopyroxene can be identified. Spinels in both garnet-absent and garnet-bearing samples show variable grain size and irregular crystal shape. Compositions of spinels in the garnet-absent samples are homogeneous. In the garnet-bearing samples, they can be divided into primary and secondary groups. The primary spinels (Sp1) occur away from garnet crystals, and are the least aluminous and largest in grain size among all spinels. These are only observed in two samples (67212 & 67225). Two sub-groups of secondary spinels are identified. One (Sp2b) is confined within the kelyphite rims of garnet. These are the most aluminous and the smallest among spinels. The other (Sp2a) is close to the kelyphite rims but not confined within them. They are intermediate in aluminium content and grain size. Careful examination reveals that there is a continuous change in garnet grain size, abundance, crystal shape and width of the kelyphite rim from sample to sample, which implies a continuous replacement of garnet by spinel and pyroxenes. It appears that the reaction has just started in 67222, in which only a very thin rim has developed around the large garnet crystals (upto 2 mm in diameter) and the secondary minerals have not yet formed (Plate 1b). The reaction has progressed to a small extent in 67210 & 67211, in which two to three layers of kelyphite rims with different crystallinity have been produced (very similar to that decribed by Reid & Dawson, 1972). The replacement has apparently advanced significantly in 67221, in which the kelyphite rims become substantially thicker and even develop within garnet crystals (Plate 1c). The reaction is perhaps near completion in 67212 & 67225, in which a very small amount of relict, small and irregular-shaped garnet crystals are preserved (Plate 1d). The transition

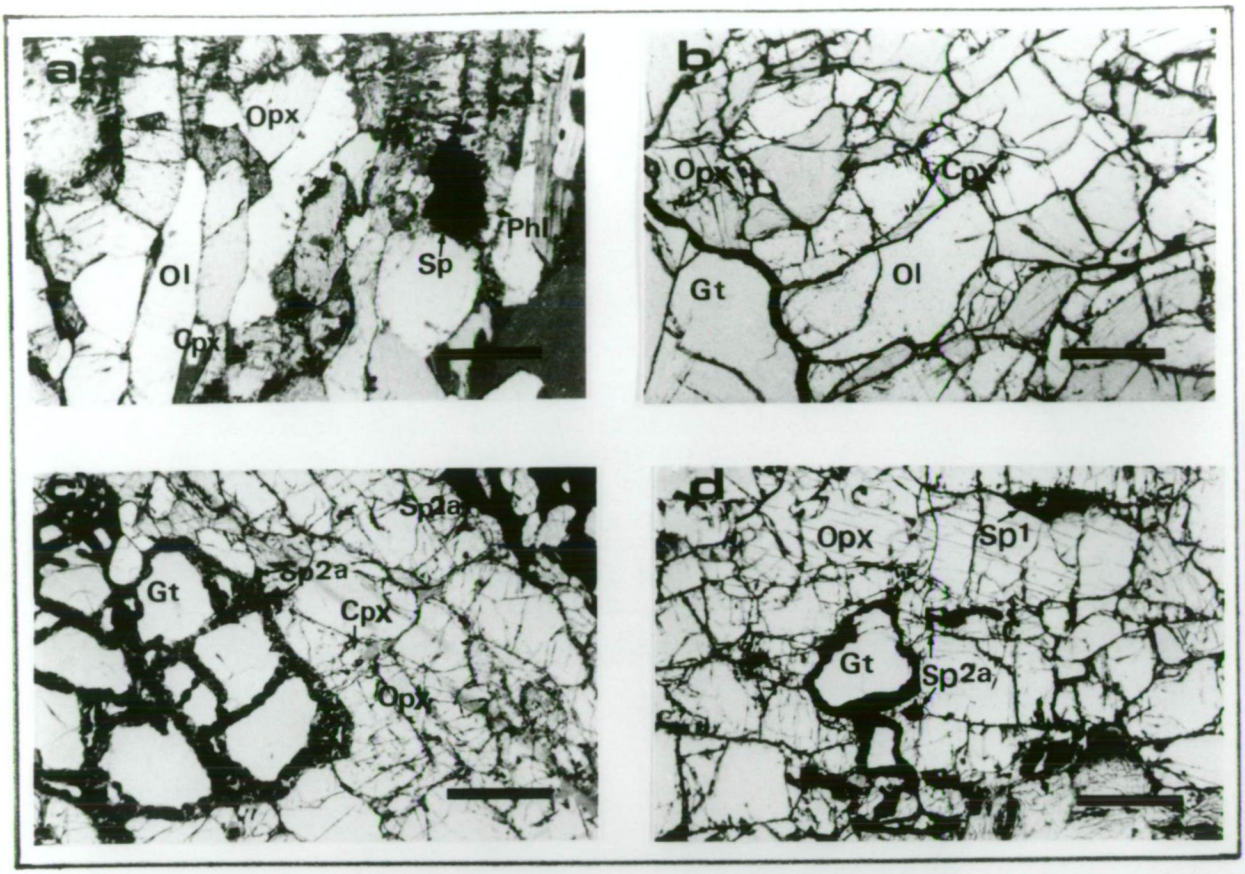

Plate 1a. Phlogopite-bearing spinel lherzolite 76209 with clear foliation;
Plate 1b. Garnet lherzolite 76222 with granoblastic texture. The garnet rim is very thin and does not contain recongizable individual secondary minerals.

Plate 1c. Garnet lherzolite with the presence of two groups of secondary spinels (76221): one within the kelyphite rims of garnet (Sp2b), the other separated from the kelyphite rims (Sp2a). The replacement of garnet by spinel + pyroxenes is shown by the development of kelyphite rims to be substantial.

Plate 1d. Garnet + spinel lherzolite 76225 with primary spinels (Sp1) and secondary spinels (Sp2a). Garnet crystals are very small and rare, indicating very extensive transformation of garnet to spinel + pyroxenes. (Scales bars: 1 mm)

process is presumably related to decompression of original stable garnet (± spinel) lherzolites and/or heating by the host magma, perhaps further catalysed by infiltration of alkali-rich fluids from the host magma (see discussion below).

1.4 Mineral Chemistry

Major and minor element compositions of the minerals were analysed by a JEOL JX-50A electron microprobe in the EDS mode. Normal beam current was 0.7 nA on a Cu metal standard and the accelerating voltage was 15 kV. Calcium and nickel in olivine were determined by a CAMECA SX-50 microprobe, using the WDS analytical system with PET as the diffraction crystal. The trace-element analysis programme supplied by CAMECA was used for Ca & Ni analysis, with a beam current of 100 nA, accelerating voltage of 15 kV and peak counting time of 60 seconds (half for background counting). The detection limits for Ca & Ni are 50 and 100 ppm respectively.

To facilitate discussion, compositions of most minerals are represented by three parameters: Mg# ($=\frac{100Mg}{Mg+Fe^{2+}}$), Cr# ($=\frac{100Cr}{Al+Cr+Fe^{3+}}$), and Ca# ($=\frac{100Ca}{Mg+Fe^{2+}+Ca}$). Clinopyroxene is described by an additional parameter An#($=\frac{100Ca}{Na+Ca}$) due to the presence of a significant amount of sodium. Mineral names are abbreviated as follows: Ol - olivine, Opx - orthopyroxene, Cpx - clinopyroxene, Gt - garnet, Sp - spinel, Phl - phlogopite.

1.4.1 Composition variation within individual minerals

Olivine: Compositions of olivine range in Mg# from 89.67 to 91.42; NiO (wt%) from 0.34 to 0.4 % and CaO (wt%) from 0.018 to 0.134 % (Table 1.2). Olivine in sample 76222 (the only garnet-only lherzolite) has the lowest Mg#, and in 76216 (a spinel lherzolite) has the highest Mg#. In general, olivines in the Gt-bearing samples are slightly lower in Mg# and have CaO contents in a narrower range (0.070 - 0.109%) than in the Gt-absent samples (0.068 - 0.134%). There is a positive correlation between CaO and Mg#, probably indicating substitution of Fe by Ca (Fig.1.2). On the other hand, NiO and MnO are nearly constant for all the samples.

Orthopyroxene: The Mg# of Opx varies from 90.07 to 92.15; Cr# from 4.72 to 22.14; Ca# from 1.44 to 2.75 (Table 1.3). The three parameters are positively correlated with each other (Fig. 1.3a & b). Orthopyroxene in 76222 (garnet lherzolite) has the lowest Mg#, Cr#, and Ca#, and in 76216 (spinel lherzolite) the highest Mg#, Cr# and Ca#. Those in the Gt-bearing samples have a more restricted range of all the three parameters than in the Gt-free samples. Ca is negatively correlated with Fe (Fig.1.3c), suggesting a Fe^{2+} = Ca substitution. The positive correlation of Ca and Cr may indicate

Table 1.2 Olivine Compositions in the Ming-xi Lherzolites

Sample #	76210	76211	76212	76213	76217	76218	76221	76224	76225	76222	76209	76214	76215	76216	76219	76220	76223	76226	76227	76228
Rock Type	GSL	GSL	GSL	GSL	GSL	GSL	GSL	GSL	GSL	GL	Phl-SL	SL	SL	SL	SL	SL	SL	SL	SL	SL
SiO2	41.11	41.15	41.26	41.36	40.99	41.33	41.30	41.12	41.25	41.04	41.39	41.12	41.43	41.56	41.39	41.37	41.27	41.24	41.52	41.31
FeO	9.34	9.44	8.94	8.86	9.61	9.17	8.74	9.04	9.06	9.97	8.64	9.77	8.68	8.30	8.60	8.58	8.67	9.38	8.39	8.67
NiO	0.368	0.338	0.394	0.335	0.394	0.382	0.378	0.373	0.402	0.383	0.378	0.360	0.399	0.372	0.382	0.389	0.380	0.378	0.387	0.377
MgO	49.11	48.99	49.30	49.35	48.91	49.03	49.49	49.37	49.19	48.54	49.51	48.69	49.41	49.63	49.50	49.56	49.58	48.93	49.63	49.55
CaO	0.072	0.074	0.109	0.095	0.098	0.087	0.094	0.093	0.105	0.070	0.080	0.068	0.082	0.130	0.134	0.101	0.097	0.070	0.084	0.090
Sum	100	100	100	100	100	100	100	100	100	100	100	100	100	100	100	100	100	100	100	100
Oxygen	4	4	4	4	4	4	4	4	4	4	4	4	4	4	4	4	4	4	4	4
Si	1.0051	1.0062	1.0067	1.0083	1.0037	1.0090	1.0067	1.0042	1.0070	1.0061	1.0083	1.0069	1.0094	1.0107	1.0082	1.0077	1.0059	1.0080	1.0100	1.0067
Fe	0.1909	0.1931	0.1825	0.1807	0.1968	0.1873	0.1781	0.1845	0.1850	0.2045	0.1760	0.2000	0.1768	0.1689	0.1752	0.1748	0.1768	0.1918	0.1706	0.1768
Ni	0.0072	0.0066	0.0077	0.0066	0.0078	0.0075	0.0074	0.0073	0.0079	0.0075	0.0074	0.0071	0.0078	0.0073	0.0075	0.0076	0.0074	0.0074	0.0076	0.0074
Mg	1.7897	1.7858	1.7935	1.7936	1.7856	1.7848	1.7985	1.7974	1.7903	1.7740	1.7979	1.7774	1.7945	1.7991	1.7974	1.7996	1.8014	1.7830	1.7997	1.8001
Ca	0.0019	0.0019	0.0028	0.0025	0.0026	0.0023	0.0025	0.0024	0.0027	0.0018	0.0021	0.0018	0.0021	0.0034	0.0035	0.0026	0.0025	0.0018	0.0022	0.0024
Sum	2.9949	2.9938	2.9933	2.9917	2.9963	2.9910	2.9933	2.9958	2.9930	2.9939	2.9917	2.9931	2.9906	2.9893	2.9918	2.9923	2.9941	2.9920	2.9900	2.9933
Mg#	90.36	90.24	90.77	90.85	90.07	90.5	90.99	90.69	90.63	89.67	91.08	89.89	91.03	91.42	91.12	91.14	91.06	90.29	91.34	91.06

Rock types: SL - spinel lherzolite; GL - garnet lherzoltie; GSL - garnet + spinel lherzolite.

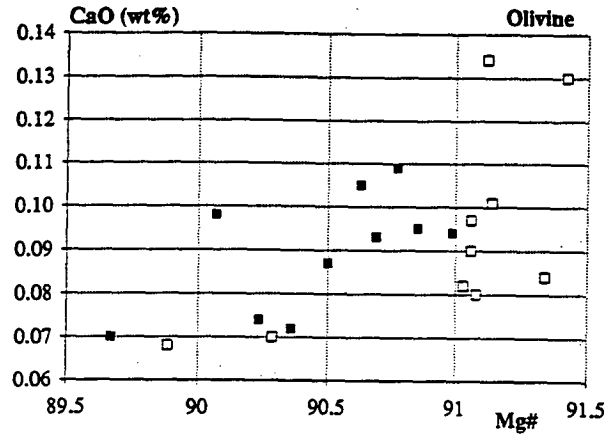

Figure 1.2. Mg# - CaO variation diagram of olivine (Filled symbols are Gt-bearing samples; empty symbols are Gt-free samples).

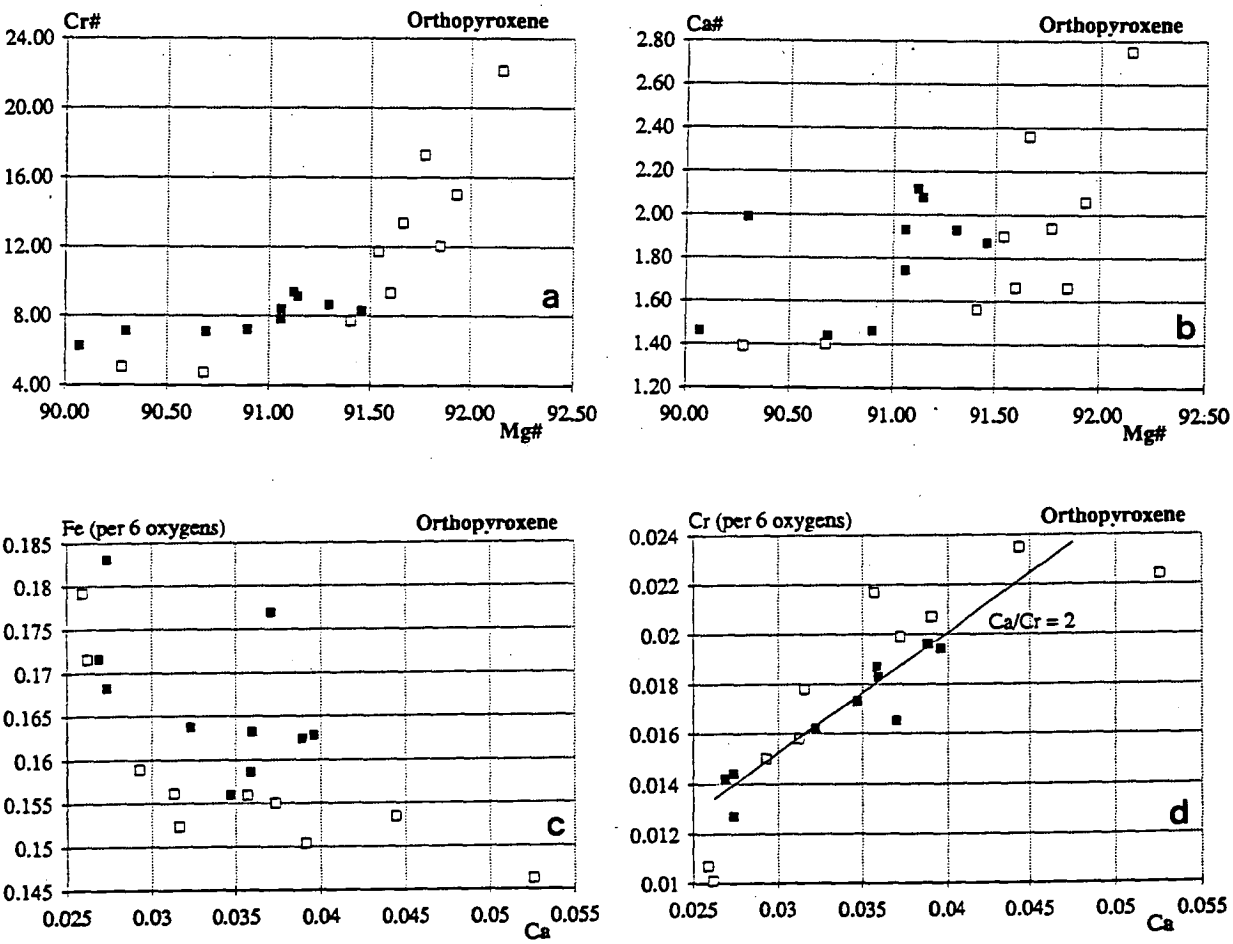

Figure 1.3. (a) Mg# - Cr# variation diagram of orthopyroxene

(b) Mg# - Ca# correlation diagram of orthopyroxene

(c) negative correlation of Cr - Fe in orthopyroxene (cations per 6 oxygens)

(d) positive correlation of Cr - Ca in orthopyroxene (cations per 6 oxygens).

The line marks the constant ratio of Ca/Cr = 2.

Table 1.3 Orthopyroxene Compositions in the Ming-xi Lherzolites

Sample#	76210	76211	76212	76213	76217	76218	76221	76224	76225	76222	76209	76214	76215	76216	76219	76220	76223	76226	76227	76228
Rock Type	GSL	GSL	GSL	GSL	GSL	GSL	GSL	GSL	GSL	GL	Phl-SL	SL	SL	SL	SL	SL	SL	SL	SL	SL
SiO2	55.57	55.45	55.24	55.37	54.82	55.63	55.65	55.33	55.40	55.32	55.52	55.12	56.11	57.23	55.97	56.60	56.82	55.40	56.45	55.89
TiO2		0.17			0.17			0.17		0.19	0.19	0.21								
Al2O3	4.56	4.61	4.82	4.91	5.28	4.72	4.74	4.87	4.63	4.65	4.42	4.96	3.81	1.95	3.76	2.90	2.34	5.02	3.22	4.03
Cr2O3	0.53	0.52	0.72	0.67	0.60	0.60	0.64	0.69	0.71	0.46	0.55	0.39	0.58	0.83	0.86	0.76	0.73	0.37	0.66	0.80
FeO	5.85	5.96	5.64	5.67	6.13	5.69	5.42	5.51	5.65	6.35	5.53	6.22	5.43	5.09	5.33	5.23	5.39	5.96	5.30	5.42
MgO	32.75	32.57	32.53	32.41	32.00	32.49	32.61	32.46	32.53	32.29	33.00	32.39	33.22	33.48	32.88	33.44	33.70	32.54	33.52	32.90
CaO	0.74	0.73	1.05	0.98	1.00	0.88	0.94	0.97	1.07	0.74	0.80	0.70	0.85	1.43	1.21	1.06	1.01	0.71	0.86	0.97
Sum	100	100	100	100	100	100	100	100	100	100	100	100	100	100	100	100	100	100	100	100
Oxygen	6	6	6	6	6	6	6	6	6	6	6	6	6	6	6	6	6	6	6	6
Si	1.912	1.909	1.903	1.906	1.892	1.914	1.912	1.904	1.908	1.908	1.910	1.900	1.928	1.967	1.926	1.945	1.954	1.906	1.939	1.922
Ti		0.004			0.004			0.004		0.005	0.005	0.006								
Al	0.185	0.187	0.196	0.199	0.215	0.191	0.192	0.198	0.188	0.189	0.179	0.202	0.154	0.079	0.152	0.117	0.095	0.204	0.130	0.163
Cr	0.014	0.014	0.020	0.018	0.017	0.016	0.017	0.019	0.019	0.013	0.015	0.011	0.016	0.022	0.024	0.021	0.020	0.010	0.018	0.022
Fe	0.168	0.172	0.162	0.163	0.177	0.164	0.156	0.159	0.163	0.183	0.159	0.179	0.156	0.146	0.153	0.150	0.155	0.172	0.152	0.156
Mg	1.680	1.672	1.671	1.663	1.647	1.666	1.671	1.665	1.670	1.661	1.692	1.665	1.702	1.715	1.687	1.713	1.728	1.669	1.716	1.687
Ca	0.027	0.027	0.039	0.036	0.037	0.032	0.035	0.036	0.040	0.027	0.029	0.026	0.031	0.053	0.044	0.039	0.037	0.026	0.032	0.036
Sum	3.988	3.986	3.990	3.986	3.988	3.983	3.983	3.984	3.988	3.986	3.989	3.988	3.987	3.982	3.986	3.986	3.989	3.987	3.987	3.985
Mg#	90.90	90.69	91.14	91.06	90.30	91.06	91.46	91.30	91.12	90.07	91.41	90.28	91.60	92.15	91.66	91.93	91.77	90.68	91.85	91.54
Cr#	7.21	7.06	9.10	8.39	7.11	7.82	8.27	8.63	9.37	6.27	7.71	5.05	9.31	22.14	13.37	15.00	17.30	4.72	12.04	11.73
Ca#	1.46	1.44	2.08	1.93	1.99	1.74	1.87	1.93	2.12	1.46	1.56	1.39	1.66	2.75	2.36	2.06	1.94	1.40	1.66	1.90

existence of a component $Ca_2Si_2O_6*\frac{1}{2}Cr_2O_3$ in the Opx (Fig. 1.3d). Most minor elements (Ti, Mn, Ni, Na) are below detection limit.

Clinopyroxene: Cpx has higher Mg# and Cr# , and wider variation ranges than coexisting Ol and Opx. The Mg# varies from 89.5 to 93.0; Cr# from 7.5 to 30.4; Ca# from 40.4 to 45.2; An# from 85 to 100 (Table 1.4). The Mg#, Cr# and An# display a positive correlation (Fig. 1.4a & b). Clinopyroxene in 76222 still has the lowest Mg#, Cr#, and An#, but the highest Mg#, Cr#, An# are found in Cpx of 76223 (not 76216). TiO_2 ranges from below detection limit to 0.x%wt% and shows a negative correlation with Mg# (Fig. 1.4c) and a positive correlation with Na_2O (Fig. 1.4d). Ca and Fe again display negative correlation but Ca - Cr relationships are not straightforward.

Garnet: The garnet composition has a very limited range: Mg# 83.1 - 85.5; Cr# 3.4 - 7.4; Ca# 12.1 - 15.0 (Table 1.5). As for Opx, the three parameters are positively correlated with each other (Fig.1.5a & b). They are of typical chrome-pyrope type (the G9 garnets of Dawson & Stephens, 1975), lower in Cr and higher in Ca than the diamond-associated G10 garnets. No chemical zoning in garnet has been detected in any of the garnet grains. Garnet in 76222 has the lowest Mg#, Cr#, and Ca#; and in 76212 & 76225 the highest Cr# and Ca# but not Mg#. In fact garnets in the latter two samples have the lowest Mg-cations among all the samples in this suite. Such "Mg-depletion" is believed to be a direct consequence of the extensive reaction (transformation) from garnet to spinel + orthopyroxene (± clinopyroxene). Ca and Fe again show a negative correlation (Fig.1.5c); and Ca and Cr show positive correlation (Fig.1.5d).

Spinel: Spinels in samples with garnet and without garnet exhibit contrasting trends in the Mg# versus Cr# plot (Fig.1.6). In samples without garnet, they show wide variation (Mg# 70.70 - 81.17; Cr# 11.53 - 65.52; Table 1.6) and negative correlation of Mg# and Cr#, which is typical for all the spinel peridotite suites enclosed in alkali-basalts and for Alpine and abyssal peridotites. In samples with garnet the Mg# and Cr# of the spinels are within very restricted range (Mg# 78.99 - 81.6, Cr# 18 - 20.73; Table 1.6) and manifest a positive correlation, a feature characteristic of coexisting silicate minerals such as garnet and pyroxenes. Such positive correlation can be explained by direct transformation of these spinels from garnet, which is consistent with petrographic observations noted earlier. In this sense, all these spinels are secondary in origin. Primary spinels (Sp1), which were once in equilibrium with garnet and pyroxenes at higher pressure, are found in a continuous reaction relationship with garnet and pyroxenes in samples 76212 & 76225, where different primary spinel grains have continuously variable composition (e.g. from the highest Cr# for the "most" primary spinels to the lowest Cr# for the secondary spinels (Sp2a) close to but not confined within the kelyphite rims). Table 1.6 gives the two extreme compositions for these two samples. The primary spinels are also different from secondary spinels in that they conform with the trend on the

Table 1.4 Clinopyroxene Compositions in the Ming-xi Lherzolites

Sample#	76210	76211	76212	76213	76217	76218	76221	76224	76225	76222	76209	76214	76215	76216	76219	76220	76223	76226	76227	76228
Rock Type	GSL	GSL	GSL	GSL	GSL	GSL	GSL	GSL	GSL	GL	Phl-SL	SL	SL	SL	SL	SL	SL	SL	SL	SL
SiO2	52.92	52.65	52.79	52.70	52.32	52.75	52.89	52.62	52.90	52.50	52.85	52.05	53.33	54.48	53.47	53.97	54.22	52.45	53.62	53.22
TiO2	0.31	0.46		0.26	0.40	0.38	0.26	0.31		0.59	0.28	0.86						0.44		0.19
Al2O3	6.02	6.44	5.28	6.11	6.81	5.96	5.90	6.28	5.15	6.77	5.24	7.22	3.76	2.30	3.88	2.81	2.47	6.78	3.09	5.16
Cr2O3	1.23	1.22	1.19	1.31	1.25	1.36	1.39	1.43	1.21	1.14	1.06	0.89	0.99	1.50	1.28	1.24	1.17	0.82	1.03	1.70
FeO	2.75	2.93	2.94	3.01	3.34	2.86	2.76	2.82	2.91	3.20	2.63	3.04	2.47	2.88	2.74	2.45	2.46	2.76	2.46	2.83
MgO	15.89	15.56	17.17	16.51	16.17	16.29	16.49	16.33	17.11	15.35	16.50	15.27	17.48	18.91	18.12	18.04	18.36	15.56	17.61	16.73
CaO	19.36	19.06	19.94	18.83	18.20	19.10	19.04	18.80	20.02	18.65	20.55	18.97	21.69	19.39	20.21	21.22	21.33	19.64	21.80	18.79
Na2O	1.51	1.68	0.70	1.27	1.52	1.31	1.28	1.42	0.69	1.81	0.89	1.69	0.28	0.55	0.29	0.27	0.00	1.54	0.39	1.38
Sum	100	100	100	100	100	100	100	100	100	100	100	100	100	100	100	100	100	100	100	100
Oxygen	6	6	6	6	6	6	6	6	6	6	6	6	6	6	6	6	6	6	6	6
Si	1.906	1.897	1.903	1.897	1.884	1.900	1.903	1.894	1.908	1.892	1.907	1.876	1.926	1.961	1.926	1.947	1.954	1.889	1.939	1.916
Ti	0.009	0.012		0.007	0.011	0.010	0.007	0.008		0.016	0.008	0.023						0.012		0.005
Al	0.255	0.273	0.224	0.259	0.289	0.253	0.250	0.266	0.219	0.288	0.223	0.307	0.160	0.098	0.165	0.120	0.105	0.288	0.132	0.219
Cr	0.035	0.035	0.034	0.037	0.036	0.039	0.039	0.041	0.034	0.032	0.030	0.025	0.028	0.043	0.037	0.035	0.034	0.023	0.030	0.048
Fe	0.083	0.088	0.089	0.091	0.101	0.086	0.083	0.085	0.088	0.097	0.080	0.092	0.075	0.087	0.083	0.074	0.074	0.083	0.074	0.085
Mg	0.853	0.836	0.923	0.886	0.868	0.875	0.884	0.876	0.920	0.824	0.887	0.821	0.941	1.015	0.973	0.970	0.987	0.836	0.949	0.898
Ca	0.747	0.736	0.770	0.726	0.702	0.737	0.734	0.725	0.774	0.720	0.794	0.733	0.839	0.748	0.780	0.820	0.824	0.758	0.844	0.725
Na	0.106	0.117	0.049	0.089	0.106	0.091	0.090	0.099	0.048	0.127	0.063	0.118	0.019	0.039	0.021	0.019	0.000	0.108	0.027	0.096
Sum	3.994	3.995	3.992	3.992	3.996	3.990	3.990	3.994	3.990	3.995	3.991	3.994	3.989	3.988	3.984	3.985	3.977	3.997	3.995	3.993
Mg#	91.15	90.43	91.25	90.71	89.62	91.02	91.42	91.17	91.28	89.52	91.78	89.97	92.66	92.13	92.19	92.93	93.02	90.94	92.74	91.34
Cr#	12.05	11.31	13.09	12.60	10.95	13.26	13.62	13.25	13.60	10.13	11.99	7.64	14.97	30.39	18.12	22.84	24.20	7.50	18.29	18.10
Ca#	44.38	44.33	43.23	42.64	42.03	43.41	43.14	43.00	43.43	43.87	45.10	44.54	45.24	40.43	42.49	44.00	43.71	45.21	45.22	42.44
An#	87.61	86.24	94.06	89.10	86.85	88.98	89.14	87.98	94.13	85.06	92.70	86.11	97.75	95.09	97.45	97.78	100.00	87.57	96.87	88.30

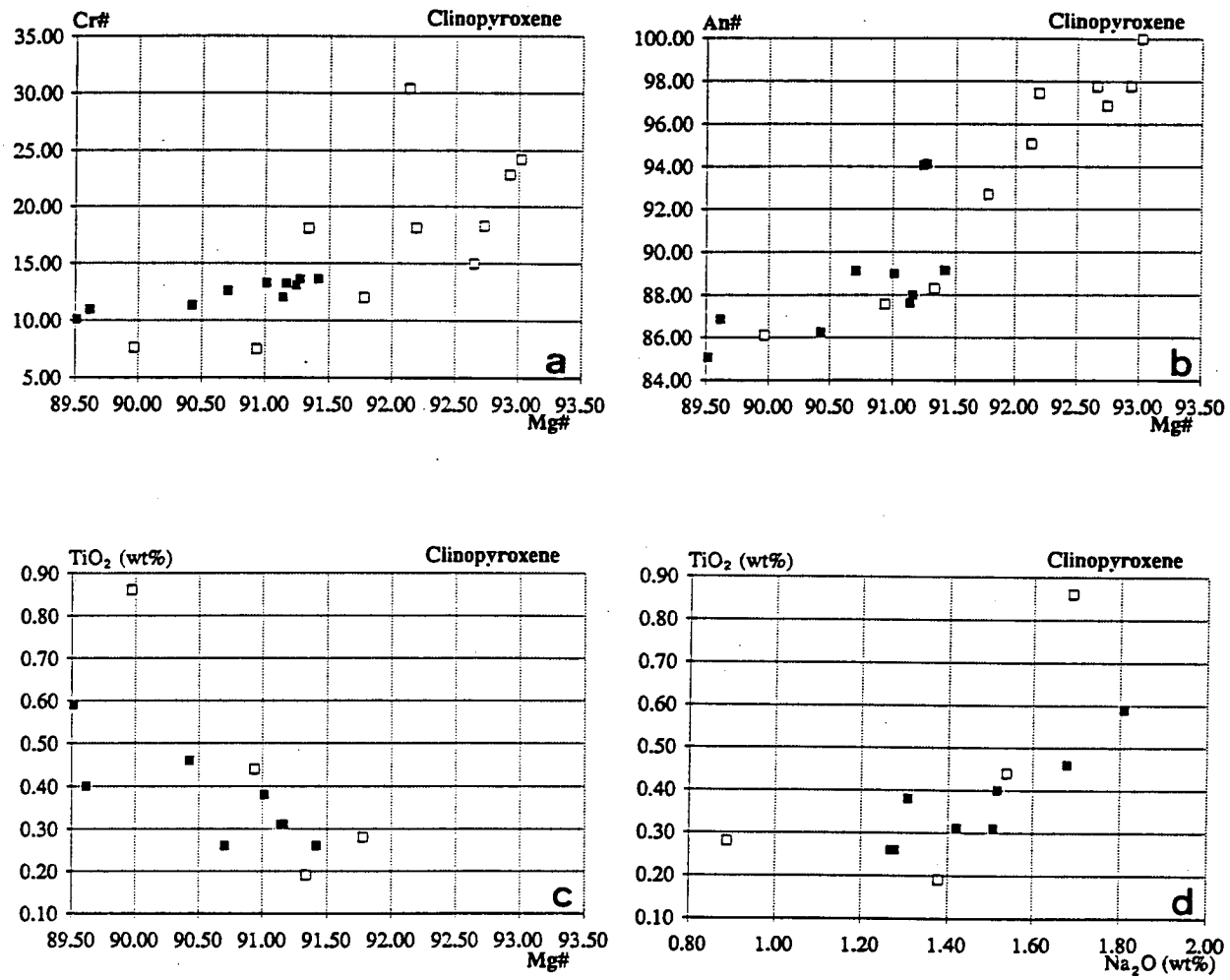

Figure 1.4. (a) Mg# - Cr# variation diagram of clinopyroxene
(b) Mg# - An# correlation diagram of clinopyroxene
(c) negative correlation of TiO_2 and Mg# in clinopyroxene
(d) positive correlation of TiO_2 and Na_2O in clinopyroxene.

Table 1.5 Garnet Compositions in the Ming-xi Lherzolites

Sample#	76210	76211	76212	76213	76217	76218	76221	76224	76225	76222
Rock Type	GSL	GSL	GSL	GSL	GSL	GSL	GSL	GSL	GSL	GL
SiO2	42.23	42.32	42.32	42.46	42.36	42.35	42.20	42.27	42.18	42.32
TiO2	0.18	0.22		0.18	0.21	0.19	0.28	0.23		0.17
Al2O3	23.11	23.06	22.11	22.61	22.72	22.81	22.34	22.41	22.15	23.18
Cr2O3	1.47	1.37	2.64	1.97	1.70	1.80	2.40	2.27	2.54	1.21
FeO	7.04	7.17	6.35	6.49	6.84	6.60	6.31	6.43	6.53	7.47
MnO	0.30	0.26	0.25	0.28	0.29	0.25	0.29	0.27	0.24	0.25
MgO	20.65	20.72	20.43	20.80	20.90	20.78	20.85	20.87	20.49	20.64
CaO	5.01	4.88	5.90	5.21	4.99	5.20	5.32	5.25	5.87	4.76
Sum	100	100	100	100	100	100	100	100	100	100
Oxygen	12	12	12	12	12	12	12	12	12	12
Si	2.987	2.993	3.002	3.001	2.996	2.994	2.988	2.992	2.995	2.994
Ti	0.010	0.011		0.010	0.011	0.010	0.015	0.012		0.009
Al	1.927	1.922	1.849	1.884	1.893	1.901	1.864	1.870	1.854	1.932
Cr	0.082	0.077	0.148	0.110	0.095	0.101	0.135	0.127	0.143	0.068
Fe	0.416	0.424	0.377	0.384	0.405	0.390	0.374	0.380	0.388	0.442
Mn	0.018	0.016	0.015	0.017	0.017	0.015	0.018	0.016	0.014	0.015
Mg	2.178	2.185	2.161	2.192	2.204	2.190	2.201	2.202	2.168	2.177
Ca	0.380	0.370	0.448	0.395	0.378	0.394	0.404	0.398	0.446	0.361
Sum	7.998	7.997	8.000	7.992	7.999	7.995	7.998	7.998	8.007	7.997
Mg#	83.95	83.75	85.16	85.11	84.49	84.87	85.48	85.27	84.83	83.12
Cr#	4.10	3.83	7.43	5.53	4.77	5.03	6.73	6.37	7.14	3.37
Ca#	12.77	12.41	15.02	13.28	12.66	13.25	13.55	13.36	14.86	12.11

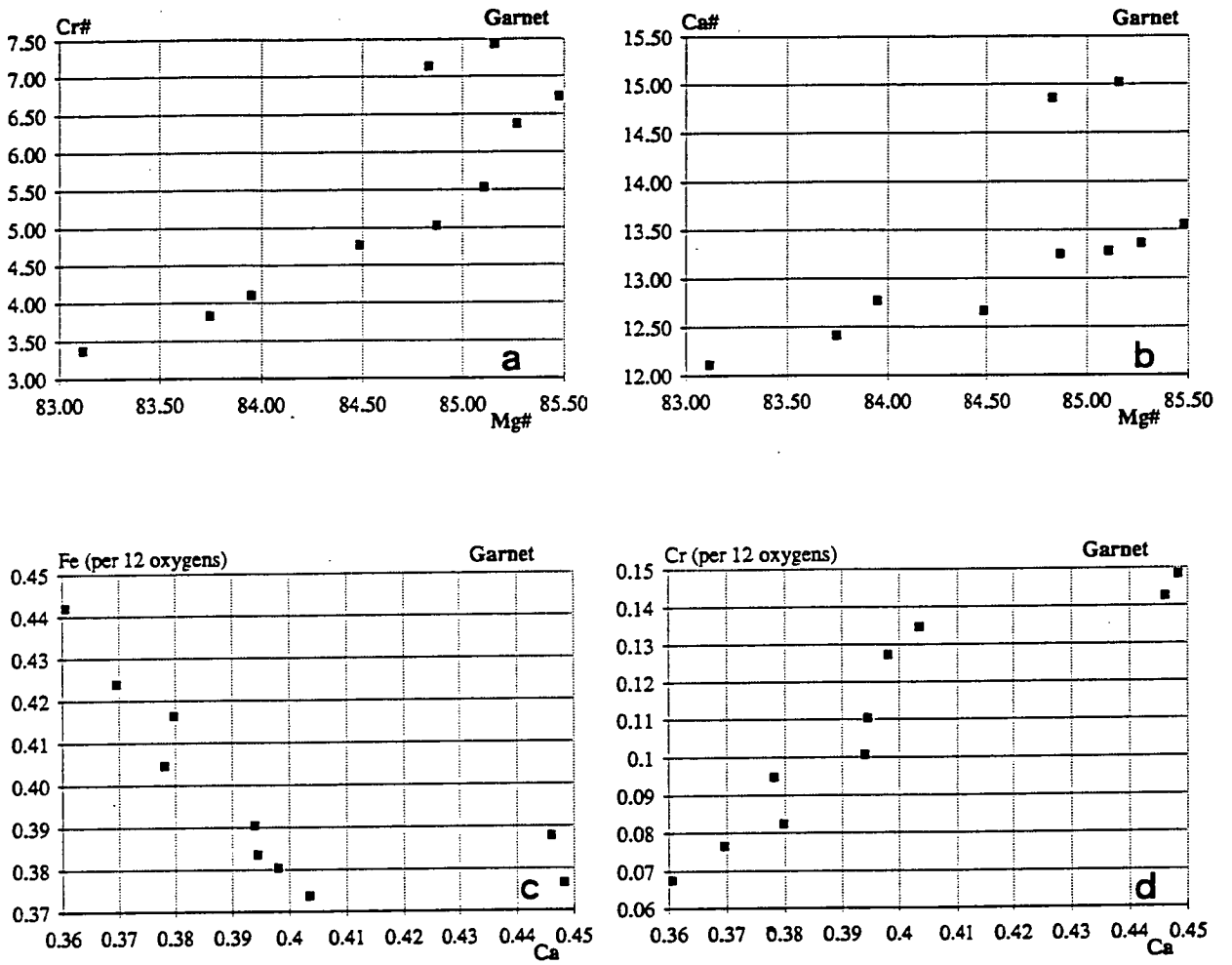

Figure 1.5. (a) Mg# - Cr# correlation in garnet

(b) Mg# - Ca# correlation in garnet

(c) negative correlation of Cr - Fe in garnet (cations per 12 oxygens)

(d) positive correlation of Cr - Ca in garnet (cations per 12 oxygens).

Table 1.6 Representative Spinel Compositions in the Ming-xi Lherzolites

Sample#	76212*	76225*	76210	76211	76212	76213	76217	76218	76221	76224	76225	76209	76214	76215	76216	76219	76220	76223	76226	76227	76228
Rock Type	GSL	GSL	GSL	GSL	GSL	GSL	GSL	GSL	GSL	GSL	GSL	Phl-SL	SL	SL	SL	SL	SL	SL	SL	SL	SL
	primary		secondary							secondary											
TiO2	0.17		0.24	0.29	0.19	0.22	0.26	0.31	0.22	0.27	0.1997	0.27	0.38		0.47		0.20	0.24	0.20	0.19	0.37
Al2O3	44.92	44.63	49.98	50.13	47.99	48.95	50.51	49.50	48.93	49.17	47.478	47.61	55.04	43.62	17.48	36.48	29.57	24.74	56.87	35.42	38.46
Cr2O3	23.21	23.64	17.86	17.16	20.22	18.62	16.53	18.20	19.07	19.04	20.332	20.52	11.98	25.35	49.49	32.76	39.31	43.64	11.04	32.17	29.12
FeO	12.20	12.16	11.41	11.95	11.50	11.49	12.37	11.24	10.87	10.69	11.762	11.63	11.47	11.42	16.98	11.81	13.60	15.21	10.50	13.87	12.66
NiO	0.35	0.46	0.37	0.38	0.37	0.40	0.42	0.44	0.40	0.38	0.3944	0.37	0.36	0.34		0.34			0.34	0.37	0.36
MgO	19.14	19.10	20.14	20.09	20.09	20.32	19.91	20.30	20.51	20.46	20.099	19.60	20.77	19.28	15.58	18.61	17.32	16.18	21.04	17.99	19.02
Sum	100	100	100	100	100	100	100	100	100	100	100	100	100	100	100	100	100	100	100	100	100
TiO2	0.17		0.24	0.29	0.19	0.22	0.26	0.31	0.22	0.27	0.20	0.27	0.38		0.47		0.20	0.24	0.20	0.19	0.37
Al2O3	44.80	44.50	49.85	49.98	47.85	48.79	50.34	49.36	48.79	49.05	47.31	47.50	54.89	43.51	17.37	36.37	29.47	24.64	56.76	35.27	38.31
Cr2O3	23.15	23.57	17.81	17.11	20.16	18.56	16.48	18.15	19.01	18.99	20.26	20.47	11.95	25.29	49.19	32.66	39.17	43.46	11.02	32.03	29.00
Fe2O3	2.75	2.98	2.64	3.08	2.97	3.25	3.24	2.81	2.91	2.50	3.44	2.35	2.74	2.51	6.03	3.04	3.47	4.10	2.00	4.27	3.96
FeO	9.70	9.45	9.00	9.14	8.79	8.53	9.41	8.69	8.22	8.41	8.63	9.49	8.96	9.13	11.44	9.03	10.43	11.45	8.68	9.97	9.04
NiO	0.35	0.46	0.37	0.38	0.37	0.40	0.42	0.44	0.40	0.38	0.39	0.37	0.36	0.34		0.34	0.00	0.00	0.34	0.37	0.36
MgO	19.09	19.05	20.09	20.03	20.03	20.25	19.84	20.24	20.45	20.41	20.03	19.55	20.71	19.23	15.49	18.55	17.26	16.11	21.00	17.91	18.94
Sum	100	100	100	100	100	100	100	100	100	100	100	100	100	100	100	100	100	100	99.99	100.01	100
Oxygen	4	4	4	4	4	4	4	4	4	4	4	4	4	4	4	4	4	4	4	4	4
Ti	0.004		0.005	0.006	0.004	0.004	0.005	0.006	0.004	0.005	0.004	0.006	0.007		0.011		0.005	0.005	0.004	0.004	0.008
Al	1.438	1.431	1.563	1.567	1.511	1.534	1.578	1.549	1.532	1.539	1.498	1.506	1.685	1.402	0.634	1.208	1.012	0.869	1.728	1.181	1.261
Cr	0.499	0.508	0.375	0.360	0.427	0.392	0.347	0.382	0.401	0.400	0.430	0.435	0.246	0.547	1.204	0.728	0.903	1.028	0.225	0.720	0.640
Fe3+	0.056	0.061	0.053	0.062	0.060	0.065	0.065	0.056	0.058	0.050	0.070	0.048	0.054	0.052	0.141	0.065	0.076	0.092	0.039	0.091	0.083
Fe2+	0.221	0.215	0.200	0.203	0.197	0.190	0.209	0.193	0.183	0.187	0.194	0.213	0.195	0.209	0.296	0.213	0.254	0.287	0.188	0.237	0.211
Ni	0.008	0.010	0.008	0.008	0.008	0.009	0.009	0.009	0.009	0.008	0.008	0.008	0.008	0.008		0.008			0.007	0.008	0.008
Mg	0.775	0.775	0.797	0.794	0.800	0.806	0.787	0.804	0.813	0.810	0.802	0.784	0.805	0.784	0.715	0.780	0.750	0.719	0.809	0.759	0.789
Sum	3	3	3	3	3	3	3	3	3	3	3	3	3	3	3	3	3	3	3	3	3
Mg#	77.82	78.24	79.92	79.62	80.23	80.89	78.99	80.61	81.60	81.23	80.54	78.60	80.46	78.97	70.70	78.55	74.68	71.49	81.17	76.22	78.88
Cr#	25.01	25.42	19.34	18.68	21.38	20.33	18.00	19.79	20.73	20.62	21.54	22.43	12.74	28.05	65.52	37.59	47.14	54.19	11.53	37.86	33.69
Fe3:Fe2	0.26	0.28	0.26	0.30	0.31	0.34	0.31	0.29	0.32	0.27	0.36	0.22	0.28	0.25	0.47	0.30	0.30	0.32	0.21	0.39	0.39

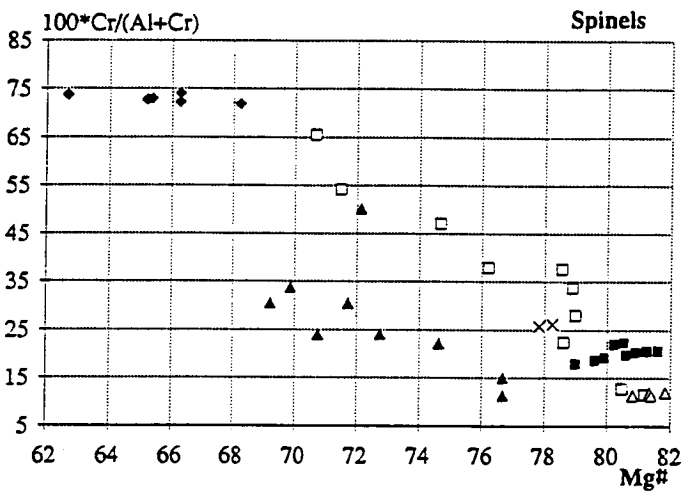

Figure 1.6. Mg# - Cr# correlation in spinels (open squares: spinels in Ming-xi xenoliths without garnet; solid squares: secondary spinels in Ming-xi xenoliths with garnet; crosses: primary spinels in Ming-xi xenoliths with garnet; open triangles: spinels in French spinel + garnet lherzolites reported by Berger, 1979 and Berger & Vannier, 1984; Solid triangles: spinels in Malaita spinel + garnet lherzolites presented by Neal, 1988; solid diamonds: spinels in Lesotho spinel + garnet lherzolites given by Nixon & Boyd, 1973).

Mg# versus Cr# plot defined by spinels in samples without garnet (Fig.1.6). The spinels coexisting with garnet in xenoliths from Massif Central of France (Berger, 1979; Berger & Vennier, 1984) show a positive correlation trend between Mg# and Cr#, and are therefore probably also decomposition product of garnet (Fig.1.6). On the other hand, spinels in the spinel + garnet lherzolite xenoliths from Malaita, Solomon Islands (Neal, 1988) and Lesotho, southern Africa (Nixon & Boyd, 1973) display negative correlation between Mg# and Cr# (Fig.1.6). They are most likely primary, in chemical equilibrium with the coexisting silicate minerals.

Phlogopite: Phlogopite is only found in one sample (76209). Several flakes occur in a vein-like schlieren, parallel to the tabular texture of the rock (Plate 1a). The concentration of these flakes made polishing difficult and some have been removed during polishing, but their composition is homogeneous and comparable to phlogopite in a garnet + spinel lherzolite from the same locality reported by Cao & Zhu (1987). Both are rich in TiO_2 and Cr_2O_3 (Table 1.7) and therefore are probably of secondary origin according to the classification of Carswell (1975) and Dawson & Smith (1975). Its presence connotes a small scale, late stage modal metasomatism.

1.4.2 Relationships between mineral chemistry and whole-rock chemistry

The mineral compositions are apparently related to the whole-rock compositions. In chapter two, whole-rock compositions of eight representative samples are reported. They are related to respective mineral compositions in Figs.1.7a & b, which clearly show that the Cr# of all minerals and the Mg# of all but spinel are positively correlated with the whole-rock Cr# and Mg# (definitions of whole-rock Mg# and Cr# are the same as those of the minerals', i.e. atomic proportions). Due to the negative correlation of whole-rock MgO and Al_2O_3 (Chapter Two; Maaløe & Aoki, 1977), and the positive correlation of Mg and Al in spinels, and due to the low abundance of spinels with high-Al concentration, the whole rock Mg# is negatively correlated with the Mg# of spinels. These correlation trends and the composition variation trends shown by individual minerals (above discussion) and the whole-rocks (Chapter Two) are consistent with a continuous depletion of basaltic components (mainly Al, Ca, Ti, and Na) from the sample with the lowest Mg# and Cr# to the samples with higher Mg# and Cr#. Thus they all consistently depict a partial melting trend. This topic is addressed in more detail in the next chapter.

Table 1.7 Comparison of Phlogopite Compositions

Sample #	76209	MD10/10	megacryst	primary	secondary
No. analyses	[4]		[9]	[5]	[5]
Reference	this study	(1)	(2)	(3)	(4)
SiO2	39.04	38.84	41.30	41.30	39.30
TiO2	4.58	5.64	1.06	0.32	1.11
Al2O3	17.24	16.29	12.01	12.60	14.90
Cr2O3	1.66	1.29	0.30	0.70	1.51
FeO	4.17	4.78	4.90	2.77	3.06
MnO		0.01	0.01	0.02	0.07
NiO	0.38		0.11		
MgO	20.73	20.02	24.30	26.80	24.90
Na2O	0.60	0.41	0.16	0.74	1.22
K2O	9.26	9.70	10.40	9.35	8.37
Cl	0.24				
Sum	97.89	96.98	94.55	94.60	94.44
Oxygen	22	22	22	22	22
Si	5.4091	5.4451	5.9389	5.8561	5.5903
Ti	0.4767	0.5946	0.1146	0.0341	0.1187
Al	2.8148	2.6916	2.0354	2.1057	2.4979
Cr	0.1818	0.1430	0.0341	0.0785	0.1698
Fe	0.4826	0.5604	0.5893	0.3285	0.3640
Mn		0.0012	0.0012	0.0024	0.0084
Ni	0.0423		0.0127		
Mg	4.2818	4.1841	5.2092	5.6651	5.2802
Na	0.1598	0.1114	0.0446	0.2034	0.3365
K	1.6372	1.7348	1.9079	1.6913	1.5189
Cl	0.0564				
Sum	15.4862	15.4662	15.8879	15.9651	15.8848
Mg#	89.87	88.19	89.84	94.52	93.55
Cr#	6.07	5.04	1.65	3.59	6.37
K#	91.11	93.96	97.72	89.26	81.86

(1). Cao & Zhu (1987); (2), (3), (4). Dawson & Smith (1975);
(1). in a garnet + spinel lherzolite from Ming-xi;
(2). megacrysts from South African kimberlites;
(3) & (4). in garnet lherzolites of South African kimberlites.

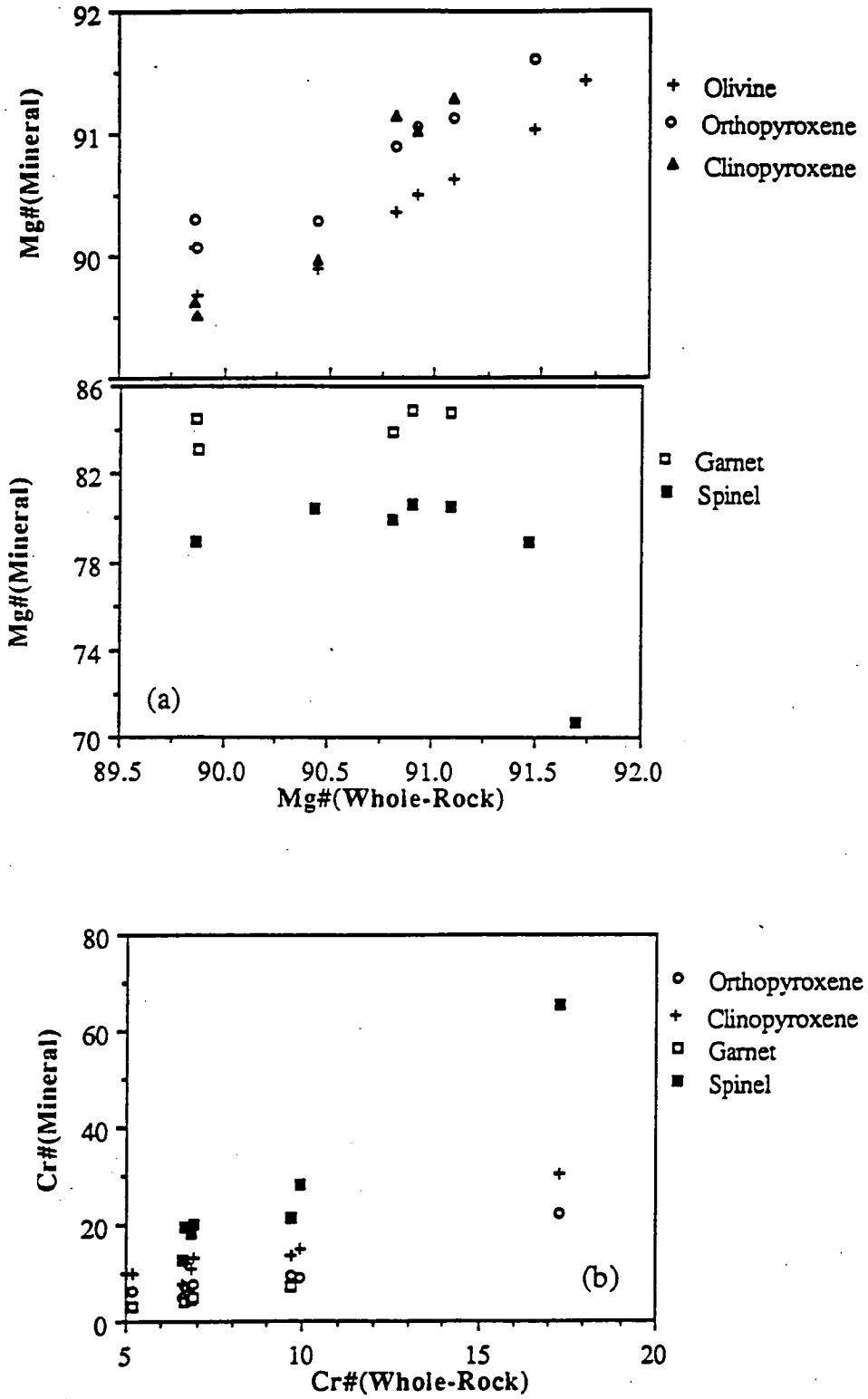

Figure 1.7. correlation of mineral composition with whole-rock composition:

(a) Mg# of whole - rock versus Mg# of minerals

(b) Cr# of whole - rock versus Cr# of minerals

1.4.3 Element partitioning between minerals, and the equilibration conditions of the xenoliths

An extensive literature search of coexisting olivine and orthopyroxene compositions in peridotites from different thermal and tectonic environments suggests that the Fe^{2+}/Mg partitioning between olivine and orthopyroxene is overwhelmingly composition dependent and insensitive to pressure and temperature (Fig.1.8). A linear regression analysis of 247 pairs of coexisting olivine and orthopyroxene (122 pairs in xenoliths enclosed in alkali-basalts including those from Ming-xi, 125 pairs in xenoliths included in kimberlites, data sources are listed in Table 1.8) produces the following empirical relation ($K_d=\frac{(Fe^{2+}/Mg)^{Opx}}{(Fe^{2+}/Mg)^{Ol}}$):

$$Mg\#(ol) = \frac{100}{1.007+1.034(Fe^{2+}/Mg)^{opx}}; \quad \text{or} \quad \ln K_d^{Opx/Ol} = -0.11\ (\pm 0.06)\ .$$

This relation can be useful for prediction of Mg# of olivine from coexisting orthopyroxene when the olivine is difficult to analyse (or vice versa). Similarly, Mg#s of olivine and clinopyroxene, orthopyroxene and clinopyroxene are also closely correlated with each other. Variations in their partition coefficients (K_ds) are small and show slight but insignificant (in the composition range of interest) temperature dependency.

Previous experimental studies (e.g. O'Neill & Wood, 1979; Harley, 1984; Råheim & Green, 1974a) have established that the partitioning of Fe^{2+}/Mg between olivine and garnet, between orthopyroxene and garnet, and between clinopyroxene and garnet are sensitive to temperature. The partition coefficents for all the garnet-bearing samples are very similar, suggesting that these xenoliths were equilibrated under very similar temperatures. Estimation of the equilibration temperature by using the thermometers formulated by Kawasaki (1979), Carswell & Harley (1989) and in Chapter Six produces the following results (details in Table 1.9):

$$Kd_{Fe^{2+}\text{-}Mg}^{Gt\text{-}Ol} = 1.73\ (\pm 0.04); \quad T = 1150° \pm 50°C$$

$$Kd_{Fe^{2+}\text{-}Mg}^{Gt\text{-}Opx} = 1.82\ (\pm 0.06); \quad T = 1150° \pm 50°C$$

$$Kd_{Fe^{2+}\text{-}Mg}^{Gt\text{-}Cpx} = 1.79\ (\pm 0.04); \quad T = 1050° \pm 50°C.$$

Fe^{2+}/Mg partitioning between olivine and spinel is known to be temperature-dependent (e.g. Fabries, 1977; Engi, 1983). Its strong composition dependence (particularly on Cr/Cr+Al of spinel, Fig.1.9a) makes the thermometer based on this partitioning relation less reliable. The three calibrations by Fabries (1977), O'Neill & Wall (1987), and Ballhaus et al. (1991) yield slightly different equilibrium temperatures (Table 1.9), mostly ranging from 1000° to 1100°C, with an average of 1050°C. The Fe^{2+}/Mg partitioning between garnet and spinel, and between pyroxenes and spinel all show a strong control exerted by the Cr/Cr+Al of spinel (Figs.1.9b, c & d).

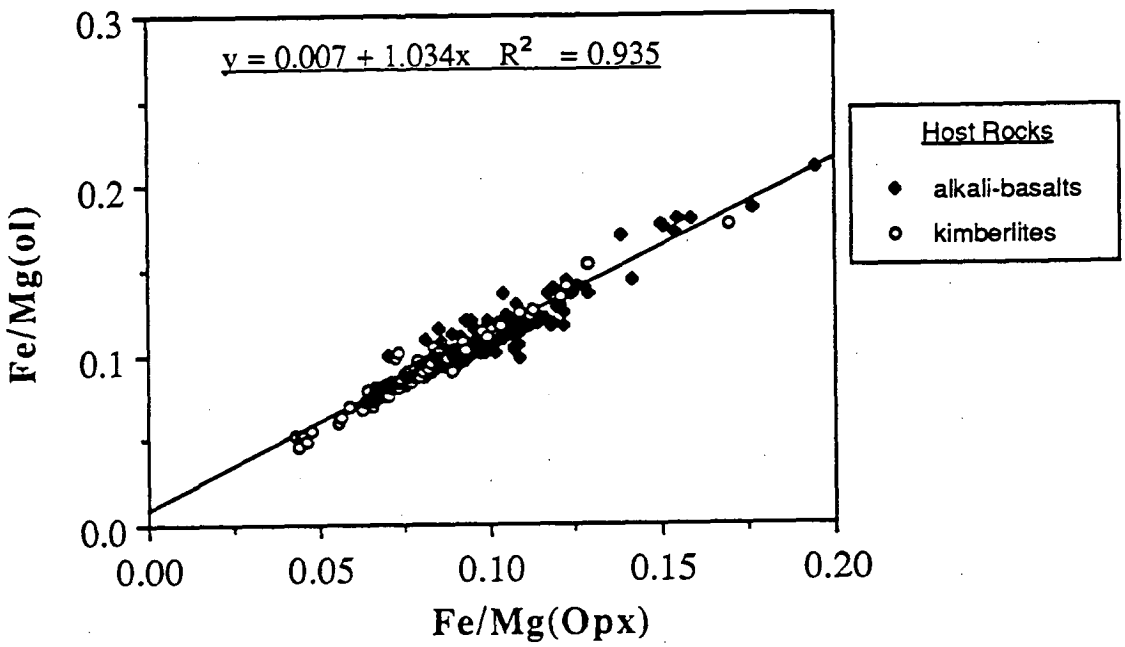

Figure 1.8. Fe^{2+}/Mg partitioning between olivine and orthopyroxene in ultramafic xenoliths

Table 1.8 Data Sources for Fe2+/Mg Partitioning between Olivine and Orthopyroxene

xenoliths in alkali-basalts	xenoliths in kimberlites
1 Frey & Prinz (1978)	15 Nixon & Boyd (1973)
2 Galer & O'Nions (1989)	16 Danchin & Boyd (1976)
3 Francis (1987)	17 Shee et al. (1982)
4 Chen et al. (1989)	18 Mori (1976)
5 Stolz & Davies (1988)	19 Mitchell (1984)
6 Preß et al. (1986)	20 MacGregor (1979)
7 Berger (1979)	21 Carswell et al. (1979)
8 Berger & Vennier (1984)	22 Cox et al. (1987)
9 Ferguson et al. (1977)	23 Boyd & Mertzman (1987)
10 Ferguson & Sheraton (1979)	
11 Sutherland et al. (1984)	
12 Skewes & Stern (1979)	
13 Liang & Elthon (1990)	
14 this study	

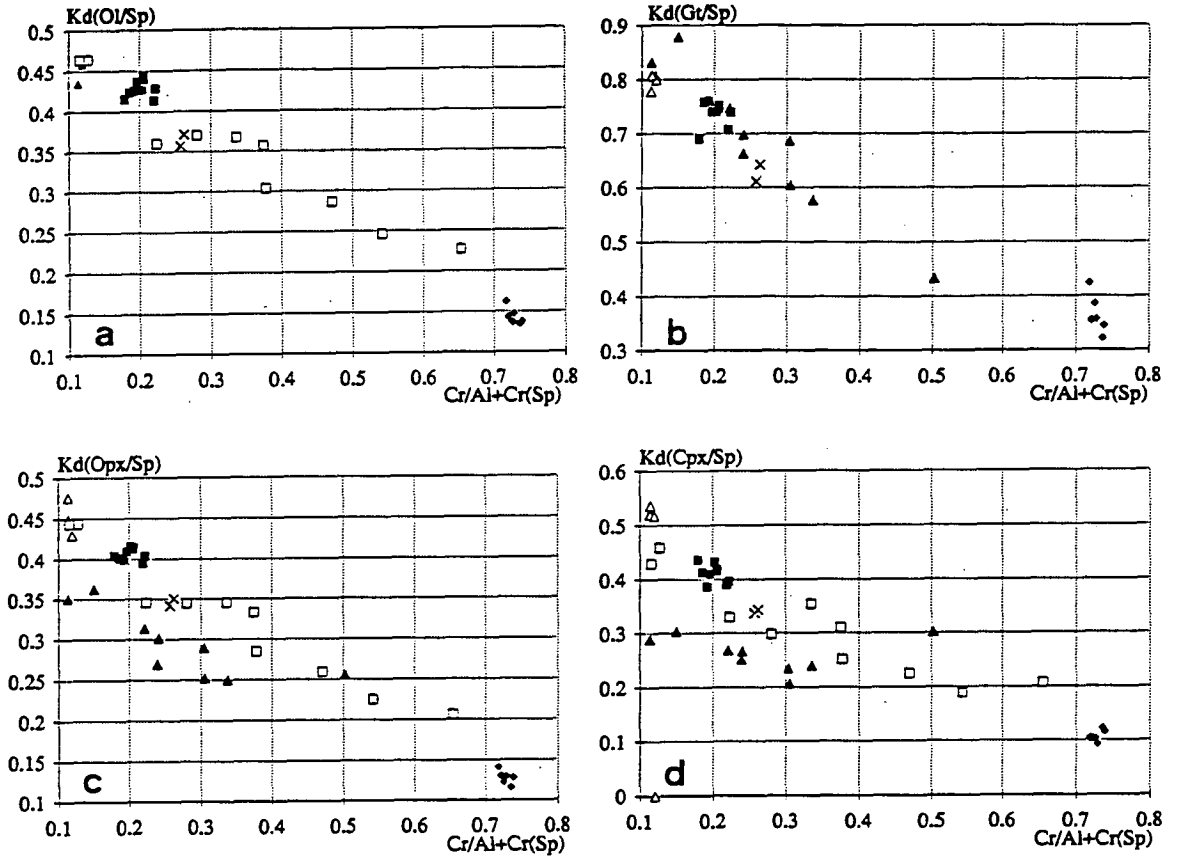

Figure 1.9. strong correlation between Cr/Cr+Al (spinels) and

(a) the olivine - spinel Fe^{2+}/Mg partitioning K_d;

(b) the garnet - spinel Fe^{2+}/Mg partitioning K_d

(c) the orthopyroxene - spinel Fe^{2+}/Mg partitioning K_d

(d) the clinopyroxene - spinel Fe^{2+}/Mg partitioning K_d (symbols as for Figure 1.6).

The mutual solubilities of diopside and enstatite components in orthopyroxene and clinopyroxene have long been recognised as useful temperature indicators (e.g. Davis & Boyd, 1966; Wood & Banno, 1973; Akella, 1974; Mori & Green, 1975). Applying the thermometers developed by Wells (1977), Kretz (1982), Bertrand & Mercier (1985), and Brey & Köhler (1990), a consistent equilibrium temperature of 1100° ± 50°C for all the samples (both garnet-free and garnet-bearing) is obtained (Table 1.9). This temperature is in broad agreement with the temperatures calculated from the Fe^{2+}/Mg partitioning relations between olivine and garnet, between orthopyroxene and garnet, between clinopyroxene and garnet, and between olivine and spinel.

The Al_2O_3-solubility in orthopyroxene coexisting with spinel is known to be temperature-sensitive. The calibrations of Webb & Wood (1986) and Witt-Eickschen & Seck (1991) give similar temperatures at 1000° - 1050°C. The garnet-bearing samples record slightly higher temperature than the garnet-free samples according to the two thermometers (Table 1.9).

Equilibration pressure estimates for garnet-bearing xenoliths are lower (20.5 ± 0.5 kbar) by the Nickel & Green (1985) method than by the Nickel (1989) method (25 - 30 kbar). The former is based on the Al_2O_3-solubility in orthopyroxene coexisting with garnet and the latter is based on Cr-partitioning between orthopyroxene and garnet. The spinel lherzolite to garnet lherzolite transition barometer derived in Chapter Four generates a pressure of 27 (± 1) kbar. The MC74 barometer formulated by Finnerty & Boyd (1984) based on the experimental data of Al_2O_3 solubility in orthopyroxene of MacGregor (1974) consistently produces pressures higher than the Nickel & Green (1985) barometer but lower than the transition barometer from Chapter Four (Table 1.9). These inconsistencies remain a problem for future investigation. Because of the wide application of the Nickel & Green (1985) barometer, the pressure estimate obtained from this barometer is chosen for temperature and oxygen fugacity calculation whenever necessary. The temperatures necessary for all the pressure calculations are derived from the Wells (1977) thermometer. A summary of the calculation results is given in Table 1.9.

Ballhaus et al. (1991) have experimentally calibrated an empirical oxygen barometer to estimate mantle oxygen fugacity from the spinel-orthopyroxene-olivine paragenesis. This oxygen barometer yields consistently - 0.5 (± 0.5) log units relative to the FMQ buffer for both the garnet-free and garnet-bearing samples, in agreement with the results from the Wood et al. (1990) calibration, but is one log unit higher than the estimate by the O'Neill & Wall (1987) method (Table 1.9).

Table 1.9 The Estimated Equilibrium Conditions of the Ming-xi Lherzolites

Sample #	76210	76211	76212	76213	76217	76218	76221	76222	76224	76225	76209	76214	76215	76216	76219	76220	76223	76226	76227	76228
P(kbar)	19.26	19.59	20.76	20.61	20.14	20.33	20.57	19.57	20.95	21.30	20.50	20.50	20.50	20.50	20.50	20.50	20.50	20.50	20.50	20.50
T°C	1044	1035	1114	1104	1101	1085	1096	1037	1091	1110	1052	1033	1066	1173	1155	1103	1128	1020	1043	1099
P(kbar)																				
Nickel(1989)	25.79	25.18	29.61	26.96	26.44	27.06	29.64	25.06	28.12	29.23										
BK90	17.41	17.85	18.75	18.85	18.43	18.50	18.71	17.89	19.13	19.29										
NG85	19.26	19.59	20.76	20.61	20.14	20.33	20.57	19.57	20.95	21.30										
MC74	23.19	22.64	25.71	24.99	23.82	24.64	25.09	22.64	24.48	26.10										
Chapter Four	25.96	25.79	27.63	26.78	25.53	26.62	27.64		27.47	27.71										
T(°C)																				
BM85	1056	1047	1127	1132	1134	1108	1126	1053	1124	1122										
BK90	1112	1114	1160	1177	1184	1155	1167	1125	1169	1157	1098	1117	1081	1214	1183	1124	1142	1087	1058	1174
Wells(1977)	1044	1035	1114	1104	1101	1085	1096	1037	1091	1110	1052	1033	1066	1173	1155	1103	1128	1020	1043	1099
Kretz(1982)>	1045	1044	1087	1103	1117	1079	1090	1057	1094	1080	1019	1034	1017	1175	1115	1067	1078	1011	1018	1113
<1080	1021	1019	1125	1170	1207	1106	1135	1050	1144	1108	962	995	956	1381	1202	1076	1103	943	959	1196
Chapter Six	962	1021	1078	1106	1173	1050	1053	1073	1070	1056										
CH89	1110	1119	1187	1183	1217	1164	1165	1140	1170	1169										
OW79	1166	1160	1294	1239	1296	1274	1268	1180	1299	1275										
K79	1075	1069	1189	1133	1168	1157	1154	1084	1177	1177										
Fabries(1979)	1014	1016	1032	1046	998	1046	1064		1060	1076	925	1010	1004	1090	1079	1037	1023	969	1013	1088
OW87	943	940	972	978	918	982	1003		1006	1015	869	920	960	1134	1073	1048	1039	878	984	1069
BBG91	1040	1038	1063	1075	1015	1081	1102		1105	1108	952	1036	1034	1143	1129	1083	1061	998	1036	1134
WW86	1009	986	1057	1059	1075	1029	1037		1023	1033	982	988	958	863	1002	919	854	1016	923	1027
WS91-1	1011	994	1059	1057	1068	1027	1033		1018	1041	1001	969	987	1003	1037	985	942	980	997	1069
WS91-2	1024	1014	1105	1091	1074	1055	1070	995	1086	1095	1016	980	1011	1021	1112	1038	1004	985	1012	1100
Δlog(fo2)																				
OW87	-1.46	-1.24	-1.46	-1.28	-1.26	-1.45	-1.40		-1.70	-1.27	-1.67	-1.33	-1.77	-0.88	-1.79	-1.64	-1.49	-1.71	-1.04	-1.22
WBJ90	-0.62	-0.42	-0.55	-0.44	-0.41	-0.61	-0.56		-0.84	-0.38	-0.74	-0.57	-0.75	0.57	-0.66	-0.34	-0.07	-0.95	0.05	-0.22
BBG91	-0.86	-0.64	-0.75	-0.62	-0.60	-0.82	-0.76		-1.04	-0.55	-0.98	-0.83	-0.99	0.45	-0.82	-0.53	-0.26	-1.26	-0.11	-0.35

abbreviations: BK90 - Brey & Köhler (1990); NG85 - Nickel & Green (1985); MC74 - Finnerty & Boyd (1984); BM85 - Bertrand & Mercier (1985); CH89 - Carswell & Harley (1989); OW79 - O'Neill & Wood (1979); K79 - Kawasaki (1979); OW87 - O'Neill & Wall (1987); BBG91 - Ballhaus et al. (1991); WW86 - Webb & Wood (1986); WS91 - Witt-Eickschen & Seck (1991); WBJ - Wood et al. (1990).

1.5 The Kelyphite Rims around Garnet

Instability of garnet in xenoliths enclosed in kimberlites and alkali basalts is well documented. It is variously explained as a result of several processes, including (1) heating by the host magma (Padovani & Carter, 1973); (2) decompression (Reid & Dawson, 1972); (3) interaction with fluids released from the host magma (Nixon et al., 1963; Exley et al., 1982); (4) incongruent melting of garnet fluxed by volatiles (Hunter & Taylor, 1982); or a combination of these processes. In the Ming-xi samples all the garnet grains developed a kelyphite rim, where secondary spinel and pyroxenes can be found. These spinels are confined within the kelyphite rims and have the lowest Cr# and highest Mg# among all the spinels in the garent-bearing samples (Table 1.10). Their secondary origin is self-evident.

Pyroxenes in the kelyphite rims are like those reported in the literature (e.g. Reid & Dawson, 1972; Lock & Dawson, 1980). Compared with primary pyroxenes, they have characteristically high Al_2O_3, high MnO and low Mg#. There is much less clinopyroxene present in the rims than orthopyroxene. Clinopyroxene has undetectable amounts of Na_2O, and orthopyroxene usually has very high CaO content. Their compositions always show wide variation (Table 1.11). Temperatures of 1085° - 1350°C are obtained when the two-pyroxene thermometers are applied to a few selected Opx - Cpx pairs (Table 1.11). These temperatures may indicate the arrested reaction temperatures, assuming that the selected pyroxene pairs are locally in mutual equilibrium.

Apart from secondary spinels and pyroxenes in the kelyphite rims of garnet, alkali-rich glasses have also been found. There are two types of glasses: K-rich and Na-rich. Their compositions are very similar to feldspar composition, except that the weight total is sometimes much less than 100% (Table 1.12). Similar glasses in xenoliths in the Fayette county kimberlite, Pennsylvania, were interpreted by Hunter & Taylor (1982) to be the result of incongruent melting of garnet, promoted by the metasomatic fluxing of alkalis and volatiles. Occurrence of glasses in Ming-xi samples is not restricted to garnet-bearing samples. In sample 76220 (a spinel lherzolite), glass compositionally similar to that in 76217 is also found. It may have been associated with garnet before and the garnet has been reacted out (but there is no petrographic evidence for the expected kelyphite); alternatively, the glass may be the product of interaction between fluxing fluids from the host magma and the xenoliths (not necessarily garnet). In either case it suggests experience of a late stage invasive metasomatism. The compositions of both types of glass are very similar to feldspar microlite compositions in the host basalts (Table 1.12); these are presumably devitrification product of residual melt from the cooling and crystallizing basalts. This similarity suggests that the likely fluid source is the host basalts.

Table 1.10 Composition Range of the Secondary Spinels within the Kelyphite Rims of Garnet

Sample #	76210		76211		76212		76213		76217		76218		76221		76224		76225	
SiO2							0.18	0.24					0.11	0.24			0.13	0.71
TiO2			0.26				0.11				0.30	0.30	0.22	0.05	0.57	0.46		
Al2O3	63.54	63.38	62.90	65.64	58.53	57.89	60.13	61.10	62.09	65.83	59.79	63.59	58.86	60.46	58.20	58.63	60.40	56.64
Cr2O3	5.31	5.63	6.13	5.70	10.19	11.13	6.52	6.04	4.52	4.60	7.09	5.62	7.99	8.05	8.04	8.15	6.92	10.09
FeO	11.72	9.88	9.47	10.26	10.81	10.95	10.46	10.46	10.56	11.48	10.16	9.89	10.45	9.87	12.23	11.67	10.30	12.38
MnO							0.17										0.20	0.32
NiO							0.23						0.14				0.26	
MgO	20.62	21.32	22.44	21.79	22.00	21.60	20.53	20.02	22.97	21.56	21.53	22.53	21.98	20.60	21.02	21.47	21.05	18.73
Sum	101.19	100.21	101.20	103.39	101.53	101.57	98.14	97.62	100.14	103.47	98.87	101.93	99.64	99.03	100.06	100.38	99.14	98.16
TiO2			0.26				0.11				0.30	0.30	0.22	0.05	0.57	0.46		
Al2O3	63.54	63.38	62.90	65.64	58.53	57.89	60.13	61.10	62.09	65.83	59.79	63.59	58.86	60.46	58.20	58.63	60.40	56.64
Cr2O3	5.31	5.63	6.13	5.70	10.19	11.13	6.52	6.04	4.52	4.60	7.09	5.62	7.99	8.05	8.04	8.15	6.92	10.09
Fe2O3	0.88	0.42	1.32	0.12	2.94	2.52	1.33	0.17	4.16	1.00	1.87	1.52	3.05	0.07	2.86	2.93	1.82	1.05
FeO	10.92	9.50	8.28	10.16	8.17	8.68	9.26	10.30	6.81	10.58	8.48	8.53	7.70	9.81	9.65	9.04	8.67	11.44
MnO							0.17										0.20	0.32
NiO							0.23						0.14				0.26	
MgO	20.62	21.32	22.44	21.79	22.00	21.60	20.53	20.02	22.97	21.56	21.53	22.53	21.98	20.60	21.02	21.47	21.05	18.73
Sum	101.28	100.25	101.33	103.40	101.82	101.82	98.27	97.64	100.56	103.57	99.06	102.08	99.95	99.04	100.35	100.67	99.32	98.27
Oxygen	4	4	4	4	4	4	4	4	4	4	4	4	4	4	4	4	4	4
Ti			0.0049				0.0022				0.0058	0.0056	0.0042	0.0010	0.0110	0.0088		
Al	1.8780	1.8801	1.8449	1.8879	1.7409	1.7290	1.8362	1.8725	1.8321	1.8929	1.8085	1.8509	1.7716	1.8330	1.7597	1.7619	1.8246	1.7679
Cr	0.1053	0.1120	0.1206	0.1100	0.2033	0.2230	0.1335	0.1242	0.0895	0.0887	0.1439	0.1097	0.1613	0.1637	0.1631	0.1643	0.1403	0.2112
Fe3+	0.0167	0.0079	0.0248	0.0021	0.0558	0.0481	0.0259	0.0034	0.0784	0.0184	0.0360	0.0282	0.0586	0.0013	0.0553	0.0561	0.0351	0.0209
Fe2+	0.2291	0.2001	0.1723	0.2073	0.1723	0.1840	0.2007	0.2241	0.1427	0.2158	0.1820	0.1761	0.1645	0.2110	0.2071	0.1927	0.1858	0.2533
Mn							0.0037										0.0044	0.0072
Ni							0.0047						0.0029				0.0054	
Mg	0.7709	0.7999	0.8325	0.7927	0.8277	0.8160	0.7931	0.7759	0.8573	0.7842	0.8237	0.8295	0.8368	0.7900	0.8039	0.8161	0.8044	0.7395
Sum	3	3	3	3	3	3	3	3	3	3	3	3	3	3	3	3	3	3
Mg#	77.09	79.99	82.85	79.27	82.77	81.60	79.80	77.59	85.73	78.42	81.90	82.49	83.57	78.92	79.51	80.90	81.24	74.49
Cr#	5.31	5.62	6.06	5.50	10.17	11.15	6.69	6.21	4.48	4.44	7.24	5.52	8.35	8.20	8.48	8.53	7.14	10.67
Fe3:Fe2	0.07	0.04	0.14	0.01	0.32	0.26	0.13	0.02	0.55	0.09	0.20	0.16	0.36	0.01	0.27	0.29	0.19	0.08

Table 1.11 Representative Compositions of the Secondary Pyroxenes in the Kelyphite Rims of Garnet

Sample #	76210		76213-1		76213-2		76221		76224-1		76224-2		76225	
	Opx	Cpx	Opx	Cpx	Opx	Cpx	Opx	Cpx	Opx	Cpx	Opx	Cpx	Opx	Cpx
SiO2	52.56	46.86	51.39	52.29	52.29	51.02	50.67	51.90	51.53	51.43	49.52	46.97	47.14	46.02
TiO2		0.21	0.12	0.26		0.44	0.23	0.36	0.45	0.66	0.20	1.18		0.17
Al2O3	7.24	14.87	8.66	6.32	8.09	9.16	9.84	7.10	8.36	6.70	11.12	11.12	15.15	13.14
Cr2O3	0.37	1.15	1.11	1.22	1.68	0.51	1.27	0.77	0.66	0.84	1.66	2.17	2.23	2.14
FeO	7.76	4.05	7.34	2.85	6.93	4.00	6.85	4.22	6.91	4.42	6.83	4.32	6.67	4.46
MnO	0.31	0.24	0.37		0.32		0.35	0.28				0.29	0.24	0.39
MgO	28.97	13.48	29.52	16.11	29.34	17.70	27.74	17.33	29.32	17.59	28.55	15.24	26.61	15.41
CaO	1.57	20.22	2.03	19.10	1.96	16.05	2.55	16.85	1.41	15.90	1.26	17.05	1.75	18.62
Na2O				1.16				1.17		0.98		0.76		
Sum	98.78	101.08	100.56	99.31	100.62	100.03	99.50	99.98	98.64	98.52	99.14	99.10	99.78	100.36
Oxygen	6	6	6	6	6	6	6	6	6	6	6	6	6	6
Si	1.8553	1.6832	1.7900	1.8948	1.8158	1.8271	1.7811	1.8693	1.8155	1.8748	1.7417	1.7234	1.6537	1.6730
Ti		0.0057	0.0033	0.0071		0.0117	0.0062	0.0098	0.0119	0.0181	0.0053	0.0326		0.0047
Al	0.3012	0.6295	0.3557	0.2699	0.3311	0.3866	0.4076	0.3014	0.3471	0.2878	0.4610	0.4809	0.6265	0.5628
Cr	0.0103	0.0327	0.0306	0.0350	0.0462	0.0143	0.0353	0.0218	0.0184	0.0242	0.0462	0.0629	0.0617	0.0616
Fe	0.2291	0.1217	0.2139	0.0864	0.2011	0.1199	0.2014	0.1272	0.2036	0.1347	0.2009	0.1326	0.1956	0.1356
Mn	0.0093	0.0073	0.0111		0.0094		0.0104	0.0084				0.0090	0.0071	0.0121
Mg	1.5244	0.7218	1.5332	0.8703	1.5189	0.9448	1.4535	0.9305	1.5400	0.9559	1.4970	0.8336	1.3918	0.8350
Ca	0.0594	0.7782	0.0758	0.7415	0.0731	0.6157	0.0959	0.6502	0.0532	0.6210	0.0475	0.6703	0.0658	0.7251
Na				0.0815				0.0814		0.0693		0.0541		
Sum	3.9890	3.9800	4.0135	3.9864	3.9956	4.0010	3.9913	4.0000	3.9898	3.9858	3.9994	3.9992	4.0022	4.0101
T°C														
BM85		1126		1141		1349		1267		1287		1228		1212
BK90		1172		1141		1304		1251		1274		1245		1232
Wells(1977)		1085		1132		1353		1238		1262		1188		1223

Table 1.12 Compositions of the Alkali-rich Glasses Associated with the Kelyphite Rims of Garnet and the Feldspar Microlites in the Matrix of the Host Basalts

Sample#	76210		76213		76221			76213	76568	76569
	mean	s.d.	mean	s.d.	mean	s.d.		Feldspar Microlites		
No. of analyses	[4]		[16]		[3]					
SiO2	46.91	1.19	58.88	3.10	47.46	0.93	SiO2	65.15	63.81	49.58
TiO2	0.24	0.03	0.19	0.13	0.17	0.1	TiO2	0.32	1.05	0.27
Al2O3	22.63	1.29	22.93	2.22	22.97	0.18	Al2O3	21.51	21.33	25.75
FeO	0.44	0.14	0.92	1.09	0.40	0.10	CaO	4.45	1.53	9.02
MgO	0.78	0.15	2.33	3.55	0.35	0.18	Na2O	7.79	5.25	0.00
CaO	8.12	0.78	5.72	1.25	7.31	0.52	K2O	2.07	6.17	7.96
Na2O	0.31	0.07	6.08	0.94	0.25	0.21	Sum	100.09	99.14	92.58
K2O	6.68	1.33	1.88	1.53	1.20	0.51				
Sum	85.50	1.74	98.67	1.85	79.99	0.43	Oxygen	8	8	8
							Si	2.8713	2.8752	2.4801
							Ti	0.0053	0.0357	0.0101
							Al	1.1166	1.1320	1.5202
							Ca	0.2103	0.0735	0.4847
							Na	0.6652	0.4584	
							K	0.0579	0.3549	0.5091
							Sum	4.9267	4.9297	5.0042
							Ca	22.56	8.29	48.77
							Na	71.29	51.68	0
							K	6.14	40.04	51.23

1.6 Discussion

Numerous studies of mantle xenoliths have concluded that most of the Cr-diopside spinel lherzolites are partial melting residues, accidentally carried to the surface by their host magmas (e.g. Forbes & Kuno, 1967; Jackson & Wright, 1970; Frey & Green, 1974; Varne, 1977; Frey & Prinz, 1978; Nickel & Green, 1984). Therefore, they are representative of the mantle wall-rocks and carry information about the constitution, composition, thermal conditions, mechanical, seismic, electric and rheological properties of the upper mantle. A consensus among mantle petrologists is that all upper mantle xenoliths record experience of partial melting process, followed by recrystallization under ambient mantle thermal conditions, and possible metasomatism at different stages and to variable extents. The Ming-xi lherzolite suite is one typical example. The systematic variation in individual mineral compositions is consistent with variation of the whole-rock compositions (Fig.1.7a & b). Both are best interpreted as a partial melting trend. The consistent positive correlation of Mg# and Cr# (and An# for clinopyroxene) in all the silicate minerals suggests that individual xenoliths are not simple mechanical mixtures of different proportions of various minerals but are the partial melting product of a relatively homogeneous source. This source is adequately represented by the sample 76222, which not only has the lowest Mg# (of all the silicate minerals) but also has the highest modal abundances of garnet and clinopyroxene. It is the least depleted end-member of all the samples in this suite. The difference in the mineral chemistry of the xenoliths implies that each xenolith experienced different degrees of partial melting and that the melt in equilibrium with each xenolith has different composition from one another. In the next chapter, this partial melting process is modelled in detail to determine the composition of these melts and to estimate the extent of the melting.

Whereas the early partial melting process is recorded by the bulk rock and the individual mineral compositions, the petrography and composition exchange between minerals suggest experience of mantle metamorphism -- recrystallization under mantle thermal conditions. Application of mineral thermometers and barometers to these xenoliths suggests that they are all well equilibrated around 20.5 (± 0.5) kbar (the Nickel & Green pressure) and 1050° - 1100°C (average of the calculated temperatures from all the thermometers). The PT estimates plot between the southeastern Australia geotherm (O'Reilly & Griffin, 1985) and the eastern margin of the Australian craton geotherm (Pearson et al., 1991) (Fig.1.10). The available mineral barometers and thermometers are not accurate enough to construct a geotherm from these xenoliths. An uncertainty of 50°C in temperature estimate corresponds to an uncertainty of 2 kbar in pressure. Thus although

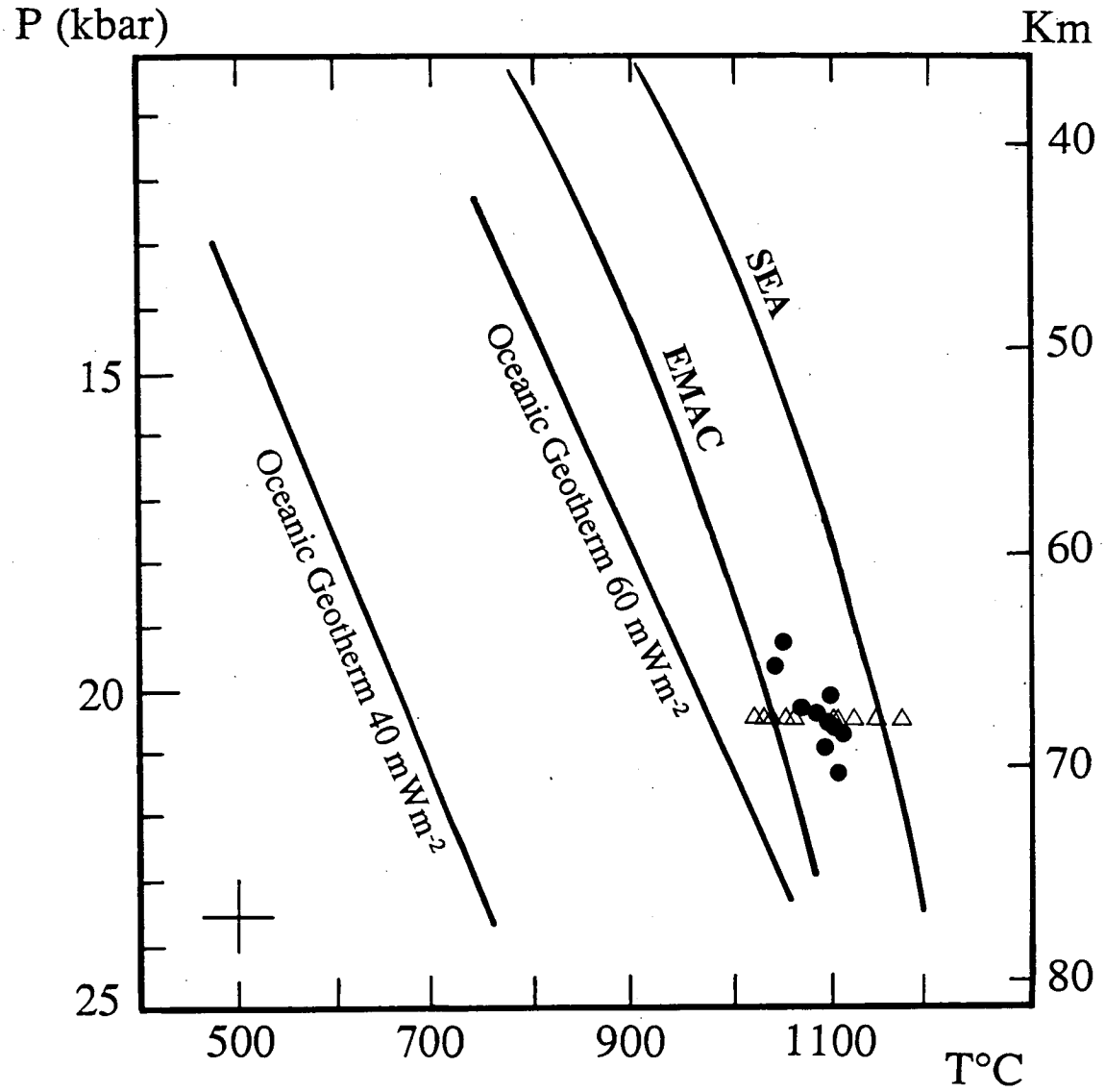

Figure 1.10. the equilibration PT conditions of Ming-xi lherzolites compared with Australian xenolith geotherms and theoretical oceanic geotherms (solid dots: garnet-bearing samples; empty triangles: garnet-free spinel lherzolites. SEA: southeastern Australian geotherm of O'Reilly & Griffin, 1985; EMAC: eastern margin of the Australian craton geotherm of Pearson et al., 1991; Oceanic geotherms: Chapman & Pollack, 1977).

there seems to be a trend in the PT plot from the garnet-bearing xenoliths, all the data points are within the error range and do not represent a true geotherm.

The oxygen fugacities recorded by the Ming-xi xenoliths fall in the group of "lightly metasomatised" xenoliths of Ballhaus et al. (1991). They are slightly more oxidised than the so-called primitive mantle samples such as those reported by Preß et al. (1986). This agrees with the presence of phlogopite in one sample and alkali-rich glasses in several samples, which indicates some degree of metasomatism. The secondary phlogopite may suggest a local event of modal metasomatism and the presence of alkali-rich glasses in some garnet rims and in at least one garnet-absent sample registers the signature of a very late metasomatism. This late metasomatism may well be synchronous with transport of the xenoliths by the host magma. The similarity between the glass compositions in the xenoliths and in the host basalt strongly implies that these metasomatic elements are directly from the host magma. However, this metasomatic process is insignificant in that it has not resulted in any obvious change in mineral and whole-rock major element geochemistry. The growth of kelyphite rims and the partial conversion of garnet lherzolite to spinel lherzolite seen in the growth of secondary spinels outside of obvious kelyphite rims seems to be an isochemical process.

The experimental study on spinel-lherzolite to garnet-lherzolite transition in Chapter Four has demonstrated that the appearance (or disappearance) of garnet in a lherzolite system is principally controlled by pressure, with a major influence due to whole-rock composition (Cr# in particular). Thermobarometric calculation indicates that all the xenoliths reported in this study have equilibrated under very similar PT conditions (20.5 kbar, 1050° - 1100°C). It is therefore reasonable to suggest that the presence/absence of garnet in these xenoliths is related to their bulk compositions. Because Cr_2O_3 (and Al_2O_3 to large extent) in the whole-rock is mainly stored in spinel, the Cr# of spinel is a good indicator of the whole-rock Cr# (Fig. 1.7b). Comparison of the Cr# of spinels between the garnet-free and garnet-bearing samples reveals that the former are greater than the latter with two exceptions: spinels in samples 76214 & 76226, which in fact have the lowest Cr# among all the spinels in the suite (not including those confined within the kelyphite rims of garnet) (Table 1.6). The highest Cr# ($\approx$ 25.5) in the garnet-bearing samples belongs to the primary spinels in 76212 & 76225 and probably represents the limit of garnet appearance under these PT conditions (i.e. garnet is not expected to be found in samples with spinel Cr# > 25.5; but is expected to be found in samples with spinel Cr# < 25.5). Spinels in the phl-bearing spinel lherzolite 76209 have Cr# (22.43) less than this limit, which implies that garnet should be stable in this sample as well. Another phl-bearing garnet lherzolite with the presence of spinel has been found in the same locality and the Cr# of the spinel in this sample is 17 (Cao & Zhu, 1987), which is consistent with the garnet-bearing suite. The absence of garnet in 76209, 76214,

76226 may suggest that these equilibrated under different pressure and temperature from the garnet-bearing lherzolites and the spinel-only lherzolites (spinel Cr# > 25.5). The implication is that the host basalt sampled from one locality in the mantle (20.5 kbar, 1050°C) at which there was a chemically controlled transition from garnet lherzolite to spinel lherzolite suite. It also sampled from a slightly shallower zone (represented by samples 76209, 76214, 76226) at which garnet was not stable. An alternative explanation could be that sampling of the garnet lherzolite to spinel lherzolite wallrock locality included a portion of the mantle which had suffered a prior heating event (responsible for the growth of secondary Sp2a group spinels and for spinel lherzolites 76209, 76214, 76226). Against this possibility these three samples do not have a higher equilibrium temperature or different fO_2 on spinel or two-pyroxene thermometers. On the contrary, they indicate a slightly lower temperature. Therefore, it seems more likely that samples 76209, 76214, 76226 came from a slightly shallower part of the mantle than other samples, and both regions have been affected by a late and local phlogopite veining event.

Chapter Two

Geochemistry of a Suite of Lherzolite Xenoliths from Fu-jian, Southeastern China

Chapter Two

Geochemistry of a Suite of Lherzolite Xenoliths from Fu-jian, Southeastern China

2.1 Introduction

Petrologic and geochemical studies of mantle xenoliths world-wide have shown that they are residues of a partial melting process, and that many, if not all, have been altered by metasomatic processes (e.g. Carter, 1970; Frey & Green, 1974; Frey & Prinz, 1978; Carswell, 1980). The first process is responsible for the regular variations in both mineral and whole-rock major element geochemistry (e.g. Berg & O'Hara, 1973; Maaløe & Aoki, 1977; Chapter One) and the latter process is responsible for trace element and isotopic heterogeneities (e.g. Wass & Rogers, 1980; Bailey, 1982; Roden & Murthy, 1985).

There are two approaches in quantitative modelling of the partial melting process: the mineral/melt equilibria approach (e.g. Hanson & Langmuir, 1978) and the empirical bulk-rock series approach (e.g. O'Hara et al., 1975; Reid & Woods, 1978; Nickel & Green, 1984). The mineral/melt equilibria approach makes use of mineral-melt partition coefficients and stoichiometric constraints imposed by the residual minerals to solve for extent of melting and composition of the melts. A major problem in this approach is that most minerals have re-equilibrated to ambient mantle thermal conditions after the melting process and no longer retain their compositions from the conditions of melting. The empirical bulk-rock series approach assumes a source - residue relationship between the bulk-rock compositions of fertile and depleted samples, and estimates the melt composition and degree of melting empirically. Frey et al. (1985) summarize three models under this scenario: (1) uniform degree of melting followed by incomplete segregation of the compositionally homogeneous melt (the two-component mixing model); (2) variable degree of melting with complete or incomplete segregation of compositionally homogeneous melt (similar to the invariant melting observed in simple systems in the laboratory, hence the invariant melting model); and (3) variable degree of melting with complete or partial extraction of compositionally different melts (the heterogeneous melting model). Models (1) and (2) are indistinguishable on major element basis (Frey et al., 1985). Experimental results on partial melting of model peridotites (e.g. Jaques & Green, 1980; Falloon et al., 1988) indicate that compositions of partial melts change systematically with degree of melting, temperature and pressure; and that the melting path is determined by progressive elimination of phases along multiple-phase cotectic paths. The overall melting pattern is thus inconsistent with model (2). Model (3) is an extension of model (1). Although the heterogeneous melting model

is discussed by Frey et al. (1985), it is the mineral/melt equilibria approach that was used by them to obtain the degree of melting and melt compositions. In this chapter, an empirical method is described under the heterogeneous melting model, utilising the Ming-xi lherzolite xenoliths as an example. A basic assumption in this method is that each one of the xenoliths in this suite represents a residue after melting of a homogeneous source (equivalent to the most fertile composition in the suite). An implication is that the melts extracted must lie on the trend defined by the xenoliths. The minerals may have re-equilibrated under subsolidus conditions, but each residue as a whole should maintain a closed system after the partial melting process, unless modified by modal metasomatism. Therefore, the correlation relations defined by the xenoliths are equally applicable to the extracted melts.

2.2 Whole-rock Geochemistry of the Xenoliths

Of twenty samples from Ming-xi on which mineralogical data were obtained, eight have been analysed for major and a few trace elements by a Philips PW1140/00 XRF spectrometer at the Geology Department, University of Tasmanina (Table 2.1). One of them is garnet lherzolite; three are spinel lherzolite; and four are spinel-bearing garnet lherzolite. Interpretation of these results should take into account problems of representative sampling due to the small sample size and yet large mineral grain size, and of low concentrations of some minor elements such as Na_2O and TiO_2 (Nickel & Green, 1984). Most samples analysed have Na_2O concentrations below the XRF detection limit (0.2%). The Na_2O concentrations given in Table 2.1 are calculated on the basis of Na_2O contents in clinopyroxenes and modal% of clinopyroxene in the samples (assuming clinopyroxene is the only significant Na_2O-bearing phase). The eight samples were selected so as to cover the wide MgO range exhibited by this suite of lherzolites. Thus any systematic variation can be readily recognised.

Additional thirty-three analyses from the Chinese literature (Sun & Lai, 1980; Zhang, 1982; Cao & Zhu, 1983; Zhou & Chen, 1984; Zhang & Cong, 1987) are compiled in Table 2.2 for comparison. Both Fe_2O_3 and FeO were usually given in the original references but are all converted to FeO* (FeO as the total iron). The majority of these analyses plot close to each other and define obvious trends in the oxide versus MgO diagrams (Fig.2.1). They have the same variation range and correlation trends as spinel peridotites from western USA (Wilshire et al., 1988; Fig.2.2a) and eastern Australia (Nickel & Green, 1984; O'Reilly & Griffin, 1988; 1987; Stolz & Davies, 1988; Chen et al., 1990; Fig.2.2b). Spinel peridotites from Mongolia (Preß et al., 1986; Fig.2.2c) and French Massif Central (Hutchison et al., 1975; Fig.2.2d), and spinel ± garnet lherzolites from Pali-Aike (Skewes & Stern, 1979; Stern et al., 1989; Fig.2.2d) plot within the variation trends defined by the Ming-xi xenoliths, although they are in a smaller range of variation (probably due to limited number of samples available)

Table 2.1 XRF Analyses of Eight Representative Ming-xi Lherzolites

sample #	76210	76214	76215	76216	76217	76218	76222	76225
SiO2	44.12	44.94	44.37	45.36	44.58	44.27	45.1	44.66
TiO2	0.07	0.21	0.04	0.08	0.09	0.08	0.15	0.02
Al2O3	3.22	3.23	1.68	1.09	3.50	2.86	4.62	2.12
Cr2O3	0.41	0.41	0.38	0.53	0.46	0.39	0.43	0.44
FeO*	8.07	8.27	7.98	7.70	8.68	8.29	8.16	8.05
MnO	0.13	0.13	0.13	0.13	0.14	0.13	0.14	0.14
NiO	0.26	0.25	0.28	0.27	0.26	0.27	0.22	0.28
MgO	39.77	39.01	42.67	42.41	38.37	41.35	36.09	41.05
CaO	2.71	2.65	1.63	0.98	2.83	2.11	3.81	1.99
Na2O	0.19	0.23	0.02	0.03	0.22	0.13	0.32	0.07
K2O	0.04	0.02	0.02	0.10	0.02	0.01	< 0.01	0.02
P2O5	0.03	0.05	< 0.03	0.04	< 0.03	0.04	< 0.03	< 0.03
ignition loss	-0.30	-0.34	-0.24	0.19	0.11	0.17	0.06	-0.22
total	98.91	98.91	99.01	99.84	99.12	100	98.86	98.85
Trace elements (ppm)								
V	69	76	46	41	80	57	92	59
Nb	< 1.0	< 1.0	1.2	2	< 1.0	< 1.0	< 1.0	< 1.0
Zr	1.3	6.3	2.5	9.3	4.5	2.7	7.3	< 1.2
Y	3.2	2.8	2.1	2.3	6.3	3.7	5	2.6
Sr	33	276.3	3.4	9.3	10.4	12.5	14.9	3.7
Rb	2.7	< 1.5	< 1.5	< 1.5	< 1.5	< 1.5	< 1.5	< 1.5
Mg#(ol)	90.36	89.89	91.03	91.42	90.07	90.5	89.67	90.63
FeO/MgO(ol)	0.190	0.201	0.176	0.167	0.196	0.187	0.205	0.184
modal%*								
olivine	64.52	58.92	69.66	65.05	58.65	68.58	53.42	64.94
orthopyroxene	15.75	25.54	21.95	30.37	21.58	15.63	17.07	24.23
clinopyroxene	11.89	13.46	6.8	3.18	13.79	8.83	17.16	8.55
garnet	7.28	0	0	0	4.65	6.34	12.35	1.23
spinel	0.55	2.09	1.59	1.4	1.32	0.62	0	1.05

* mineral modes were calculated from whole-rock and mineral compositions.

Table 2.2 Additional Major Element Analyses of Ming-xi Peridotites from Chinese Literature

Reference	Sun & Lai (1980)			Cao & Zhu (1983)			Zhang (1982)				Zhang & Cong (1987)					
Sample #	53	54	55	T2--3	T2--4	T2--5	M9	B38	B162	B171	B7	d01	d02	d06-1	d05	d07
Rock Type	GL	GL	GL	GL	GL	GL	GL	GL	GL	GH	GH	GL	GL	GL	GL	GL
SiO2	44.30	43.16	43.08	43.05	43.55	43.35	44.35	43.29	43.93	43.78	40.01	44.72	43.69	44.03	43.71	43.43
TiO2	0.20	0.16	0.16	0.17	0.15	0.14	0.20	0.14	0.15	0.15	0.27	0.28	0.10	0.14	0.28	0.08
Al2O3	4.17	3.31	1.97	3.17	3.19	3.15	3.76	3.20	2.90	1.90	5.44	3.27	2.35	3.03	5.05	2.59
Cr2O3							0.39	0.38	0.39	0.39	0.49	0.42	0.49	0.23	0.20	0.44
FeO*	8.83	7.96	8.22	8.67	8.75	9.36	11.31	9.25	8.90	8.68	13.22	9.30	11.33	9.33	9.51	10.90
MnO	0.14	0.18	0.18	0.15	0.16	0.16	0.13	0.19	0.12	0.25	0.16	0.17	0.16	0.17	0.20	0.16
NiO							0.23	0.27	0.28	0.29	0.28	0.28	0.27	0.27	0.25	0.30
MgO	38.46	41.22	42.72	39.60	40.38	39.55	36.87	39.69	39.83	40.77	35.20	36.28	38.02	35.22	34.20	39.75
CaO	2.68	1.77	1.01	3.24	2.32	3.04	2.77	2.83	2.87	2.34	1.41	3.97	2.90	7.17	5.69	2.15
Na2O	0.35	0.17	0.15	0.55	0.47	0.39	0.23	0.26	0.23	0.09	0.14	0.30	0.23	0.04	0.05	
K2O	0.06	0.06	0.05	0.09	0.07	0.03	0.07	0.03	0.06	0.10	0.04	0.03	0.05	0.04	0.05	0.03
P2O5	0.03	0.11	0.08	0.05	0.04	0.04	0.05	0.08	0.06	0.11	0.37	0.20	0.03	0.20	0.24	0.03
Sum	99.22	98.10	97.62	98.74	99.08	99.21	100.37	99.61	99.72	98.85	97.03	99.22	99.62	99.87	99.43	99.86

Reference	Zhou & Chen (1984)			Zhang (1982)									Zhang & Cong (1987)				
Sample #	M18-1	M18-2	M4	M25	M3	B167	B248	B33	B29	B27	B235	B224	B199	d08	d10	d11	d12
Rock Type	SL	SL	SL	SL	SL	SL	SL	SL	SL	SL	SH	SH	SH	SL	SL	SL	SL
SiO2	44.19	43.42	44.65	44.56	43.79	43.42	44.21	43.76	44.28	44.54	44.55	42.92	43.71	43.51	43.88	45.07	44.07
TiO2	0.13	0.15	0.13	0.18	0.12	0.14				0.19	0.18	0.32	0.41		0.25	0.20	0.14
Al2O3	3.13	3.80	2.69	2.75	1.44	0.55	2.22	4.10	2.64	3.45	1.52	3.81	2.28	1.38	1.25	3.02	3.70
Cr2O3	0.37	0.44	0.37	0.32	0.37	0.31	0.45	0.38	0.38	0.42	0.45	0.46	0.34	0.13	0.19	0.41	0.34
FeO*	9.35	8.58	8.96	8.02	9.85	8.76	9.13	8.88	8.46	8.88	8.23	9.87	11.36	9.99	9.12	9.18	10.97
MnO	0.13	0.11	0.15	0.11	0.13	0.15	0.14	0.12	0.12	0.14	0.13	0.13	0.12	0.17		0.18	0.17
NiO	0.26	0.28	0.26	0.27	0.29	0.27	0.30	0.37	0.30	0.27	0.31	0.25	0.26	0.34	0.34	0.28	0.28
MgO	39.32	38.70	39.36	39.36	41.77	44.19	40.73	38.15	40.99	38.31	42.42	38.19	39.54	42.58	42.97	34.97	36.45
CaO	2.66	2.60	1.43	2.99	1.30	1.54	1.90	3.19	2.38	3.20	1.83	1.98	1.41	1.10	1.30	4.41	3.68
Na2O	0.51	0.28	0.27	0.38	0.27	0.04	0.09	0.35	0.25	0.32	0.16	0.20	0.23	0.04	0.03	0.05	0.24
K2O	0.07	0.08	0.04	0.09	0.10	0.08	0.03	0.12	0.05	0.06	0.09	0.09	0.18	0.04	0.03	0.05	0.03
P2O5	0.03	0.07	0.04	0.05	0.08	0.07	0.08	0.07	0.07	0.09	0.06	0.11	0.11	0.13	0.03	0.08	0.03
Sum	100.14	98.51	98.35	99.09	99.50	99.52	99.28	99.49	99.92	99.87	99.93	98.33	99.95	99.41	99.39	97.90	100.10

GL - garnet lherzolite; GH - garnet harzburgite; SL - spinel lherzolite; SH - spinel harzburgite.

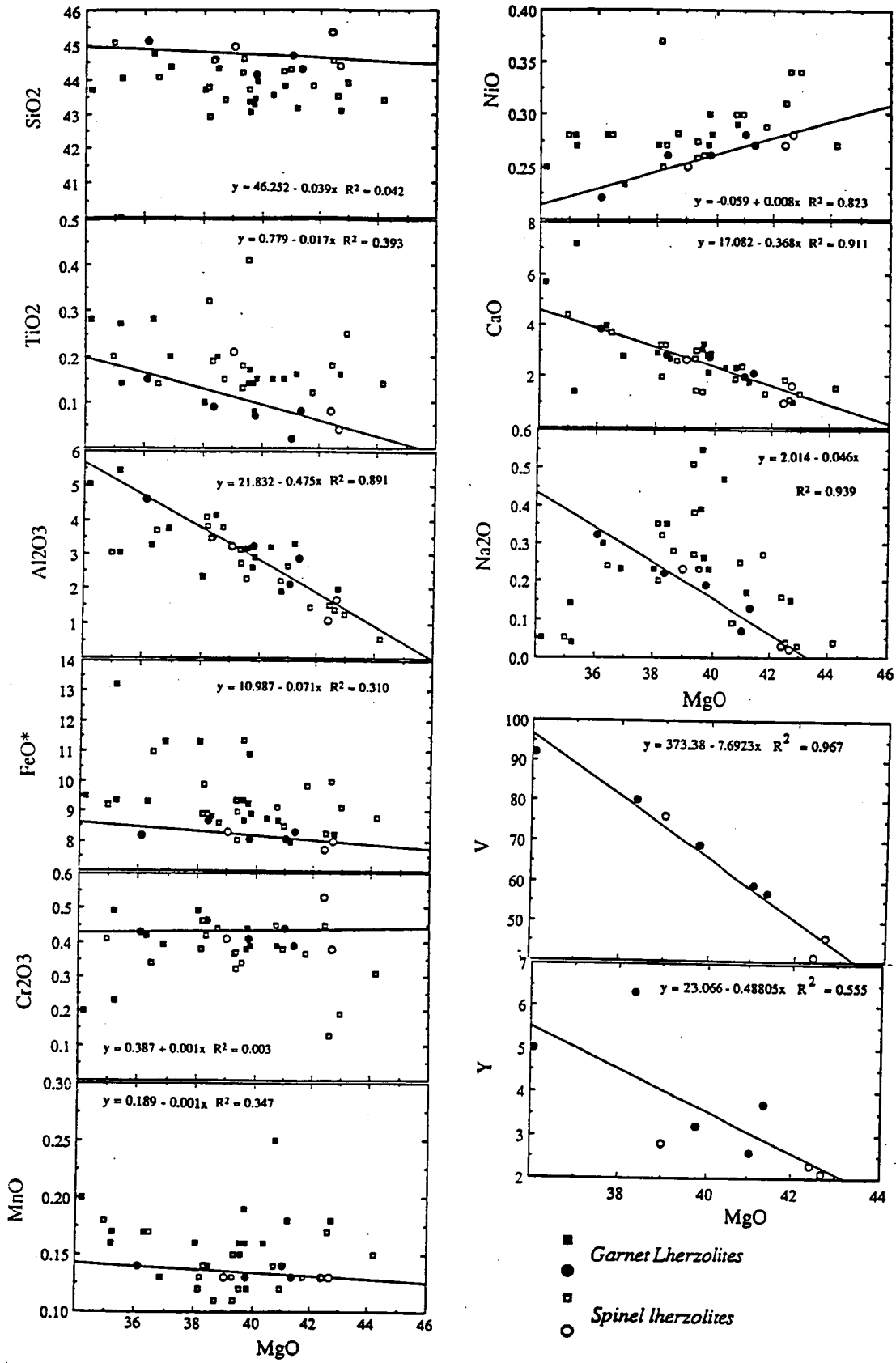

Figure 2.1. Major and trace element variation diagrams for peridotites from Ming-xi, Fu-jian Province, southeastern China. Circles represent analyses given in this study; squares represent analyses from Chinese literature. The line marks the best fit of the eight analyses given in this study. V and Y values are in ppm.

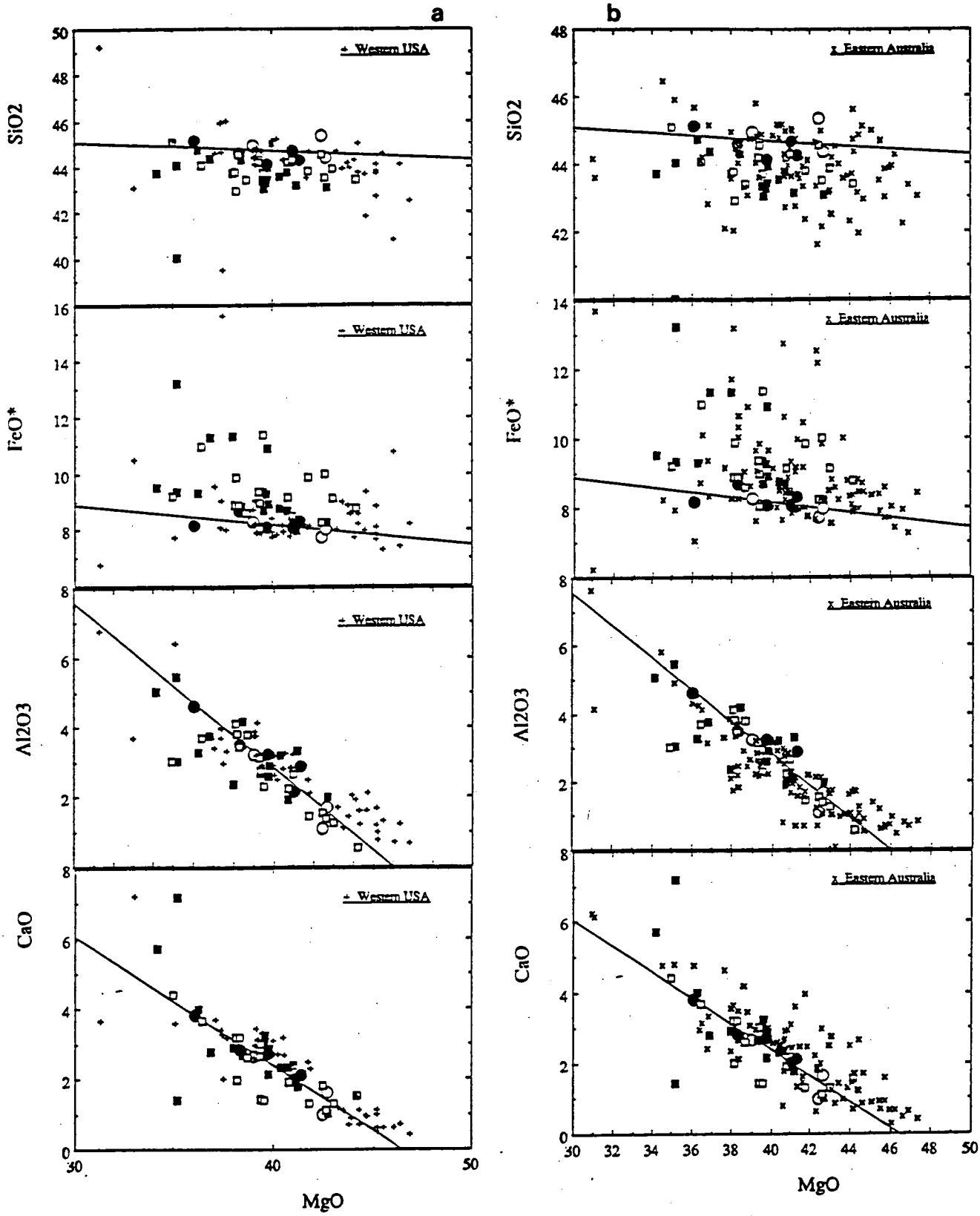

Figure 2.2. Comparison of some major elements between Ming-xi peridotites and peridotites from (a) western USA; (b) eastern Australia; (c) Mongolia; (d) French Massif Central, and Pali-Aike (data sources are given in the text).

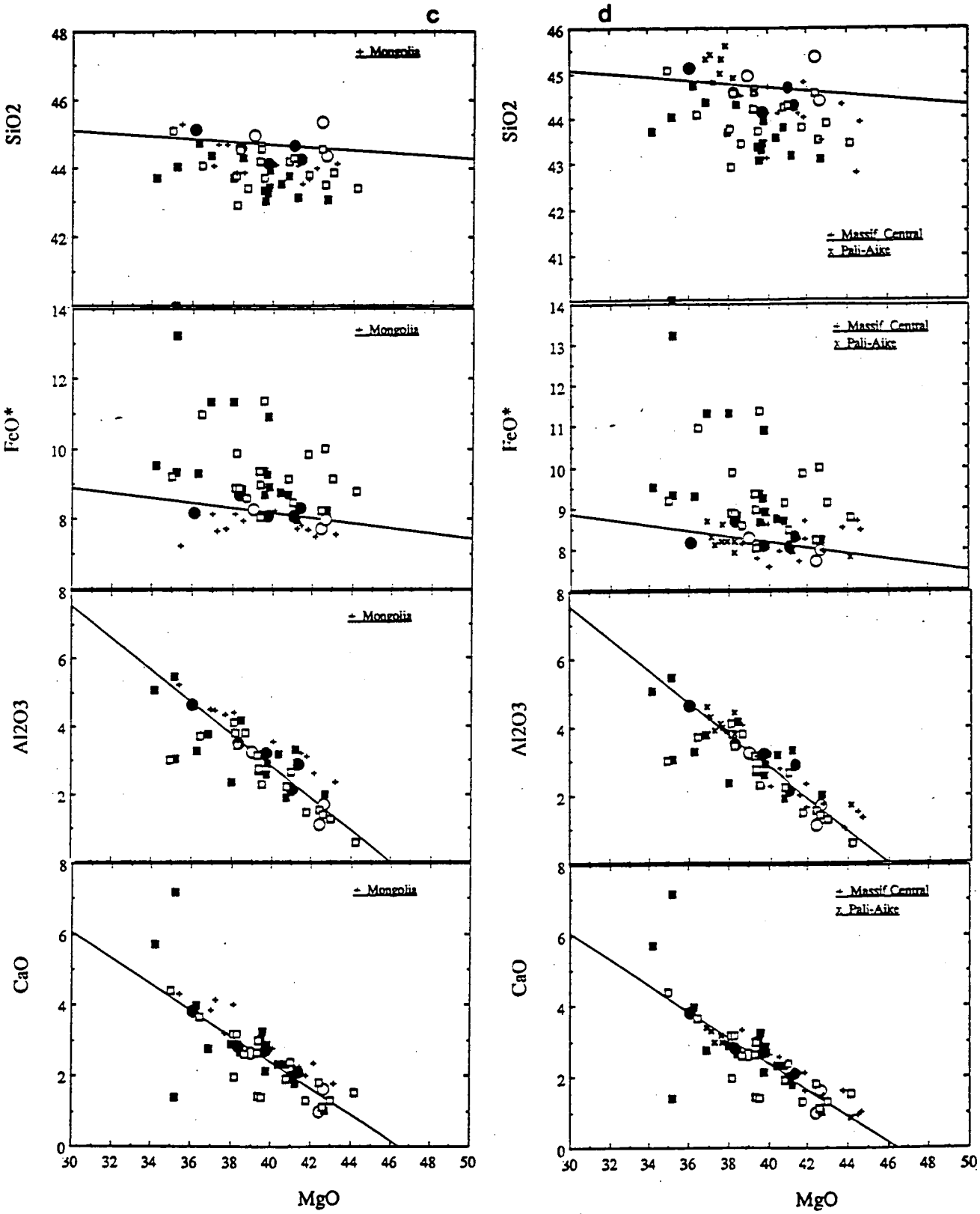
c
d
SiO2
FeO*
Al2O3
CaO
MgO
+ Mongolia
+ Massif Central
x Pali-Aike

and are slightly lower in FeO* than the Ming-xi samples. The comparison suggests that the Ming-xi suite is a typical suite of xenoliths in alkali-basalts, thus the modelling can have a broad implication.

Within the Ming-xi suite, there is an overlap in major element composition between garnet-bearing and garnet-absent samples. Bulk rock MgO is positively related to modal% of olivine and negatively related to modal% of clinopyroxene (Table 2.1). Positive correlations of CaO, Al_2O_3, V and Zr (except in 76216) respectively with modal% of clinopyroxene imply that these elements are mainly stored in clinopyroxene. These correlations again indicate a gradual depletion of low fusion-point components, and are consistent with a partial melting origin. The sample 76222 has the highest modal proportions of clinopyroxene and garnet, and is the least depleted sample analyzed. The close similarities in major and the analyzed trace element compositions between this sample and previously estimated model mantle compositions (Ringwood, 1975; Jagoutz et al., 1979; Sun & McDonough, 1989) reinforce the use of 76222 as a representative of the source composition for the Ming-xi xenoliths. Most of the trace elements in these rocks are near the detection limit (1 - 2 ppm). Exceptionally high Sr in 76210 and particularly in 76214, and high Zr in 76216 may be related to melt penetration from the host basalts as inferred from the presence of alkali-rich glasses in some xenoliths (Chapter One).

Simple least square regression analysis was performed with the eight samples analyzed in Tasmania to obtain oxide - MgO relations (regression line shown in Fig.2.1). Analyses from Chinese literature were not included because of uncertainties in the data reliability. Regression parameters are listed in Table 2.3, where they are compared with those of some representative peridotite suites reported in the literature. Among those listed in Table 2.3, the Ming-xi suite is the most fertile suite, less depleted than the average young continental spinel lherzolite estimated by Maaløe & Aoki (1977). An interesting observation is the difference between young continental spinel lherzolites and oceanic spinel lherzolites. Although Maaløe & Aoki (1977) did not infer a difference between the two groups of xenoliths, Table 2.3 suggests that on average the oceanic spinel lherzolites are more depleted than the young continental spinel lherzolites.

2.3 Estimation of the Equilibrium Melt Composition

A necessary assumption in the partial melting modelling is that olivine composition remains the same as at the time of melting. Thus the equilibrium melt actually means the melt in equilibrium with olivine in the xenoliths (not other minerals). This assumption is justified by experimental results reported in chapter three: under subsolidus conditions in the temperature range of 1200° - 1500°C, pressure range of 20 - 35 kbar, FeO/MgO ratio of olivine changes little with temperature and pressure, whereas compositions of other minerals

Table 2.3 Regression Parameters for Some Peridotite Suites

$y = a + bx$ (where x = MgO in wt%)

Type	young continental spinel lherzolite								oceanic spinel lherzolite						peridotite massif	
locality	Ming-xi		Mongolia		Lake Bullenmerri		world-wide		Alligator Lake		Ocean floor		world-wide		Ronda	
	a	b	a	b	a	b	a	b	a	b	a	b	a	b	a	b
SiO2	46.250	-0.039	49.432	-0.133	51.497	-0.185	54.976	-0.250	54.666	-0.242	47.213	-0.052	58.321	-0.331	53.155	-0.217
TiO2	0.779	-0.017	1.016	-0.022	0.653	-0.013	0.584	-0.013	0.596	-0.013	0.945	-0.020	1.050	-0.022	0.693	-0.015
Al2O3	21.832	-0.475	17.838	-0.357	15.824	-0.330	16.281	-0.337	16.371	-0.345	17.923	-0.378	14.739	-0.294	18.570	-0.384
Cr2O3	0.387	0.001	0.480	-0.024	0.636	-0.006	0.468	-0.001	0.119	0.007					0.321	0.001
FeO*	10.987	-0.071	8.043	-0.007	14.179	-0.129	8.788	-0.016	11.988	-0.079	12.184	-0.092	12.759	-0.106	9.965	-0.047
MnO	0.167	-0.001	0.127		0.229	-0.002	0.210	-0.002	0.223	-0.002	0.514	-0.009	0.675	-0.012	0.148	-0.0004
NiO	-0.059	0.008	-0.074	0.009	-0.100	0.009	-0.174	0.011	-0.180	0.011			-0.280	0.013	-0.018	0.007
CaO	17.082	-0.368	16.512	-0.342	14.792	-0.297	16.943	-0.354	14.221	-0.305	14.651	-0.323	10.483	-0.217	16.249	-0.335
Na2O	2.014	-0.046	1.526	-0.032	1.621	-0.031	1.096	-0.022	1.477	-0.031	1.115	-0.022	1.178	-0.022	1.547	-0.033
K2O			0.078	-0.002			0.172	-0.003	0.097	-0.002	0.858	-0.019				
V	373.38	-7.69			321.28	-6.43										
Y	23.07	-0.49			12.00	-0.24										
data source*	1		2		3		4		5		6		4		7	

*) 1 - this study; 2 - Preß et al. (1986); 3 - Nickel & Green (1984); 4 - Maaløe & Aoki (1977);
5 - Francis (1987); 6 - Shibata & Thompson (1986); 7 - Frey et al. (1985).

vary significantly. Accepting this assumption, and based on the heterogeneous melting model outlined above, the following procedure is followed to obtain the melt composition in equilibrium with (olivine in) each individual xenolith:

(1) from the olivine FeO/MgO ratio and the well-known olivine - melt partition coefficient Kd = 0.35 (this number is preferred according to Frey et al., 1975; Francis, 1987), the melt FeO/MgO is derived:

$$(FeO/MgO)^{melt} = \frac{(FeO/MgO)^{olivine}}{0.35}$$

(2) substituting the $FeO = a_{FeO} + b_{FeO}MgO$ relation (Table 2.3), the MgO in the melt can be determined:

$$MgO^{melt} = \frac{0.35a_{FeO}}{(FeO/MgO)^{olivine} - 0.35b_{FeO}}$$

(3) from the oxide - MgO relations given in Table 2.3, other oxides in the equilibrium melt can be obtained.

(4) the degree of melting f can be estimated from the relation between the source, the residue and the melt:

$$C^i_{source} = fC^i_{melt} + (1 - f)C^i_{residue}$$

This is readily achieved by employing the Genmix program (Le Maitre, 1979).

Results of the calculation for the Ming-xi xenoliths are summarized in Table 2.4. The calculated equilibrium melts have MgO ranging from 17 - 20%. The extent of melting varies from 11% to 29%. When plotted in the melting grid of the CIPW molecular normative basalt tetrahedron (Fig. 2 of Falloon & Green, 1988), these melts locate near the locus of experimental melts in equilibrium with olivine + orthopyroxene + clinopyroxene ± spinel at 30 kbar (Fig.2.3). Because the melting temperatures for typical mantle peridotites at 30 kbar are above 1500°C under anhydrous conditions (extrapolated from Fig.1 of Jaques & Green, 1980), these melts are believed to be generated at T > 1500°C (at 30 kbar). Compared with some experimentally determined melts (Table 2.5), these calculated equilibrium melts have similar composition to those produced at 1550°C, 25 - 30 kbar. This is clearly illustrated in the CIPW normative diagram: the experimental melts formed at 25 - 30 kbar, 1550°C plot close to the calculated melts, whereas those at P < 25 kbar plot far away from them in the lower pressure region (Fig.2.3). This comparison suggests that the inferred melting probably took place at 25 - 30 kbar, 1550°C (± 50°C).

The method outlined above has been used to calculate equilibrium melt compositions for a number of peridotite suites reported in the literature. These include Mongolia spinel lherzolites (Preß et al., 1986), spinel peridotites from Lake Bullenmerri, Victoria, Australia (Nickel & Green, 1984), from Alligator Lake, Yukon, Canada (Francis, 1987), and Ronda peridotite Massif (Frey et al., 1985). The calculated melts have the following MgO% range: 12.4 - 16 (Mongolia), 15.5 - 23 (Alligator Lake), 14.2 - 23.4 (Lake Bullenmerri), and 13.4 - 19.4 (Ronda). The extents of melting these peridotites have experienced are 6.9 -

Table 2.4 Representative Compositions of Calculated Ming-xi Melts

Sample #	76210	76214	76215	76216	76217	76218	76225
SiO2	45.55	45.59	45.50	45.47	45.57	45.54	45.53
TiO2	0.47	0.49	0.45	0.44	0.48	0.47	0.47
Al2O3	13.34	13.73	12.72	12.32	13.58	13.21	13.09
Cr2O3	0.41	0.41	0.41	0.41	0.41	0.41	0.41
FeO*	9.72	9.78	9.63	9.57	9.75	9.70	9.68
MnO	0.15	0.15	0.15	0.15	0.15	0.15	0.15
NiO	0.08	0.08	0.09	0.10	0.08	0.09	0.09
MgO	17.88	17.05	19.18	20.02	17.37	18.15	18.40
CaO	10.50	10.81	10.02	9.71	10.69	10.40	10.31
Na2O	1.19	1.23	1.13	1.09	1.21	1.18	1.17
Sum	99.30	99.31	99.29	99.28	99.30	99.30	99.30
melt%	16.20	13.31	27.60	29.22	11.02	21.62	22.03
CIPW molecular normative projection							
Qz	31.80	32.37	30.92	30.37	32.15	31.61	31.45
JdTs	26.40	27.43	24.82	23.82	27.03	26.07	25.77
Ol	41.81	40.20	44.26	45.81	40.83	42.32	42.79
Qz	8.92	8.37	9.70	10.17	8.59	9.09	9.24
Di	22.00	23.44	19.93	18.70	22.87	21.55	21.15
Ol	69.08	68.18	70.37	71.13	68.54	69.36	69.61

28%(Mongolia, source composition Mo105), 7.6 - 35% (Alligator Lake, source composition 10046), 2 - 38% (Lake Bullenmerri, source composition BME15), and 3.6 - 30.8% (Ronda, source composition R717) according to this method. These melts are projected on the CIPW molecular normative diagram (Fig.2.3). With reference to the experimentally determined melting grid of Falloon et al. (1988), it can be observed that (1) individual samples in a suite cover a wide pressure range; (2) these melts plot in a wider range and at lower pressure than the Ming-xi melts; (3) these melts are in the clinopyroxene-out region, whereas the Ming-xi melts are in the clinopyroxene-in region of the Tinaquillo lherzolite system (its bulk composition is relatively more depleted than those of the MORB-pyrolite and the Hawaiian pyrolite).

These observations suggest that (a) individual samples within these suites have compositions determined by melt extractions at different depth in the mantle column being melted. There are two extreme possibilities: (i) they originated from different vertical depth of the mantle; (ii) they represent different parts of a upwelling mantle diapir. Samples from the interior part of the diapir experienced higher degree of melting than those from outside part of the diapir (as has been suggested by Frey et al, 1985 for Ronda peridotite massif); (b) they indicate inefficient melt extraction. This is deduced from the melt composition and the small extent of melting for some samples. Compositions of melts from small degrees of melting (< 5%) are expected to be very different (high normative Ne) from those from large degrees of melting. For the less compatible elements such as Ti and Na, their abundances should be significantely higher in the low degree melts than in the high degree melts. However, the calculated melts all have similar compositions. The implication is that all samples experienced large extent of melting, but not all the melts segregated completely from the residue. Some residues thus have very similar composition to the source composition because of this incomplete melt extraction; (c) the xenolith suites from other localities originated from shallower depth than the Ming-xi xenoliths. The presence of garnet in some Ming-xi xenoliths supports this suggestion; (d) depth of melting for the peridotite suites are in the following order of decreasing depth: Ming-xi, Mongolia, Lake Bullenmerri, Ronda, and Alligator Lake.

2.4 Discussion

Partial melting is a common and complex process, responsible for much of the chemical differentiation and homogenization of the upper mantle. Mantle xenoliths, peridotite massifs, and basalts only represent some end products of this complex process. The details of this process have often been overprinted by late processes such as mantle metamorphism and metasomatism. The systematic variations in mineral and whole-rock major element geochemistry seem to be the only evidence of operation on partial melting in mantle xenoliths. Thus the modelling method presented in this study can only be the simplest

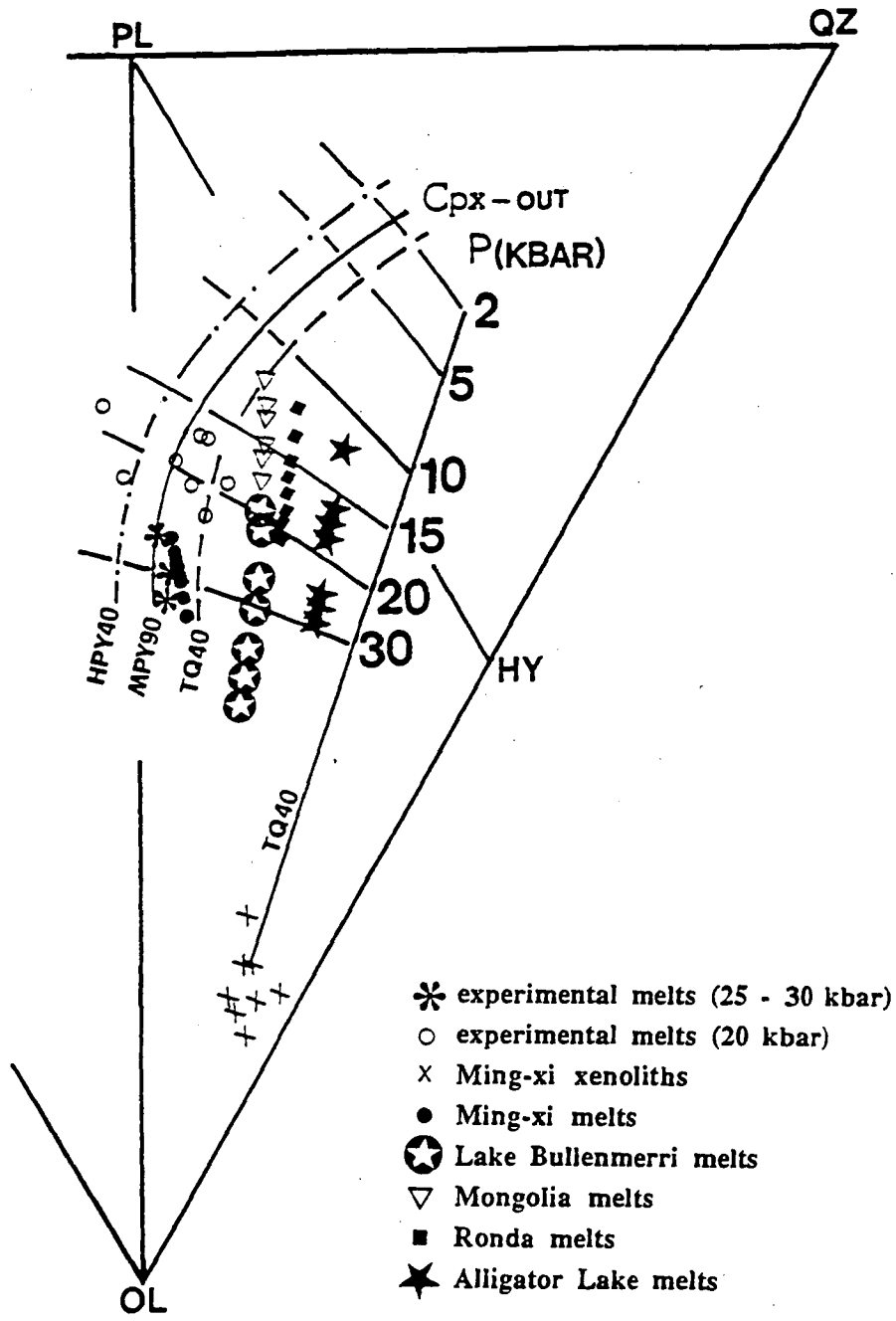

Figure 2.3. Compositions of calculated melts in equilibrium with Ming-xi lherzolites and some spinel peridotite suites from literature plotted on the JdTs-Ol-Qz plane of the basalt tetrahedron (molecular Norms) with references to the melting grid of Falloon et al. (1988). Some representative Ming-xi xenoliths are also shown on the plot. Cpx-out lines mark the disappearance of clinopyroxene with increasing melting temperature in three different peridotite systems (Hawaiian pyrolite minus 40% olivine; Morb pyrolite minus 40% olivine; and Tinaquillo lherzolite minus 40% olivine). Compositions of the experimental melts are given in Table 2.5.

Table 2.5 Representative Compositions of Experimental Melts

Ref.	1	2	3	4	4	4	5	5	5	6	6	6	6	6
S. M.	519-16	KLB-1	359	KRB	KRB	L45	TQ40	HPY40	HPY40	MPY90	MPY90	MPY87	MPY87	MPY87
P(Kb)	20	30	20	20	25	30	20	20	20	18	25	20	20	20
T(°C)	1450	1550	1250	1400	1425	1550	1475	1450	1500	1450	1550	1380	1405	1430
SiO2	46.86	46.90	47.85	49.72	48.77	47.50	47.52	46.09	48.15	47.88	46.86	46.94	47.52	47.39
TiO2	0.72	0.90	0.76	1.14	1.66	1.08	0.52	2.56	2.35	0.66	0.66	0.70	0.73	0.60
Al2O3	14.59	11.00	14.60	13.51	15.32	11.88	12.96	14.71	10.76	15.16	13.73	15.44	14.39	14.26
Cr2O3	0.14	0.40	0.09	0.15	0.10	0.11	0.39	0.31	0.60	0.36	0.38	0.20	0.38	0.28
FeO*	10.30	7.80	10.70	10.36	8.70	9.21	8.29	10.34	10.16	8.12	8.06	9.83	9.62	9.44
MnO	0.12	0.20	0.17	0.11	0.14	0.21								
MgO	15.98	19.20	12.67	14.25	12.18	18.71	17.79	13.90	16.27	14.58	17.75	14.24	14.51	15.46
CaO	9.29	12.20	11.31	8.02	8.80	8.84	12.09	10.24	9.38	11.64	10.92	10.53	10.98	10.94
Na2O	1.94	1.20	1.71	2.34	3.09	2.11	1.03	1.29	1.87	1.56	1.60	2.30	1.84	1.60
K2O	0.10		0.17	0.63	1.26	0.09		0.55	0.39					
P2O5				0.16	0.30									
Sum	100.04	99.80	100.03	100.39	100.32	99.74	100.59	99.99	99.93	99.96	99.96	100.18	99.97	99.97
Mg#	73.44	81.44	67.85	71.03	71.39	78.36	79.28	70.56	74.06	76.19	79.70	72.09	72.89	74.49

S.M.: Starting mix.
Ref: 1 - Stolper (1980); 2 - Takahashi (1986); 3 - Kushiro (1990); 4 - Takahashi & Kushiro (1983); 5 - Falloon et al. (1988); 6 - Falloon & Green (1988).

approach to this complex problem. However, it is a method that makes the maximum use of the major element geochemistry of the xenoliths. Compared with previous modelling methods, it is based on less assumptions and gives reasonable estimates of melt compositions and extent of melting. The precision of the method depends critically on the relationship between individual xenoliths in the suite, which determines the regression relations for the calculation. The assumption that xenoliths in a suite are related by the same partial melting event(s) may not always be true; and there is no guarantee that only one part of the mantle is sampled by the host basalts. Nevertheless, petrography and thermobarometric calculations often suggest that most xenoliths in a suite do have similar origin. Therefore, the assumption is acceptable in most cases. An advantage of this method is that the caculated melt compositions can be directly compared with results from experimental studies of peridotite melting; which enables an estimation of the likely melting conditions (pressure and temperature). The pressure thus obtained can also be regarded as the depth of origin for the xenoliths. This information is particularly useful for spinel peridotites because of the lack of reliable geobarometry for this type of rocks.

Because the major element geochemistry represents the final product of the complex partial melting process, the calculation can give no more information than the final results of this process. Details of this complex process, such as initiation of melting, melting styles (batch, fractional, or continuous - concept of Hanson & Langmuir, 1978), melt segregation and migration, can not be learned from the major element geochemistry alone. Recent progress in theoretical analysis of this dynamic process has introduced new methods to investigate these problems (e.g. Waff, 1980; Stolper et al., 1981; McKenzie, 1984; Scott & Stevenson, 1989). Detailed and systematic studies of trace element geochemistry in mantle samples may also help to unravel some parts of the partial melting mystery. However, these studies can not be separated from one another. Results obtained from different approaches should be consistent if they are close to reality. In this sense, the modelling method detailed in this study may provide some crude measure for other approaches.

Chapter Three

A Comprehensive Dataset of Mineral Chemistry in a Model Lherzolite System under Upper Mantle Conditions

Chapter Three

A Comprehensive Dataset of Mineral Chemistry in a Model Lherzolite System under Upper Mantle Conditions

3.1 Introduction

Extensive studies of mantle-derived samples (e.g. inclusions in diamonds, xenoliths in kimberlites and alkali-basalts, ultramafic intrusions and peridotites in the ophiolite complexes) have convincingly demonstrated that the upper mantle is predominantly made of peridotites (Ringwood, 1975; Nixon, 1987; Menzies, 1990). The mineralogy of the peridotitic upper mantle was initially inferred and then experimentally confirmed to vary from the plagioclase-lherzolite facies, to the spinel-lherzolite facies, and to the garnet-lherzolite facies with increasing pressure/depth (Green & Ringwood, 1963,1967a). Mineral composition variation in the peridotitic upper mantle has partly been studied empirically and experimentally in association with the development of various mineral geothermometers and geobarometers (e.g. Davis & Boyd, 1966; Wood & Banno, 1973; MacGregor, 1974; Råheim & Green, 1974a; Lindsley & Dixon, 1976; Wells, 1977; Mori & Green, 1978; O'Neill & Wood, 1979; Sachtleben & Seck, 1981; Harley, 1984a & b; Nickel & Green, 1985; Nickel, 1989; Brey et al., 1990). These studies have shown that the change in mineral chemistry with pressure and temperature should be gradual and systematic. The present study aims to investigate the details of such systematic change. Furthermore, mineral chemistry is a fundamental aspect of petrology. The dataset presented here may be useful in understanding both peridotite and basalt petrogenesis, and is relevant to studies of mantle petrology and geodynamics.

3.2 Experimental Details

Experiments were conducted in a single-stage, 0.5" piston-cylinder apparatus hosted at the Geology Department, University of Tasmania, using techniques similar to those described by Green & Ringwood (1967b). Experimental pressure covers 20 - 35 kbar; temperature ranges from 1200°C to 1500°C. Samples were contained in specpure graphite capsules, surrounded by inner graphite heater, pyrex glass, and outer talc sleeve (the Dry-assembly type of Nickel, 1983). No special oxygen-buffer was employed.

The experimental temperature was controlled by a Eurotherm Model 818P controller/programmer connected with a $W_{97}Re_3/W_{75}Re_{25}$ thermocouple. The ramping function of this controller allowed a standard procedure to be adopted for the heating of all

experiments to desired run temperature, as follows: from the ambient temperature to 650°C, the heating rate was set at 80°C per minute; from 650°C to the temperature 40°C below the desired experimental run temperature, heating rate was increased to 90°C per minute; in the last 40°C before reaching the experimental temperature, the temperature was brought very slowly to the run value at the rate of 20°C per minute. This prevented temperature overshoot. After the set point was reached, run temperature was maintained by the automatic controller to within ± 2°C of the desired value. A pressure correction of -10% relative to the nominal piston pressure was applied for all runs. Pressure was raised to the experimental value well before the heating of the samples started and was constantly monitored. For runs overnight, pressure could drop by upto 0.6 kbar.

Experimental duration was determined by trial and error, and varies according to the run temperature. Because all experiments were anhydrous, relatively long run times were anticipated. It was believed that 7 days at 1200°C, 3 - 4 days at 1300°C, 1 - 2 days at 1400°C, and 3 - 6 hours at 1500°C were practically long enough to reach equilibrium. This is supported by two reversal runs (details below).

The starting material for the set of experiments was sintered oxides, prepared in the manner described by Falloon et al. (1988). The composition is a modified Tinaquillo lherzolite, TQ40 (Jaques & Green, 1980), representative of a relatively depleted upper mantle. The experimental run details are given in Table 3.1.

Analysis of the experimental products was performed on a Cameca SX50 electron microprobe in the WDS mode. Three elements were analysed simultaneously at one time through three diffraction crystals: Na, Mg, Al, Si (TAP); K, Ca, Ti, Cr (PET); and Mn, Fe, Ni (LiF). The analytical conditions were 15 kV, 20 nA with counting time of 20 seconds each for most elements except Si, Al, and Mg (10 seconds each). Mineral standards used are from Jarosewich et al. (1980). Pure metals are used as Mn and Ni standards. The detection limit for each element is: Na 0.03; Mg 0.063; Al 0.039; Si 0.054; Ca 0.039; Ti 0.048; Cr 0.064; Mn 0.051; Fe 0.069; Ni 0.058 (wt%). The X-ray data were processed by an in-house PDP mini-computer with the PAP data reduction scheme. All analyses were made in a spot-mode with the electron beam size varing between 1 and 5 microns. The results are normalised to 100% to facilitate comparison.

3.3 Equilibrium Evaluation

For the experimental data to be useful it is necessary to demonstrate attainment of equilibrium. This can be very difficult, particularly in complex multi-component systems (Perkins & Newton, 1980; Brey et al., 1990). The idea of approaching equilibrium from different chemical directions (Brey et al. 1990) is theoretically sound, but practically difficult. To host more than two starting mixes in a small capsule with fixed volume limits

Table 3.1 Experimental Run Details

starting mix		Run#	P(kbar)	T(°C)	Duration(h)	Product	observations
	TQ40	T3101	25	1200	73	Gt Sp 2px Ol	
		T3105	22	1200	72	Sp 2px Ol	
SiO2	47.51	T3108	23	1200	72	Sp 2px Ol	
TiO2	0.13	T3126	27	1200	173.3	Gt Sp 2px Ol	
Al2O3	5.35	T3130	25	1300	72	Sp 2px Ol	
Cr2O3	0.75	T3136	27	1300	72	Gt Sp 2px Ol	
Fe2O3	0.15	T3141	23	1300	57	Sp 2px Ol	
FeO	7.38	T3145	20	1200	168	Sp 2px Ol	
MnO	0.18	T3151	30	1200	168	Gt 2px Ol	+ metastable Sp
NiO	0.43	T3158	20	1300	76.6	Sp 2px Ol	
MgO	32.8	T3160	30	1300	74.6	Gt Sp 2px Ol	
CaO	4.97	T3163	30	1400	26	Gt 2px Ol	+ metastable Sp
Na2O	0.3	T3164	25	1400	24.3	Sp 2px Ol	
K2O	0.03	T3167	27	1400	24	Gt Sp 2px Ol	
P2O5	0.02	T3168	25	1200	96.3	Gt Sp 2px Ol	buffer assembly
Sum	100	T3239	20	1200	168	Gt Sp 2px Ol	reversal of T3168
		T3247	27	1300	75.5	Gt Sp 2px Ol	buffer assembly
		T3249	30	1500	3	Gt Sp 2px Ol	tiny Sp
		T3299	35	1400	24	Gt 2px Ol	
		T3302	35	1500	3	Gt 2px Ol	
		T3306	35	1200	168	Gt 2px Ol	
		T3316	20	1300	96	Sp 2px Ol	reversal of T3247
		T3342	35	1400	48	Gt 2px Ol	reversal of T3247
		T3345	35	1300	96.5	Gt 2px Ol	
		T3355	26	1300	94	Gt Sp 2px Ol	
		T3360	26	1400	25	Sp 2px Ol	
		T3364	28	1300	86.5	Gt Sp 2px Ol	
		T3378	28	1500	3	Gt Sp 2px Ol	
		T3430	30	1500	3	Gt Sp 2px Ol	tiny Sp
		T3453	28	1400	39	Gt Sp 2px Ol	
		T3454	28	1200	168	Gt Sp 2px Ol	Sp metastable ?
		T3524	22.5	1400	48.3	Sp 2px Ol	
		T3526	29	1400	49	Gt Sp 2px Ol	
		T3527	32	1500	5	Gt 2px Ol	

the amount of mixes to be loaded into the capsule. In the first few runs we followed the sample arrangement method of Brey et al. (1990) and loaded three different starting mixes in one graphite capsule, with each sample weighing less than 5 milligrams. The results showed that these small samples did not consistently match the prepared starting compositions and non-equilibrium mineral assemblages were produced (indicated by the presence of quartz in the charges). As a result, the multi-mix method was not adopted, and only one composition (TQ40) was used. Most runs in the present study are of the synthesis type, and are believed to closely approach equilibrium. This is demonstrated in three ways. Firstly, three duplication runs were conducted, each pair under identical P, T conditions. Each pair produced minerals with identical compositions within the experimental and analytical errors. Secondly, two sets of "reversal" type experiments were performed to explore the possibility of "strictly" reversing mineral composition in the complex multi-component system. Thirdly, within the analytical limit, all the minerals except spinels in the run products are reasonably homogeneous. They show systematic variations in composition with changing pressure and temperature. The details of the first two points are discussed below. The third point is illustrated in the analysis of the experimental results.

In the three pairs of runs under identical P, T conditions, one pair was made at 1500°C, 30 kbar, and lasted 3 hours. The dry assembly was used in both runs (T3249 & T3430, Table 3.1). Both produced garnet, two pyroxenes and olivine. The compositions of these phases agree closely (Table 3.2). For example, garnet in T3249 has Mg# ranging from 85.9 to 87.1, Cr# ranging from 6.8 to 8.36. In T3430 its Mg# is 86.14 - 86.57, and Cr# is 7.75 - 8.57. There is a small difference in the sample arrangement for the other two pairs. For the pair at 1200°C, 25 kbar (T3101 & T3168) a buffer assembly was used for T3168 but a dry assembly for T3101. The buffer assembly was made with a large graphite capsule (with about twice as much capacity as the small capsule in the dry assembly) sealed inside a platinum capsule, surrounded by boron nitride, pyrex glass and outer talc-sleeve. Both T3168 & T3101 produced spinel, garnet, two pyroxenes and olivine. The amount of olivine and clinopyroxene present in the two charges is similar, but there is appreciably more orthopyroxene and spinel, and less garnet in T3101 (dry assembly) than in T3168 (buffer assembly). The compositions of orthopyroxene, spinel, garnet in the two runs are slightly different. This may be directly related to the type of capsule used with possible small P, T calibration difference between the small and large capsule assemblies. The buffer assembly may require <10% pressure correction or the "hot spot" may be 20 - 30°C different from the thermocouple. If the bulk composition is the same in the two runs then the difference in the mineral proportion and composition must reflect different P, T, fO_2 conditions. However, the other pair (T3136 & T3247) at 1300°C, 27 kbar gives an opposite sense of P, T difference. The run with dry assembly

(T3136) has more garnet, less spinel and orthopyroxene (i.e. higher P, lower T) than the run with the buffer assembly (T3247). An additional problem may arise for the small capsule in that the composition of the starting mix loaded into each capsule may be slightly different. This would produce different mineral proportions but in the five-phase assemblage should not give mineral proportions matching different P, T conditions. Despite this problem, the mineral compositions in the respective pairs are very similar (Table 3.2), indicating less than 0.5 kbar difference.

The first of the two sets of reversal runs involves re-equilibration of minerals synthesized at higher pressure (T3168, 1200°C, 25 kbar) at the same temperature but lower pressure (T3239, 1200°C, 20 kbar). Some garnet metastably persisted in T3239. However, the change in mineral compositions relative to the original starting composition (T3168) indicates that these minerals are in the progress of re-equilibration at the lower pressure. This is clearly shown by a decrease in the amount of olivine and garnet, and an increase in the amount of spinel and orthopyroxene in T3239 relative to T3168. Thus the reaction Olivine + Garnet = Spinel + Orthopyroxene is proceeding to the right in T3239.

The other set of reversal experiments consists of two runs, one at lower pressure (T3316, 1300°C, 20 kbar), the other at higher pressure and temperature (T3342, 1400°C, 35 kbar) relative to the synthesis conditions of the starting minerals (T3247, 1300°C, 27 kbar). This set is very successful. Not only the garnet in the starting mix is completely eliminated at the lower pressure (T3316), and the spinel completely consumed at the higher pressure (T3342), but also the mineral compositions match those of the synthesis runs at these pressure, temperature conditions (T3158, 1300°C, 20 kbar; T3299, 1400°C, 35 kbar; Table 3.2). It is deduced that the metastable persistence of garnet in the first set of reversal runs is probably due to a slow reaction rate at the relatively lower temperature of T3239.

Based on these repeated and reversal experiments it was concluded that synthesis runs at the chosen pressure, temperature conditions and run durations can produce equilibrium mineral assemblages.

3.4 Experimental Results

All runs reported in this study are anhydrous and subsolidus. Run products are composed of olivine and two pyroxenes, with the presence of spinel, or garnet, or both. No melt is detected in the run products. Typical examples are shown in Plate.3. Olivine, orthopyroxene, clinopyroxene form large tabular crystals. Garnet grains are commonly large, subhedral, and poikilitic. The average size of garnet grains and the amount of inclusions tend to decrease with increasing pressure. Spinel is normally less than 5 microns in diameter and less than 3% in the charge. Because of this, analysis of spinel is

Table 3.2 Comparison of Mineral Compositions and Calculated Modes in the Repeated and Reversal Runs

	T3101		T3168		T3136		T3247		T3145		T3239		T3316		T3158		T3342		T3299		T3249		T3430	
P(kbar)	25		25		27		27		20		20		20		20		35		35		30		30	
T(°C)	1200		1200		1300		1300		1200		1200		1300		1300		1400		1400		1500		1500	
	mean	s.d.	mean	s.d.	mean	s.d.	mean	s.d.	mean	s.d.	mean	s.d.	mean	s.d.	mean	s.d.	mean	s.d.	mean	s.d.	mean	s.d.	mean	s.d.
Ol%§	32.90		33.97		34.74		33.83		30.75		33.93		30.86		30.39		35.50		34.45		34.26		33.72	
Mg#	89.22	0.12	89.48	0.19	89.22	0.20	88.68	0.47	89.56	0.18	88.89	0.12	89.13	0.19	89.70	0.03	89.16	0.16	89.92	0.11	89.82	0.22	89.84	0.09
CaO%	0.12	0.01	0.17	0.04	0.19	0.02	0.22	0.01	0.27	0.03	0.16	0.03	0.24	0.04	0.31	0.08	0.19	0.04	0.22	0.02	0.33	0.09	0.31	0.05
Opx%	37.16		32.19		33.68		32.85		42.52		33.54		42.42		42.09		26.05		24.67		26.35		25.44	
Mg#	89.81	0.01	90.15	0.09	89.77	0.01	90.20	0.95	89.71	0.34	89.87		89.59	0.14	89.94	0.17	89.59	0.18	90.36	0.01	90.44	0.28	90.35	0.22
Cr#	7.95	0.80	12.01	2.20	8.71	0.28	7.68	0.14	7.03	0.78	11.38		8.84	0.50	9.16	0.76	9.93	0.60	13.02	0.70	9.12	0.59	8.51	1.41
CaO	1.76	0.47	1.44	0.06	1.74	0.03	1.99	0.07	1.93	0.12	1.47		1.88	0.04	2.01	0.07	2.01	0.17	2.00	0.06	2.51	0.09	2.44	0.01
Na2O	0.13	0.02	0.15	0.01	0.15	0.01	0.17	0.01	0.10	0.01	0.13				0.11	0.01	0.17	0.01	0.20	0.05	0.15	0.01	0.14	0.01
Cpx%	19.89		22.08		21.78		24.70		23.90		20.31		23.95		25.30		23.80		24.92		28.65		31.03	
Mg#	89.05	0.64	89.96	0.06	89.01		88.87	1.46	88.91	0.22	89.68		89.05		89.20	0.27	89.03	0.49	89.49	0.47	89.72	0.43	89.20	0.85
Cr#	9.83	0.25	10.16	0.57	10.50		8.95	0.32	9.49	0.15	13.66		12.93		10.72	0.59	12.84	0.33	13.06	3.11	10.97	0.74	10.69	0.85
CaO	18.55	0.17	17.69	0.16	17.59		15.63	0.42	17.61	0.09	18.52		17.24		16.45	0.12	15.06	0.11	14.70	0.87	13.16	1.22	12.35	0.98
Na2O	1.02	0.04	1.03	0.04	0.97		0.97	0.04	0.77	0.01	1.04		0.57		0.64	0.03	0.89	0.01	0.85	0.05	0.60	0.03	0.54	0.15
Gt%	9.18		11.25		9.34		7.71				11.73						14.66		15.96		10.78		10.20	
Mg#	82.70	0.32	83.89	0.17	83.71	0.43	84.16				82.79						83.59	0.59	85.86	0.04	87.07	0.36	86.53	0.27
Cr#	5.67	0.17	4.56	0.93	5.86	1.06	5.25				4.72						5.71	1.46	6.51	1.92	8.13	0.88	8.12	0.23
CaO	6.25	0.20	6.50	0.06	6.23	0.03	5.87				6.28						5.58	0.14	5.88	0.10	5.93	0.36	6.12	0.17
	*composition range of spinels																							
Sp%	0.86		0.51		0.47		0.91		2.83		0.49		2.77		2.22									
Mg#	77.89	79.20	78.32	80.30	78.42	81.70	76.19	81.10	81.45	83.50	79.36	81.70	80.69	79.50	80.91	81.63								
Cr#	20.73	17.30	21.30	18.50	24.29	15.10	26.77	14.50	21.22	12.30	18.22	9.41	17.34	23.97	14.77	18.98								
Fe3:Fe2	0.21	0.19	0.24	0.24	0.23	0.28	0.23	0.27	0.26	0.26	0.24	0.17	0.19	0.25	0.09	0.22								

§). mineral modes (in wt%) were calculated from starting composition and mineral compositions.

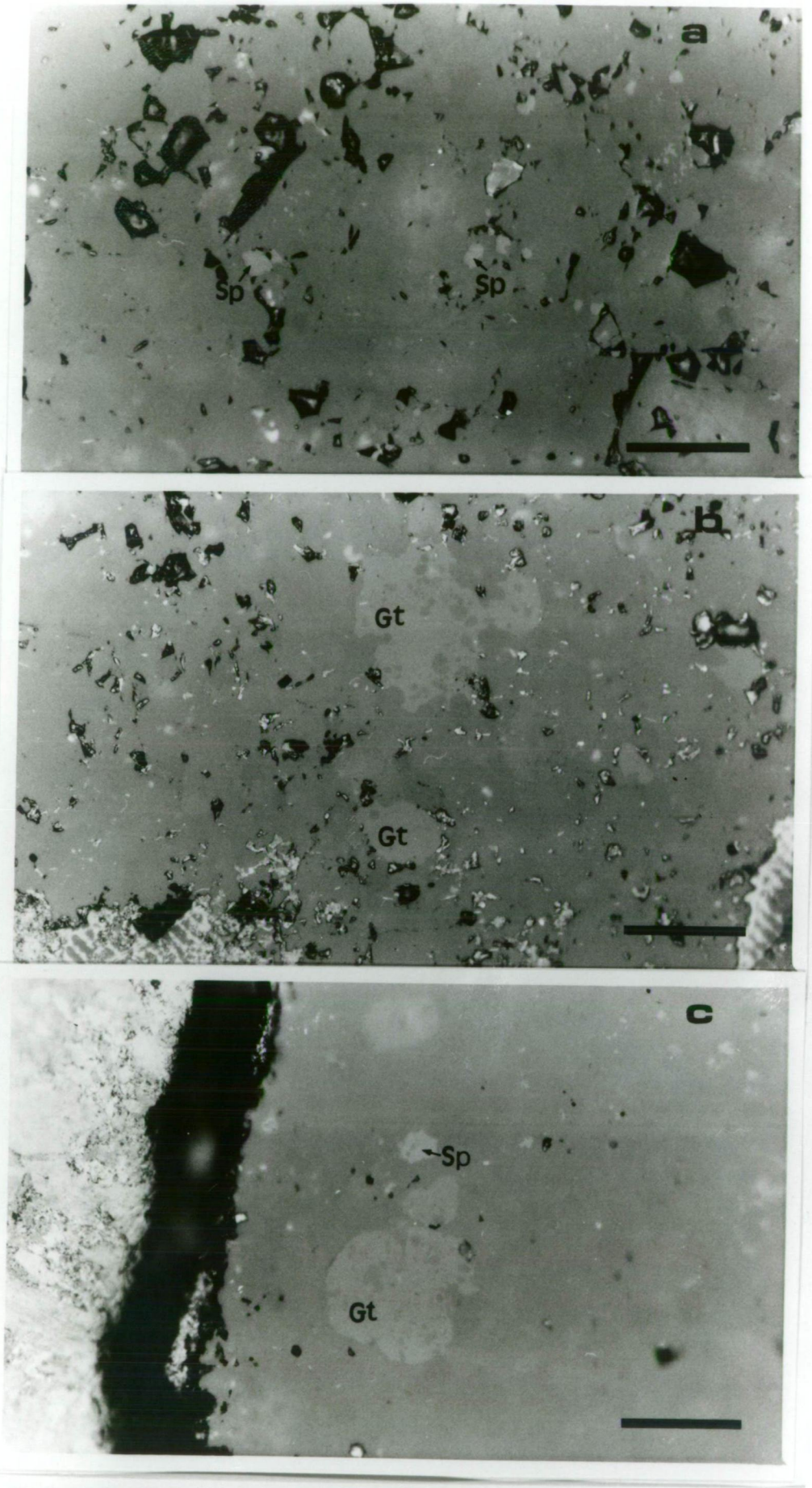

Plate 3. Typical experimental run products

(a) spinel lherzolite, T3108, 1200°C, 23kbar, 72 hours;

(b) garnet lherzolite, T3163 1400°C, 30 kbar, 26 hours;

(c) spinel and garnet lherzolite, T3101, 1200°C, 25 kbar, 73 hours.

(scale bar = 5 μm)

very difficult. Its analytical quality is poorer than other minerals'. Care was taken to avoid analysis of inclusions in garnet. Good stoichiometry for garnet (Si = 3.00 ± 0.02, total cations = 8.00 ± 0.02 per 12 oxygens) is used to distinguish true compositions from contaminated ones (Nickel, 1989).

One of the main objectives of this study is to locate the precise position of the spinel-lherzolite to garnet-lherzolite transition boundary in this system. It is known that this transition is a univariant line in the simple MAS and CMAS systems but changes to a divariant field in the complex multi-component system (e.g. Green & Ringwood, 1967a; O'Neill, 1981; Newton, 1989). In this study the garnet-in boundary is located within ± 0.3 kbar, and the spinel-out boundary within ± 0.6 kbar. In the experimental pressure, temperature range, the two boundaries are approximated by two straight lines (Fig.3.1). At lower temperatures, they are likely to be curves similar to the univariant line in the MAS system (Newton, 1989). The appearance of garnet is very sensitive to pressure. A barometer based on this was developed by O'Neill (1981) and further improved by Webb & Wood (1986). It will be shown that the two versions of the barometer do not adequately describe the spinel-facies to the garnet-facies transition, based on the data presented here and further experimental results in high-Cr systems (Chapter Four). Chapter Four discusses details of these problems and presents a new barometer for peridotites with coexisting equilibrium spinel and garnet.

3.4.1 Composition Variations of Individual Mineral in P-T Space

Olivine: The composition of olivine does not change greatly in the experimental pressure, temperature range (Table 3.3). Its Mg# varies between 89 and 90; NiO content ranges from 0.60 to 1.00%; MnO, from 0.10 to 0.22%; and CaO, from 0.11 to 0.38%. The high NiO content is due to the initial high NiO in the starting mix, a result of subtraction of 40% Ni-free olivine $(Mg_{91.9}Fe_{8.0}Mn_{0.1})_2SiO_4$ from the original Tinaquillo lherzolite composition. CaO solubility in olivine increases with increasing temperature and decreasing pressure. This is broadly consistent with result of ion-probe analyses of CaO in natural olivines (Hervig, et al., 1986): olivine as inclusions in diamond and in kimberlite-borne *cold* garnet lherzolites have the lowest CaO content, whereas those in the *hot* garnet lherzolite contain the highest CaO. This is also consistent with the experimental results in the simple CFMS system (Adams and Bishop, 1986) and the complex system with the bulk composition SC1 (Köhler & Brey, 1990). The effect of temperature on this solubility is greater than that of pressure (Fig.3.2), implying better potential as a temperature-indicator than as a pressure-indicator.

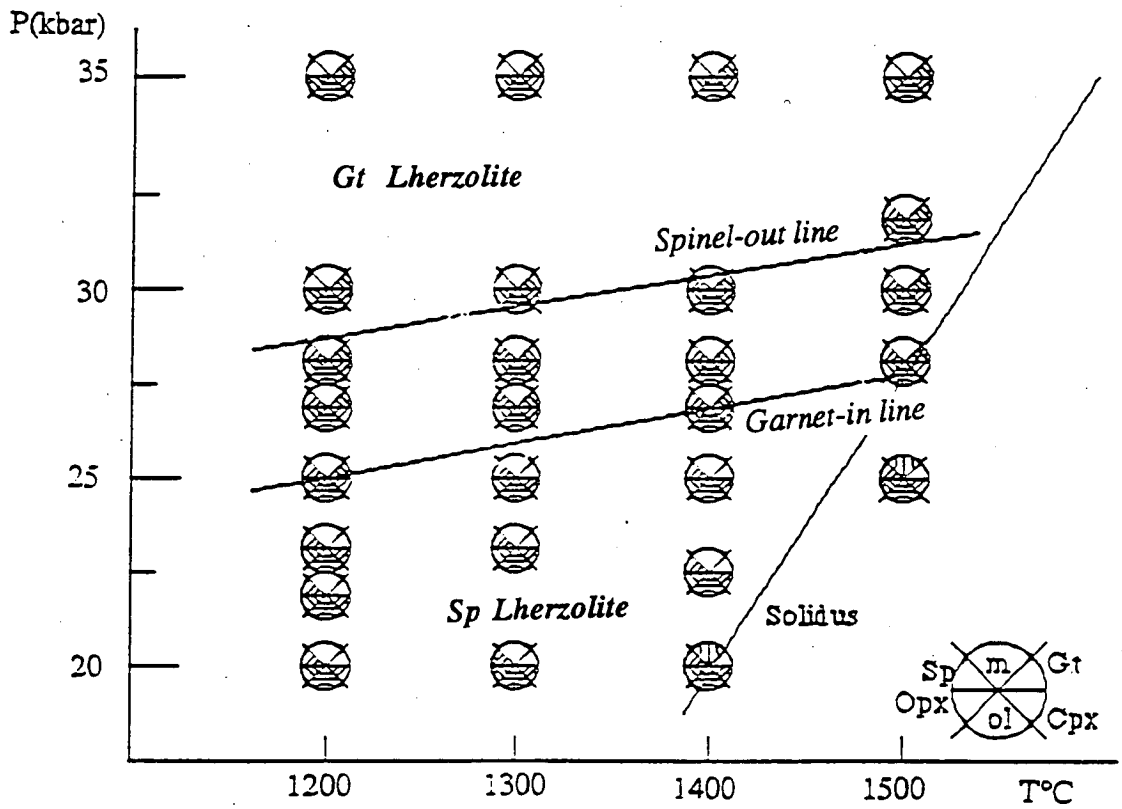

Figure 3.1. Phase relations in the TQ40 lherzolite system.
(ol: olivine, Opx: orthopyroxene, Cpx: clinopyroxene, Sp: spinel, Gt: garnet, m: melt)

Table 3.3 Representative Compositions of Experimental Olivines

Run#	T3145	T3239	T3105	T3108	T3101	T3168	T3126	T3454	T3151	T3306	T3316	T3158	T3141	T3130	T3355	T3136	T3247	T3364
P(kbar)	20	20	22	23	25	25	27	28	30	35	20	20	23	25	26	27	27	28
T(°C)	1200	1200	1200	1200	1200	1200	1200	1200	1200	1200	1300	1300	1300	1300	1300	1300	1300	1300
Ol wt%	30.75	33.93	32.28	31.46	32.9	33.97	34.18	33.79	34.2	35.26	30.86	30.39	32.61	32.61	34.08	34.74	33.83	34.59
SiO2	40.62	40.47	40.64	40.34	40.25	40.64	40.54	40.09	40.46	40.70	40.56	40.76	40.92	40.65	40.55	40.84	40.37	40.60
FeO	10.10	10.67	10.54	10.34	10.38	10.11	10.67	10.16	10.46	10.07	10.43	9.88	10.27	10.38	10.20	10.27	10.86	10.22
MnO	0.19	0.09	0.16	0.17	0.15	0.15	0.14	0.14	0.13	0.19	0.13	0.16	0.15	0.15	0.16	0.20	0.14	0.18
NiO	0.21	0.75	0.79	0.82	0.95	0.70	0.85	1.00	0.85	0.88	0.70	0.62	0.81	0.90	1.00	0.77	0.67	0.93
MgO	48.61	47.86	47.74	48.09	48.15	48.23	47.62	48.50	47.98	48.00	47.94	48.28	47.64	47.63	47.91	47.73	47.75	47.93
CaO	0.27	0.16	0.13	0.24	0.12	0.17	0.18	0.11	0.12	0.16	0.24	0.31	0.21	0.28	0.18	0.19	0.22	0.14
Sum	100	100	100	100	100	100	100	100	100	100	100	100	100	100	100	100	100	100
Total*	99.52	99.68	99.42	101.22	99.04	99.74	99.96	98.96	100.31	99.79	100.1	100.66	100.61	99.53	98.7	100.92	100.26	99.23
Oxygen	4	4	4	4	4	4	4	4	4	4	4	4	4	4	4	4	4	4
Si	0.998	0.999	1.002	0.996	0.994	1.000	1.001	0.990	0.998	1.002	1.000	1.002	1.008	1.003	1.000	1.006	0.997	1.001
Fe	0.208	0.220	0.217	0.214	0.214	0.208	0.220	0.210	0.216	0.207	0.215	0.203	0.211	0.214	0.210	0.212	0.224	0.211
Mn	0.004	0.002	0.003	0.004	0.003	0.003	0.003	0.003	0.003	0.004	0.003	0.003	0.003	0.003	0.003	0.004	0.003	0.004
Ni	0.004	0.015	0.016	0.016	0.019	0.014	0.017	0.020	0.017	0.018	0.014	0.012	0.016	0.018	0.020	0.015	0.013	0.018
Mg	1.781	1.761	1.755	1.769	1.773	1.770	1.753	1.785	1.765	1.762	1.762	1.769	1.749	1.752	1.762	1.752	1.759	1.762
Ca	0.007	0.004	0.004	0.006	0.003	0.005	0.005	0.003	0.003	0.004	0.006	0.008	0.006	0.007	0.005	0.005	0.006	0.004
Sum	3.002	3.001	2.998	3.004	3.006	3.000	2.999	3.010	3.002	2.998	3.000	2.998	2.993	2.997	3.000	2.994	3.003	2.999
Mg#	89.56	88.88	88.98	89.23	89.21	89.48	88.83	89.49	89.10	89.47	89.13	89.70	89.22	89.10	89.33	89.22	88.68	89.32
C**	0.36	0.21	0.17	0.32	0.16	0.23	0.24	0.15	0.16	0.21	0.32	0.41	0.28	0.38	0.24	0.25	0.29	0.19
M	89.24	88.69	88.82	88.95	89.07	89.27	88.62	89.36	88.96	89.28	88.84	89.33	88.97	88.77	89.12	89.00	88.42	89.15
F	10.40	11.10	11.00	10.73	10.77	10.50	11.14	10.50	10.88	10.51	10.84	10.26	10.75	10.86	10.64	10.75	11.28	10.66

*) the original totals.

**) $Mg\# = \frac{100Mg}{Mg + Fe^{2+}}$ $Cr\# = \frac{100Cr}{Al + Cr}$ $Ca\# = \frac{100Ca}{Ca + Na}$ $C = \frac{100Ca}{Ca + Mg + Fe^{2+}}$ $M = \frac{100Mg}{Ca + Mg + Fe^{2+}}$ $F = \frac{100Fe^{2+}}{Ca + Mg + Fe^{2+}}$

Table 3.3 Representative Compositions of Experimental Olivines (cont'd)

Run#	T3160	T3345	T3524	T3164	T3360	T3167	T3453	T3526	T3163	T3342	T3299	T3378	T3249	T3430	T3527	T3302
P(kbar)	30	35	22.5	25	26	27	28	29	30	35	35	28	30	30	32	35
T(°C)	1300	1300	1400	1400	1400	1400	1400	1400	1400	1400	1400	1500	1500	1500	1500	1500
Ol%	34.08	35.14	31.71	32.66	32.29	34.45	34.35	33.14	35.16	35.5	34.45	34.76	34.26	33.72	33.71	34.05
SiO2	40.70	40.80	40.40	40.56	40.63	40.52	40.70	40.38	40.76	40.69	40.79	40.78	40.80	40.63	40.47	40.90
FeO	9.54	10.31	10.01	10.18	9.95	10.50	10.25	10.25	10.19	10.34	9.71	9.53	9.73	9.73	9.96	9.24
MnO	0.14	0.15	0.15	0.16	0.14	0.16	0.18	0.16	0.14	0.17	0.10	0.22	0.13	0.19	0.18	0.17
NiO	0.70	0.90	0.96	0.78	0.70	0.77	0.92	0.81	0.86	0.91	0.60	0.86	0.86	0.87	0.80	0.71
MgO	48.67	47.71	48.26	48.05	48.35	47.80	47.72	48.12	47.77	47.70	48.57	48.28	48.15	48.27	48.21	48.65
CaO	0.25	0.14	0.22	0.27	0.23	0.25	0.23	0.27	0.28	0.19	0.22	0.34	0.33	0.31	0.38	0.33
Sum	100	100	100	100	100	100	100	100	100	100	100	100	100	100	100	100
Total	100.29	99.26	98.27	99.82	98.57	99.92	99.9	98.31	99.89	99.71	99.99	100.43	99.61	99.24	98.42	99.57
Oxygen	4	4	4	4	4	4	4	4	4	4	4	4	4	4	4	4
Si	1.000	1.005	0.996	1.000	1.000	1.000	1.003	0.996	1.004	1.003	1.002	1.002	1.003	1.000	0.997	1.003
Fe	0.196	0.212	0.206	0.210	0.205	0.217	0.211	0.212	0.210	0.213	0.199	0.196	0.200	0.200	0.205	0.189
Mn	0.003	0.003	0.003	0.003	0.003	0.003	0.004	0.003	0.003	0.004	0.002	0.005	0.003	0.004	0.004	0.004
Ni	0.014	0.018	0.019	0.016	0.014	0.015	0.018	0.016	0.017	0.018	0.012	0.017	0.017	0.017	0.016	0.014
Mg	1.782	1.753	1.774	1.765	1.773	1.758	1.754	1.770	1.755	1.753	1.778	1.769	1.765	1.771	1.771	1.779
Ca	0.007	0.004	0.006	0.007	0.006	0.007	0.006	0.007	0.007	0.005	0.006	0.009	0.009	0.008	0.010	0.009
Sum	3.001	2.995	3.004	3.001	3.000	3.000	2.997	3.004	2.996	2.997	2.999	2.998	2.997	3.000	3.003	2.997
Mg#	90.09	89.19	89.57	89.38	89.65	89.03	89.24	89.32	89.31	89.16	89.92	90.03	89.82	89.84	89.61	90.38
C	0.33	0.19	0.30	0.36	0.31	0.33	0.31	0.37	0.38	0.26	0.29	0.45	0.44	0.42	0.50	0.44
M	89.79	89.02	89.31	89.06	89.37	88.73	88.97	89.00	88.98	88.93	89.65	89.62	89.42	89.46	89.16	89.98
F	9.88	10.79	10.39	10.58	10.32	10.93	10.72	10.64	10.65	10.81	10.05	9.92	10.13	10.12	10.34	9.58

Table 3.4 Representative Compositions of Experimental Orthopyroxenes

Run#	T3145	T3239	T3105	T3108	T3101	T3168	T3126	T3454	T3151	T3306	T3316	T3158	T3141	T3130	T3355	T3136	T3247
P(kbar)	20	20	22	23	25	25	27	28	30	35	20	20	23	25	26	27	27
T(°C)	1200	1200	1200	1200	1200	1200	1200	1200	1200	1200	1300	1300	1300	1300	1300	1300	1300
Opx%	42.52	33.54	41.63	42.01	37.16	32.19	34.54	31.46	29.68	27.18	42.42	42.09	41.05	41.22	34.69	33.68	32.85
SiO2	53.88	54.50	53.91	53.22	54.16	54.64	53.85	55.23	55.41	55.64	53.54	53.00	53.52	53.89	54.54	54.11	53.93
TiO2	0.12	0.09	0.15	0.11	0.13	0.11	0.13	0.11	0.15	0.13	0.13	0.12	0.15	0.11	0.16	0.14	0.14
Al2O3	5.66	4.64	5.85	6.49	4.95	4.40	5.31	3.66	3.19	2.83	5.81	6.28	6.32	6.13	4.93	5.29	5.83
Cr2O3	0.63	0.89	0.56	0.72	0.64	0.90	0.84	0.78	0.51	0.51	0.84	0.94	0.80	0.67	0.69	0.75	0.73
FeO	6.36	6.35	6.45	6.05	6.37	6.20	6.43	6.26	6.44	6.22	6.42	6.18	6.15	6.33	6.31	6.32	5.99
MnO	0.11	0.13	0.21	0.20	0.16	0.12	0.19	0.13	0.15	0.14	0.16	0.14	0.19	0.13	0.16	0.14	0.14
NiO	0.10	0.22	0.28	0.29	0.23	0.20	0.25	0.22	0.22	0.31	0.18	0.25	0.23	0.13	0.28	0.23	0.19
MgO	31.10	31.59	31.15	31.06	31.46	31.85	31.20	32.30	32.60	32.86	31.03	30.99	30.90	30.83	31.16	31.14	30.91
CaO	1.93	1.47	1.34	1.74	1.76	1.43	1.66	1.20	1.19	1.20	1.88	2.00	1.64	1.66	1.63	1.73	1.98
Na2O	0.10	0.13	0.10	0.12	0.13	0.15	0.13	0.12	0.15	0.16		0.11	0.11	0.13	0.14	0.15	0.17
Sum	100	100	100	100	100	100	100	100	100	100	100	100	100	100	100	100	100
total	99.79	100.23	99.79	99.66	99.78	100.38	99.93	100.07	100.27	99.66	99.7	100.67	101.18	100.52	99.89	100.75	100.4
Oxygen	6	6	6	6	6	6	6	6	6	6	6	6	6	6	6	6	6
Si	1.872	1.893	1.872	1.849	1.883	1.896	1.874	1.915	1.922	1.929	1.863	1.846	1.858	1.870	1.893	1.880	1.872
Ti	0.003	0.002	0.004	0.003	0.003	0.003	0.003	0.003	0.004	0.003	0.003	0.003	0.004	0.003	0.004	0.004	0.004
Al	0.232	0.190	0.239	0.266	0.203	0.180	0.218	0.149	0.130	0.116	0.238	0.258	0.259	0.251	0.202	0.217	0.238
Cr	0.017	0.024	0.015	0.020	0.018	0.025	0.023	0.021	0.014	0.014	0.023	0.026	0.022	0.018	0.019	0.021	0.020
Fe	0.185	0.184	0.187	0.176	0.185	0.180	0.187	0.182	0.187	0.180	0.187	0.180	0.179	0.184	0.183	0.184	0.174
Mn	0.003	0.004	0.006	0.006	0.005	0.004	0.006	0.004	0.004	0.004	0.005	0.004	0.006	0.004	0.005	0.004	0.004
Ni	0.003	0.006	0.008	0.008	0.006	0.006	0.007	0.006	0.006	0.009	0.005	0.007	0.006	0.004	0.008	0.006	0.005
Mg	1.611	1.635	1.612	1.609	1.630	1.648	1.618	1.669	1.686	1.698	1.609	1.608	1.600	1.595	1.613	1.613	1.599
Ca	0.072	0.055	0.050	0.065	0.066	0.053	0.062	0.045	0.044	0.045	0.070	0.075	0.061	0.062	0.061	0.064	0.074
Na	0.007	0.009	0.007	0.008	0.009	0.010	0.009	0.008	0.010	0.011		0.007	0.007	0.009	0.009	0.010	0.011
Sum	4.004	4.002	4.000	4.009	4.008	4.004	4.007	4.001	4.007	4.008	4.003	4.013	4.001	3.997	3.997	4.003	4.001
Mg#	89.71	89.87	89.59	90.15	89.80	90.16	89.63	90.19	90.03	90.40	89.59	89.94	89.96	89.68	89.80	89.77	90.20
Cr#	6.96	11.38	6.04	6.95	8.00	12.02	9.59	12.51	9.75	10.82	8.86	9.16	7.83	6.80	8.58	8.73	7.72
C	3.85	2.91	2.70	3.49	3.49	2.84	3.32	2.35	2.32	2.33	3.76	4.00	3.32	3.36	3.27	3.46	3.99
M	86.25	87.26	87.17	87.00	86.66	87.60	86.66	88.07	87.94	88.30	86.22	86.35	86.98	86.67	86.87	86.67	86.60
F	9.90	9.83	10.13	9.51	9.85	9.56	10.03	9.58	9.74	9.38	10.01	9.66	9.71	9.98	9.86	9.87	9.41

Table 3.4 Representative Compositions of Experimental Orthopyroxenes (cont'd)

Run#	T3364	T3160	T3345	T3524	T3164	T3360	T3167	T3453	T3526	T3163	T3342	T3299	T3378	T3249	T3430	T3527	T3302
P(kbar)	28	30	35	22.5	25	26	27	28	29	30	35	35	28	30	30	33	35
T(°C)	1300	1300	1300	1400	1400	1400	1400	1400	1400	1400	1400	1400	1500	1500	1500	1500	1500
Opx%	31.68	29.27	26.25	41.17	38.87	38.01	35.1	29.1	32.91	31.05	26.05	24.67	22.61	26.35	25.44	22.76	20.09
SiO2	54.70	54.21	55.64	52.73	53.36	53.62	53.00	53.81	53.75	53.29	54.71	55.05	53.25	53.77	52.95	53.82	54.72
TiO2	0.13	0.09	0.13	0.12	0.11	0.06	0.09	0.09	0.13	0.11	0.09	0.07	0.09	0.03	0.14	0.22	0.05
Al2O3	4.43	5.08	2.85	7.08	6.29	6.21	6.90	5.54	5.40	6.58	4.30	3.76	6.66	5.70	6.73	5.18	4.50
Cr2O3	0.64	0.87	0.46	0.80	0.95	0.95	1.06	0.90	0.81	0.95	0.71	0.84	0.95	0.85	0.93	0.79	0.92
FeO	6.31	5.77	6.54	6.05	6.19	5.96	6.32	5.98	6.39	5.94	6.44	6.04	5.72	5.80	5.81	6.08	5.35
MnO	0.19	0.08	0.14	0.14	0.19	0.12	0.20	0.16	0.09	0.15	0.17	0.09	0.13	0.11	0.06	0.09	0.14
NiO	0.31	0.31	0.35	0.27	0.22	0.26	0.16	0.27	0.29	0.18	0.32	0.23	0.26	0.28	0.29	0.34	0.26
MgO	31.57	31.42	32.22	30.48	30.47	30.73	30.21	31.10	31.03	30.50	31.09	31.72	30.30	30.79	30.50	30.97	31.58
CaO	1.55	2.02	1.49	2.18	2.09	1.97	1.93	2.03	1.94	2.15	2.00	2.00	2.51	2.51	2.44	2.34	2.32
Na2O	0.16	0.16	0.17	0.14	0.14	0.13	0.14	0.13	0.16	0.15	0.17	0.20	0.13	0.15	0.14	0.15	0.17
Sum	100	100	100	100	100	100	100	100	100	100	100	100	100	100	100	100	100
total	99.45	100.41	99.82	98.65	101.03	100.49	100.47	100.23	99.42	100.63	100.39	100.16	99.22	99.59	99.67	98.97	100.5
Oxygen	6	6	6	6	6	6	6	6	6	6	6	6	6	6	6	6	6
Si	1.900	1.882	1.933	1.835	1.857	1.862	1.845	1.870	1.871	1.852	1.904	1.912	1.851	1.869	1.842	1.874	1.897
Ti	0.003	0.002	0.003	0.003	0.003	0.002	0.002	0.002	0.003	0.003	0.002	0.002	0.002	0.001	0.004	0.006	0.001
Al	0.182	0.208	0.117	0.290	0.258	0.254	0.283	0.227	0.222	0.269	0.177	0.154	0.273	0.234	0.276	0.213	0.184
Cr	0.018	0.024	0.013	0.022	0.026	0.026	0.029	0.025	0.022	0.026	0.020	0.023	0.026	0.023	0.026	0.022	0.025
Fe	0.183	0.167	0.190	0.176	0.180	0.173	0.184	0.174	0.186	0.173	0.188	0.175	0.166	0.169	0.169	0.177	0.155
Mn	0.006	0.002	0.004	0.004	0.006	0.004	0.006	0.005	0.003	0.004	0.005	0.003	0.004	0.003	0.002	0.003	0.004
Ni	0.009	0.009	0.010	0.008	0.006	0.007	0.005	0.008	0.008	0.005	0.009	0.006	0.007	0.008	0.008	0.010	0.007
Mg	1.635	1.626	1.668	1.581	1.581	1.591	1.567	1.612	1.610	1.580	1.613	1.642	1.570	1.596	1.582	1.607	1.632
Ca	0.058	0.075	0.056	0.081	0.078	0.073	0.072	0.075	0.072	0.080	0.075	0.074	0.094	0.094	0.091	0.087	0.086
Na	0.011	0.011	0.012	0.010	0.009	0.009	0.009	0.009	0.011	0.010	0.011	0.013	0.009	0.010	0.010	0.010	0.011
Sum	4.003	4.006	4.005	4.011	4.003	4.001	4.002	4.006	4.009	4.002	4.002	4.005	4.002	4.006	4.008	4.008	4.003
Mg#	89.91	90.67	89.78	89.98	89.78	90.19	89.50	90.27	89.65	90.15	89.58	90.35	90.43	90.44	90.35	90.08	91.32
Cr#	8.87	10.27	9.77	7.06	9.19	9.27	9.31	9.81	9.19	8.87	9.93	13.00	8.71	9.12	8.51	9.26	12.01
C	3.07	4.02	2.90	4.42	4.23	3.99	3.95	4.05	3.87	4.36	3.98	3.93	5.11	5.03	4.93	4.67	4.60
M	87.15	87.02	87.17	86.00	85.98	86.59	85.96	86.61	86.17	86.22	86.02	86.80	85.81	85.89	85.89	85.87	87.12
F	9.78	8.96	9.93	9.58	9.79	9.42	10.09	9.34	9.95	9.42	10.00	9.27	9.08	9.08	9.18	9.46	8.28

Orthopyroxene: most elements in orthopyroxene show small but significant variation in pressure, temperature-space (Table 3.4). Si increases with increasing pressure and decreasing temperature; Al is opposite, increasing with rising temperature and falling pressure (Fig.3.3a); Cr and Ca are similar to Al, increasing with increasing temperature, but only slightly increasing with decreasing pressure. With rising temperature, Ti, Mg, and Fe show minor decreases. Na increases with increasing pressure, and only slightly with increasing temperature. Ni and Mn do not perceptibly change. It is worth noting that there is no dramatic change in all these elements (in orthopyroxene) when the garnet-in and spinel-out boundaries are crossed, indicating that the appearance of garnet and disappearance of spinel are results of gradual change in mineral compositions in the system. This is further supported by the composition variation of other minerals in the system.

The weak correlation between Cr_2O_3 concentration and pressure, and the generally low concentration of Cr_2O_3 in natural orthopyroxenes (in the garnet-facies) may be two main reasons for the barometer based on Cr_2O_3-in-orthopyroxene (Nickel, 1989) to be less accurate than that based on Al_2O_3-in-orthopyroxene (Nickel & Green, 1985). The strong SiO_2 - pressure correlation (Fig.3.3b) suggests the possibility of formulating a barometer based on SiO_2-in-orthopyroxene (in the garnet-facies).

Clinopyroxene: Si, Ti, and Al behave the same way as they do in orthopyroxene in response to the pressure, temperature change. The CaO and Na_2O contents show sensitive dependence on temperature: both decrease with increasing temperature, and increase very little with increasing pressure (Fig.3.4). Opposite to their negative correlation with temperature in orthopyroxene, both Mg and Fe in clinopyroxene increase with increasing temperature (Fig.3.5). There are small variations in Cr_2O_3, NiO and MnO contents. Overall, clinopyroxene shows more sensitive composition change with temperature and pressure than orthopyroxene (Table 3.5).

Garnet: Unlike in pyroxenes, Fe and Mg in garnet behave differently in response to temperature change. Fe decreases but Mg increases with increasing temperature (Fig.3.6). Thus garnet alone can fractionate Fe and Mg in a temperature change process. This property of garnet underpins the fundamental usefulness of the garnet-olivine, and garnet-pyroxene Fe^{2+}/Mg exchange thermometers. Mn seems to follow Fe, slightly decreasing with increasing temperature. Both Ti and Cr show very small increase with rising temperature. Ca tends to decrease with increase in both temperature and pressure. Si and Al do not change significantly in the pressure, temperature-range of interest (Table 3.6).

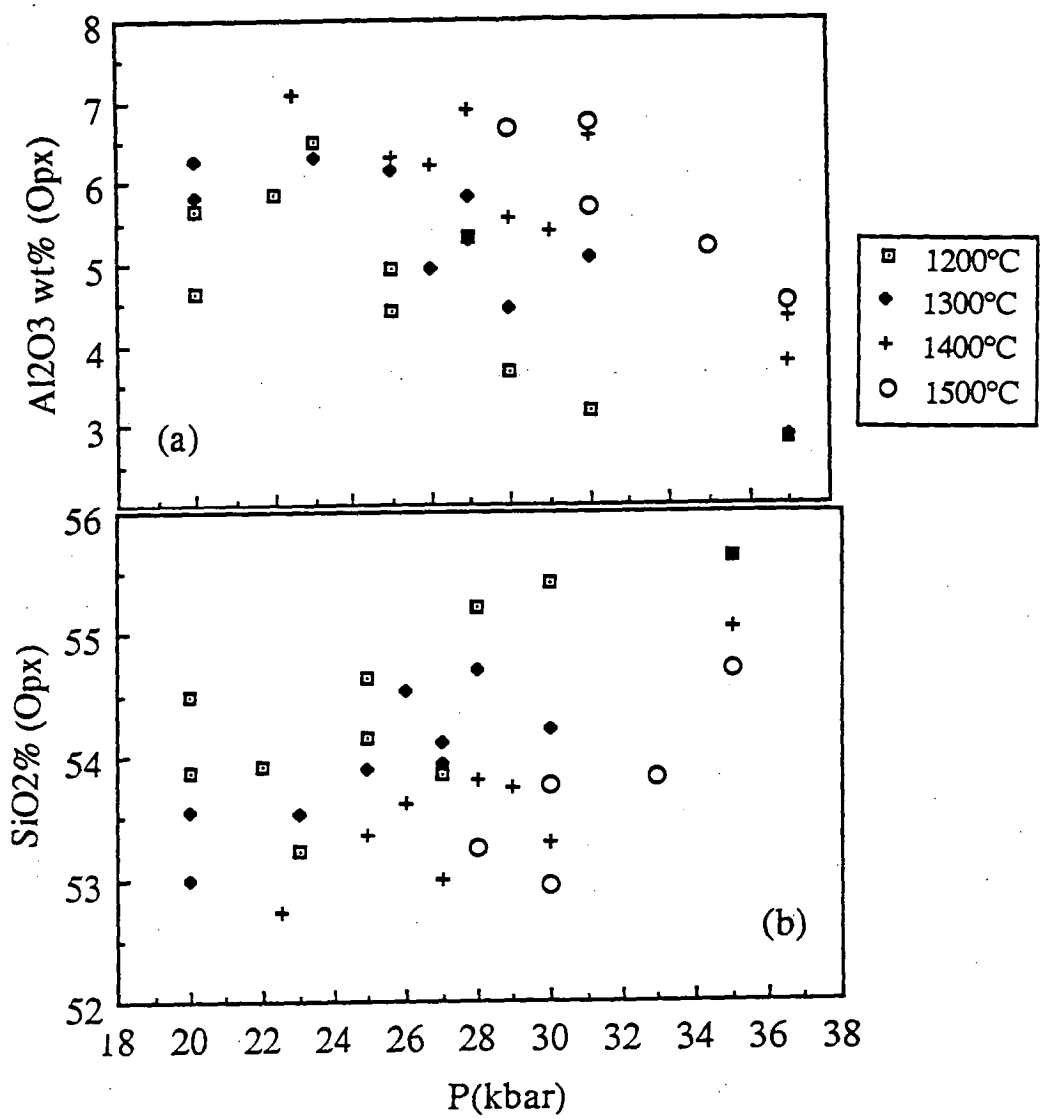

Figure 3.3 (a) Al_2O_3 solubility in orthopyroxene correlates with pressure and temperature. Al_2O_3 increases with rising temperature and falling pressure. (b) SiO_2 (in orthopyroxene) - pressure correlation diagram. SiO_2 increases with increasing pressure and decreasing temperature.

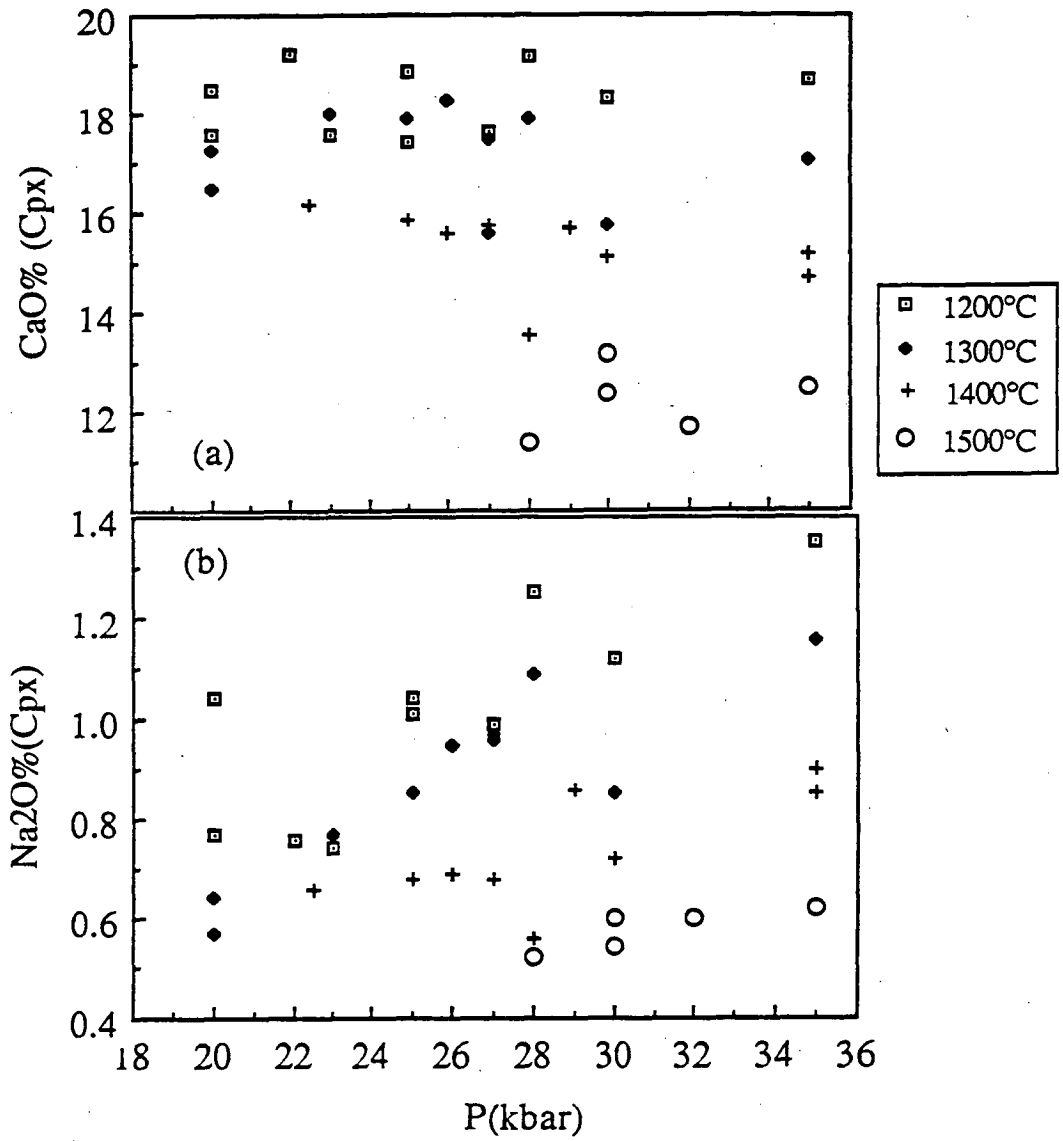

Figure 3.4. CaO and Na_2O in clinopyroxene as a function of pressure and temperature. Both show obvious temperature dependence. Na_2O increases with increasing pressure; effect of pressure on CaO is insignificant.

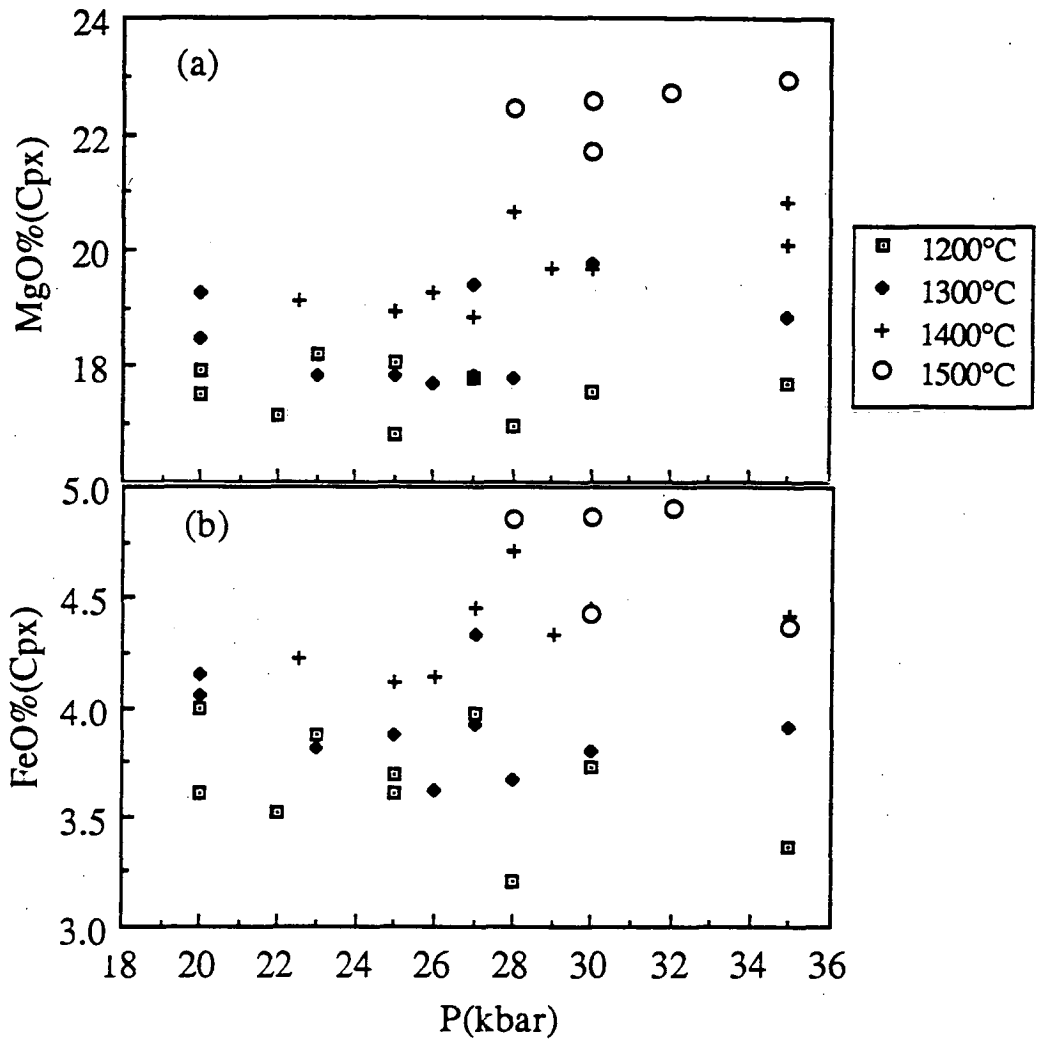

Figure 3.5. FeO and MgO (in clinopyroxene) variation in P-T space. They are also strongly dependent on temperature. Correlation with pressure is very weak.

Table 3.5 Representative Compositions of Experimental Clinopyroxenes

Run#	T3145	T3239	T3105	T3108	T3101	T3168	T3126	T3454	T3151	T3306	T3316	T3158	T3141	T3130	T3355	T3136	T3247
P(kbar)	20	20	22	23	25	25	27	28	30	35	20	20	23	25	26	27	27
T(°C)	1200	1200	1200	1200	1200	1200	1200	1200	1200	1200	1300	1300	1300	1300	1300	1300	1300
Cpx%	23.9	20.31	23.16	24.54	19.89	22.08	21.6	19.13	19.97	19.87	23.95	25.3	23.96	23.78	21.16	21.78	24.7
SiO2	51.26	52.29	51.93	51.24	52.01	52.05	51.57	52.08	52.86	53.93	51.73	51.16	51.27	50.94	51.87	51.65	52.37
TiO2	0.27	0.35	0.27	0.23	0.34	0.30	0.30	0.35	0.28	0.26	0.17	0.21	0.24	0.32	0.24	0.26	0.32
Al2O3	6.92	5.24	6.14	7.00	5.98	6.11	6.24	5.33	4.50	3.51	6.20	6.63	6.68	7.06	5.97	6.42	5.85
Cr2O3	1.08	1.24	0.78	0.98	0.98	1.03	1.24	1.39	1.40	0.95	1.37	1.19	1.13	0.91	1.11	1.12	0.86
FeO	3.99	3.60	3.52	3.87	3.69	3.60	3.97	3.21	3.73	3.36	4.05	4.15	3.81	3.87	3.62	3.92	4.33
MnO	0.14	0.17	0.11	0.11	0.13	0.19	0.10	0.14		0.13		0.17	0.10	0.13	0.13	0.14	0.18
NiO	0.07	0.08	0.13	0.07	0.14	0.21	0.19	0.14	0.25	0.16	0.18	0.12	0.17	0.20	0.15	0.22	0.16
MgO	17.91	17.54	17.13	18.21	16.84	18.07	17.78	16.96	17.55	17.69	18.46	19.26	17.85	17.83	17.68	17.83	19.41
CaO	17.60	18.46	19.23	17.56	18.86	17.43	17.62	19.14	18.32	18.68	17.27	16.46	17.98	17.90	18.27	17.48	15.56
Na2O	0.77	1.04	0.76	0.74	1.04	1.01	0.99	1.25	1.12	1.35	0.57	0.64	0.77	0.85	0.95	0.96	0.97
Sum	100	100	100	100	100	100	100	100	100	100	100	100	100	100	100	100	100
total	100.03	100.34	99.52	100.09	98.34	101.37	99.4	99.82	100.05	100.05	99.83	99.94	101.27	100.38	99.62	100.64	100.39
Oxygen	6	6	6	6	6	6	6	6	6	6	6	6	6	6	6	6	6
Si	1.850	1.890	1.876	1.847	1.881	1.876	1.864	1.886	1.911	1.946	1.865	1.844	1.852	1.841	1.874	1.865	1.881
Ti	0.007	0.010	0.007	0.006	0.009	0.008	0.008	0.010	0.008	0.007	0.005	0.006	0.006	0.009	0.007	0.007	0.009
Al	0.294	0.223	0.261	0.298	0.255	0.259	0.266	0.228	0.192	0.149	0.264	0.282	0.285	0.301	0.254	0.273	0.248
Cr	0.031	0.035	0.022	0.028	0.028	0.030	0.035	0.040	0.040	0.027	0.039	0.034	0.032	0.026	0.032	0.032	0.024
Fe	0.120	0.109	0.106	0.117	0.112	0.108	0.120	0.097	0.113	0.101	0.122	0.125	0.115	0.117	0.110	0.119	0.130
Mn	0.004	0.005	0.003	0.003	0.004	0.006	0.003	0.004		0.004		0.005	0.003	0.004	0.004	0.004	0.006
Ni	0.002	0.002	0.004	0.002	0.004	0.006	0.006	0.004	0.007	0.005	0.005	0.004	0.005	0.006	0.004	0.006	0.005
Mg	0.964	0.945	0.923	0.979	0.908	0.971	0.958	0.916	0.946	0.951	0.992	1.035	0.961	0.961	0.952	0.960	1.039
Ca	0.681	0.715	0.744	0.678	0.731	0.673	0.682	0.743	0.710	0.722	0.667	0.636	0.696	0.693	0.707	0.676	0.599
Na	0.054	0.073	0.054	0.052	0.073	0.071	0.069	0.088	0.079	0.094	0.040	0.045	0.054	0.059	0.067	0.068	0.067
Sum	4.007	4.007	4.001	4.010	4.005	4.007	4.012	4.015	4.005	4.006	3.999	4.015	4.010	4.017	4.010	4.009	4.008
Mg#	88.90	89.68	89.67	89.36	89.05	89.96	88.86	90.41	89.36	90.38	89.05	89.21	89.30	89.14	89.69	89.01	88.87
Cr#	9.48	13.66	7.89	8.57	9.87	10.20	11.75	14.91	17.24	15.37	12.93	10.75	10.15	7.93	11.12	10.50	8.95
Ca#	92.67	90.78	93.30	92.92	90.95	90.47	90.81	89.42	90.04	88.44	94.35	93.42	92.81	92.12	91.37	90.93	89.90
C	38.57	40.41	41.98	38.25	41.76	38.41	38.76	42.31	40.12	40.68	37.45	35.40	39.26	39.14	39.97	38.55	33.87
M	54.61	53.44	52.03	55.18	51.87	55.41	54.42	52.16	53.50	53.61	55.70	57.63	54.24	54.25	53.84	54.70	58.77
F	6.82	6.15	5.99	6.57	6.38	6.19	6.82	5.53	6.37	5.71	6.85	6.97	6.50	6.61	6.19	6.76	7.36

Table 3.5 Representative Compositions of Experimental Clinopyroxenes (cont'd)

Run#	T3364	T3160	T3345	T3524	T3164	T3360	T3167	T3453	T3526	T3163	T3342	T3299	T3378	T3249	T3430	T3527	T3302
P(kbar)	28	30	35	22.5	25	26	27	28	29	30	35	35	28	30	30	32	35
T(°C)	1300	1300	1300	1400	1400	1400	1400	1400	1400	1400	1400	1400	1500	1500	1500	1500	1500
Cpx%	20.65	23.73	20.84	25.73	26.34	27.53	25.3	30.11	24.27	25.19	23.8	24.92	36.35	28.65	31.03	33.09	30.35
SiO2	52.67	52.83	53.54	50.98	51.74	51.33	51.31	51.33	52.18	51.54	53.41	53.35	52.09	52.26	52.16	52.39	53.34
TiO2	0.27	0.19	0.24	0.26	0.20	0.18	0.14	0.19	0.18	0.18	0.19	0.13	0.18	0.12	0.10	0.11	0.07
Al2O3	5.05	5.37	3.82	7.33	7.11	7.25	7.29	7.65	5.78	6.66	4.45	4.48	7.08	6.24	5.98	6.15	4.66
Cr2O3	1.20	1.17	0.97	1.00	1.19	1.23	1.13	1.10	1.04	1.31	0.98	1.00	1.06	1.15	1.07	1.03	1.14
FeO	3.67	3.80	3.91	4.23	4.11	4.14	4.46	4.71	4.33	4.46	4.42	4.36	4.86	4.43	4.87	4.90	4.37
MnO	0.18	0.13	0.19	0.04	0.11	0.10	0.15	0.13	0.11	0.13	0.17	0.16	0.17	0.16	0.14	0.18	0.19
NiO	0.15	0.11	0.27	0.21	0.11	0.23	0.22	0.17	0.12	0.23	0.22	0.19	0.27	0.20	0.21	0.24	0.21
MgO	17.81	19.78	18.85	19.11	18.93	19.28	18.86	20.64	19.70	19.68	20.09	20.81	22.43	21.68	22.58	22.69	22.95
CaO	17.89	15.76	17.03	16.17	15.83	15.58	15.76	13.53	15.70	15.09	15.18	14.68	11.36	13.16	12.35	11.71	12.45
Na2O	1.09	0.85	1.16	0.66	0.68	0.69	0.68	0.56	0.86	0.72	0.90	0.85	0.52	0.60	0.54	0.60	0.62
Sum	100	100	100	100	100	100	100	100	100	100	100	100	100	100	100	100	100
total	99.92	99.64	99.88	99.26	101.05	100.48	99.77	100.59	99.11	100.23	99.17	100.09	100.88	100.29	99.34	99.2	99.84
Oxygen	6	6	6	6	6	6	6	6	6	6	6	6	6	6	6	6	6
Si	1.901	1.893	1.930	1.835	1.857	1.844	1.846	1.836	1.876	1.853	1.916	1.911	1.852	1.865	1.862	1.866	1.899
Ti	0.007	0.005	0.007	0.007	0.005	0.005	0.004	0.005	0.005	0.005	0.005	0.004	0.005	0.003	0.003	0.003	0.002
Al	0.215	0.227	0.162	0.311	0.301	0.307	0.309	0.322	0.245	0.282	0.188	0.189	0.297	0.263	0.252	0.258	0.195
Cr	0.034	0.033	0.028	0.028	0.034	0.035	0.032	0.031	0.030	0.037	0.028	0.028	0.030	0.032	0.030	0.029	0.032
Fe	0.111	0.114	0.118	0.127	0.123	0.124	0.134	0.141	0.130	0.134	0.133	0.131	0.144	0.132	0.145	0.146	0.130
Mn	0.006	0.004	0.006	0.001	0.003	0.003	0.005	0.004	0.003	0.004	0.005	0.005	0.005	0.005	0.004	0.006	0.006
Ni	0.004	0.003	0.008	0.006	0.003	0.007	0.006	0.005	0.004	0.007	0.006	0.006	0.008	0.006	0.006	0.007	0.006
Mg	0.959	1.057	1.013	1.026	1.013	1.032	1.012	1.101	1.055	1.055	1.075	1.111	1.189	1.154	1.201	1.205	1.218
Ca	0.692	0.605	0.658	0.624	0.609	0.599	0.607	0.518	0.605	0.581	0.584	0.564	0.433	0.503	0.472	0.447	0.475
Na	0.076	0.059	0.081	0.046	0.048	0.048	0.048	0.039	0.060	0.050	0.062	0.059	0.036	0.041	0.038	0.042	0.043
Sum	4.005	4.001	4.009	4.012	3.995	4.004	4.003	4.002	4.012	4.008	4.002	4.006	3.998	4.005	4.013	4.008	4.007
Mg#	89.63	90.26	89.57	88.95	89.15	89.25	88.29	88.64	89.02	88.72	89.02	89.49	89.17	89.72	89.20	89.20	90.36
Cr#	13.75	12.79	14.56	8.36	10.08	10.25	9.44	8.78	10.76	11.63	12.86	13.02	9.13	10.97	10.69	10.09	14.12
Ca#	90.06	91.08	89.01	93.07	92.76	92.61	92.74	93.05	91.00	92.07	90.34	90.53	92.41	92.40	92.62	91.45	91.72
C	39.29	34.07	36.77	35.10	34.89	34.13	34.64	29.45	33.78	32.84	32.59	31.22	24.50	28.14	25.96	24.86	26.05
M	54.42	59.51	56.63	57.73	58.04	58.78	57.70	62.54	58.96	59.59	60.01	61.55	67.32	64.48	66.04	67.02	66.82
F	6.29	6.42	6.60	7.17	7.06	7.08	7.65	8.01	7.27	7.57	7.40	7.23	8.18	7.39	7.99	8.12	7.13

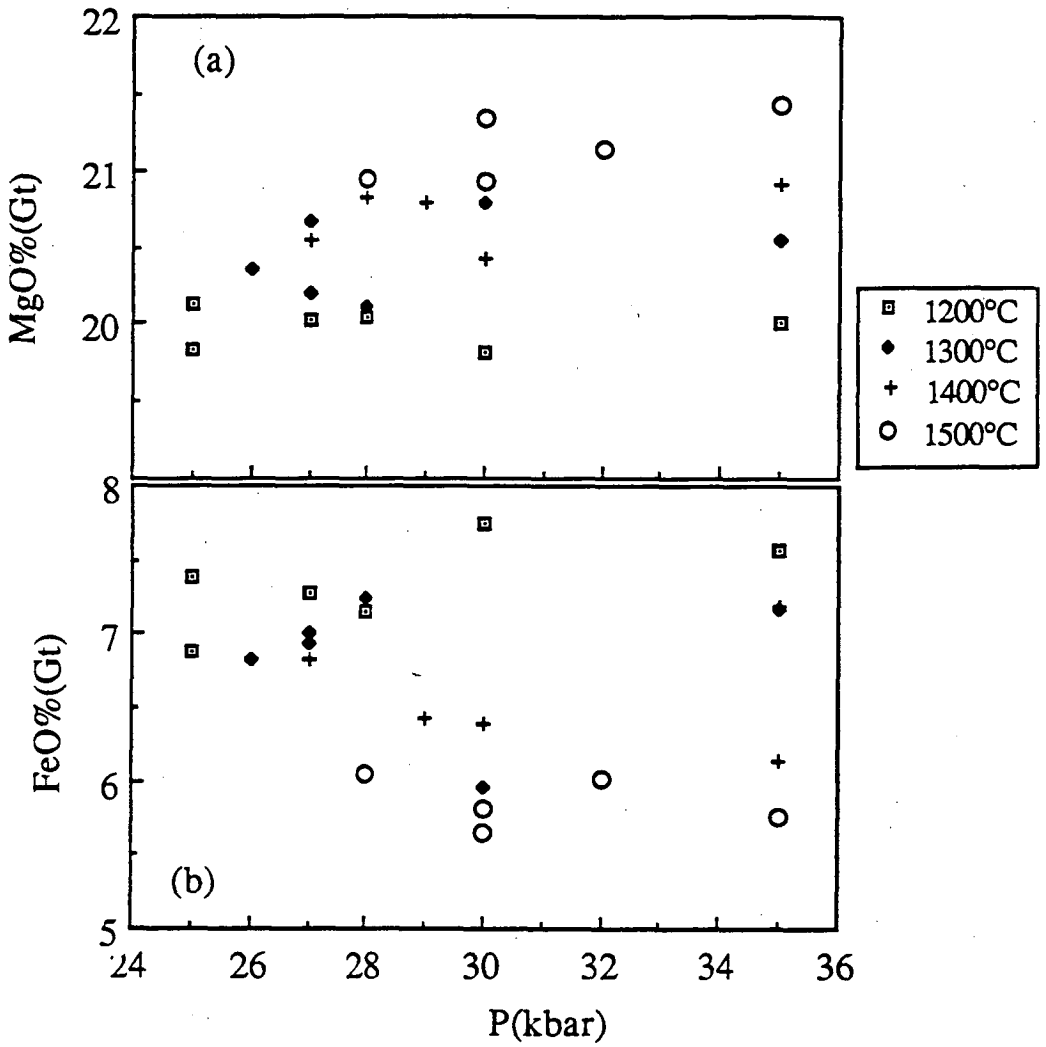

Figure 3.6. FeO and MgO (in garnet) variation with pressure and temperature. With increasing temperature, MgO increases but FeO decreases. Thus garnet is able to fractionate MgO and FeO during a temperature change process such as cooling.

Table 3.6 Representative Compositions of Experimental Garnets

Run#	T3239	T3101	T3168	T3126	T3454	T3151	T3306	T3355	T3136	T3247	T3364	T3160	T3345	T3167
P(kbar)	20	25	25	27	28	30	35	26	27	27	28	30	35	27
T(°C)	1200	1200	1200	1200	1200	1200	1200	1300	1300	1300	1300	1300	1300	1400
Gt%	11.73	9.18	11.25	9.46	15.89	16.15	17.69	9.21	9.34	7.71	12.74	12.74	17.77	4.91
SiO2	42.26	42.13	41.96	41.92	42.17	41.68	41.91	42.11	41.96	42.41	41.76	42.22	41.98	41.92
TiO2	0.33	0.28	0.34	0.18	0.26	0.25	0.21	0.26	0.26	0.26	0.27	0.23	0.30	0.29
Al2O3	21.74	21.74	22.31	22.11	21.36	21.77	22.73	22.50	21.92	21.61	22.18	21.79	21.61	21.81
Cr2O3	1.61	1.95	1.59	2.23	2.47	2.41	1.67	1.61	2.04	1.79	2.02	2.77	2.20	2.38
FeO	7.45	7.39	6.88	7.27	7.15	7.75	7.56	6.83	7.00	6.93	7.24	5.95	7.16	6.83
MnO	0.28	0.33	0.35	0.26	0.36	0.35	0.41	0.33	0.40	0.33	0.28	0.28	0.34	0.24
NiO			0.04	0.03	0.09	0.12	0.07		0.07	0.06		0.04	0.15	
MgO	20.11	19.83	20.12	20.02	20.04	19.82	20.01	20.36	20.19	20.67	20.11	20.78	20.55	20.55
CaO	6.22	6.35	6.42	5.99	6.10	5.84	5.45	6.00	6.17	5.93	6.14	5.94	5.70	5.99
Sum	100	100	100	100	100	100	100	100	100	100	100	100	100	100
total	100.92	98.34	101.24	99.77	100.58	101.38	100.99	100.25	100.91	99.07	100.48	101	99.45	100.84
Oxygen	12	12	12	12	12	12	12	12	12	12	12	12	12	12
Si	3.010	3.005	2.985	2.987	3.009	2.981	2.981	2.989	2.989	3.014	2.976	2.995	2.992	2.983
Ti	0.018	0.015	0.018	0.010	0.014	0.013	0.011	0.014	0.014	0.014	0.015	0.012	0.016	0.016
Al	1.825	1.827	1.870	1.857	1.796	1.835	1.906	1.882	1.841	1.810	1.863	1.822	1.815	1.829
Cr	0.091	0.110	0.089	0.126	0.139	0.136	0.094	0.090	0.115	0.101	0.114	0.155	0.124	0.134
Fe	0.444	0.441	0.409	0.433	0.427	0.464	0.450	0.405	0.417	0.412	0.432	0.353	0.427	0.407
Mn	0.017	0.020	0.021	0.016	0.022	0.021	0.025	0.020	0.024	0.020	0.017	0.017	0.021	0.015
Ni			0.002	0.002	0.005	0.007	0.004		0.004	0.003		0.002	0.009	
Mg	2.135	2.108	2.133	2.126	2.132	2.114	2.122	2.154	2.144	2.190	2.137	2.197	2.184	2.180
Ca	0.475	0.485	0.489	0.457	0.466	0.448	0.415	0.456	0.471	0.452	0.469	0.451	0.435	0.457
Sum	8.014	8.012	8.018	8.013	8.010	8.019	8.008	8.011	8.019	8.016	8.021	8.005	8.022	8.020
Mg#	82.79	82.71	83.90	83.08	83.32	82.01	82.51	84.16	83.72	84.17	83.20	86.16	83.65	84.29
Cr#	4.73	5.68	4.56	6.34	7.20	6.91	4.70	4.58	5.88	5.26	5.76	7.86	6.39	6.82
C	15.54	15.99	16.14	15.16	15.42	14.80	13.91	15.13	15.53	14.79	15.44	15.04	14.29	15.01
M	69.92	69.48	70.37	70.48	70.48	69.88	71.04	71.43	70.71	71.72	70.35	73.20	71.69	71.64
F	14.53	14.53	13.50	14.36	14.11	15.33	15.06	13.44	13.75	13.49	14.21	11.76	14.01	13.36

Table 3.6 Representative Compositions of Experimental Garnets (cont'd)

Run#	T3453	T3526	T3163	T3342	T3299	T3378	T3249	T3430	T3527	T3302
P(kbar)	28	29	30	35	35	28	30	30	32	35
T(°C)	1400	1400	1400	1400	1400	1500	1500	1500	1500	1500
Gt%	5.92	9.15	8.89	14.66	15.96	5.85	10.78	10.2	10.44	15.51
SiO2	42.22	42.18	42.13	42.14	42.19	42.23	42.50	42.05	42.07	42.19
TiO2	0.26	0.24	0.23	0.26	0.22	0.24	0.18	0.25	0.29	0.17
Al2O3	22.26	22.23	21.76	21.95	22.06	22.04	21.06	21.71	21.98	21.43
Cr2O3	2.00	2.09	2.50	1.98	2.29	2.44	2.78	2.86	2.57	3.03
FeO	6.07	6.43	6.40	7.19	6.14	6.05	5.65	5.81	6.01	5.75
MnO	0.35	0.28	0.34	0.28	0.37	0.24	0.42	0.24	0.21	0.24
NiO		0.06	0.14	0.10	0.03	0.02	0.06	0.04	0.10	0.08
MgO	20.82	20.79	20.43	20.55	20.91	20.94	21.34	20.93	21.14	21.43
CaO	6.01	5.71	6.09	5.55	5.80	5.80	5.93	6.12	5.62	5.69
Sum	100	100	100	100	100	100	100	100	100	100
total	100.64	100.38	100.62	100.54	101.35	101.47	100.02	100.56	100.63	101.44
Oxygen	12	12	12	12	12	12	12	12	12	12
Si	2.991	2.990	2.996	2.997	2.991	2.992	3.016	2.984	2.982	2.992
Ti	0.014	0.013	0.012	0.014	0.012	0.013	0.010	0.013	0.016	0.009
Al	1.858	1.857	1.823	1.840	1.843	1.840	1.761	1.816	1.836	1.791
Cr	0.112	0.117	0.141	0.111	0.128	0.137	0.156	0.161	0.144	0.170
Fe	0.360	0.381	0.381	0.428	0.364	0.358	0.335	0.345	0.356	0.341
Mn	0.021	0.017	0.021	0.017	0.022	0.014	0.025	0.014	0.013	0.014
Ni		0.003	0.008	0.006	0.002	0.001	0.003	0.002	0.006	0.005
Mg	2.199	2.197	2.166	2.179	2.210	2.212	2.258	2.214	2.234	2.265
Ca	0.456	0.434	0.464	0.423	0.441	0.440	0.451	0.465	0.427	0.432
Sum	8.010	8.010	8.010	8.014	8.012	8.007	8.016	8.015	8.013	8.019
Mg#	85.94	85.22	85.05	83.59	85.86	86.05	87.07	86.53	86.25	86.92
Cr#	5.68	5.93	7.16	5.71	6.51	6.91	8.13	8.12	7.27	8.66
C	15.13	14.40	15.41	13.96	14.61	14.62	14.81	15.39	14.15	14.23
M	72.94	72.95	71.94	71.92	73.31	73.47	74.17	73.21	74.04	74.55
F	11.93	12.66	12.64	14.12	12.08	11.91	11.02	11.40	11.81	11.22

Spinel: Analysis of spinel crystals in the charges was extremely difficult, due to their small size and low abundance. The major elements of the spinels in most charges show great inhomogeneity. Initially it was thought that this was perhaps due to contamination by surrounding silicates. After carefully analysing the largest crystals in the charges and selecting the analyses with the minimum SiO_2 and CaO, large variation within individual runs still persist. This inhomogeneity is found to exist even at 1500°C, as long as the runs were subsolidus. In runs with melt present, however, spinels seem to be homogeneous (Ballhaus et al., 1991). The inhomogeneity under subsolidus conditions is probably caused by rapid nucleation of small spinel crystals early in the course of heating to run temperature and inhomogeneity in "local bulk composition" from which these small spinel crystals grew. Because of their small size, it is impossible to detect any chemical zoning in these crystals. Apparently this problem of inhomogeneity was also encountered in the study of Nickel (1986) in the simple CMAS-Cr system. Nickel (1986) argues that in experiments with spinel as the only aluminous phase, the Cr/Al ratio of the spinel is independent of pressure and temperature, and only dependent on bulk composition. To test this suggestion, Cr/Al ratios of coexisting orthopyroxene and spinel in a number of natural peridotite suites enclosed in alkali-basalts and kimberlites (reference sources given in Table 1.8) are plotted in Figure 3.7. Two obvious trends can be observed in this plot. One is defined mainly by garnet-bearing spinel peridotites enclosed in kimberlites (the high-Cr trend); and the other (the low Cr-trend), defined by most of the spinel peridotites (some are garnet-bearing) included in alkali-basalts, and by some spinel peridotite inclusions in kimberlites. Some alkali-basalt-borne spinel peridotites also plot close to the high-Cr trend and these are mostly associated with amphibole and glass. All the spinels on the high-Cr trend have Cr/(Cr + Al) ratio greater than 0.60; and most of the spinels on the low-Cr trend have the Cr/(Cr + Al) ratio smaller than 0.60. Because the majority of the experimental spinels have Cr-ratios smaller than 0.60, the low-Cr trend is assumed to be applicable to equilibrated orthopyroxene + spinel assemblages. Thus the Cr/Al of orthopyroxene in the experiments can be used to infer the equilibrium composition of spinels from the observed composition spread in the experimental products. These inferred or selected compositions are listed in Table 3.7. In two runs at high pressure & temperature (e.g. T3430, 1500°C, 30 kbar) spinel is very small and very scarce. The analyses selected probably do not represent the equilibrium compositions. They are shown for reference only.

Systematic variation is shown by the spinel compositions thus determined (Table 3.7). There is a clear positive correlation between pressure and TiO_2 in Spinel (Fig.3.8). Al_2O_3 decreases with increasing pressure and decreasing temperature; whereas Cr_2O_3 is opposite. With increasing temperature, MgO increases but FeO decreases, a feature very

Table 3.7 Representative Compositions of Experimental Spinels

Run#	T3145	T3239	T3105	T3108	T3101	T3168	T3126	T3454	T3316	T3158	T3141	T3130	T3355	T3136	T3247	T3364
P(kbar)	20	20	22	23	25	25	27	28	20	20	23	25	26	27	27	28
T(°C)	1200	1200	1200	1200	1200	1200	1200	1200	1300	1300	1300	1300	1300	1300	1300	1300
Sp%	2.83	0.49	2.93	2.00	0.86	0.51	0.22	-0.26	2.77	2.22	2.38	2.39	0.86	0.47	0.91	0.35
SiO2	0.48	0.77	0.18	0.22		0.62	0.52	0.24	0.23	0.42	0.26	0.44	0.21	0.28	0.44	0.24
TiO2	0.19	0.21	0.26	0.23	0.24	0.32	0.31	0.64	0.19	0.20	0.17	0.27	0.32	0.37	0.48	0.58
Al2O3	47.30	49.51	53.17	52.84	46.58	47.51	43.84	38.29	44.59	49.11	48.77	47.75	49.30	45.33	42.62	41.80
Cr2O3	19.60	16.95	13.46	14.62	18.15	19.82	21.33	28.50	21.67	18.07	18.48	18.19	18.09	21.68	24.13	23.73
FeO	10.27	11.21	10.68	9.74	11.30	11.81	11.81	13.48	10.83	9.88	10.29	10.62	10.89	11.46	12.49	12.53
MnO	0.09	0.12	0.21	0.14		0.06	0.61	0.09	0.16	0.09	0.12	0.15	0.11	0.04	0.24	0.14
NiO	0.05	0.29	0.74	0.75	0.73	0.54	0.10	0.65	0.53	0.49	0.57	0.61	0.80	0.63	0.61	0.70
MgO	20.04	19.57	19.62	19.48	18.41	19.32	18.23	17.37	18.91	19.37	19.44	18.75	19.24	19.04	18.22	18.11
CaO		0.16		0.05		0.07	0.09	0.09		0.15	0.05	0.06	0.06		0.11	0.12
Sum	97.54	97.86	98.14	97.80	95.41	99.38	96.23	99.02	96.88	97.21	97.84	96.34	98.75	98.55	98.79	97.59
TiO2	0.19	0.21	0.26	0.24	0.25	0.32	0.32	0.64	0.20	0.21	0.17	0.28	0.32	0.37	0.48	0.59
Al2O3	48.37	50.47	54.08	54.00	48.71	47.69	45.44	38.57	45.92	50.46	49.77	49.48	49.84	45.89	43.03	42.71
Cr2O3	20.04	17.28	13.69	14.94	18.98	19.89	22.11	28.71	22.31	18.57	18.86	18.85	18.29	21.95	24.36	24.24
Fe2O3	2.43	2.43	1.72	0.58	2.31	2.53	2.67	2.65	2.44	1.12	1.66	1.58	1.65	2.39	2.61	2.96
FeO	8.31	9.24	9.32	9.43	9.74	9.58	9.83	11.19	8.95	9.15	9.00	9.60	9.52	9.45	10.26	10.13
MnO	0.09	0.12	0.21	0.14		0.06	0.63	0.09	0.16	0.09	0.12	0.16	0.11	0.04	0.24	0.14
NiO	0.05	0.30	0.75	0.77	0.76	0.54	0.10	0.65	0.55	0.50	0.58	0.63	0.81	0.64	0.62	0.72
MgO	20.49	19.95	19.96	19.91	19.25	19.39	18.90	17.50	19.47	19.90	19.84	19.43	19.45	19.28	18.39	18.50
Sum	100	100	100	100	100	100	100	100	100	100	100	100	100	100	100	100
Oxygen	4	4	4	4	4	4	4	4	4	4	4	4	4	4	4	4
Ti	0.0038	0.0043	0.0052	0.0046	0.0051	0.0065	0.0066	0.0136	0.0040	0.0041	0.0035	0.0056	0.0065	0.0076	0.0100	0.0123
Al	1.5207	1.5800	1.6717	1.6694	1.5405	1.5124	1.4566	1.2783	1.4647	1.5796	1.5624	1.5588	1.5679	1.4657	1.3957	1.3862
Cr	0.4228	0.3629	0.2839	0.3099	0.4027	0.4233	0.4754	0.6383	0.4775	0.3899	0.3972	0.3984	0.3860	0.4702	0.5301	0.5279
Fe3+	0.0489	0.0486	0.0340	0.0115	0.0467	0.0513	0.0548	0.0562	0.0498	0.0223	0.0334	0.0317	0.0331	0.0488	0.0542	0.0614
Fe2+	0.1855	0.2053	0.2043	0.2068	0.2185	0.2155	0.2236	0.2632	0.2026	0.2032	0.2005	0.2144	0.2126	0.2141	0.2361	0.2335
Mn	0.0022	0.0028	0.0047	0.0032		0.0014	0.0146	0.0022	0.0038	0.0021	0.0028	0.0035	0.0025	0.0009	0.0056	0.0033
Ni	0.0012	0.0063	0.0159	0.0162	0.0165	0.0117	0.0023	0.0148	0.0119	0.0108	0.0125	0.0136	0.0174	0.0139	0.0136	0.0158
Mg	0.8149	0.7900	0.7803	0.7784	0.7701	0.7779	0.7661	0.7335	0.7857	0.7881	0.7878	0.7741	0.7740	0.7787	0.7547	0.7596
Sum	3	3	3	3	3	3	3	3	3	3	3	3	3	3	3	3
Mg#	81.45	79.38	79.25	79.01	77.90	78.31	77.41	73.60	79.50	79.50	79.71	78.31	78.45	78.43	76.17	76.49
Cr#	21.22	18.22	14.27	15.56	20.24	21.30	23.93	32.36	23.97	19.58	19.93	20.03	19.42	23.69	26.77	26.72
Fe3:Fe2	0.26	0.24	0.17	0.06	0.21	0.24	0.25	0.21	0.25	0.11	0.17	0.15	0.16	0.23	0.23	0.26

Table 3.7 Representative Compositions of Experimental Spinels (cont'd)

Run#	T3160	T3524	T3164	T3360	T3167	T3453	T3526	T3163	T3378	T3430	T3249
P(kbar)	30	22.5	25	26	27	28	29	30	28	30	30
T(°C)	1300	1400	1400	1400	1400	1400	1400	1400	1500	1500	1500
Sp%	0.17	1.40	2.14	2.17	0.24	0.52	0.53	-0.30	0.44	-0.39	-0.04
SiO2	0.39	0.36	0.28	0.80	0.29	0.82	0.83	0.34	0.40	0.80	2.17
TiO2	0.41	0.15	0.24	0.23	0.29	0.29	0.35	0.24	0.22	0.17	0.21
Al2O3	45.64	51.11	47.60	48.37	43.51	43.17	47.78	48.97	41.44	50.68	44.65
Cr2O3	20.87	15.15	19.71	17.54	23.93	21.02	21.45	18.53	27.59	16.04	21.38
FeO	10.40	9.10	9.84	10.18	11.31	10.49	11.17	10.18	9.57	9.14	9.92
MnO	0.02	0.02	0.09	0.11	0.06	0.07	0.17	0.17	0.08	0.19	0.09
NiO	0.61	0.76	0.65	0.54	0.58	0.75	0.75	0.66	0.71	0.65	0.78
MgO	18.57	19.68	19.68	20.39	18.83	18.43	20.56	19.50	18.68	20.06	20.55
CaO	0.07	0.05	0.08	0.04	0.14	0.04	0.14	0.09	0.10	0.05	0.13
Sum	96.52	95.97	97.81	97.37	98.51	94.22	102.23	98.25	98.29	96.91	97.59
TiO2	0.42	0.16	0.24	0.24	0.29	0.31	0.34	0.24	0.22	0.18	0.21
Al2O3	47.24	53.20	48.58	49.51	44.07	45.70	46.59	49.77	42.13	52.20	45.57
Cr2O3	21.60	15.77	20.12	17.95	24.24	22.25	20.92	18.83	28.05	16.52	21.82
Fe2O3	1.03	1.14	1.78	3.32	2.25	2.55	3.09	1.54	0.75	1.61	4.13
FeO	9.83	8.44	8.44	7.44	9.43	8.81	8.11	8.95	9.06	7.96	6.40
MnO	0.02	0.02	0.09	0.11	0.06	0.07	0.17	0.17	0.08	0.20	0.09
NiO	0.63	0.79	0.66	0.55	0.59	0.79	0.73	0.67	0.72	0.67	0.80
MgO	19.22	20.48	20.09	20.87	19.07	19.51	20.05	19.82	18.99	20.66	20.97
Sum	100	100	100	100	100	100	100	100	100	100	100
Oxygen	4	4	4	4	4	4	4	4	4	4	4
Ti	0.0086	0.0031	0.0049	0.0047	0.0060	0.0063	0.0069	0.0049	0.0046	0.0034	0.0042
Al	1.5013	1.6443	1.5296	1.5478	1.4183	1.4589	1.4784	1.5626	1.3654	1.6178	1.4440
Cr	0.4605	0.3270	0.4249	0.3766	0.5233	0.4765	0.4452	0.3967	0.6098	0.3434	0.4638
Fe3+	0.0210	0.0226	0.0357	0.0661	0.0463	0.0521	0.0626	0.0309	0.0155	0.0319	0.0837
Fe2+	0.2218	0.1851	0.1887	0.1650	0.2153	0.1995	0.1826	0.1996	0.2082	0.1751	0.1439
Mn	0.0005	0.0005	0.0021	0.0026	0.0014	0.0017	0.0038	0.0039	0.0019	0.0043	0.0022
Ni	0.0137	0.0167	0.0143	0.0117	0.0129	0.0173	0.0158	0.0144	0.0160	0.0141	0.0173
Mg	0.7727	0.8008	0.7999	0.8254	0.7764	0.7878	0.8047	0.7871	0.7785	0.8100	0.8408
Sum	3	3	3	3	3	3	3	3	3	3	3
Mg#	77.70	81.23	80.91	83.34	78.29	79.80	81.50	79.77	78.90	82.23	85.38
Cr#	23.23	16.40	21.35	18.92	26.32	23.98	22.42	19.93	30.63	17.23	23.29
Fe3:Fe2	0.09	0.12	0.19	0.40	0.22	0.26	0.34	0.16	0.07	0.18	0.58

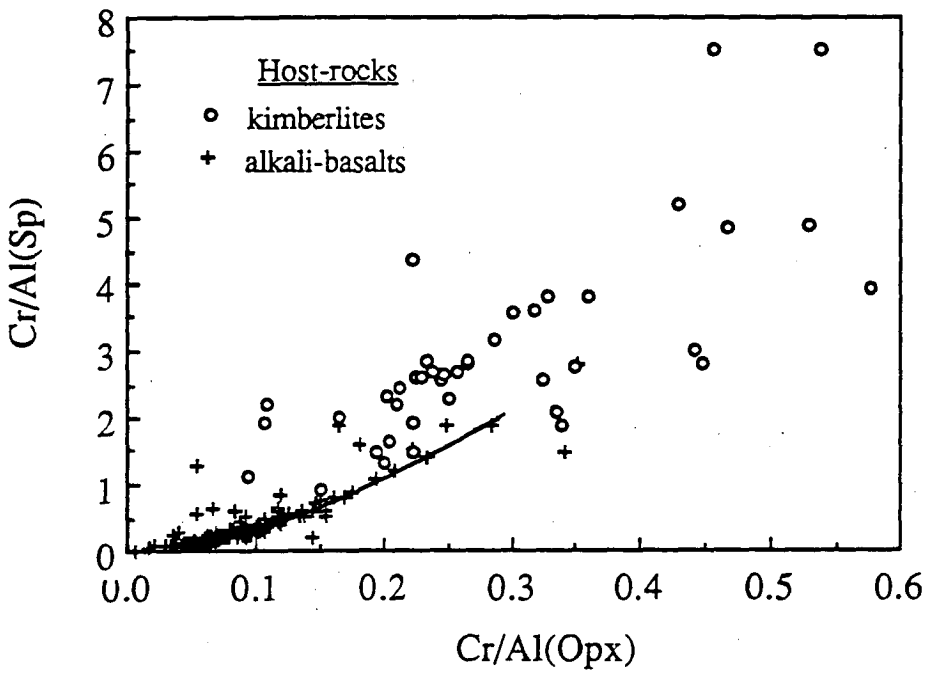

Figure 3.7. Correlation of Cr/Al ratio of spinel with that of orthopyroxene in a number of natural peridotite suites. The low-Cr trend (solid line) is constrained by mostly low-pressure spinel peridotites enclosed in alkali-basalts. Spinel peridotites included in kimberlites define the high-Cr trend. The low-Cr trend is used to infer the experimental equilibrium spinel compositions from the analysed experimental range, using the compositions of the coexisting orthopyroxene. Data sources are give in Table 1.8.

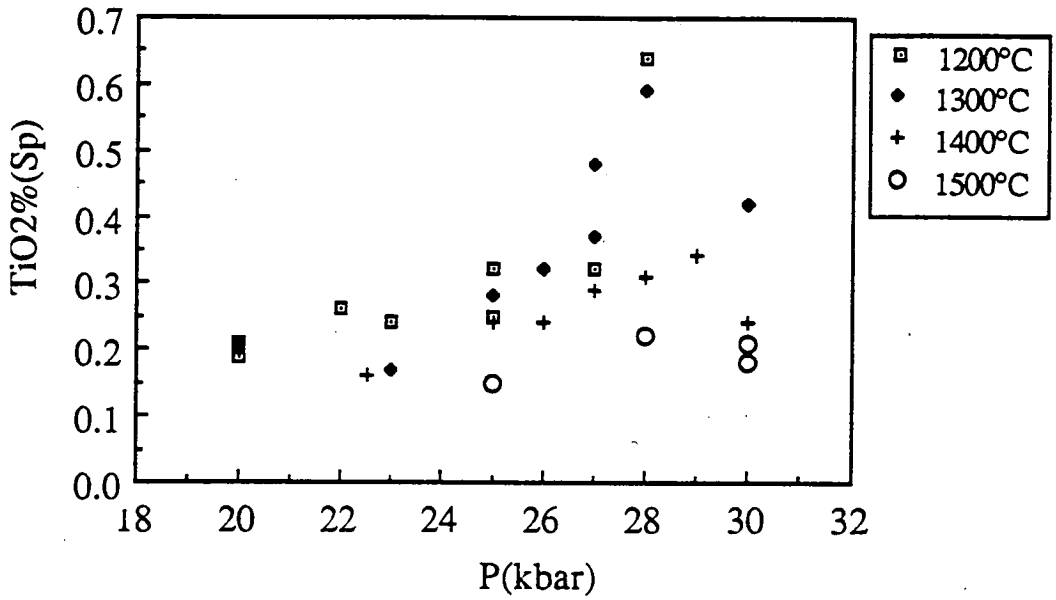

Figure 3.8. Pressure dependence of TiO_2 in the experimental spinels. Although not well defined, the positive correlation trend is discernible.

similar to garnet. There is a tendency for Fe_2O_3 (calculated on the basis of perfect stoichiometry) to increase and MnO to decrease with increasing pressure.

The experimental study of Brey et al. (1990) covers a wider P-T field than the present study. Most of their runs are in the garnet-facies field. Their pressure interval is about 10 kbar, greater than the present study. Thus the results from these two studies are complementary. Variation in their mineral compositions (olivine, two pyroxenes & garnet) are systematic and consistent with the above discussion.

3.4.2 Element Partitioning between Minerals

The variation trends of different elements in P-T space provide clues to the partitioning behaviour of these elements between different minerals. For a given bulk composition and a given mineral paragenesis the partitioning behaviour of an element is entirely dependent on external physical conditions (e.g. pressure & temperature). However, each element has different sensitivity to changes in pressure & temperature. Some elements, e.g. Ca in pyroxenes, Fe^{2+}/Mg in garnet, show sensitive temperature-dependence; whereas others, e.g. Si in garnet, do not seem to respond very much to pressure & temperature variation (at least in the pressure,temperature range of interest). The results of the present study (and of previous studies such as Nickel, 1989; Brey et al., 1990) indicate that partitioning of Si, Al and Cr between orthopyroxene and garnet, and of Si and Al between clinopyroxene and garnet, are strongly dependent on pressure & temperature (Fig.3.9). Partitioning of Ca between olivine and clinopyroxene also shows strong temperature & pressure dependence (Fig.3.10).

For the Fe^{2+}/Mg partitioning between olivine (/ orthopyroxene / clinopyroxene) and garnet, and between olivine and clinopyroxene, temperature has the dominant effect over pressure (Fig.3.11). These partitioning relationships have been investigated before through many individual experimental studies designed to calibrate individual thermometers (e.g. Råheim & Green, 1974a; Mori & Green, 1978; O'Neill & Wood, 1979; Harley, 1984a).

Ca-partitioning between orthopyroxene and clinopyroxene is the basis of the well-known two-pyroxene thermometers (e.g. Wells, 1977; Kretz, 1982; Bertrand & Mercier, 1985; Brey & Köhler, 1990). The partition behaviour of Na between orthopyroxene and clinopyroxene is very much like Ca. Although two empirical calibrations of the thermometer based on this have been published before (Hervig & Smith, 1980; Brey & Köhler, 1990), this study offers the first experimental dataset for Na-partitioning between orthopyroxene and clinopyroxene. Fitting of the experimental data at 25, 30, 35 kbar in the form of the thermometer given by Brey & Köhler (1990) produces the following expression:

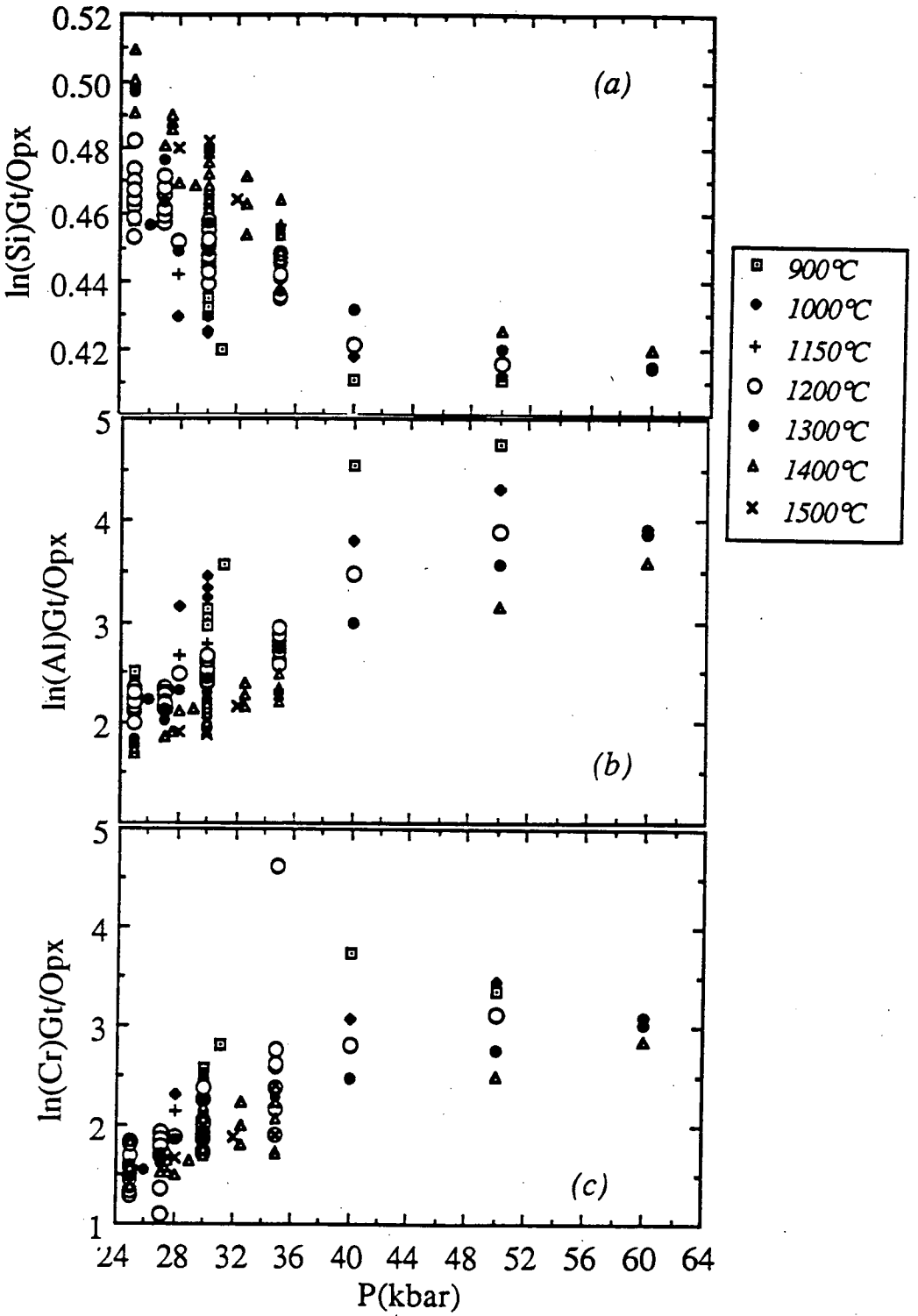

Figure 3.9. Partitioning of Si (a), Al (b) and Cr (c) between garnet and clinopyroxene controlled by pressure and temperature. They show clear pressure dependence. Additional data are from Nickel (1989) and Brey et al. (1990).

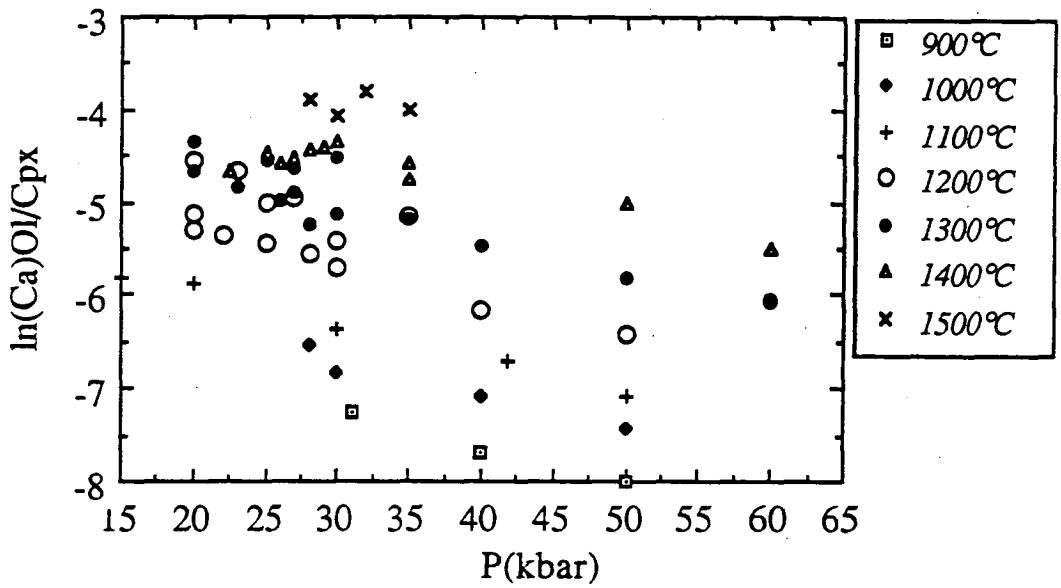

Figure 3.10. Partitioning of Ca between olivine and clinopyroxene as a function of pressure and temperature. The dominant effect of temperature over pressure is clearly demonstrated. Additional data are from Brey et al. (1990) and Köhler & Brey (1990).

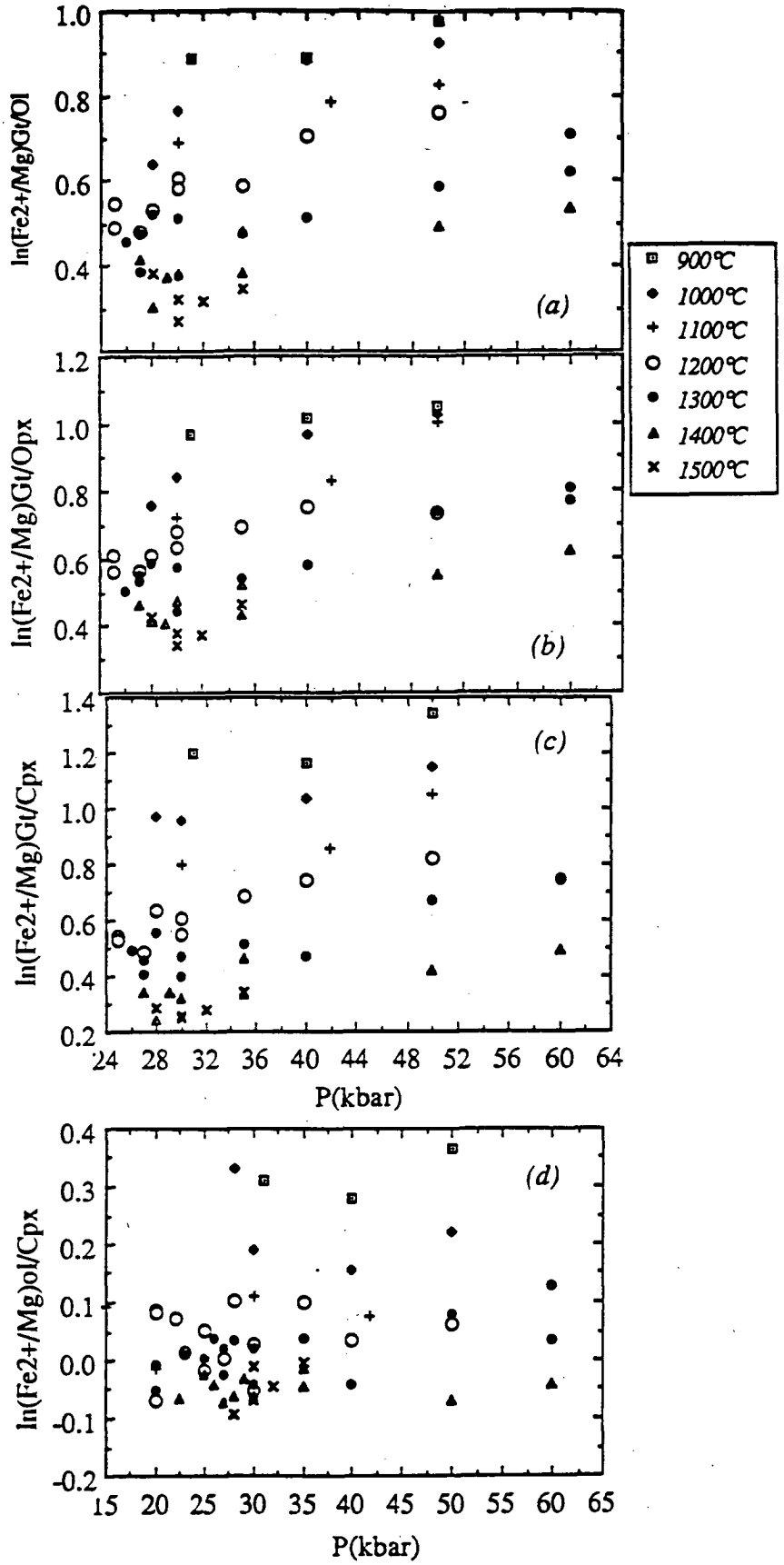

Figure 3.11. Fe^{2+}/Mg partitioning between garnet and olivine (a), between garnet and orthopyroxene (b), between garnet and clinopyroxene (c), and between olivine and clinopyroxene (d) as a function of pressure and temperature. All are dominantly controlled by temperature. Additional data are from Brey et al. (1990).

$$\{\ln(D)\}^2 = \frac{26477}{T(K)} - 13.268 \quad (r^2 = 0.945) \quad \text{where } D = \frac{Na^{Opx}}{Na^{Cpx}}$$

(where Na is the number of Na-ions per 6-oxygen in the pyroxene structure) which translates into a new calibration of the thermometer:

$$T(K) = \frac{26477}{13.268 + \{\ln(D)\}^2}.$$

The available data do not show clear pressure-effect on the ln(D).

Comparison of the experimental temperatures in this study with those estimated by the Brey & Köhler (1990) calibration indicates that the calibration underestimates temperature at the high-temperature end and overestimates temperature at the low-temperature end (Fig.3.12b). The Hervig & Smith (1980) calibration generally underestimates the equilibrium temperatures by about 100°C (Fig.3.12a). The new calibration appears to be an improvement on these earlier calibrations (Fig.3.12c).

Podvin (1988) provides experimental evidence to support temperature-dependence of Ni-Mg partitioning between orthopyroxene and olivine observed by Berger & Vannier (1978) in natural lherzolites. Based on his experimental data at 1 atm, 1075° - 1225°C, Podvin (1988) formulated a simple thermometer. The experimental data presented in this study do not support this lnKd - temperature relationship. On the contrary, our data show little dependence of lnKd ($Kd = \frac{(Ni/Mg)^{Ol}}{(Ni/Mg)^{Opx}}$) on temperature and pressure (Fig.3.13).

Carswell (1974) suggests temperature control on Mn/Mg partitioning between garnet and clinopyroxene. A Mn-thermometer was formulated by Delaney et al. (1979). However, this dataset does not support the suggestion, and application of the Mn-thermometer to the dataset yields temperature values too low compared with the run temperatures.

It was mentioned in the previous section that Ti increases in garnet, and decreases in clinopyroxene and orthopyroxene with increasing temperature. A temperature dependence for $\ln Ti_{(Garnet/Clinopyroxene)}$ [similarly $\ln Ti_{(Garnet/Orthopyroxene)}$] is illustrated in Figure 3.14.

As with garnet, Fe^{2+}/Mg partitioning between spinel and olivine (/orthopyroxene /clinopyroxene) is sensitive to temperature change. More important is the discovery of the strong pressure dependence of Ti partitioning between spinel and pyroxenes (Fig.3.15), which may be formulated as a useful barometer for spinel peridotites. The details are discussed in Chapter Four, where more experimental data are presented to support this observation.

3.4.3 fO_2 estimation

Although the experiments reported here were not oxygen-buffered explicitly, the run conditions (dry experiments in graphite capsules) limited the possible fO_2 range

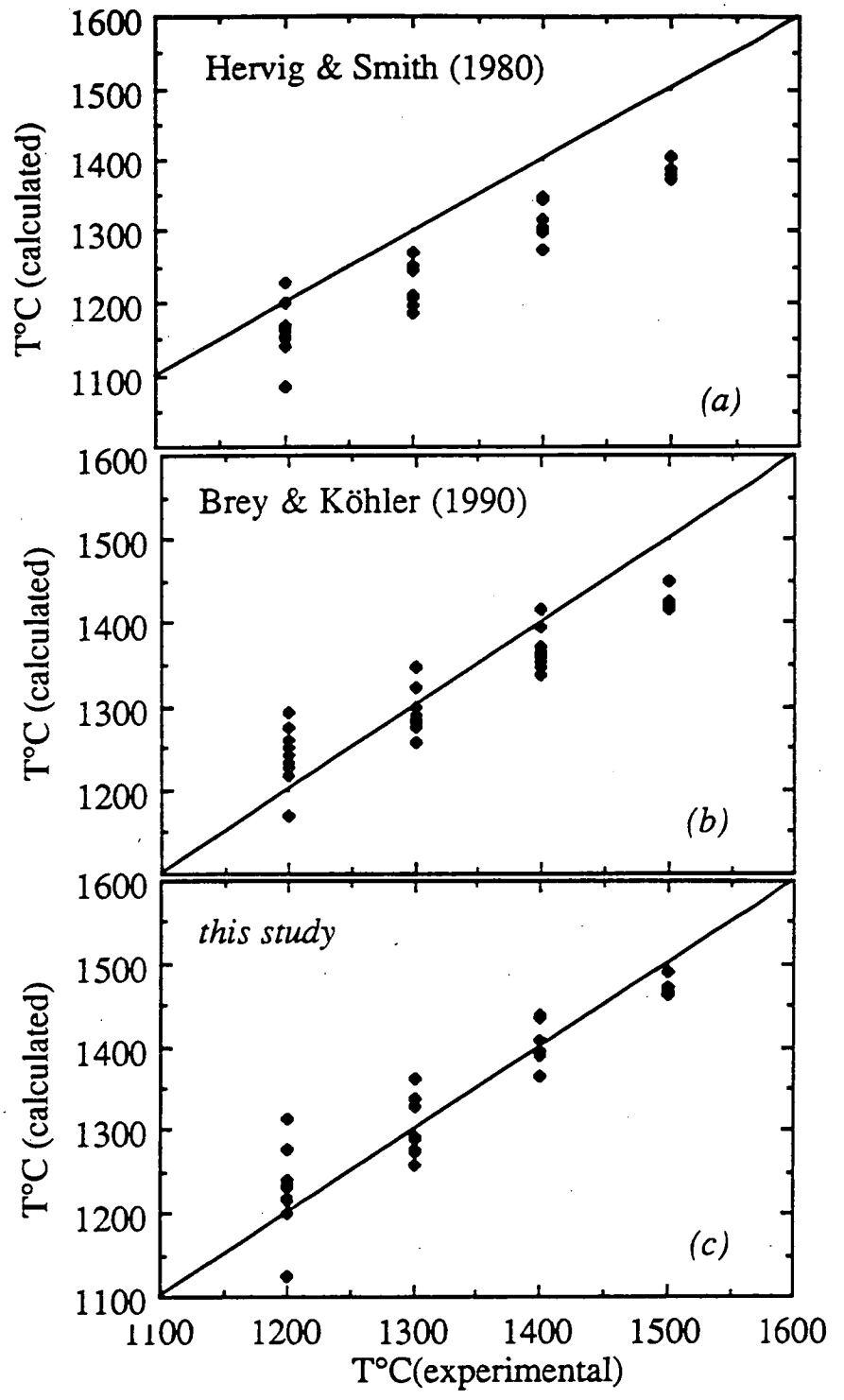

Figure 3.12. Results of calculated equilibrium temperatures from three sodium-thermometers compared with experimental run temperatures.

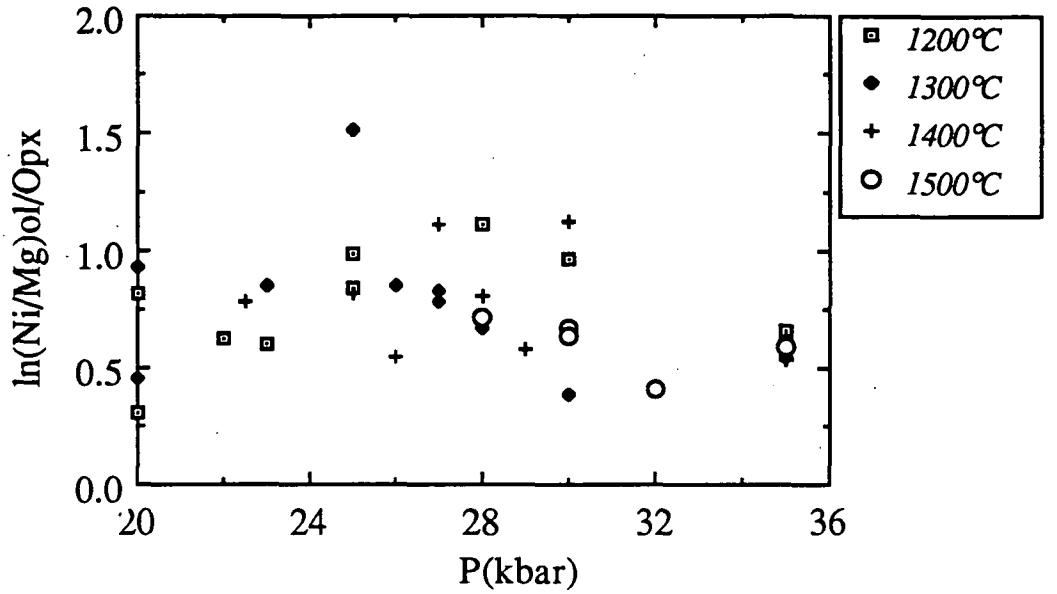

Figure 3.13. Ni/Mg partitioning between olivine and orthopyroxene as a function of pressure and temperature. There is no obvious correlation between $\ln(Ni/Mg)^{Ol/Opx}$ and temperature or pressure. Most of the data points fall in the range between 0.5 and 1.0.

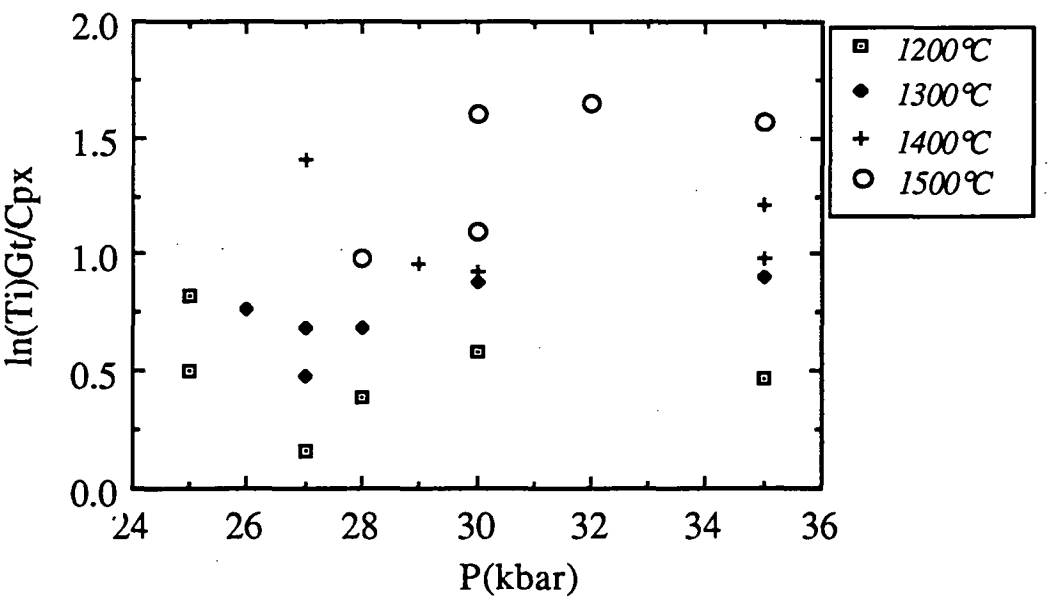

Figure 3.14. Temperature dependence of Ti partitioning between garnet and clinopyroxene is noticeable in this plot. Several points off the trend probably indicate poor quality of these analyses.

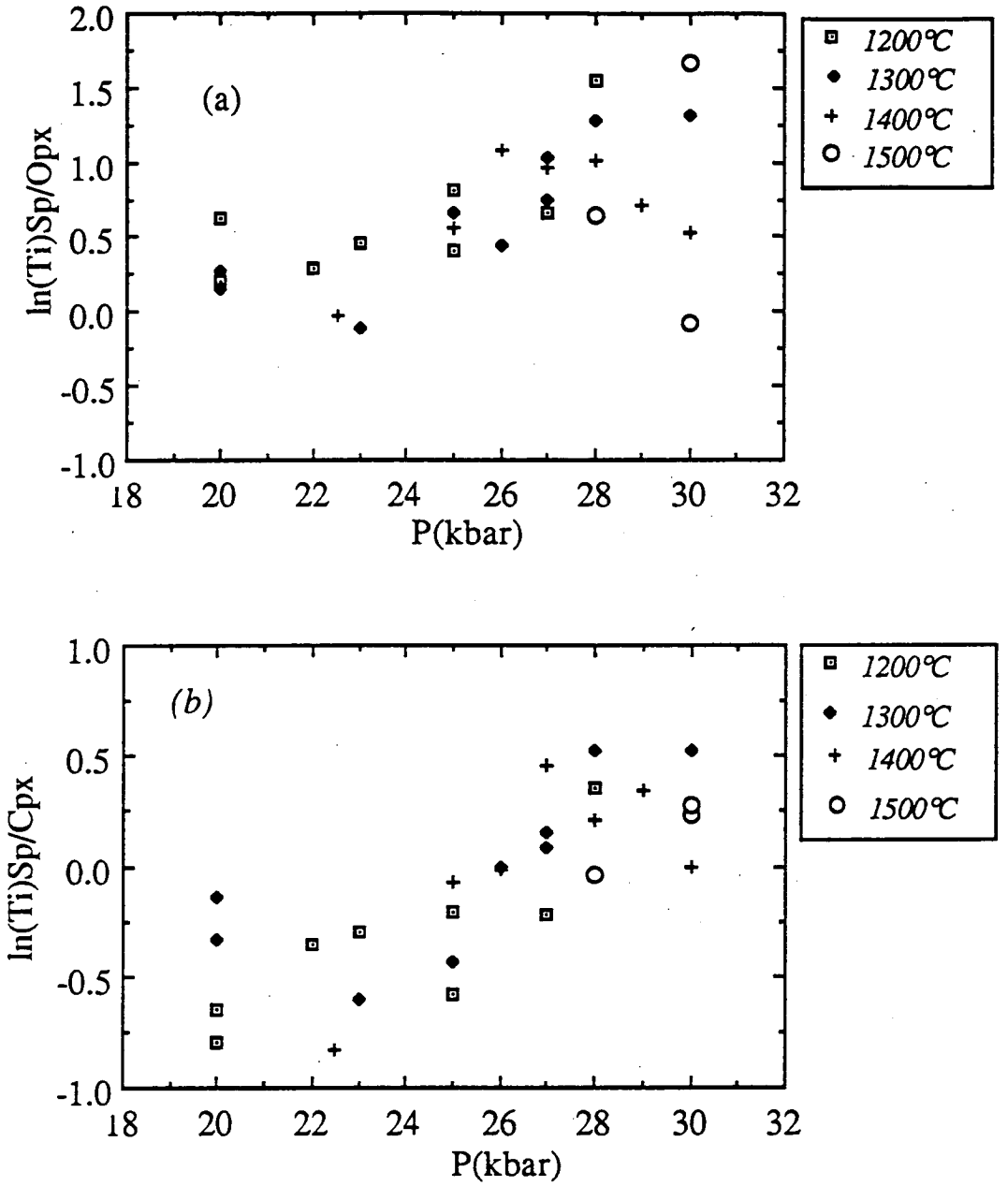

Figure 3.15. The partitioning of Ti between spinel and orthopyroxene (a) and between spinel and clinopyroxene (b) is clearly dependent on pressure. Judging from the slope of the trends, the ln(Ti) - P relationships should make reasonable barometers for spinel peridotites. Some points off the trends in both diagrams imply poor quality of these data (especially spinel analyses at 1500°C).

Table 3.8 Buffer equations used to infer the fO_2 conditions of the experiements (from Taylor, 1985)

---

the *FMQ* buffer:

$$\log fO_2 \text{ (bar)} = 8.746 - \frac{25035}{T(K)} + \frac{0.0944P}{T(K)} - 2.2 \times 10^{-6}P - \frac{10^{-7}P^2}{T(K)}$$

the *graphite - CO* buffer:

$$\log fO_2 \text{ (bar)} = 2.0815 + 0.25754\ln T - \frac{21060}{T(K)} + \frac{0.17112P}{T(K)} - \frac{7.4268 \times 10^{-4}P^2}{T^2}$$

the *graphite - H_2O* buffer:

$$\log fO_2 \text{ (bar)} = 5.0186 - 0.065844\ln T - \frac{22674}{T(K)} + \frac{0.12858P}{T(K)} - \frac{6.6384 \times 10^{-4}P^2}{T^2}$$

---

during these experiments. Assuming that the graphite-CO equilibrium prevailed over the experimental P,T range of this study, the "furnace buffer" should be around 1.2 ± 0.5 log units below the FMQ buffer (buffer equations are listed in Table 3.8). However, if H_2O was present during the experiments, graphite-H_2O equilibrium in the P,T range of interest should correspond to 2.25 ± 0.5 log units below the FMQ buffer. Calculation of the furnace fO_2 by using the olivine-spinel-orthopyroxene oxygen sensor of Ballhaus et al. (1991) gives 1.5 ± 0.5 log units below the FMQ buffer for most of the runs (Table 3.9), in accord with the fO_2 conditions suggested by the graphite-CO equilibrium.

3.4.4 Assessment of existing mineral barometers and thermometers

This experimental dataset provides a good opportunity for assessment of the predicability of existing mineral barometers and thermometers. There are a large number of mineral barometers and thermometers applicable to peridotitic rocks. Some of them are shown by previous studies to give unrealistic estimates [e.g. the garnet - clinopyroxene Fe^{2+}/Mg exchange thermometer of Saxena (1979) seriously underestimates equilibrium temperatures according to Carswell & Gibb, 1987] and are not discussed here. The calculated experimental conditions using various barometers and thermometers are compared with the actual run pressures and temperatures in Table 3.9.

There are four types of barometers in the lherzolite system. The Ca-in-olivine coexisting with clinopyroxene barometer by Köhler & Brey (1990) produces pressure estimates with large uncertainty (upto 20 kbar less than experimental pressure, Fig. 3.16a), probably due to the large analytical uncertainties in the measurement of the low Ca concentrations in the experimental olivines. The spinel lherzolite to garnet lherzolite transition barometer developed by O'Neill (1981) and further modified by Webb & Wood (1986) also gives scatter in the calculated pressure (± 3.5 kbar, Fig.3.16b), and the Webb & Wood (1986) version consistently under-estimates pressure by 3.5 kbar. The Al_2O_3-in-orthopyroxene coexisting with garnet barometer of Nickel & Green (1985) satisfactorily reproduces the experimental run pressure (± 2 kbar, Fig.3.16c). Modification of this barometer according to the suggestion of Taylor & Green (1991) under-estimates pressure by as much as 5 kbar. The Brey & Köhler (1990) barometer gives reasonable results (± 3 kbar, Fig.3.16d) but tends to under-estimate pressure at pressures greater than 30 kbar. The MC74 formulation of Finnerty & Boyd (1984) and the PE81, PN80 barometers of Finnerty & Boyd (1987) consistently over-estimate equilibrium pressure (upto 10 kbar, Fig.3.16e). The WO74c formulation of Finnerty & Boyd (1984) generates reasonable pressure estimates (± 3 kbar) but tends to under-estimate pressure at pressure lower than 30 kbar and over-esimate pressure at pressure greater than 30 kbar (Fig.3.16e). The Cr_2O_3-in-orthopyroxene coexisting with garnet barometer formulated by Nickel (1989)

Table 3.9a Comparison of Calculated Pressures with Experimental Run Pressures

Run#	T3145	T3239	T3105	T3108	T3101	T3168	T3126	T3454	T3151	T3306	T3316	T3158	T3141	T3130	T3355	T3136	T3247
T(°C)	1200	1200	1200	1200	1200	1200	1200	1200	1200	1200	1300	1300	1300	1300	1300	1300	1300
P(kbar)	20	20	22	23	25	25	27	28	30	35	20	20	23	25	26	27	27
Ca-in-Olivine																	
Köhler & Brey90	1.0	16.1	21.9	4.1	23.8	12.7	11.4	26.8	23.0	16.3	18.4	10.0	23.3	14.9	27.6	25.2	17.7
Sp-Gt transition																	
O'Neill81	26.2	25.3	24.0	24.1	25.9	26.2	27.0	29.4			27.8	26.2	26.5	26.5	26.3	27.7	28.7
Webb & Wood86	22.7	21.9	20.6	20.7	22.4	22.8	23.5	25.9			24.1	22.4	22.7	22.7	22.5	24.0	25.0
Al-barometer																	
Nickel & Green85		25.3			24.0	26.1	23.3	28.6	30.4	32.9					28.0	26.5	25.6
Taylor & Green91		23.7			21.9	24.2	21.3	26.7	27.9	30.4					25.7	24.4	23.4
Brey & Köhler90		24.1			22.4	24.9	21.8	27.6	29.3	32.3					27.5	25.9	24.9
MC74	27.2	30.3	26.7	25.2	29.3	31.1	28.2	33.9	35.9	37.8	31.3	30.0	29.9	30.4	33.9	32.8	31.2
WO74c		23.2			21.6	23.7	21.3	27.2	28.8	30.8					26.0	24.6	23.3
PE81	26.5	28.8	26.1	24.9	28.1	29.4	27.2	31.6	33.2	34.6	29.0	28.1	28.0	28.4	31.1	30.2	29.0
PN80	22.7	25.8	22.2	20.5	24.8	26.6	23.7	29.5	31.6	33.5	26.3	25.0	24.9	25.4	29.0	27.8	26.2
Cr-barometer																	
Nickel89		22.1			28.7	21.5	26.6	29.3	34.2	29.2					25.4	27.9	26.8

Run#	T3364	T3160	T3345	T3524	T3164	T3360	T3167	T3453	T3526	T3163	T3342	T3299	T3378	T3249	T3430	T3527	T3302
T(°C)	1300	1300	1300	1400	1400	1400	1400	1400	1400	1400	1400	1400	1500	1500	1500	1500	1500
P(kbar)	28	30	35	22.5	25	26	27	28	29	30	35	35	28	30	30	32	35
Ca-in-Olivine																	
Köhler & Brey90	34.3	14.3	32.9	33.0	26.8	30.9	28.9	26.5	25.8	24.2	36.0	30.5	23.2	28.7	28.6	20.9	26.9
Sp-Gt transition																	
O'Neill81	28.8	27.2		26.2	27.8	27.5	29.3	28.7	28.4	27.3			30.9	29.8	27.4		
Webb & Wood86	25.1	23.5		21.9	23.7	23.4	25.5	24.8	24.5	23.2			27.2	25.8	22.7		
Al-barometer																	
Nickel & Green85	29.1	27.3	36.2				25.9	29.8	30.1	26.7	34.2	36.3	30.4	32.1	29.3	35.0	36.9
Taylor & Green91	26.9	25.2	33.5				23.9	27.7	27.8	24.4	31.8	34.0	27.9	29.9	26.7	31.5	34.6
Brey & Köhler90	28.7	26.8	36.5				26.1	30.1	30.5	26.8	35.0	37.2	31.5	33.2	30.4	36.4	38.0
MC74	35.7	33.5	42.8	32.3	34.4	34.6	32.8	36.5	37.0	33.6	40.9	43.2	37.7	40.5	37.5	42.2	44.8
WO74c	27.4	25.8	34.6				24.6	28.0	28.6	24.9	32.3	34.6	28.7	30.7	28.3	33.7	35.9
PE81	32.4	30.7	37.9	29.2	30.8	31.0	29.6	32.5	32.8	30.2	35.8	37.6	32.8	35.0	32.6	36.3	38.3
PN80	30.8	28.5	38.1	26.8	28.9	29.1	27.2	31.1	31.6	28.1	35.6	38.0	31.7	34.6	31.5	36.4	39.1
Cr-barometer																	
Nickel89	29.9	30.2	36.5				25.5	25.2	27.6	28.1	29.3	28.7	28.3	33.4	31.6	32.7	33.3

Table 3.9b Comparison of Calculated Temperatures with Experimental Run Temperatures

Run#	T3145	T3239	T3105	T3108	T3101	T3168	T3126	T3454	T3151	T3306	T3316	T3158	T3141	T3130	T3355	T3136	T3247
P(kbar)	20	20	22	23	25	25	27	28	30	35	20	20	23	25	26	27	27
T(°C)	1200	1200	1200	1200	1200	1200	1200	1200	1200	1200	1300	1300	1300	1300	1300	1300	1300
two-pyroxene																	
Wells77	1214	1154	1137	1233	1122	1198	1196	1095	1137	1110	1244	1290	1207	1205	1176	1203	1299
Kretz82	1204	1163	1119	1214	1122	1214	1200	1112	1168	1159	1231	1275	1190	1192	1174	1206	1303
BM85	1249	1178	1154	1259	1154	1251	1236	1118	1185	1158	1277	1311	1231	1231	1209	1249	1340
Brey & Köhler90	1254	1202	1184	1267	1196	1261	1256	1163	1225	1205	1271	1295	1247	1248	1230	1265	1330
Ca-in-Opx																	
Brey & Köhler90	1281	1190	1174	1261	1279	1211	1270	1173	1183	1211	1272	1293	1242	1258	1258	1283	1331
Fe2+/Mg(Gt-Ol)																	
O'Neill & Wood79		1344			1305	1420	1421	1339	1249	1256					1478	1442	1629
Kawasaki79		1233			1232	1317	1320	1265	1203	1218					1354	1340	1469
Fe2+/Mg(Gt-Opx)																	
Harley84		1119			1159	1202	1210	1178	1126	1150					1263	1243	1225
Carswell & Harley89		1157			1199	1244	1252	1219	1165	1191					1307	1286	1268
Sen & Battacharya84		1121			1126	1185	1178	1122	1034	1020					1263	1222	1198
Lee & Ganguly88(T1)		1286			1331	1381	1383	1348	1285	1307					1445	1424	1400
Lee & Ganguly88(T2)		1286			1291	1284	1285	1295	1286	1294					1253	1275	1279
Fe2+/Mg(Gt-Cpx)																	
Chapter Six		1064			1184	1168	1240	1099	1141	1102					1213	1278	1319
Sp-Opx-Ol equilibria																	
Lane & Ganguly80(Ta)	1424	1263	1470	1601	1344	1261	1416	1173	1121	1099	1451	1538	1566	1543	1347	1411	1502
Lane & Ganguly80(Tb)	1384	1227	1428	1555	1302	1220	1371	1130	1077	1050	1411	1496	1521	1496	1304	1366	1455
Webb & Wood86	1304	1100	1238	1332	1186	1111	1316	1114			1388	1373	1399	1382	1170	1301	1477
Witt-Eicksch&Seck91(Ca)	1152	999	1092	1161	1078	1010	1155	1027			1176	1183	1194	1199	1051	1149	1269
Witt-Eicksch&Seck91(Al)	1112	1168	1093	1184	1088	1161	1178	1083	965	950	1191	1257	1203	1148	1105	1145	1159
Fe2+/Mg(Sp-Ol)																	
Ballhaus et al91	1256	1138	1054	1014	1068	1089	1145	1045			1207	1058	1142	1082	1067	1158	1138
O'Neill&Wall87	960	877	822	779	817	831	871	772			913	801	873	826	817	881	859
Fabries79	1194	1104	1016	963	1023	1039	1084	983			1152	1012	1085	1025	1008	1087	1070
Na-in-two-pyroxene																	
Hervig & Smith80	1162	1152	1164	1228	1154	1200	1168	1084	1168	1139		1244	1185	1208	1196	1211	1252
Brey & Köhler90	1227	1218	1234	1294	1233	1275	1251	1168	1259	1243		1299	1257	1283	1275	1290	1324
this study	1230	1217	1233	1312	1220	1278	1239	1124	1239	1200		1330	1260	1289	1274	1292	1339
Δlogfo2																	
Ballhaus et al91	-1.29	-1.26	-1.77	-3.63	-1.39	-1.23	-1.34	-1.25			-1.36	-2.49	-2.00	-2.10	-2.00	-1.50	-1.41

Table 3.9b Comparison of Calculated Temperatures with Experimental Run Temperatures (cont'd)

Run#	T3364	T3160	T3345	T3524	T3164	T3360	T3167	T3453	T3526	T3163	T3342	T3299	T3378	T3249	T3430	T3527	T3302
P(kbar)	28	30	35	22.5	25	26	27	28	29	30	35	35	28	30	30	32	35
T(°C)	1300	1300	1300	1400	1400	1400	1400	1400	1400	1400	1400	1400	1500	1500	1500	1500	1500
two-pyroxene																	
Wells77	1174	1305	1207	1302	1297	1310	1298	1379	1304	1334	1314	1342	1478	1422	1467	1459	1456
Kretz82	1191	1308	1248	1279	1285	1300	1285	1379	1306	1321	1327	1355	1459	1407	1437	1453	1444
BM85	1222	1354	1273	1327	1344	1351	1338	1412	1343	1371	1370	1391	1468	1440	1452	1464	1460
Brey & Köhler90	1244	1339	1289	1311	1322	1333	1325	1379	1327	1354	1353	1372	1406	1391	1400	1407	1420
Ca-in-Opx																	
Brey & Köhler90	1252	1356	1279	1339	1339	1323	1322	1345	1336	1378	1383	1381	1427	1440	1429	1425	1438
Fe2+/Mg(Gt-Ol)																	
O'Neill & Wood79	1354	1683	1452				1571	1886	1675	1665	1445	1673	1662	2007	1856	1834	1771
Kawasaki79	1276	1528	1379				1426	1665	1510	1524	1369	1554	1492	1771	1663	1650	1626
Fe2+/Mg(Gt-Opx)																	
Harley84	1198	1360	1292				1315	1376	1392	1328	1307	1412	1362	1488	1443	1461	1378
Carswell & Harley89	1240	1407	1337				1361	1425	1441	1374	1353	1462	1410	1541	1493	1513	1426
Sen & Battacharya84	1151	1357	1208				1329	1406	1421	1310	1230	1375	1386	1555	1483	1491	1325
Lee & Ganguly88(T1)	1371	1551	1468				1502	1573	1585	1517	1483	1606	1553	1698	1647	1660	1564
Lee & Ganguly88(T2)	1293	1220	1295				1221	1182	1171	1248	1287	1233	1187	1100	1149	1144	1250
Fe2+/Mg(Gt-Cpx)																	
Chapter Six	1177	1358	1273				1413	1563	1417	1476	1330	1497	1481	1549	1579	1544	1473
Sp-Opx-Ol equilibria																	
Lane & Ganguly80(Ta)	1285	1397	1104	1729	1578	1567	1724	1460	1446	1674	1312	1232	1677	1503	1710	1430	1339
Lane & Ganguly80(Tb)	1241	1349	1055	1679	1531	1519	1670	1413	1398	1619	1261	1182	1624	1453	1654	1380	1287
Webb & Wood86	1202	1237		1444	1420	1384	1697	1340	1297	1453			1693	1367	1415		
Witt-Eicksch&Seck91(Ca)	1101	1109		1228	1208	1179	1365	1167	1141	1225			1368	1187	1194		
Witt-Eicksch&Seck91(Al)	1069	1181	935	1240	1262	1258	1328	1211	1174	1275	1091	1118	1276	1205	1273	1150	1176
Fe2+/Mg(Sp-Ol)																	
Ballhaus et al91	1115	1020		1137	1242	1424	1199	1250	1366	1160			1163	1785	1235		
O'Neill&Wall87	842	767		877	950	1112	904	954	1055	891			855	1392	959		
Fabries79	1046	946		1077	1156	1338	1118	1162	1262	1076			1062	1608	1139		
Na-in-two-pyroxene																	
Hervig & Smith80	1198	1271	1198	1316	1298	1274	1301	1344	1274	1304	1275	1348	1379	1373	1386	1373	1405
Brey & Köhler90	1281	1348	1300	1360	1354	1339	1362	1394	1347	1372	1364	1416	1416	1418	1425	1423	1450
this study	1276	1361	1277	1408	1389	1364	1393	1436	1365	1396	1365	1439	1467	1462	1473	1462	1489
Δlogfo2																	
Ballhaus et al91	-1.11	-2.77		-2.58	-2.01	-1.00	-1.69	-1.48	-1.22	-2.30			-3.49	-0.89	-2.20		

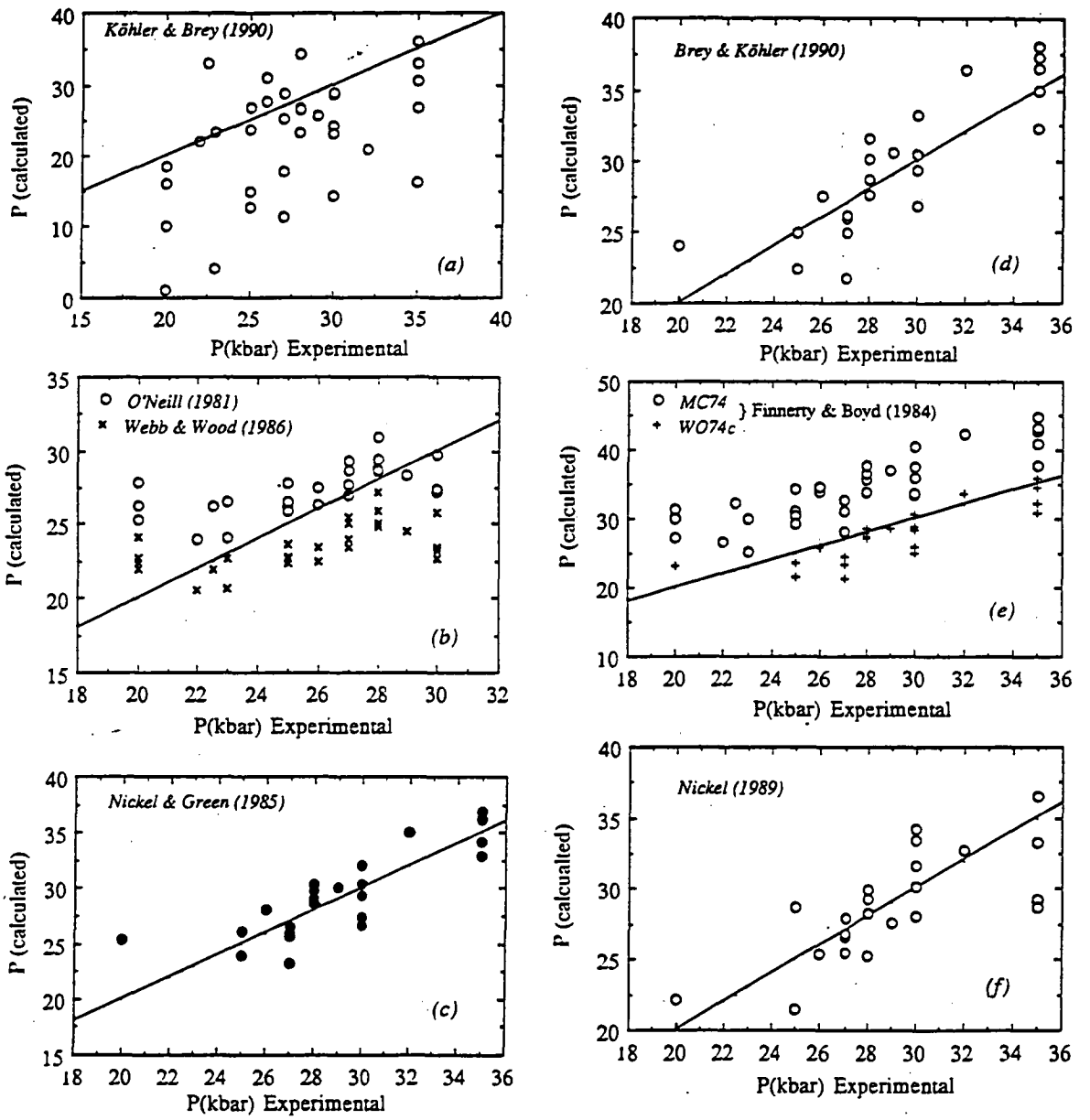

Figure 3.16. Comparison of experimental pressures with pressure estimates from

(a) the Ca-barometer of Köhler & Brey (1990);

(b) the spinel peridotite to garnet peridotite transition barometer of O'Neill (1981) and Webb & Wood (1986);

(c) the Al-barometer of Nickel & Green (1985);

(d) the Al-barometer of Brey & Köhler (1990);

(e) the Al-barometer MC74 and WO74c of Finnerty & Boyd (1984);

(f) the Cr-barometer of Nickel (1989).

offers reasonable pressure estimates with relatively large uncertainty (± 4 kbar, Fig.3.16f). Among all these barometers discussed, the Nickel & Green (1985) barometer produces the closest pressure estimates to the experimental pressure.

Among the two-pyroxene thermometers, the Bertrand & Mercier (1985) version gives the most accurate temperature estimates (± 100°C, Fig.3.17a). The Wells (1977) and Kretz (1982) thermometers produce similar results (± 125°C, Fig.3.17a). The Brey & Köhler (1990) formulation offers no improvemnet over the Bertrand & Mercier (1985) version and tends to under-estimate experimental temperature by 100°C at temperatures higher than 1300°C (Fig.3.17a). Brey & Köhler (1990) formulated a new thermometer on the basis of Ca concentration in orthopyroxene alone. This thermometer is very similar to their two-pyroxene thermometer and reproduces the experimental temperatures within ± 75°C (Fig.3.17b). The two garnet - olivine Fe^{2+}/Mg exchange thermometers of O'Neill & Wood (1979) and Kawasaki (1979) can seriously over-estimate temperature by as much as 200 - 400°C (Fig.3.17c). The thermometer based on garnet - orthopyroxene Fe^{2+}/Mg exchange formulated by Carswell & Harley (1989) generates good temperature estimates (± 50°C, Fig.3.17d), but those by Harley (1984a) and Sen & Battacharya (1984) consistently under-estimate experimental temperatures by as much as 150°C (Fig.3.17d). Thermometers based on garnet - clinopyroxene Fe^{2+}/Mg exchange are discussed in details in Chapter Six and a new version is formulated there. This new thermometer gives reasonable temperature estimates (± 60°C). None of the spinel - olivine Fe^{2+}/Mg exchange thermometers (Fabries, 1979; O'Neill & Wall, 1987; Ballhaus et al., 1991) is found satisfactory. All of these three versions under-estimate experimental temperatures by as much as 300 - 500°C (Fig.3.17e). Further discussions are presented in Chapter Five. Thermometers based on orthopyroxene-spinel-olivine equilibria formulated by Lane & Ganguly (1980) and by Witt-Eicksch & Seck (1991) produce scattered temperature estimates (± 250°C, Fig.3.17f). The two thermometers of Witt-Eicksch & Seck (1991) consistently under-estimate experimental temperatures by 250°C. The Webb & Wood (1986) modification of the Gasparik & Newton (1984) thermometer reproduces experimental temperatures within ± 120°C (Fig.3.17f). In summary, two thermometers (Bertrand & Mercier, 1985; Carswell & Harley, 1989) produce the closest temperature estimates to the experimental temperatures; the thermometers by Wells (1977) and Kretz (1982) and the one formulated in Chapter Six also give acceptable results.

3.5 Subsolidus Mineral Reactions

The gradual change in mineral composition and mineral modes with pressure and temperature is a manifestation of mineral reactions under the subsolidus conditions. Two basic types of mineral reactions are recognised in the lherzolite system. One is pressure-

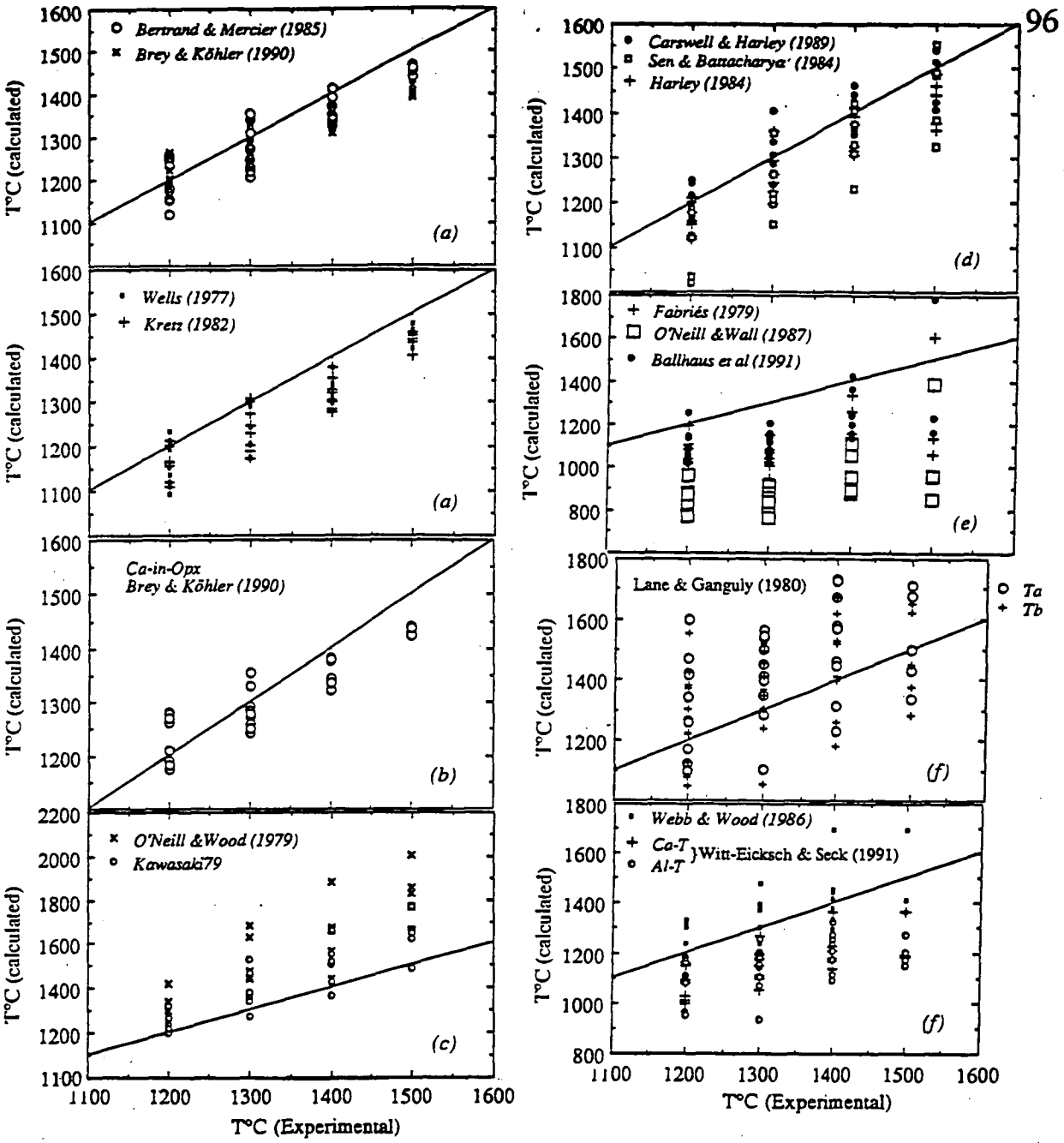

Figure 3.17. Comparison of experimental temperatures with temperature estimates from

(a) the two-pyroxene thermometer of Bertrand & Mercier (1985), Wells (1977), Kretz (1982), and Brey & Köhler (1990);

(b) the Ca-in-Opx thermometer of Brey & Köhler (1990);

(c) the garnet - olivine Fe^{2+}/Mg partitioning thermometer of O'Neill & Wood (1979) and Kawasaki (1979);

(d) the garnet - orthopyroxene Fe^{2+}/Mg partitioning thermometer of Carswell & Harley (1989), Harley (1984), and Sen & Battacharya (1984);

(e) the spinel - olivine Fe^{2+}/Mg partitioning thermometer of Fabriés (1977), O'Neill & Wall (1987), and Ballhaus et al. (1991);

(f) the spinel - orthopyroxene - olivine equilibria thermometer of Lane & Ganguly (1980), Witt-Eicksch & Seck (1991), and Webb & Wood (1986).

dependent and involves formation of garnet at the expense of spinel and orthopyroxene with increasing pressure; the other type is temperature-dependent and concerns formation of clinopyroxene at the expense of spinel, orthopyroxene, and garnet with increasing temperature. In the spinel-facies field, there is no significant element variation correlating with pressure change. Some minor elements [such as Ca in olivine (Köhler & Brey, 1990, this study) and Ti in spinel (this study)] exhibit substantial pressure-dependence but their abundances are so small as to have little influence on the modal abundances of their host minerals. In the garnet-facies field, garnet formation is through the well-known reaction approximated by

$$\underset{\text{Opx}_{ss}}{MgAl_2SiO_6} + Mg_2Si_2O_6 = \underset{\text{Garnet}}{Mg_3Al_2Si_3O_{12}}$$

which has been calibrated as a geobarometer(e.g. Wood, 1974; Harley & Green, 1982; Nickel & Green, 1985; Brey & Köhler, 1990). In the transition zone from the spinel-facies to the garnet-facies, formation of garnet is accompanied by olivine via the reaction

$$\underset{\text{Spinel}}{MgAl_2O_4} + 2\,\underset{\text{Opx}_{ss}}{Mg_2Si_2O_6} = \underset{\text{Garnet}}{Mg_3Al_2Si_3O_{12}} + \underset{\text{Olivine}}{Mg_2SiO_4}$$

which has also been calibrated as a barometer by O'Neill (1981) (with modification by Webb & Wood, 1986).

The temperature-dependent reactions are represented by the following reactions: in the Spinel-facies field:

$$\underset{\text{Spinel}}{MgAl_2O_4} + \underset{\text{Opx}_{ss}}{CaMgSi_2O_6} = \underset{\text{Cpx}_{ss}}{CaAl_2SiO_6} + \underset{\text{Olivine}}{Mg_2SiO_4}$$

in the Garnet-facies field:

$$\underset{\text{Garnet}}{Mg_3Al_2Si_3O_{12}} + \underset{\text{Opx}_{ss}}{CaMgSi_2O_6} = \underset{\text{Cpx}_{ss}}{CaAl_2SiO_6} + 2\,\underset{\text{Cpx}_{ss}}{Mg_2Si_2O_6}$$

and in both the Spinel-facies and the Garnet-facies fields:

$$\underset{\text{Opx}_{ss}}{CaMgSi_2O_6} = \underset{\text{Cpx}_{ss}}{CaMgSi_2O_6}; \qquad \underset{\text{Opx}_{ss}}{Mg_2Si_2O_6} = \underset{\text{Cpx}_{ss}}{Mg_2Si_2O_6}$$

The last two reactions (two-pyroxene equilibria) have been thoroughly investigated from the simple CMAS system to the complex natural system. The thermometer based on the first of the two is one of the most frequently-used thermometers in the literature (e.g. Wells, 1977; Bertrand & Mercier, 1985; Brey & Köhler, 1990). The first two reactions are potentially useful macroscopic thermometers.

3.6 Conclusions

Several important conclusions can be drawn from this study:

1. There is no abrupt composition change across the spinel-lherzolite to garnet-lherzolite transition boundary. The compositions of all phases present in the lherzolite system change continuously and gradually. This gradual change with temperature and pressure produces changes in modal mineralogy. Thus at 1500°C in the spinel lherzolite field there is < 1% spinel present with relatively Al-rich pyroxenes. The first appearance of garnet produces around 5% modal garnet. In contrast at 1200°C there is about 2 - 2.5% spinel in the spinel lherzolite field and at garnet appearance, the modal proportion of garnet is 10 - 12%. This quantifies the nature of mineral-based discontinuties which might be anticipated due to interaction of appropriate geotherm with the spinel lherzolite to garnet lherzolite transition boundary.

2. Two types of mineral reactions are identified in the subsolidus lherzolite system: the pressure-dependent reactions involving growth of garnet at the expense of spinel and orthopyroxene towards higher pressures and the temperature-dependent reactions involving formation of clinopyroxene at the expense of spinel, garnet and orthopyroxene towards higher temperatures. These reactions are continuous, gradual and systematic.

3. Systematic composition changes of individual mineral with pressure and temperature in the lherzolite system are thoroughly investigated and documented. The dataset provides a fundamental basis for further studies of physical properties of the upper mantle, and is necessary for better, and more accurate modelling of upper mantle processes.

4. Assessment of existing mineral barometers and thermometers with the dataset presented in this study indicates that the Nickel & Green (1985) barometer and the Bertrand & Mercier (1985), Carswell & Harley (1989) thermometers reproduce the experimental pressures and temperatures satisfactorily. The two-pyroxene thermometers formulated by Wells (1977) and Kretz (1982, the Ca-transfer thermometer), and the garnet - clinopyroxene Fe^{2+}/Mg exchange thermometer in Chapter Six also give reasonable temperature estimates.

Chapter Four

The Spinel-peridotite Facies to Garnet-peridotite Facies Transition in Simple and Complex Systems

Figures (8)
Plates (3)
Tables (7)

Abbreviations:

MAS: $MgO - Al_2O_3 - SiO_2$;
CMAS: $CaO - MgO - Al_2O_3 - SiO_2$;
CMASCr: $CaO - MgO - Cr_2O_3 - Al_2O_3 - SiO_2$;
IW: iron-wüstite; EMOG: enstatite-magnesite-olivine-graphite.

Chapter Four

The Spinel-peridotite Facies to Garnet-peridotite Facies Transition in Simple and Complex Systems

4.1 Introduction

The transition from spinel-facies to garnet-facies is a prominent phase boundary in the low-pressure part of the peridotite system. A petrologic application of this transition is its use as a geobarometer (O'Neill, 1981). The garnet-in boundary also offers an approximation of the pressure limit for spinel peridotite inclusions in alkali-basalts, for which there is no precise geobarometer available. A geophysical application of this transition is the suggestion of it being responsible for observed increases in seismic P-wave velocity (an increase of 0.2 - 0.4 km/sec) in the oceanic lithosphere at the depth of 40 - 55 km (Green & Liebermann, 1976; Webb & Wood, 1986); and partly responsible for the observed 50 - 300 m uplift of old oceanic floor relative to that predicted from the conductive cooling model (Wood & Yuen, 1983).

Experimental studies particularly designed to locate the transition boundary are mainly in simplified peridotite systems, although limited data in complex multi-component systems are also available (e.g. Green & Ringwood, 1967a; O'Hara et al., 1971). Despite the large number of experiments, there is not yet a clear picture about the exact location of the transition boundary in complex systems. The empirical model developed by O'Neill (1981) only considers the reaction

$$2\,Mg_2Si_2O_6 + MgAl_2O_4 = Mg_2SiO_4 + Mg_3Al_2Si_3O_{12} \qquad (4.1)$$

but neglects the other reaction

$$Mg_2Si_2O_6 + MgAl_2SiO_6 = Mg_3Al_2Si_3O_{12} \qquad (4.2)$$

which is equally important to garnet-growth with increasing pressure (Green & Ringwood, 1967a; Chapter Three). Therefore a better model is required to consider both reactions.

This study summarises available experimental data in simple and complex systems in the literature and presents new experimental data in three model lherzolite systems. A new empirical model predicting the pressure of garnet-incoming is formulated from these data; and its application is discussed.

4.2 Previous Experimental Studies in Simple Systems

The MAS system

The simplest peridotite system is the MAS system, where the spinel-facies to garnet-facies transition is a univariant curve in PT space. There are many experimental

studies in this system, mostly concerned with Al_2O_3-solubility in enstatite, which was found to be temperature-sensitive in the spinel-facies and pressure-sensitive in the garnet-facies. The study of MacGregor (1974) covers 900° - 1800°C, 15 - 45 kbar, and locates the transition at 1000°C/21.5 kbar, 1600°C/32.5 kbar. Danckwerth & Newton (1978) made a detailed study in the temperature range of 900° - 1100°C and found the transition boundary 2 kbar lower than that determined by MacGregor (1974). The slope of the transition curve is also slightly smaller than that of MacGregor (1974). Perkins et al. (1981) noticed the inconsistency and undertook another detailed study in the temperature range of 900° - 1600°C, and pressure range of 15 - 40 kbar. They placed the transition at 1100°C/22 kbar, 1400°C/27 kbar, about 1 kbar lower than that determined by MacGregor (1974) but with the same slope as that of MacGregor (1974). However, the location at 1200°C/22.5 kbar, 1600°C/30 kbar by Gasparik & Newton (1984) is more consistent with the study of Danckwerth & Newton (1978) at low temperatures. Newton (1989) summarised several well-controlled experiments in this system and obtained a transition boundary which is at yet lower pressure (Fig.4.1). The maximum difference between these studies is 3.5 kbar. In view of the experimental uncertainties (differences in sample assembly arrangement in particular), the transition boundary and the Al_2O_3 in enstatite data given in Figure 1 of Newton (1989) are adopted in this study as the basis of empirical modelling in complex systems.

The CMAS system

Addition of Ca to the MAS system introduces another phase, clinopyroxene, which keeps the transition univariant. The experimental study of O'Hara et al. (1971) found the transition at 1100°C/18 kbar, 1400°C/22 kbar. The large change in the slope of the transition which they found at T > 1400°C is probably caused by the presence of melt, which dissolves large amount of Al_2O_3 and CaO therefore increases the pressure of garnet-incoming. The transition at 1400°C/22 kbar is confirmed by Gasparik (1984). At lower temperatures Jenkins & Newton (1979) suggested the transition at 900°C/15 kbar and 1000°C/16 kbar, about 2 kbar lower than that suggested by O'Neill (1981) at 800°C/16.5 kbar, 1100°C/19 kbar. Most of these experimental data except that of Jenkins & Newton (1979) are consistent with each other within the experimental uncertainties of ± 0.5 kbar (Fig.4.2). They indicate a consistent decrease of about 2 kbar relative to the transition boundary in the MAS system.

The CMAS-Cr system

Further addition of Cr to the CMAS system has two important effects on the transition. Firstly it increases the degree of freedom in the system and therefore the transition changes from a univariant curve to a divariant field in PT space. Secondly the

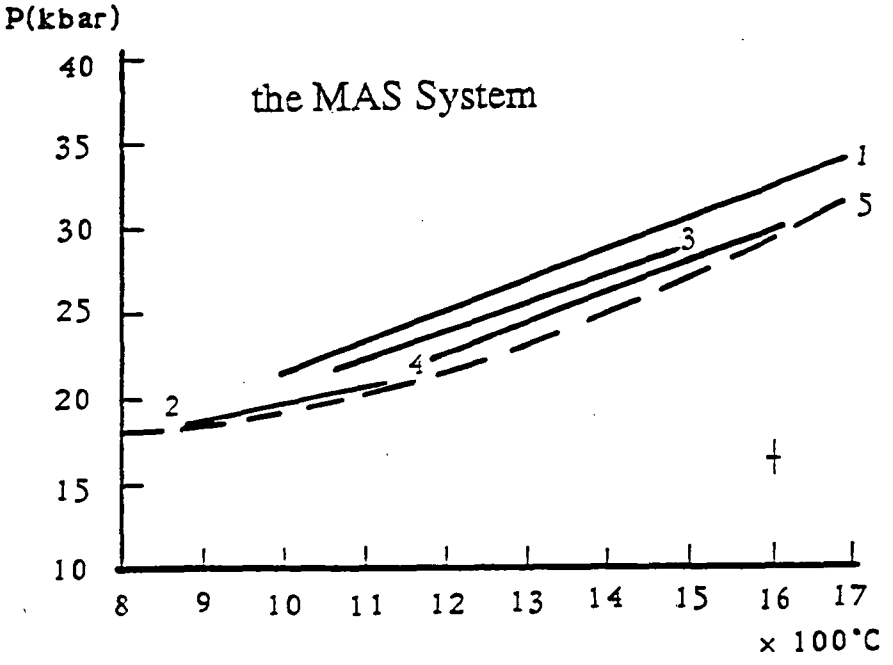

Figure 4.1. Experimentally determined spinel-peridotite to garnet-peridotite transition boundaries in the MAS system (1. MacGegor, 1974; 2. Danckwerth & Newton, 1978; 3. Perkins et al., 1981; 4. Gasparik & Newton, 1984; 5. Newton, 1989).

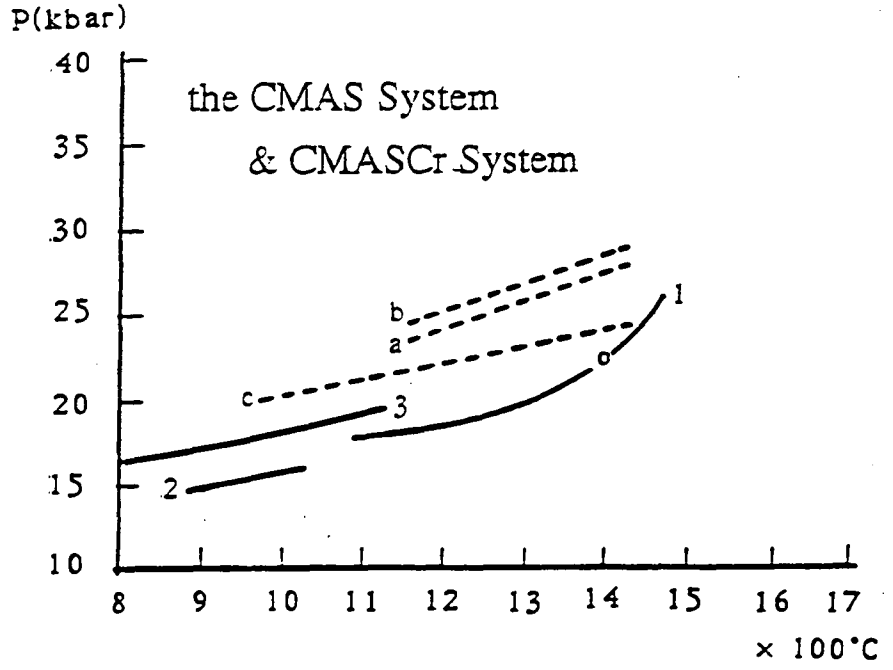

Figure 4.2. Experimentally determined garnet-in boundaries in the CMAS system (solid lines: 1. O'Hara et al. 1971; 2. Jenkins & Newton, 1979; 3. O'Neill, 1981; o. Gasparik, 1984) and in the CMASCr system (broken lines: Nickel, 1986; a. low-Cr mix, Cr#10; b. medium-Cr mix, Cr#20; c. high-Cr mix, Cr#30).

strong tendency of Cr to partition into spinel increases the pressure of the spinel-out boundary and enlarges the PT field in which both spinel and garnet coexist. Chromium also partitions into garnet and pyroxenes, and in this order. This causes a slight increase in the pressure of garnet appearance. Apart from the experimental study of O'Neill (1981), who determined the composition of spinels coexisting with garnet in the CMASCr system by X-ray diffraction method, the study by Nickel (1986) is the only one which specifically emphasises the transition boundary in PT space in this system. Nickel's study demonstrates that increase in the amount of Cr_2O_3 in the system does not simply raise the pressure of garnet appearance and the amount of pyroxenes present in the system also has significant influence on the transition. In the three sets of experiments with three different bulk Cr/Cr+Al values, the garnet-in boundary in the high-Cr system (Cr#=30) locates at lower pressure and has a shallower slope than in the low-Cr system (Cr#=10) (Fig.4.2; Nickel, 1986). This is because there is no olivine in the high-Cr system and consequently the amount of pyroxenes increased significantly relative to those in the low-Cr and medium-Cr (Cr#=20) systems. Therefore, garnet growth is facilitated due to the significantly increased amount of pyroxenes in the high-Cr system.

The discussion so far has qualitatively shown the effects of Ca and Cr on the spinel-facies to garnet-facies transition. Fe is a major component in the peridotite system, but direct experimental study of the effect of Fe on the transition is lacking. Theoretical calculations by O'Neill (1981) and Gasparik (1987) suggest a decrease of the pressure of garnet appearance with increasing FeO content in the system. O'Neill (1981) suggests that Fe_2O_3 behaves in the same way as Cr_2O_3, i.e. increasing the pressure of the garnet-in boundary, which is consistent with the experimental observation of MacGregor (1970). The effects of other minor elements such as Na, Mn and Ni are probably small and cannot be ascertained with available experimental data.

4.3 Previous Experimental Studies in Complex Systems

Green & Ringwood (1967a) determined the garnet-in boundary in the Hawaiian pyrolite model system and found that garnet growth could be achieved in the absence of spinel via the reaction (4.2). O'Hara et al. (1971) specifically designed a series of experiments to locate the garnet-in boundary in complex systems. They used three starting compositions with noticeable difference in the Cr# [unfortunately the Cr_2O_3 in one of the systems 368(v) was not determined]. Although the intention of using three different compositions was to create an experimental bracket, the actual garnet-in boundaries corresponding to each starting composition differ from one another because of the differences in the Cr#. Only experiments with the starting composition 368(v) are used to

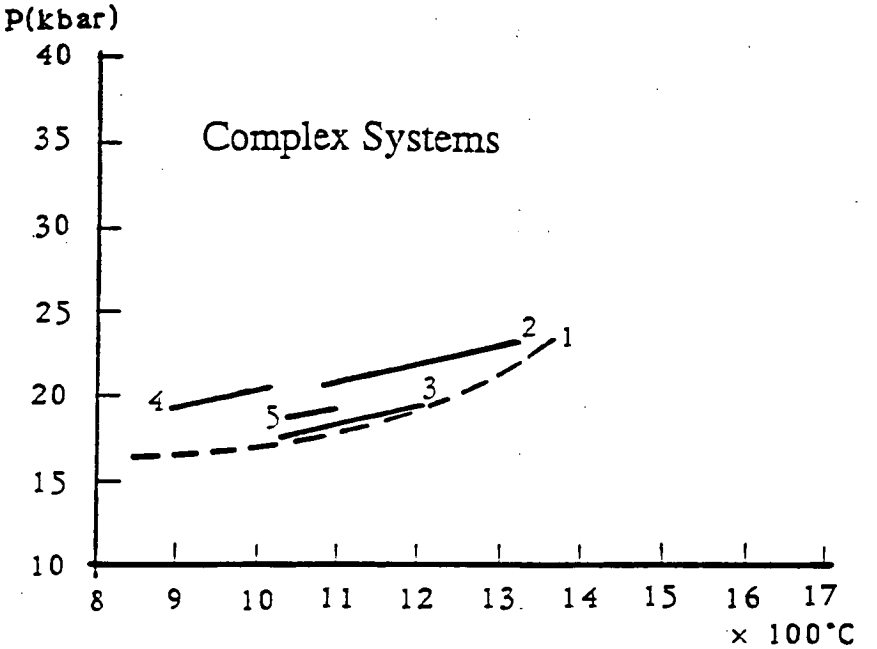

Figure 4.3. Experimentally determined garnet-in boundaries in complex systems (1. O'Hara et al., 1971; 2. Green & Ringwood, 1967a; 3. Taylor & Green, 1988; 4. Wallace & Green, 1988; 5. Niida & Green, in prep.).

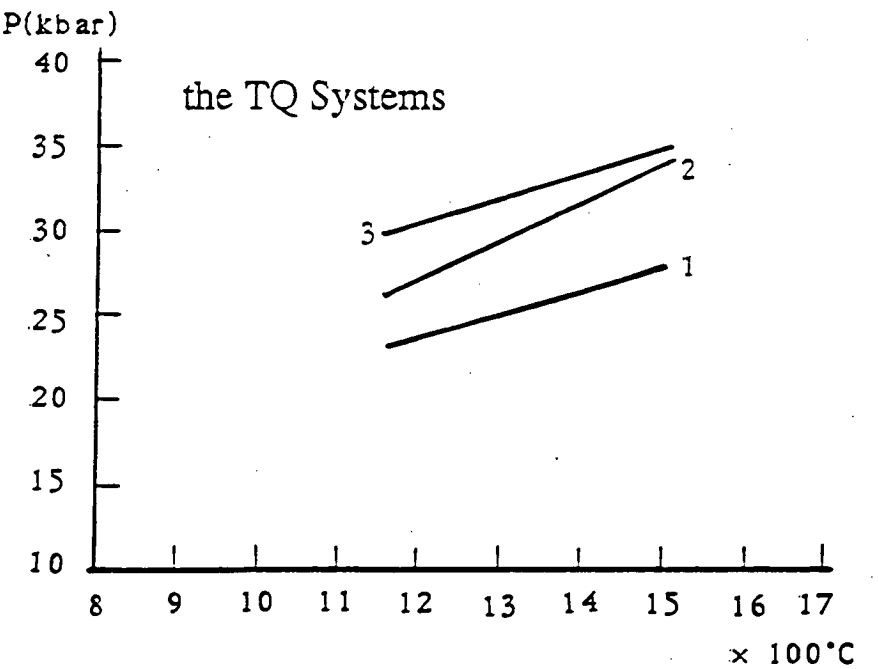

Figure 4.4. The garnet-in boundaries in the three model lherzolite systems determined in this study (1. TQ40; 2. TQ40/30a; 3. TQ40/30b).

Table 4.1 The Bulk Compositions of Six Model Lherzolite Systems

	Hawaiian Pyrolite	Morb Pyrolite	368 (v)	TQ40	TQ40/30a	TQ40/30b
reference	1	2	3	4	5	5
SiO2	45.2	47.15	48.15	47.51	46.27	47.22
TiO2	0.71	0.28	0.23	0.13	0.13	0.13
Al2O3	3.54	7.28	5.32	5.35	5.21	4.07
Cr2O3	0.43	0.75	n.d.	0.75	3.33	2.6
Fe2O3	0.48		1.11	0.15	0.15	0.15
FeO	8.04	[7.27]	5.7	7.38	7.19	7.34
MnO	0.14	0.12	0.11	0.18	0.17	0.18
NiO	0.2	0.29		0.43	0.42	0.43
MgO	37.48	30.57	33.09	32.8	31.95	32.6
CaO	3.08	5.63	4.7	4.97	4.84	4.94
Na2O	0.57	0.66	0.48	0.3	0.29	0.3
K2O	0.13		0.16	0.03	0.03	0.03
P2O5			0.06	0.02	0.02	0.02
Sum	100	100	99.11	100	100	100.01
100Mg/Mg+Fe	89.26	88.23	91.19	88.79	88.79	88.79
100Cr/Cr+Al	7.53	6.46		8.60	30.01	30.00
ΣR2O3	4.45	8.03	> 6.43	6.25	8.69	6.82
Al2O3/Cr2O3	8.23	9.71		7.13	1.56	1.57
ΣPx				39.21	39.80	44.02
ΣR2O3/ΣPx				0.1594	0.2183	0.1549

references: 1 - Green & Ringwood (1967a); 2 - Niida & Green (in prep.);
3 - O'Hara et al. (1971); 4 - Chapter Three; 5 - This chapter.
n.d.: not determined.
ΣPx: normative pyroxenes in wt%.

construct the garnet-in boundary, which is compared with the garnet-in boundary in the Hawaiian pyrolite system in Figure 4.3. Due to the higher Al_2O_3 content in the 368(v) system than in the Hawaiian pyrolite system (Table 4.1), the garnet-in boundary in the 368(v) system is 2 - 3 kbar lower than in the Hawaiian pyrolite system (Fig.4.3).

The MORB pyrolite composition has higher $Al_2O_3 + Cr_2O_3$ and lower Cr# than the Hawaiian pyrolite composition (Table 4.1). The study of Niida & Green (in prep.) locates the garnet-in boundary in MORB pyrolite system at lower pressure than in the Hawaiian pyrolite system. Both Taylor & Green (1988) and Wallace & Green (1988) used the same starting composition as Green & Ringwood (1967a) but a relatively reduced oxygen environment (about IW + 1) was created in the study of Taylor & Green (1988) and a relatively oxidised oxygen environment (about EMOG) in the study of Wallace & Green (1988). The garnet-in boundary is shifted to lower pressure in the reduced pyrolite system and to higher pressure in the oxidised pyrolite system (Fig.4.3). This presumably illustrates the influence of Fe_2O_3 and FeO on the garnet-in boundary: under low-oxygen conditions, most Fe occurs as FeO, which stabilises garnet to lower pressure; under high-oxygen conditions, some FeO would be oxidised to Fe_2O_3, which stabilises spinel and delays the appearance of garnet.

4.4 New Experimental Data in Complex Systems

An obvious imperfection of previous experimental studies in complex systems is the lack of mineral compositions associated with the spinel-facies to garnet-facies transition, which prevented a rigorous mathematical analysis of this transition. In order to overcome this problem, a detailed experimental study has been undertaken in three model lherzolite systems. The starting compositions are listed in Table 4.1. Experimental details are discussed in Chapter Three. The TQ40 composition represents a relatively depleted mantle composition (Jaques & Green, 1980) and originates from the Tinaquillo lherzolite composition of Green (1963). The TQ40/30b is derived in such a way that the ΣR_2O_3 and oxides other than Al_2O_3 and Cr_2O_3 are kept the same as in TQ40 but the Cr# is increased from 8.6 in TQ40 to 30. The TQ40/30a composition has the same Cr# as TQ40/30b but higher ΣR_2O_3 and ΣR_2O_3/Px (Px= normative pyroxenes in wt%) than TQ40/30b. In this way, the effect of Cr#, ΣR_2O_3 and ΣR_2O_3/Px on the garnet-in boundary can be evaluated.

Indeed the garnet-in boundaries in the three systems are very different from each other: the two boundaries in the TQ40 and TQ40/30b systems are parallel to each other with a pressure difference of about 7 kbar (± 0.5 kbar), but that in the TQ40/30a system has a steeper slope than these two boundaries. Although the Cr#s are the same in the two high-Cr systems, garnet is evidently stabilised to lower pressure in the TQ40/30a system

than in the TQ40/30b system (particularly at relatively low temperatures, Fig.4.4) due to the difference in ΣR_2O_3 and ΣR_2O_3/Px values. It appears that the higher the ΣR_2O_3 and ΣR_2O_3/Px in a system, the steeper the slope (dP/dT) of the garnet-in boundary becomes; and that for systems with identical Cr#, the higher the ΣR_2O_3/Px value, the lower the pressure of the garnet-in boundary.

Except where spinel is a metastable phase (indicated by its near zero modal%, Table 3.7), five-phase assemblages are only present within the spinel-facies to garnet-facies transition zone in the low-Cr system, where spinel is less than 3% in modal abundance (Table 3.7) and smaller than 5 μ (mostly around 1 - 2 μ). In the high-Cr systems, spinels are very abundant and sufficiently large for microprobe analysis. They are present in every charge. Garnet crystals are generally large, with poikilitic texture. The included minerals in garnet are usually olivine and orthopyroxene. Spinel and clinopyroxene are also detected. Plate 4 shows three representative run products in the high-Cr systems. Mineral compositions were analysed by a Cameca SX50 microprobe in the WDS mode. Probe beam size varied between 1 - 3 μ. The analytical conditions were 20 nA, 15 kV, with peak counting time 20 seconds (and half background counting time) for most elements except Si, Al, Mg, for which peak counting time of 10 seconds was chosen. The analytical data were processed by a dedicated PDP-11 mini-computer according to the PAP data-reduction method. Phase compositions in the TQ40 system are given in Chapter Three, and those in the five-phase assemblages of the high-Cr systems are summarised in Table 4.2. The optimum detection limits for all the analysed major and minor elements are 0.03 - 0.06% (Chapter Three). These compositions are averages of 5 - 15 individual analyses, lowering the detection limits by a half to a quarter. A detailed discussion on the variation of mineral compositions with pressure and temperature is given in Chapter Three for the TQ40 system. The data presented here provide further support to the subsolidus mineral reactions identified in Chapter Three, i.e., with increasing temperature, mineral reactions are involved with formation of clinopyroxene at the expense of orthopyroxene, spinel and garnet; with increasing pressure, mineral reactions are concerned with garnet growth at the expense of orthopyroxene and spinel. Such reaction trends can be readily visualised from the change of mineral abundances with pressure and temperature (Table 4.2).

4.5 An Empirical Model for the Transition

The fundamental equilibrium thermodynamic function and associated thermodynamic parameters for phases in the MAS system given by Gasparik & Newton (1984) are adopted here for the thermodynamic modelling of the spinel-facies to garnet-facies transition reaction [reactions (4.1) + (4.2)]:

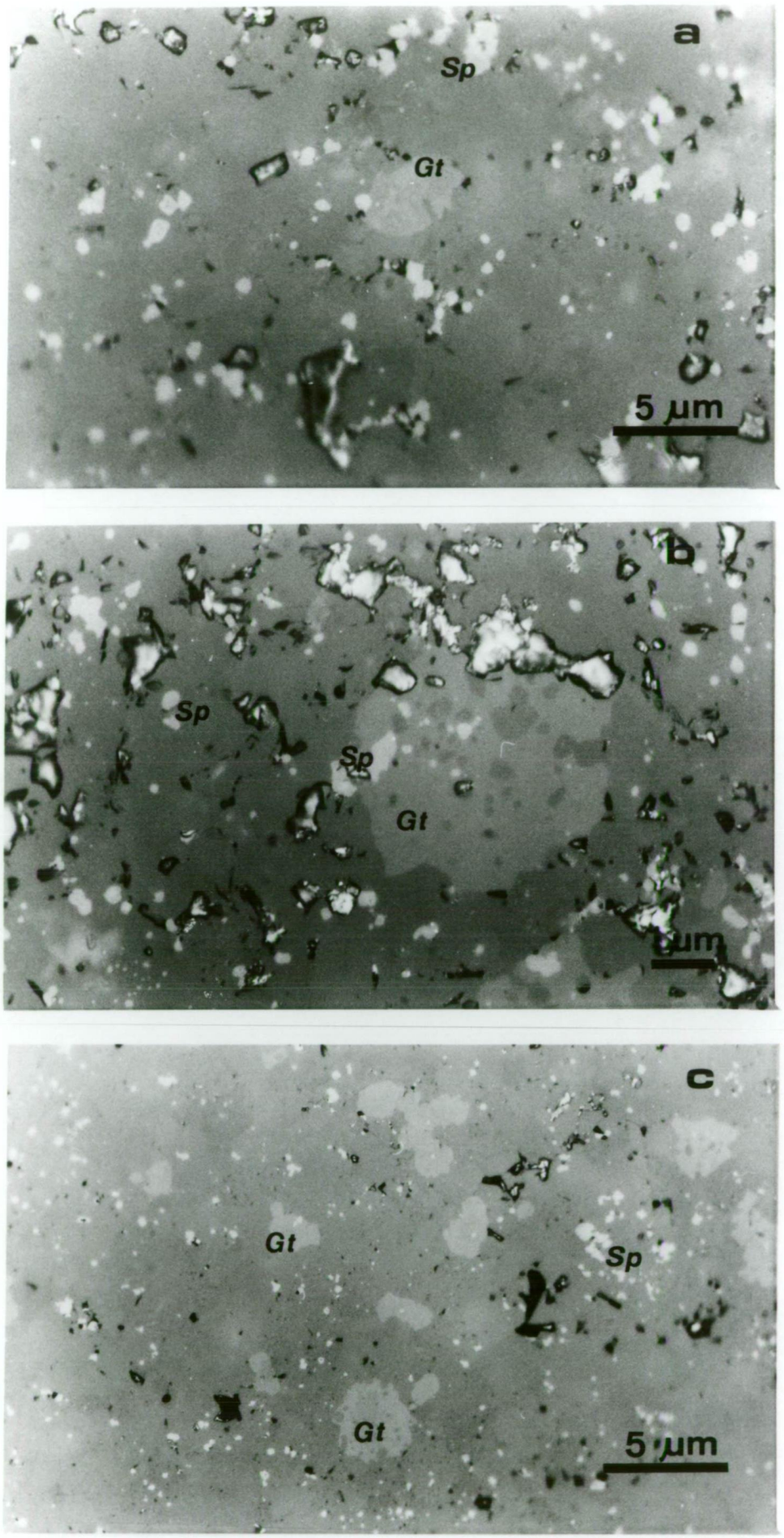

Plate 4. Coexisting spinel and garnet in the high-Cr lherzolite systems:
(a) T3429, 1500°C, 34 kbar, 3.3 hours (TQ40/30a);
(b) T3275, 1200°C, 27.5 kbar, 7 days (TQ40/30a);
(c) T3534, 1500°C, 35 kbar, 6 hours (TQ40/30b).

Table 4.2 Composition and Modal Abundance of Coexisting Minerals in the High-Cr Lherzolite Systems

TQ40/30a	T3275	T3261	T3548	T3269	T3446	T3556	T3402	T3451	T3417	T3429	T3268
T°C	1200	1200	1200	1200	1300	1300	1300	1400	1400	1500	1500
P(kb)	27.5	30	32	35	28	32	35	32	35	34	35
Ol (wt%)	29.04	28.30	29.51	31.15	27.34	31.77	31.90	28.59	30.36	29.54	30.63
SiO2	40.61	40.64	40.48	40.77	40.33	40.42	40.73	40.40	40.67	40.68	40.68
FeO	10.48	10.35	10.14	10.25	10.45	10.18	10.57	10.28	9.98	9.73	9.55
MnO	0.18	0.09	0.07	0.09	0.11	0.12		0.18	0.12	0.16	
NiO	0.81	0.80	0.79	0.77	1.00	0.82	0.89	0.81	0.46	0.76	0.75
MgO	47.76	47.89	48.42	47.99	47.89	48.29	47.66	48.13	48.54	48.40	48.69
CaO	0.16	0.23	0.09	0.12	0.23	0.18	0.14	0.21	0.22	0.27	0.32
Sum	100	100	100	100	100	100	100	100	100	100	100
Opx (wt%)	39.52	39.25	36.58	31.26	42.82	31.42	31.13	34.32	30.12	29.37	25.56
SiO2	54.46	55.00	54.82	56.12	53.91	55.81	55.66	54.32	54.88	53.76	54.19
TiO2	0.12	0.13	0.14	0.05	0.14	0.05	0.04		0.12	0.11	0.07
Al2O3	4.08	3.38	3.93	2.37	4.62	3.00	2.83	3.88	3.10	4.70	4.43
Cr2O3	1.12	0.88	1.22	0.96	1.28	1.21	1.09	1.51	1.56	1.70	1.85
FeO	6.72	6.51	6.21	6.17	6.43	6.09	6.40	6.11	6.03	5.96	5.66
MnO	0.16	0.12	0.15	0.09	0.12	0.07	0.14	0.18	0.11	0.12	0.09
NiO	0.23	0.22	0.29	0.30	0.26	0.22	0.24	0.12		0.26	0.32
MgO	31.58	32.33	32.01	32.63	31.52	31.87	32.00	31.74	32.15	30.86	30.72
CaO	1.43	1.30	1.10	1.15	1.61	1.51	1.49	1.98	1.87	2.36	2.46
Na2O	0.10	0.14	0.12	0.15	0.13	0.16	0.11	0.16	0.18	0.17	0.20
Sum	100	100	100	100	100	100	100	100	100	100	100
Cpx (wt%)	20.16	19.83	20.99	17.08	22.52	18.03	18.05	24.21	19.69	28.31	29.25
SiO2	52.87	52.99	53.19	53.49	52.13	53.73	53.59	52.69	53.22	53.09	53.42
TiO2	0.24	0.28	0.17	0.20	0.21	0.15	0.18	0.13	0.14	0.14	0.07
Al2O3	4.27	3.84	3.82	3.15	4.91	3.33	3.28	4.48	3.32	4.31	4.38
Cr2O3	1.38	1.47	1.52	1.88	1.62	1.86	1.74	1.83	2.31	1.75	1.97
FeO	3.52	3.44	3.50	3.42	3.84	3.48	3.70	4.41	4.01	4.74	4.61
MnO	0.11	0.14	0.24	0.05	0.16	0.13	0.08		0.11	0.13	0.04
NiO	0.11	0.12	0.14	0.14	0.13	0.18	0.22	0.13	0.13	0.21	0.14
MgO	17.52	17.41	17.70	17.35	18.31	18.05	18.08	20.58	20.01	22.24	22.72
CaO	18.99	19.21	18.48	19.07	17.80	18.10	18.04	14.94	15.88	12.74	12.06
Na2O	0.99	1.10	1.23	1.24	0.89	0.98	1.10	0.82	0.88	0.65	0.59
Sum	100	100	100	100	100	100	100	100	100	100	100
Gt (wt%)	5.59	6.47	7.49	16.65	1.07	15.08	15.28	8.16	16.93	8.38	10.62
SiO2	41.39	41.62	41.64	41.61	41.63	41.49	41.34	41.31	41.39	41.74	41.58
TiO2	0.27	0.29	0.28	0.42	0.26	0.25	0.33	0.25	0.33	0.22	0.29
Al2O3	20.97	20.85	20.34	19.22	20.80	19.53	19.25	19.40	18.39	19.44	20.03
Cr2O3	3.39	3.41	4.39	4.41	3.42	5.48	5.49	5.84	6.59	5.44	4.62
FeO	7.63	7.58	7.35	7.43	7.20	6.93	7.36	6.65	6.49	5.98	6.47
MnO	0.29	0.33	0.32	0.33	0.29	0.32	0.33	0.21	0.14	0.23	0.24
NiO	0.13	0.04	0.05	0.05	0.03	0.06	0.04		0.12	0.09	0.07
MgO	19.08	19.22	18.82	19.50	19.43	18.84	18.98	19.79	19.49	20.41	19.96
CaO	6.84	6.65	6.80	7.00	6.87	7.11	6.87	6.55	7.06	6.45	6.69
Sum	100	100	100	100	100	100	100	100	100	100	100
Sp (wt%)	5.69	6.16	5.44	3.87	6.25	3.70	3.65	4.71	2.90	4.41	3.94
TiO2	0.47	0.79	0.80	1.07	0.56	0.66	0.85	0.57	0.43	0.35	0.34
Al2O3	26.21	27.47	26.23	17.33	30.10	19.65	19.32	26.66	21.43	23.96	20.72
Cr2O3	41.96	39.21	40.62	49.57	37.86	48.71	48.37	41.15	48.52	44.52	48.72
Fe2O3	3.32	3.67	3.57	3.42	2.86	2.68	3.00	3.61	2.05	3.86	3.12
FeO	11.24	12.78	12.79	14.62	11.64	13.76	13.92	10.94	11.55	10.14	10.35
MnO	0.22	0.10	0.20	0.14		0.12	0.13	0.18	0.15	0.14	0.19
NiO	0.46	0.49	0.51	0.34	0.62	0.40	0.46	0.43	0.25	0.44	0.50
MgO	16.13	15.49	15.29	13.52	16.36	14.02	13.95	16.46	15.63	16.60	16.05
Sum	100	100	100	100	100	100	100	100	100	100	100

*) Mineral modes were calculated from the mineral compositions and the starting compositions.

Table 4.2 Composition and Modal Abundance of Coexisting Minerals in the High-Cr Lherzolite Systems (cont'd)

TQ40/30b	T3573	T3528	T3583	T3562	T3593	T3568	T3604	T3536	T3534	T3598
T°C	1200	1200	1300	1300	1300	1400	1400	1400	1500	1500
P(Kb)	32	35	32	35	38	32	33.5	35	35	38
Ol (wt%)	32.11	31.51	32.90	34.34	34.97	33.48	33.20	34.73	31.26	34.97
SiO2	40.67	40.34	40.65	40.62	40.88	40.69	40.69	40.78	40.51	40.97
FeO	10.44	10.14	10.62	10.91	10.34	10.52	10.42	10.19	10.16	9.77
MnO	0.18	0.14	0.17	0.19	0.10	0.17	0.19	0.14	0.21	0.23
NiO	0.90	0.98	0.98	0.92	0.94	0.88	0.87	0.95	0.90	0.91
MgO	47.67	48.28	47.41	47.21	47.60	47.56	47.61	47.72	47.96	47.82
CaO	0.13	0.12	0.17	0.15	0.14	0.19	0.22	0.22	0.25	0.30
Sum	100	100	100	100	100	100	100	100	100	100
Opx (wt%)	35.07	34.98	35.91	31.28	29.12	33.53	33.46	28.68	27.66	20.13
SiO2	55.68	55.84	54.99	55.60	55.93	54.82	54.72	55.09	53.97	55.03
TiO2	0.16	0.13	0.15	0.14	0.16	0.14	0.11	0.12	0.11	0.10
Al2O3	2.50	2.33	3.32	2.67	2.35	3.75	3.87	3.54	4.25	3.42
Cr2O3	0.92	0.84	1.21	1.15	1.17	1.34	1.50	1.43	1.66	1.80
FeO	6.36	6.19	6.57	6.36	6.20	6.46	6.21	6.20	6.16	5.74
MnO	0.17	0.16	0.19	0.21	0.15	0.18	0.15	0.21	0.18	0.17
NiO	0.28	0.30	0.27	0.28	0.36	0.35	0.32	0.29	0.29	0.31
MgO	32.63	32.83	31.58	32.01	32.03	30.86	30.95	31.05	30.77	30.87
CaO	1.17	1.25	1.54	1.42	1.48	1.92	2.03	1.86	2.42	2.35
Na2O	0.13	0.14	0.17	0.17	0.17	0.18	0.15	0.22	0.18	0.20
Sum	100	100	100	100	100	100	100	100	100	100
Cpx (wt%)	20.53	19.12	21.89	21.06	19.87	25.24	25.63	25.28	34.42	31.60
SiO2	53.05	53.39	52.99	53.93	54.01	52.82	52.96	53.63	52.42	53.96
TiO2	0.27	0.25	0.24	0.22	0.21	0.26	0.19	0.21	0.12	0.08
Al2O3	3.32	3.05	3.87	2.96	2.73	4.45	4.31	3.60	4.40	3.32
Cr2O3	1.81	1.71	1.89	1.92	1.99	1.95	1.88	2.07	2.12	2.12
FeO	3.59	3.48	3.90	3.88	3.81	4.37	4.45	4.51	5.27	4.90
MnO	0.15	0.09	0.17	0.18	0.21	0.19	0.17	0.21	0.13	0.11
NiO	0.15	0.21	0.18	0.19	0.18	0.18	0.17	0.15	0.30	0.31
MgO	17.65	17.57	17.98	18.31	18.67	19.50	19.86	19.99	23.04	22.95
CaO	18.86	19.04	17.71	17.25	17.09	15.44	15.21	14.71	11.54	11.53
Na2O	1.16	1.23	1.08	1.15	1.10	0.85	0.80	0.93	0.66	0.71
Sum	100	100	100	100	100	100	100	100	100	100
Gt (wt%)	9.05	11.64	6.06	10.96	14.40	4.60	4.53	8.99	3.93	11.59
SiO2	41.52	41.11	41.35	41.37	41.14	41.37	41.14	41.36	41.30	41.51
TiO2	0.39	0.41	0.44	0.41	0.55	0.47	0.41	0.46	0.44	0.38
Al2O3	19.50	18.82	19.78	18.87	17.81	19.02	19.25	18.29	18.68	17.85
Cr2O3	4.72	5.75	4.79	5.83	6.90	5.84	5.95	6.79	6.50	6.92
FeO	7.76	7.64	7.43	7.50	7.38	6.87	6.86	6.78	6.40	6.42
MnO	0.45	0.43	0.44	0.42	0.41	0.39	0.37	0.41	0.36	0.34
NiO	0.06	0.08		0.07	0.09	0.07	0.06	0.06	0.10	0.06
MgO	19.04	18.68	18.94	18.73	18.44	19.10	19.21	19.11	19.85	19.64
CaO	6.58	7.08	6.81	6.81	7.27	6.87	6.74	6.74	6.39	6.88
Sum	100	100	100	100	100	100	100	100	100	100
Sp (wt%)	3.24	2.75	3.24	2.36	1.64	3.16	3.18	2.32	2.74	1.71
TiO2	1.44	1.52	1.09	1.46	1.53	0.83	0.71	1.17	0.64	0.53
Al2O3	21.55	17.68	23.32	18.54	14.52	24.57	25.41	21.22	24.65	19.72
Cr2O3	44.53	47.84	43.25	46.88	51.21	43.00	42.97	45.52	43.56	49.58
Fe2O3	3.19	4.18	3.63	4.26	4.25	3.03	2.54	3.69	3.28	2.65
FeO	14.58	14.13	12.90	14.18	14.19	12.61	11.95	12.49	10.87	11.43
MnO	0.23	0.18	0.26	0.26	0.23	0.17	0.24	0.20	0.20	0.28
NiO	0.49	0.50	0.52	0.52	0.47	0.51	0.49	0.55	0.59	0.49
MgO	14.01	13.97	15.03	13.92	13.60	15.27	15.70	15.17	16.23	15.32
Sum	100	100	100	100	100	100	100	100	100	100

$$3\,Mg_2Si_2O_6 + MgAl_2SiO_6 + MgAl_2O_4 = Mg_2SiO_4 + 2\,Mg_3Al_2Si_3O_{12} \quad (4.3)$$

$$RT\ln K + \Delta H^{0}_{970;1} - T\Delta S^{0}_{970;1} - \int_{j=970}^{T}\int_{i=970}^{T}\left(\frac{\Delta Cp}{T}\partial T\right)\partial T + \int_{k=1}^{P}\Delta V^{0}_{P;T}\partial P = 0\,.$$

For simplicity we can express the terms in this thermodynamic equation as (the isobaric thermal expansion and isothermal compression coefficients α, β values and constants in the heat capacity expression are from Gasparik & Newton, 1984):

$$A \equiv \int_{k=1}^{P}\Delta V^{0}_{P;T}\partial P = [1 + \Delta\alpha(T - 298) - \frac{\Delta\beta}{2}P]P_{(kbar)}$$

$$= [-1651 + 0.110287(T - 298) - 1.5354P]P;$$

$$B \equiv \int_{j=970}^{T}\int_{i=970}^{T}\left(\frac{\Delta Cp}{T}\partial T\right)\partial T = \int_{j=970}^{T}\int_{i=970}^{T}\left[\left(\frac{a}{T} + b + \frac{c}{T^3} + \frac{d}{T^{1.5}}\right)\partial T\right]\partial T$$

$$= 0.0376246T^2 - 383.68T\ln T + 3514.65T - 35674.4\sqrt{T} - \frac{6988632.5}{T} + 233177.37.$$

In the MAS system, orthopyroxene may be treated as an ideal solid solution between enstatite (En) and Mg-Tschermak pyroxene (MgTs). Thus $RT\ln K = -RT\{\ln X^{M1}_{Al} + 3\ln(1 - X^{M1}_{Al})\}$. We further define

$$C \equiv B + RT\ln K + c_o + c_1T + c_2T^2.$$

Newton (1989) summarised the Al_2O_3 solubility in orthopyroxene data in several reversed experiments in the MAS system and obtained a best fit curve for the transition (Fig.1 of Newton, 1989). The X^{M1}_{Al}(Opx) values on this curve (Table 4.3) are used for a least-square regression analysis to solve for the constants, which are: $c_o = 39046$; $c_1 = -65.1402$; $c_2 = 0.030584$ (r^2=0.9997). Therefore the equilibrium equation for reaction (4.3) becomes

$$[-1651 + 0.110287(T - 298) - 1.5354P]P + C = 0,$$

from which we solve for P and derive the barometric expression:

$$P_{(MAS)} = \frac{[0.1103(T - 298) - 1651] + \sqrt{\{[0.1103(T - 298) - 1651]^2 + 6.1416C\}}}{3.0708}\ (kbar).$$

This barometer reproduces Newton's (1989) model data (Table 4.3) within ± 0.13 kbar (Fig.4.5).

In complex natural systems, the pressure of garnet appearance is modified by additional components such as Fe, Ca and Cr from that in the MAS system, as has been qualitatively discussed before. In order to correct for these effects, an empirical relation is assumed:

$$P_{(complex)} = a + bP_{(MAS)} + cT\ln X^{ol}_{Mg} + dT\ln X^{opx}_{Mg} + eT\ln X^{Gt}_{Mg} + fT\ln X^{Sp}_{Mg} + gT\ln X^{opx}_{Cr} +$$

Table 4.3 Experimental Data in the MAS System

P(kbar)	18	18.05	18.5	19.1	20	21.4	23	25	27.2	29.4
T(°C)	750	800	900	1000	1100	1200	1300	1400	1500	1600
X(Al)M1*	0.07	0.082	0.105	0.127	0.147	0.163	0.177	0.191	0.204	0.217

*) Values are read from the regression line in Figure 1 of Newton (1989).

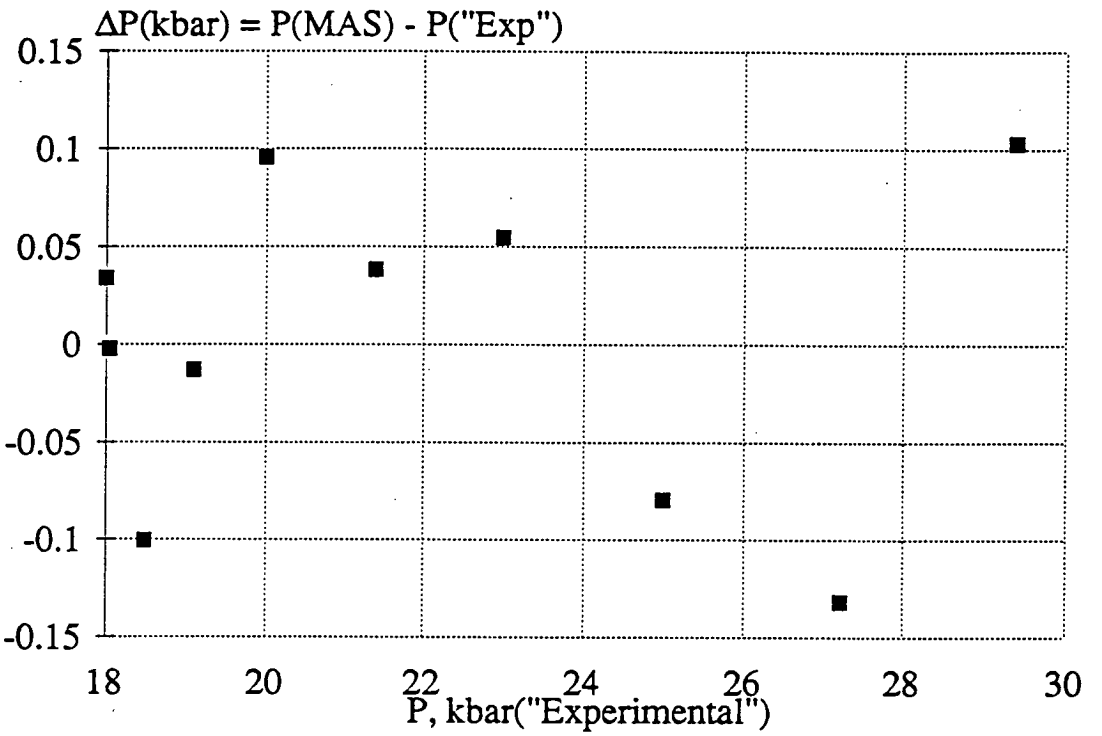

Figure 4.5. Comparison of the "experimental" pressures with calculated pressures in the MAS system (the "experimental" pressures are read from the best-fit curve in Figure 1 of Newton, 1989).

Table 4.4 Experimental Data for Empirical Modelling of the Transition in Complex Systems

Run #	P(kbar)	T(°C)	X(mg)Ol	X(mg)Opx	X(mg)Gt	X(mg)Sp	X(Cr)Opx	X(Cr+Fe3)Sp	X(Cr)Gt	X(Ca)Gt	P(MAS)	P(complex)
TO40 System												
T3101	25	1200	0.8921	0.8980	0.8271	0.7790	0.0799	0.2258	0.0568	0.1589	23.87	26.14
T3126	27	1200	0.8883	0.8963	0.8308	0.7741	0.0959	0.2669	0.0634	0.1507	23.61	25.94
T3454	28	1200	0.8949	0.9019	0.8332	0.7359	0.1254	0.3520	0.0720	0.1528	25.94	28.99
T3355	26	1300	0.8933	0.8980	0.8416	0.7845	0.0860	0.2109	0.0458	0.1503	26.02	26.65
T3136	27	1300	0.8923	0.8977	0.8372	0.7843	0.0872	0.2615	0.0588	0.1539	25.59	26.75
T3247	27	1300	0.8868	0.9020	0.8417	0.7617	0.0774	0.2951	0.0526	0.1468	24.98	26.40
T3364	28	1300	0.8932	0.8991	0.8320	0.7649	0.0889	0.2983	0.0576	0.1535	26.56	27.78
T3167	27	1400	0.8903	0.8949	0.8428	0.7829	0.0930	0.2865	0.0682	0.1494	26.41	26.48
T3453	28	1400	0.8924	0.9027	0.8594	0.7979	0.0982	0.2660	0.0568	0.1503	27.62	28.11
T3526	29	1400	0.8932	0.8965	0.8522	0.8151	0.0918	0.2557	0.0593	0.1430	27.71	27.57
T3378	28	1500	0.9003	0.9043	0.8605	0.7890	0.0870	0.3141	0.0691	0.1455	28.98	29.04
T3249	30	1500	0.8982	0.9044	0.8707	0.8539	0.0911	0.2749	0.0814	0.1468	29.75	30.19
T3430	30	1500	0.8984	0.9035	0.8653	0.8223	0.0852	0.1883	0.0812	0.1530	28.94	29.30
TO40/30a System												
T3275	27.5	1200	0.8904	0.8934	0.8168	0.7187	0.1558	0.5358	0.0979	0.1725	25.64	28.45
T3261	30	1200	0.8919	0.8984	0.8189	0.6834	0.1490	0.5106	0.0989	0.1679	26.62	29.93
T3548	32	1200	0.8949	0.9019	0.8202	0.6803	0.1720	0.5308	0.1264	0.1744	26.03	30.22
T3269	35	1200	0.8930	0.9041	0.8238	0.6225	0.2141	0.6716	0.1334	0.1741	29.22	33.58
T3446	28	1300	0.8910	0.8973	0.8278	0.7148	0.1569	0.4749	0.0995	0.1727	27.01	29.19
T3556	32	1300	0.8943	0.9032	0.8290	0.6450	0.2135	0.6363	0.1585	0.1821	30.06	33.76
T3402	35	1300	0.8893	0.8991	0.8213	0.6410	0.2044	0.6403	0.1605	0.1748	30.53	33.77
T3451	32	1400	0.8930	0.9026	0.8414	0.7284	0.2070	0.5287	0.1680	0.1661	30.65	33.48
T3417	35	1400	0.8966	0.9048	0.8426	0.7068	0.2531	0.6124	0.1939	0.1789	33.23	36.52
T3429	34	1500	0.8986	0.9022	0.8588	0.7447	0.1953	0.5749	0.1581	0.1622	32.10	33.79
T3268	35	1500	0.9009	0.9063	0.8462	0.7343	0.2192	0.6260	0.1339	0.1682	32.66	34.40
TO40/30b System												
T3573	32	1200	0.8906	0.9015	0.8140	0.6315	0.1978	0.5970	0.1396	0.1664	29.27	33.45
T3528	35	1200	0.8946	0.9044	0.8134	0.6381	0.1944	0.6629	0.1702	0.1795	29.49	34.37
T3583	32	1300	0.8884	0.8955	0.8196	0.6751	0.1969	0.5733	0.1398	0.1731	29.48	32.08
T3562	35	1300	0.8852	0.8997	0.8167	0.6364	0.2245	0.6483	0.1718	0.1742	31.30	34.72
T3593	38	1300	0.8914	0.9020	0.8166	0.6308	0.2502	0.7185	0.2062	0.1861	32.73	36.74
T3568	32	1400	0.8896	0.8950	0.8320	0.6834	0.1933	0.5561	0.1708	0.1755	31.01	32.98
T3604	33.5	1400	0.8906	0.8988	0.8330	0.7008	0.2057	0.5451	0.1717	0.1722	31.01	33.43
T3536	35	1400	0.8930	0.8993	0.8340	0.6841	0.2131	0.6078	0.1994	0.1729	31.47	34.28
T3534	35	1500	0.8938	0.8990	0.8469	0.7270	0.2078	0.5596	0.1892	0.1623	32.93	34.61
T3598	38	1500	0.8972	0.9055	0.8450	0.7050	0.2611	0.6392	0.2064	0.1740	35.29	37.87

Table 4.5 Regression Results of the Experimental Data in the Model Lherzolite Systems

Model 1	all composition terms				
	Analysis of Variance				
Source	DF*	Sum of Squares	Mean Square	F Value	Prob>F
	9	405.735	45.082	36.898	0.0001
	24	29.323	1.222		
C Total	33	435.059			
Root MSE	1.105	R-square	0.933		
Dep Mean	31.206	Adj R-sq**	0.907		
C.V.	3.542				
Variable	DF	Parameter Estimate	Standard Error	T for H0: Parameter=0	Prob > |T|
Intercept	1	14.51926	8.22453	1.765	0.0902
P(MAS)	1	0.79089	0.25801	3.065	0.0053
Tln(Xmg)Ol	1	-0.00331	0.05166	-0.064	0.9494
Tln(Xmg)Opx	1	0.09481	0.05507	1.722	0.0980
Tln(Xmg)Gt	1	-0.01509	0.02969	-0.508	0.6159
Tln(Xmg)Sp	1	-0.00306	0.00614	-0.498	0.6232
Tln(Xcr)Opx	1	-0.00029	0.00172	-0.169	0.8672
Tln(Xcr+Xfe3)sp	1	-0.00026	0.00134	-0.193	0.8484
Tln(Xcr)Gt	1	0.00194	0.00105	1.853	0.0762
Tln(Xca)Gt	1	-0.00307	0.00440	-0.696	0.4931

Model 2	only involving X(mg)Opx and X(cr)Gt				
	Analysis of Variance				
Source	DF	Sum of Squares	Mean Square	F Value	Prob>F
	3	403.940	134.647	129.804	0.0001
	30	31.119	1.037		
C Total	33	435.059			
Root MSE	1.018	R-square	0.929		
Dep Mean	31.206	Adj R-sq	0.921		
C.V.	3.264				
Variable	DF	Parameter Estimate	Standard Error	T for H0: Parameter=0	Prob > |T|
Intercept	1	19.20581	3.17029	6.058	0.0001
P(MAS)	1	0.95073	0.10755	8.840	0.0001
Tln(Xmg)Opx	1	0.06265	0.02226	2.814	0.0086
Tln(Xcr)Gt	1	0.00138	0.00038	3.612	0.0011

*) degree of freedom.
**) adjusted R-squared.

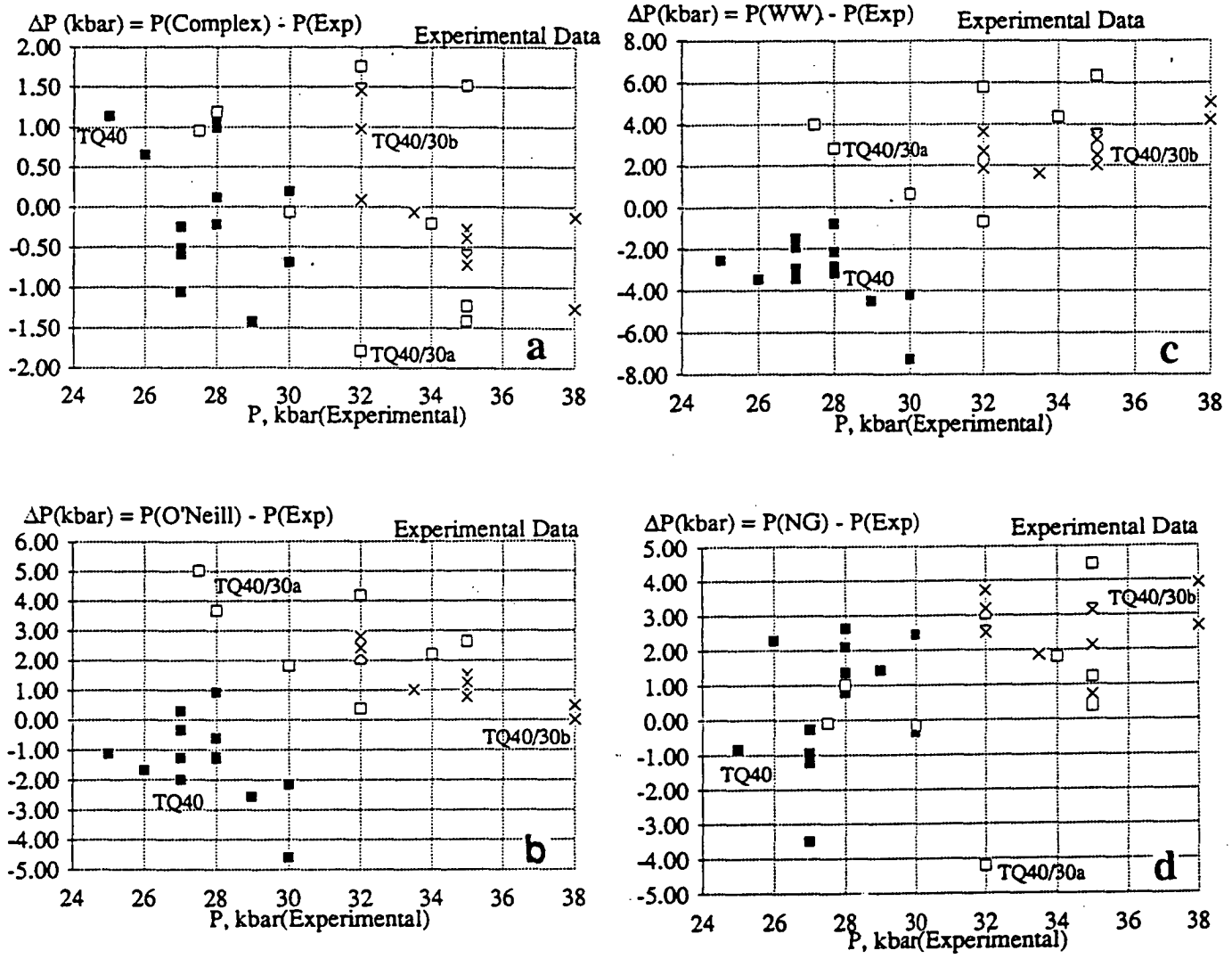

Figure 4.6. Comparison of the experimental pressures with the calculated pressures according to

(a). the empirical model in the complex systems formulated in this study.

(b). the O'Neill (1981) barometer.

(c). the modified O'Neill (1981) barometer by Webb & Wood (1986).

(d). the Nickel & Green (1985) barometer.

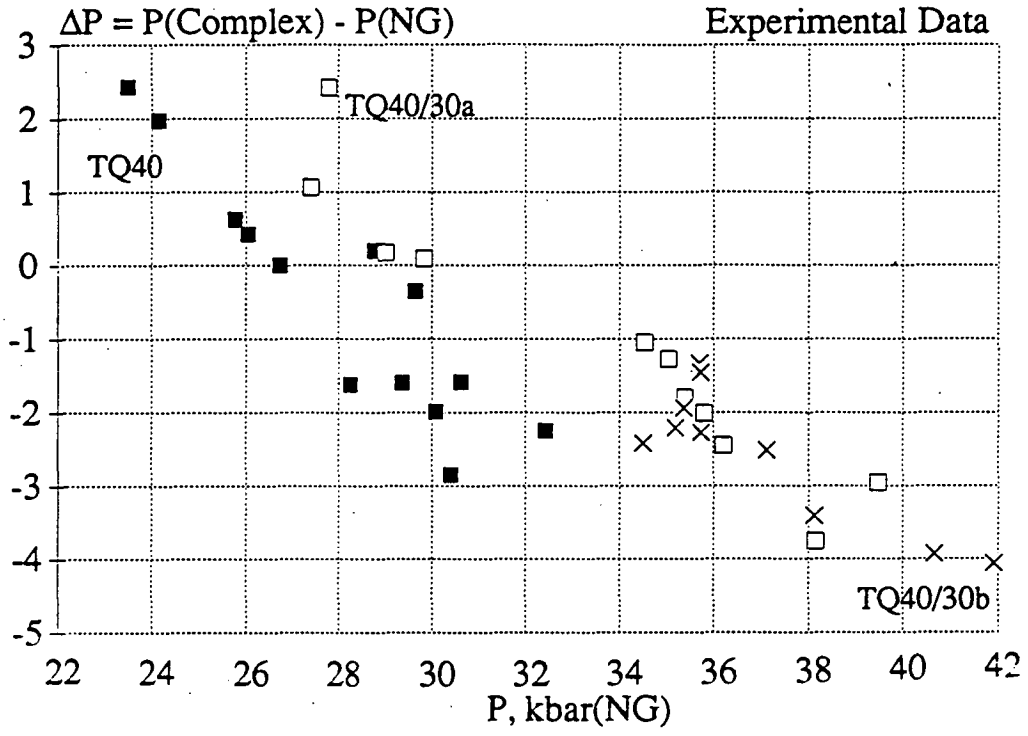

Figure 4.7. Correlation of the pressures computed by the Nickel & Green (1985) barometer with the difference between the pressures estimated by the empirical transition barometer developed in this study and by the Nickel & Green (1985) barometer for the experimental data.

$$hT\ln X_{Cr}^{Gt} + iT\ln(X_{Cr}^{Sp} + X_{Fe^{3+}}^{Sp}) + jT\ln X_{Ca}^{Gt}.$$

Fitting the experimental data in Table 4.4 to this equation by the method of multiple linear regression gives the following constants (Table 4.5):

$$P(\text{complex}) = 14.52 + 0.79P(\text{MAS}) + T\{-0.0033\ln X_{Mg}^{Ol} + 0.0948\ln X_{Mg}^{Opx} - 0.015\ln X_{Mg}^{Gt} - 0.003\ln X_{Mg}^{Sp} - 0.0003\ln X_{Cr}^{Opx} + 0.0019\ln X_{Cr}^{Gt} - 0.0003\ln(X_{Cr}^{Sp} + X_{Fe^{3+}}^{Sp}) - 0.003\ln X_{Ca}^{Gt}\} \quad (r^2 = 0.9326).$$

However, among these composition terms, only X_{Mg}^{Opx} and X_{Cr}^{Gt} are significant and the empirical barometer can be simplified to (Table 4.5):

$$P(\text{complex}) = 19.2 + 0.95P(\text{MAS}) + T\{0.0626\ln X_{Mg}^{Opx} + 0.0014\ln X_{Cr}^{Gt}\} \quad (r^2 = 0.9285).$$

This barometer reproduces the experimental pressure within ± 2 kbar (Fig.4.6a), which is better than the previous empirical barometer developed by O'Neill (1981) and its modification by Webb & Wood (1986). The difference between the calculated pressures by the O'Neill (1981) barometer and the experimental pressures is as much as 5 kbar (Fig.4.6b) and that between the calculated pressures by the Webb & Wood (1986) barometer and the experimental pressures can be as great as 6 kbar (Fig.4.6c). A significant difference between this barometer and the barometers of O'Neill (1981) and Webb & Wood (1986) is that it is not dependent on spinel composition, whereas the latter two rely heavily on X_{Cr}^{Sp}. Considering the insignificant abundance of spinel and the overwhelming abundances of orthopyroxene and garnet in spinel + garnet lherzolites, it is easy to accept that compositions of orthopyroxene and garnet should have the major effect on the reaction (4.3).

Compared with the experimental pressures, the pressures calculated by the Nickel & Green (1985) barometer (based on Al solubility in orthopyroxene in the garnet-facies field) are generally higher, with a difference as much as 4 kbar (Fig.4.6d). The difference becomes greater as the experimental pressure increases. Such a difference is transformed to a linear relation between the differences in calculated pressures by the transition barometer established in this study and by the Nickel & Green (1985) barometer and the pressures computed by the Nickel & Green (1985) barometer (Fig.4.7). This linear relation will be useful to explain the results of application of these barometers to natural spinel + garnet lherzolites.

4.6 Applications and Discussion

The empirical barometer formulated in this study has been utilised to calculate the equilibrium pressures for a number of natural spinel + garnet lherzolite inclusions in

basalts and kimberlites. The results are summarised in Table 4.6. The equilibrium temperatures are estimated according to the method of Bertrand & Mercier (1985). For sake of comparison, temperatures predicted by the two-pyroxene thermometer of Brey & Köhler (1990), by the garnet-orthopyroxene Fe^{2+}/Mg exchange thermometer of Carswell & Harley (1989), and by the garnet-clinopyroxene Fe^{2+}/Mg exchange thermometer developed in Chapter Six are also shown. Whenever required the pressure obtained from the Nickel & Green (1985) barometer is incorporated for temperature calculation; the temperature derived from the Bertrand & Mercier (1985) thermometer is incorporated for pressure estimation.

From these limited number of data it can be inferred that at 1200°C the minimum equilibrium pressure of natural spinel + garnet lherzolite inclusions in basalts is 23.5 kbar, which may be treated as the maximum pressure limit for spinel lherzolites (without garnet) at this temperature.

Comparison of the equilibrium pressures calculated by the transition barometer $P^{(complex)}$ and by the Nickel & Green (1985) barometer shows a trend that is similar to Figure 4.7 for reproduction of experimental pressures. For the spinel + garnet lherzolite xenoliths in alkali-basalts, the estimated equilibrium pressures according to the transition barometer are generally 5 ± 3 kbar higher than those by the Nickel & Green (1985) barometer; for the xenoliths in kimberlites, the difference changes from almost +10 kbar to nearly -15 kbar (Fig.4.8). This correlation trend is believed to be caused by the increasing overestimate of the equilibrium pressure by the Nickel & Green (1985) barometer as the equilibrium pressure increases (such as shown in Fig.4.7d). It should be pointed out that the transition barometer developed in this study is empirical, totally based on the experimental data in the temperature range of 1200 - 1600°C and pressure range of 20 - 38 kbar. Caution should be exercised when applying this barometer to mineral assemblages equilibrated below1200°C, which is apparently the case for most natural spinel + garnet lherzolites (Table 4.6). Four experimental runs at 20, 23, 25, and 27 kbar respectively in the TQ40 system have been conducted at 1050°C in an attempt to bring down the experimental temperature close to natural conditions. In the two runs at 25 and 27 kbar, both garnet and spinel (together with olivine and two pyroxenes) are present. In the 20 and 23 kbar runs only spinel (+ olivine and two pyroxenes) is present. Due to kinetic problems, mineral crystals in all the four charges are very small in size and ambiguous in shape (even in runs as long as 14 days). Probe analyses of these minerals show large overlap between compositions of different minerals and are therefore not reported here.

It has been advocated that the transition from spinel lherzolite to garnet lherzolite may cause a sharp increase in P-wave velocity (Green & Liebermann, 1976; Webb & Wood, 1986). Green & Liebermann (1976) suggest a 0.12 km/sec increase at around 55

Table 4.6 Estimated Equilibrium Temperatures and Pressures for Some Spinel + Garnet Lherzolites

Data Source	Sample #	T°C(BM)	T°C(BK)	T°C(CH)	T°C(Ai)	P(Ai)	P(NG)	P(O'Neill)	P(WW)
Jin et al.'91	MingXi #M3	1096	1148	1126	1071	27.15	26.07	22.75	21.70
	NuShan #N3	1192	1220	1279	1265	23.50	21.38	21.19	19.85
Chao & Zhu'87	MD-10-10	1020	1085	1109	1087	25.19	18.49	21.78	21.05
Fan & Hooper'89	HT-28	1072	1123	1160	1106	24.33	18.35	20.12	19.47
	MD-4	1042	1079	1148	918	27.27	19.97	23.24	22.19
Chapter One	76210	1069	1113	1116	971	26.12	20.19	22.40	21.45
	76211	1065	1117	1126	1042	25.96	20.71	22.30	21.38
	76212	1126	1161	1187	1081	27.72	21.13	24.73	23.38
	76212	1126	1161	1187	1081		21.13	23.72	22.49
	76213	1132	1170	1190	1106	26.99	21.58	23.33	22.12
	76217	1150	1189	1230	1195	25.85	21.84	22.86	21.64
	76218	1119	1157	1173	1065	26.82	21.40	22.99	21.85
	76221	1134	1169	1174	1068	27.94	21.88	23.42	22.20
	76224	1131	1170	1180	1093	27.80	22.40	23.27	22.07
	76225	1122	1158	1172	1061	27.81	21.70	24.73	23.39
	76225	1122	1158	1172	1061		21.70	23.87	22.62
Skewes & Stern'79	BN-4	1030	1089	1134	1041	26.31	23.23	25.98	24.35
Berger'79	Causses	1228	1251	1221	1274	25.31	22.29	21.40	19.86
	Ardeche	1253	1274	1156	1249	25.92	22.96	21.93	20.26
Berger & Vannier'84	EGL7501	1230	1249	1238	1260	24.82	21.91	21.54	19.99
Ferguson et al.'77		1060	1106	1105	995	27.81	19.88	23.30	22.22
Nixon & Boyd'79	3567	859	912	958	788	26.38	18.75	23.84	22.40
Eherenberg'82	H077	1093	1152	1056	1041	35.97	39.04	36.83	37.88
Hearn & McGee'84	GSL3	946	1011	1286	1295	38.43	38.64	40.15	49.46
Kirkley et al.'84	SD2-L11	859	896	811	626	29.72	24.77	19.11	19.42
	SD2-L189	993	1054	887	819	35.23	37.75	30.84	28.28
McCallum&Eggler'76	S1L102	1052	1116	1065	1043	41.75	47.40	37.71	39.74
Mitchell'84	14	945	1008	955	961	38.59	37.42	36.39	35.57
	32	841	883	976	836	35.33	30.37	35.92	33.37
Carswell et al.'79	PTH207	990	1073	1080	1190	45.53	53.40	23.31	22.27
		990	1073	1080	1190		53.40	37.01	37.44
	PTH403	991	1077	1055	1189	41.34	44.43	29.60	27.13
		991	1077	1055	1189		44.43	35.25	33.85
	PTH404	978	1052	1021	1112	40.78	41.77	22.25	21.48
	PTH405	992	1067	1031	1100	39.46	39.72	23.31	22.27
		992	1067	1031	1100		39.72	27.23	25.20
	PTH407	955	1021	1122	1148	39.18	38.11	22.44	21.63
	PTH409	958	1040	1033	1162	39.41	39.02	37.86	39.46
	PTH410	1018	1090	1220	1316	39.54	39.59	22.25	21.43
Boyd & Mertzman'87	FRB1008	847	853	840	575	37.34	34.81	33.16	29.17
	FRB1009	815	846	871	703	36.69	33.44	34.87	31.09
Nixon & Boyd'73	1595	878	902	918	742	38.38	35.12	31.40	32.41
	1567	925	958	971	791	37.86	35.32	32.60	34.16
	1592	943	987	980	864	38.27	36.28	33.40	35.67
	1570	948	975	977	757	38.67	37.61	32.60	34.83
	1573	963	1004	922	839	40.06	39.10	31.80	35.49
	1572	989	1053	976	981	38.99	38.90	32.70	36.85
Mori'76	K2	725	721	837	598	34.38	24.75	30.26	24.94
	K18	1027	1121	1125	1307	49.12	63.56	36.92	37.53

*) thermometers: BM - Bertrand & Mercier (1985); BK - Brey & Köhler (1990);
CH - Carswell & Harley (1989); Ai - Chapter Six;

**) barometers: Ai - the empirical transition barometer P(Complex) developed in this study;
NG - Nickel & Green (1985); O'Neill - O'Neill (1981); WW - Webb & Wood (1986).

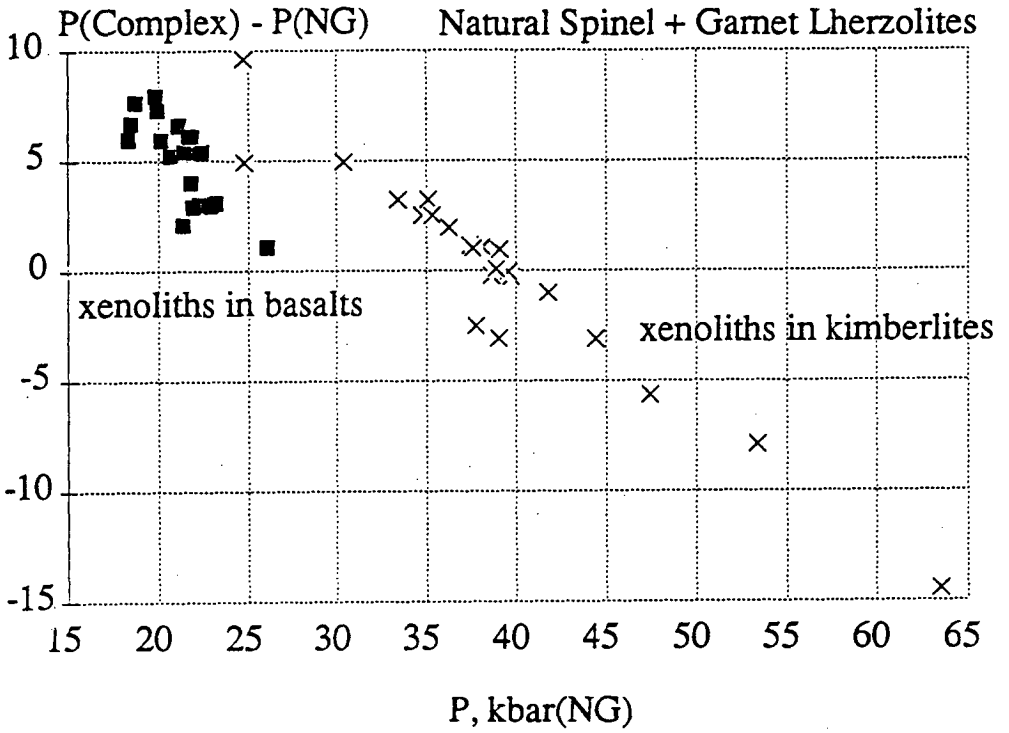

Figure 4.8. Correlation of the pressures computed by the Nickel & Green (1985) barometer with the difference between the pressures estimated by the empirical transition barometer and by the Nickel & Green (1985) barometer for some natural spinel + garnet lherzolites enclosed in basalts and kimberlites.

km (16 - 17 kbar), 850°C on the basis of this transition in the Hawaiian pyrolite system, which is confirmed by Webb & Wood (1986). Admitting that this increase is substantially smaller than the observed increase of 0.2 to 0.4 km/sec, Webb & Wood (1986) argue that uncertainties in pressure and temperature dependence of mineral elastic moduli may account for the difference. The change in P-wave velocity in the upper mantle is a direct consequence of changes in mineral association and rock density. In table 4.7 the densities of individual minerals and the rocks they constitute are calculated for the three model lherzolite systems reported in this study. The mineral compositions are from chapters three, four and five. Calculation is carried out by using the DENSCAL program of Niu & Batiza (1991) (by courtesy of Yaoling Niu). Although the compositions of the three model lherzolite systems are different from the actual mantle composition, the change in density with pressure and temperature should be similar to the natural mantle lherzolites. At constant temperature, the rock density increases gradually with increasing pressure (about 0.04 g/cm^3 per 2 kbar in the TQ40 system); at constant pressure the rock density increases with decreasing temperature (about 0.035 g/cm^3 per 100°C in the TQ40 system). The higher the Cr# in the system, the smaller the magnitude of the change. Such a systematic variation is mainly controlled by the density changes of olivine and orthopyroxene in the system. Density contributions from clinopyroxene, spinel and garnet to rock density in the pressure and temperature range of interest are relatively small.

The P-wave velocity is related to density via Birch's empirical relation $V_P = A(\overline{M}) + B\rho$, where A is a constant determined approximately by the mean atomic weight ($\overline{M}$), and B is the observed proportionality factor between velocity V_P and density ρ -- about 3 (km/sec)/(g/cm^3) for most oxides and minerals (Ringwood, 1975). The difference in density of 0.04 g/cm^3 with a pressure increase of 2 kbar would approximately correspond to 0.13 km/sec in P-wave velocity, which is similar to the value suggested by Green & Liebermann (1976) and Webb & Wood (1986); and smaller than the measured increase of 0.2 - 0.4 km/sec in the oceanic lithosphere (Webb & Wood, 1986). However, if the oceanic mantle undergoes cooling from 1350°C to 850°C at a constant pressure, its density will increase by 0.14 g/cm^3, which will produce an increase in P-wave velocity of 0.42 km/sec. As the oceanic mantle cools it becomes denser and thus sinks to deeper level. This process would favour the transition from spinel lherzolite to garnet lherzolite and would lead to a net increase in the P-wave velocity (with a major contribution from the temperature decrease), which would be very close to the observed value of 0.2 - 0.4 km/sec.

Measurements of ocean floor bathymetry show a linear dependence of depth on the square root of age for seafloor younger than 80 Ma (Parsons & Sclater, 1977). For seafloor older than 80 Ma, there is a systematic departure of the measured bathymetry from this linear relationship, with the measured ocean depth smaller than the model depth,

Table 4.7 Calculated Densities for Minerals and Rocks in the Model Lherzolite Systems

Run #	P(kbar)	T(°C)	Ol	Opx	Cpx	Gt	Sp	Rock
TQ40 System								
T3145	20	1200	3.2577	2.9490	3.3240		3.8203	3.1582
T3239	20	1200	3.2656	2.9826	3.3189	3.7115	3.7893	3.2364
T3105	22	1200	3.2709	2.9576	3.3205		3.7190	3.1651
T3108	23	1200	3.2712	2.9438	3.3450		3.7325	3.1613
T3101	25	1200	3.2778	2.9972	3.3392	3.7058	3.8020	3.2292
T3168	25	1200	3.2746	3.0115	3.3305	3.6956	3.8274	3.2524
T3126	27	1200	3.2888	2.9916	3.3589	3.6822	3.8470	3.2397
T3454	28	1200	3.2842	3.0575	3.3700	3.7011	3.9763	3.2941
T3151	30	1200	3.2953	3.1000	3.3461	3.7146		3.3152
T3306	35	1200	3.3072	3.1257	3.3762	3.6829		3.3380
T3316	20	1300	3.2486	2.9455	3.2851		3.8010	3.1441
T3158	20	1300	3.2419	2.9326	3.3316		3.7707	3.1461
T3141	23	1300	3.2574	2.9278	3.3373		3.7697	3.1534
T3130	25	1300	3.2653	2.9368	3.3702		3.7843	3.1672
T3355	26	1300	3.2659	2.9632	3.3494	3.6682	3.7738	3.2200
T3338	26	1300	3.2537	2.9035	3.3134		3.7531	3.1543
T3136	27	1300	3.2704	2.9701	3.3459	3.6995	3.8387	3.2288
T3247	27	1300	3.2769	2.9310	3.3394	3.7169	3.8740	3.2181
T3364	28	1300	3.2726	3.0040	3.3355	3.7011	3.8841	3.2576
T3160	30	1300	3.2701	2.9694	3.3211	3.6450	3.8482	3.2426
T3345	35	1300	3.2975	3.0928	3.3717	3.7330		3.3366
T3166	20	1400	3.2295	2.8706	3.2625		3.7273	3.1087
T3524	22.5	1400	3.2372	2.8900	3.3346		3.7075	3.1262
T3164	25	1400	3.2479	2.9030	3.2835		3.7687	3.1347
T3360	26	1400	3.2481	2.9093	3.3102		3.7445	3.1472
T3167	27	1400	3.2588	2.9006	3.3165	3.6883	3.8472	3.1702
T3453	28	1400	3.2597	2.9483	3.3076	3.6538	3.8026	3.2097
T3526	29	1400	3.2621	2.9743	3.3594	3.6533	3.7817	3.2295
T3163	30	1400	3.2656	2.9093	3.3352	3.6592	3.7682	3.2057
T3342	35	1400	3.2845	3.0012	3.3411	3.6997		3.2854
T3299	35	1400	3.2754	3.0213	3.3519	3.6748		3.2955
T3378	28	1500	3.2362	2.8674	3.2703	3.6313	3.8461	3.1913
T3249	30	1500	3.2456	2.9176	3.5100	3.6855	3.7467	3.2821
T3430	30	1500	3.2453	2.9003	3.3385	3.6505	3.7127	3.2260
T3527	32	1500	3.2550	2.9591	3.3245	3.6460		3.2515
T3302	35	1500	3.2563	2.9643	3.3276	3.6793		3.2849
TQ40/30a System								
T3255	20	1200	3.2582	2.9936	3.3073		4.0821	3.2229
T3280	25	1200	3.2816	2.9972	3.3160		4.0475	3.2216
T3330	26.5	1200	3.2878	3.0169	3.3251		4.0567	3.2347
T3275	27.5	1200	3.2879	3.0380	3.3367	3.7143	4.1325	3.2709
T3261	30	1200	3.2942	3.0888	3.3565	3.7139	4.1786	3.3079
T3548	32	1200	3.2972	3.0528	3.3603	3.6731	4.1920	3.2982
T3269	35	1200	3.3092	3.1005	3.3606	3.8029	4.4259	3.3785
T3476	25	1300	3.2691	2.9691	3.3344		4.0932	3.2132
T3379	27	1300	3.2732	3.0003	3.3297		4.1567	2.9467

*). desity unit in g/cm^3; uncertainty $\pm$ 0.05 g/cm^3.

**). Additonal phase compositions in the garnet-free spinel lherzolite field of the high-Cr systems are from Chapter Five.

Table 4.7 Calculated Densities for Minerals and Rocks in the Model Lherzolite Systems (cont'd)

Run #	P(kbar)	T(°C)	Ol	Opx	Cpx	Gt	Sp	Rock
TQ40/30a System								
T3446	28	1300	3.2752	3.0172	3.3477	3.7093	4.0892	3.2366
T3423	30	1300	3.2807	3.0664	3.3386	3.7348	4.1945	3.3027
T3556	32	1300	3.2846	3.0205	3.2947	3.6687	4.3072	3.2992
T3402	35	1300	3.3006	3.0662	3.3391	3.7192	4.3323	3.3365
T3481	25	1400	3.2418	2.9060	3.3014		4.0510	3.1827
T3414	27	1400	3.2567	2.9675	3.3260		4.0805	3.2132
T3540	29	1400	3.2655	2.9603	3.3272		4.1353	3.2157
T3420	30	1400	3.2665	2.9703	3.3093		4.1130	3.2167
T3544	30	1400	3.2664	2.9645	3.3370		4.0942	3.2130
T3594	31	1400	3.2668	2.9867	3.3112		4.0981	3.2235
T3470	31	1400	3.2695	2.9654	3.3215		4.0997	3.2109
T3451	32	1400	3.2726	3.0244	3.3471	3.6902	4.1225	3.2792
T3417	35	1400	3.2785	3.0581	3.3280	3.7039	4.2386	3.3217
T3515	25	1500	3.2160	2.9078	3.1981		4.1324	3.2424
T3473	27	1500	3.2383	2.9229	3.2695		4.1282	3.2130
T3252	30	1500	3.2373	2.8754	3.2526		4.1257	3.2095
T3545	31	1500	3.2464	2.9275	3.2641		4.1128	3.2244
T3517	32	1500	3.2511	2.9457	3.2900	3.6881	4.1307	3.2436
T3416	32.5	1500	3.2599	2.9493	3.2955		4.0756	3.2327
T3504	33	1500	3.2534	2.9142	3.3004		4.1224	3.2108
T3429	34	1500	3.2590	2.9552	3.3127	3.6826	4.1276	3.2591
T3268	35	1500	3.2598	2.9249	3.2837	3.6962	4.1700	3.2634
TQ40/30b System								
T3454	28	1200	3.2892	3.0898	3.3470		4.1971	3.2625
T3505	30	1200	3.2973	3.0281	3.3472		4.2039	3.2326
T3573	32	1200	3.3023	3.1051	3.3655	3.7399	4.3465	3.3196
T3528	35	1200	3.3073	3.1219	3.3767	3.7571	4.4205	3.3387
T3476	25	1300	3.2716	2.9978	3.3411		4.1960	3.2145
T3588	31	1300	3.2863	2.9810	3.2867		4.1415	3.2109
T3583	32	1300	3.2916	3.0390	3.3304	3.7091	4.2422	3.2655
T3562	35	1300	3.3054	3.0660	3.3124	3.7089	4.3792	3.3016
T3593	38	1300	3.3081	3.0669	3.3202	3.7336	4.4732	3.3206
T3481	25	1400	3.2413	2.9119	3.2776		4.1257	3.1921
T3453	28	1400	3.2562	2.9735	3.2985		4.1546	3.2038
T3470	31	1400	3.2655	2.9684	3.3057		4.1639	3.2074
T3568	32	1400	3.2766	2.9723	3.2965	3.6791	4.1977	3.2275
T3601	32.5	1400	3.2782	2.9600	3.2884		4.1868	3.2075
T3604	33.5	1400	3.2805	2.9702	3.3075	3.6831	4.1665	3.2300
T3536	35	1400	3.2828	2.9800	3.2871	3.6804	4.2754	3.2558
T3515	25	1500	3.2219	2.8813	3.2070		4.1650	3.2510
T3600	32	1500	3.2494	2.9161	3.2935		4.1511	3.1894
T3504	33	1500	3.2488	2.9528	3.2620		4.1585	3.2244
T3571	34	1500	3.2624	2.9147	3.3214		4.1448	3.2157
T3534	35	1500	3.2682	2.9653	3.3462	3.6820	4.1371	3.2517
T3598	38	1500	3.2747	2.9483	3.2861	3.7204	4.2214	3.2804
T3559	35	1600	3.2279	2.9334	3.2617		4.1852	3.2405
T3561	38	1600	3.2522	2.9227	3.2194		4.1396	3.2531
T3567	38	1600	3.2573	2.9115	3.2645		4.1340	3.2562

which gives an impression of an uplift of the oceanfloor. Wood & Yuen (1983) propose that such an uplift may be caused by mineralogic change associated with the cooling and aging of the oceanic mantle. They suggest that at $T < 900°C$, the transition has a negative Clapeyron slope (dP/dT). Assuming the temperature at the top of the lithosphere is 0°C and the ambient mantle temperature is 1350°C, they predict an uplift of 50 - 300 m as a result of the density changes induced by the transition. It is difficult to comment on this suggestion because of the lack of experimental data at such low temperatures.

Chapter Five

Empirical Geobarometers and Geothermometers for Spinel Lherzolites

Chapter Five

Empirical Geobarometers and Geothermometers for Spinel Lherzolites

5.1 Introduction

The application of equilibrium thermodynamic theory to modern petrology has resulted in a rapid development of the geothermobarometric technique. Various geobarometers and geothermometers have been formulated and utilised in petrogenetic studies. This technique is particularly useful in the study of mantle xenoliths. It provides a means of arriving at a detailed understanding of the upper mantle thermal structure. A general survey of various mineral barometers and thermometers reveals that whereas the equilibrium pressure and temperature of minerals in garnet lherzolites can be determined with reasonable accuracy and precision, the equilibration pressure of mineral assemblages in spinel lherzolites is difficult to constrain due to the lack of a suitable barometer. As well there are fewer thermometers available for temperature estimation for spinel lherzolites than for garnet lherzolites. The experimental data in the spinel lherzolite field reported in Chapters Three and Four show that Ti-partitioning between spinel and pyroxenes is strongly pressure-dependent and that Fe^{2+}/Mg partitioning between spinel and respectively, olivine, orthopyroxene, clinopyroxene, and garnet is very temperature-sensitive. These studies are particularly aimed at the P,T field where garnet lherzolite is stable with lower Cr/Al+Cr ratios, spinel lherzolite is stable with higher Cr/Al+Cr ratios, and at the P,T field in which garnet and spinel coexist in lherzolitic compositions. The latter assemblages permit the comparison of geothermometers and geobarometers developed for garnet lherzolite assemblages with those for spinel lherzolite assemblages. The starting compositions used contain low TiO_2 content and were not specifically designed to evaluate geothermometers and geobarometers involving Ti-partitioning. However, the available data are sufficient to demonstrate the empirical method, which may have a wide application in development of mineral thermobarometers. In this chapter, four empirical geobarometers based on the Ti-partition between spinel and pyroxenes and four empirical geothermometers based on the Fe^{2+}/Mg partition between spinel and silicates are formulated. Although these thermometers are shown to have great uncertainties in reproduction of the experimental temperatures, the barometers offer some promise as a new method for equilibrium pressure evaluation of spinel lherzolites. The extraction of geothermometers and geobarometers from these experimental data,

particularly those involving Ti-partitioning , also serves to guide the planning of further studies of more appropriate composition, over suitable pressure and temperature range.

5.2 Experimental Data

The experimental results in three model lherzolite systems given in Chapters Three and Four are used to formulate the empirical barometers and thermometers in this chapter. Additional mineral compositions in the garnet-free spinel lherzolite assemblages of the two high-Cr systems (Chapter Four) are presented in Table 5.1. The relevant partitioning data are summarised in Table 5.2. Details of starting compositions, experimental method and analytical techniques are described in the previous two chapters. It should be emphased that the major elements (Al, Cr, Fe, and Mg) in spinels show large scatter, but the minor elements (Ti, Mn, and Ni) are not directly correlated with the major elements and only display small variation. The "equilibrium compositions" of spinels were selected from the range of observed compositions by using coexisting orthopyroxene composition and the Cr/Al-correlation relation between spinel and orthopyroxene defined by a number of natural spinel peridotite suites (Chapter Three). It is obviously not possible to obtain any information on PT dependence of Cr/Al partition between spinel and other phases.

The optimum detection limit for TiO_2 content in the WDS mode of the CAMECA SX50 microprobe is 0.048 wt%. The experimental spinels analysed in the TQ40/8.6 system have the minimum and maximum TiO_2 contents 0.15% and 0.58% (Table 3.7), which are three and ten times the amount of the detection limit. Spinels in the high-Cr systems have even higher TiO_2 content (the minimum and maximum values are 0.21 and 1.48%). Therefore, the observation of TiO_2 increase with increasing pressure is based on reliable analytical data. The increase of TiO_2 in spinel with increasing pressure is accompanied by decrease in spinel abundance. It is possible that such an increase may merely reflect the concentration of TiO_2 in spinel because the bulk TiO_2 is fixed. However, other minor elements such as NiO and MnO do not show similar magnitude of increase with increasing pressure, which suggests that at least there is a positive effect of pressure on TiO_2 solubility in spinel.

5.3 A General Model and the Consequent Barometers and Thermometers

The two basic equilibrium thermodynamic equations that provide the theoretical foundation to the formulation of any geobarometer or geothermometer are: $\Delta G_{P,T} = \Delta H_{P,T} - T\Delta S_{P,T} + P\Delta V$ and $\Delta G_{P,T} = - RTlnK$. When combined together, a clear relation between the external physical conditions (pressure and temperature) and the composition parameters (the equilibrium constant) is established:

Table 5.1 Additional Mineral Compositions in the High-Cr Spinel Lherzolite Systems

TO40/30a

Run#	T3255	T3280	T3330	T3476	T3379	T3481	T3414	T3540	T3420	T3544	T3594	T3470	T3515	T3473	T3252	T3545	T3416	T3504
T°C	1200	1200	1200	1300	1300	1400	1400	1400	1400	1400	1400	1400	1500	1500	1500	1500	1500	1500
P(kbar)	20	25	26.5	25	27	25	27	29	30	30	31	31	25	27	30	31	32.5	33
Ol																		
SiO2	40.82	40.66	40.48	40.49	40.73	40.88	40.33	40.52	40.52	40.47	40.87	40.59	40.67	40.45	41.00	40.64	40.49	40.94
FeO	10.02	10.60	10.73	10.71	10.52	9.74	10.36	10.49	10.32	10.31	10.04	10.25	8.81	10.00	9.07	9.58	10.21	9.51
MnO	0.15	0.11				0.15	0.20	0.13	0.13	0.12	0.08	0.18	0.12	0.17	0.15	0.12	0.16	0.09
NiO	0.84	0.85	0.94	1.00	0.81	0.88	0.77	0.69	0.77	0.90	0.78	0.89	0.88	0.95	0.90	0.76	0.78	0.86
MgO	48.01	47.59	47.63	47.53	47.74	48.08	48.01	47.81	47.99	48.02	48.00	47.83	49.17	48.12	48.55	48.59	47.98	48.25
CaO	0.16	0.18	0.22	0.26	0.19	0.27	0.33	0.35	0.27	0.18	0.23	0.25	0.35	0.32	0.33	0.30	0.38	0.34
Sum	100	100	100	100	100	100	100	100	100	100	100	100	100	100	100	100	100	100
Opx																		
SiO2	55.41	54.38	54.57	54.66	54.62	54.29	53.94	53.76	54.23	53.64	54.29	54.09	54.66	53.54	54.37	54.16	53.68	54.08
TiO2	0.11	0.14	0.14	0.12	0.13	0.09	0.10	0.12	0.11	0.12	0.07	0.12	0.01	0.09	0.07	0.07	0.12	0.04
Al2O3	3.33	4.41	4.10	4.29	3.84	4.44	4.41	4.90	4.32	4.83	4.20	4.57	3.55	4.73	4.63	4.38	4.68	4.69
Cr2O3	0.92	1.03	1.12	1.11	1.17	1.59	1.54	1.44	1.36	1.42	1.49	1.40	1.94	1.75	1.88	1.75	1.75	1.82
FeO	6.58	6.42	6.61	6.21	6.49	5.93	6.13	6.20	6.13	6.29	6.32	6.23	5.04	5.84	5.49	5.54	6.02	5.62
MnO	0.23	0.18	0.15		0.19	0.13	0.07	0.12	0.13	0.18	0.07	0.13	0.02	0.06	0.11	0.10	0.06	0.10
NiO	0.21	0.22	0.25	0.32	0.27	0.32	0.26	0.28	0.31	0.22	0.23	0.31	0.22	0.30	0.24	0.26	0.27	0.25
MgO	31.61	31.42	31.46	31.35	31.38	30.76	31.23	30.96	31.14	30.86	31.16	30.93	31.58	30.89	30.56	31.07	30.81	30.73
CaO	1.49	1.69	1.47	1.81	1.78	2.31	2.19	2.04	2.11	2.29	2.03	2.09	2.88	2.66	2.66	2.51	2.46	2.50
Na2O	0.11	0.11	0.11	0.13	0.13	0.14	0.14	0.17	0.15	0.14	0.14	0.13	0.10	0.13		0.16	0.15	0.17
Sum	100	100	100	100	100	100	100	100	100	100	100	100	100	100	100	100	100	100
Cpx																		
SiO2	52.67	52.43	52.49	52.11	52.20	52.28	52.22	52.19	52.55	52.19	52.55	52.10	53.23	52.86	53.24	53.06	54.11	54.02
TiO2	0.25	0.22	0.26	0.25	0.15	0.14	0.13	0.20	0.17	0.23	0.12	0.21	0.08	0.10	0.05	0.07	0.12	0.02
Al2O3	4.55	4.76	4.70	4.65	4.80	4.51	4.68	5.05	4.82	4.95	4.56	4.83	4.84	4.56	4.35	4.62	3.31	3.41
Cr2O3	1.56	1.60	1.47	1.81	1.81	1.91	1.95	1.92	1.99	1.87	2.06	2.14	2.27	1.99	2.05	2.16	1.35	1.49
FeO	3.64	3.80	3.81	3.96	4.02	4.34	4.57	4.69	4.08	4.80	4.14	4.27	5.14	5.12	4.89	4.73	5.13	4.38
MnO		0.10	0.04		0.14	0.12	0.08	0.11	0.10	0.07	0.11	0.10	0.10	0.15	0.23	0.10	0.17	0.11
NiO		0.21	0.25	0.22	0.14	0.31	0.22	0.18	0.17	0.12	0.20	0.17	0.22	0.22	0.20	0.16	0.25	0.31
MgO	17.36	17.63	17.48	18.50	18.64	21.34	21.05	20.21	20.17	20.10	19.92	19.68	25.10	23.99	23.84	23.80	23.63	22.68
CaO	19.01	18.32	18.55	17.67	17.27	14.54	14.41	14.60	15.13	14.85	15.59	15.78	8.69	10.56	10.70	10.82	11.33	12.91
Na2O	0.96	0.92	0.93	0.84	0.82	0.52	0.68	0.84	0.82	0.80	0.75	0.72	0.33	0.46	0.45	0.47	0.60	0.67
Sum	100	100	100	100	100	100	100	100	100	100	100	100	100	100	100	100	100	100
Sp																		
TiO2	0.49	0.51	0.54	0.64	0.56	0.32	0.44	0.54	0.51	0.59	0.38	0.50	0.22	0.23	0.23	0.29	0.43	0.28
Al2O3	31.55	33.95	32.28	30.24	26.42	28.30	27.79	26.02	26.95	26.93	27.94	27.59	21.36	22.09	23.66	23.64	28.27	24.07
Cr2O3	36.99	34.06	35.81	37.88	41.53	41.27	40.80	42.05	41.32	40.52	41.59	41.01	49.51	47.94	47.02	45.58	40.40	45.72
Fe2O3	2.15	2.41	2.43	2.31	3.06	2.12	2.97	3.18	3.04	3.94	1.92	2.65	1.94	2.53	1.93	3.30	2.99	2.59
FeO	12.11	11.90	11.81	12.26	12.26	10.64	10.77	11.71	11.31	10.72	11.28	11.26	9.99	10.46	10.03	9.93	10.43	10.25
MnO	0.18	0.12	0.18	0.10	0.11	0.16	0.15	0.07	0.17	0.21	0.14	0.14	0.05	0.19		0.20	0.09	0.07
NiO	0.26	0.45	0.57	0.58	0.43	0.58	0.50	0.56	0.49	0.58	0.48	0.59	0.58	0.49	0.49	0.42	0.50	0.52
MgO	16.28	16.59	16.38	15.98	15.63	16.61	16.60	15.87	16.20	16.53	16.26	16.25	16.34	16.08	16.64	16.64	16.90	16.50
Sum	100	100	100	100	100	100	100	100	100	100	100	100	100	100	100	100	100	100

Table 5.1 Additional Mineral Compositions in the High-Cr Spinel Lherzolite Systems (Cont'd)

TQ40/30b

Run #	T3454	T3505	T3476	T3588	T3481	T3453	T3470	T3601	T3515	T3600	T3504	T3571	T3559	T3561	T3567
T°C	1200	1200	1300	1300	1400	1400	1400	1400	1500	1500	1500	1500	1600	1600	1600
P(kbar)	28	30	25	31	25	28	31	32.5	25	32	33	34	35	38	38
Ol															
SiO2	40.41	40.59	40.57	40.73	40.99	40.71	40.77	40.40	41.19	40.96	40.86	40.92	41.23	41.21	40.90
FeO	10.47	10.56	10.90	10.46	9.64	10.03	9.97	10.57	9.17	9.46	9.19	9.93	8.06	9.09	9.52
MnO	0.21	0.22	0.20	0.28	0.13	0.17	0.09	0.17	0.19	0.18	0.14	0.17	0.19	0.19	0.21
NiO	0.89	0.84	0.80	0.80	0.63	0.69	0.72	0.81	0.81	0.86	0.77	0.87	0.85	0.83	0.82
MgO	47.89	47.58	47.34	47.55	48.35	48.15	48.22	47.83	48.26	48.22	48.75	47.84	49.35	48.36	48.21
CaO	0.13	0.20	0.19	0.18	0.26	0.24	0.22	0.23	0.39	0.31	0.29	0.27	0.31	0.32	0.35
Sum	100	100	100	100	100	100	100	100	100	100	100	100	100	100	100
Opx															
SiO2	54.50	54.07	54.55	54.41	55.05	54.33	54.85	54.59	54.98	54.78	54.63	54.68	55.48	55.49	54.48
TiO2	0.15	0.14	0.14	0.10	0.12	0.11	0.00	0.12	0.08	0.09	0.03	0.11	0.03	0.08	0.08
Al2O3	3.69	4.03	3.78	3.99	3.54	3.99	3.88	3.93	3.25	3.88	3.66	3.99	2.83	3.48	4.05
Cr2O3	1.01	1.31	1.20	1.46	1.43	1.46	1.46	1.54	1.84	1.78	1.67	1.59	2.13	1.57	1.99
FeO	6.51	6.45	6.54	6.25	5.56	6.11	5.84	6.14	5.46	5.62	5.53	5.75	4.77	5.49	5.49
MnO	0.15	0.21	0.19	0.27	0.25	0.18	0.19	0.21	0.17	0.19	0.15	0.28	0.14	0.23	0.16
NiO	0.29	0.35	0.30	0.34	0.21	0.26	0.23	0.30	0.29	0.31	0.29	0.34	0.29	0.36	0.31
MgO	32.37	31.44	31.38	31.07	31.22	31.31	31.39	30.90	30.93	30.87	31.31	30.61	31.73	30.86	30.58
CaO	1.21	1.87	1.79	1.97	2.51	2.08	2.04	2.11	2.88	2.32	2.54	2.47	2.44	2.29	2.67
Na2O	0.12	0.11	0.13	0.14	0.12	0.16	0.13	0.16	0.13	0.16	0.19	0.18	0.15	0.16	0.18
Sum	100	100	100	100	100	100	100	100	100	100	100	100	100	100	100
Cpx															
SiO2	52.73	52.26	52.11	52.96	52.82	52.53	52.79	53.07	54.53	53.49	53.63	52.68	52.53	54.55	53.53
TiO2	0.30	0.24	0.23	0.20	0.16	0.17	0.16	0.17	0.09	0.11	0.10	0.17	0.10	0.05	0.09
Al2O3	3.89	4.42	4.30	4.29	4.16	4.44	4.03	4.19	3.01	3.42	3.72	4.37	4.71	3.50	4.05
Cr2O3	1.50	1.91	1.86	1.98	1.93	2.13	2.03	2.01	1.90	1.81	2.28	2.00	2.57	2.06	2.17
FeO	3.56	3.87	4.09	4.32	4.80	4.55	4.32	4.47	5.22	4.28	4.71	4.96	5.80	4.72	5.11
MnO	0.20	0.17	0.18	0.19	0.21	0.17	0.12	0.22	0.10	0.14	0.13	0.21	0.21	0.29	0.39
NiO	0.16	0.17	0.19	0.21	0.20	0.20	0.19	0.18	0.23	0.25	0.17	0.27	0.31	0.28	0.25
MgO	17.85	18.39	18.64	19.56	22.31	20.56	20.17	20.57	26.39	21.67	23.78	22.33	23.12	25.16	24.88
CaO	18.86	17.66	17.54	15.49	12.86	14.49	15.53	14.37	8.22	14.27	10.93	12.30	10.18	8.89	9.00
Na2O	0.96	0.91	0.85	0.80	0.53	0.75	0.66	0.75	0.32	0.56	0.56	0.70	0.48	0.50	0.53
Sum	100	100	100	100	100	100	100	100	100	100	100	100	100	100	100
Sp															
TiO2	0.91	0.63	0.78	0.73	0.36	0.56	0.51	0.65	0.31	0.42	0.40	0.63	0.22	0.36	0.45
Al2O3	26.32	24.08	21.85	27.11	23.55	24.58	25.08	23.54	19.39	21.83	21.68	24.38	17.12	21.49	23.05
Cr2O3	41.24	43.95	45.80	40.97	46.08	44.15	43.99	45.16	51.06	48.05	48.04	44.27	54.20	48.43	46.44
Fe2O3	2.47	2.95	3.20	2.57	2.57	2.70	2.34	2.49	2.32	2.18	2.63	2.74	2.16	2.58	2.70
FeO	13.29	12.59	12.63	12.02	10.49	11.50	11.76	12.01	10.26	10.92	10.40	11.23	9.30	10.05	10.15
MnO	0.24	0.16	0.32	0.26	0.17	0.23	0.18	0.29	0.25	0.27	0.25	0.21	0.18	0.28	0.26
NiO	0.50	0.52	0.67	0.54	0.47	0.39	0.36	0.43	0.42	0.58	0.44	0.58	0.51	0.54	0.50
MgO	15.02	15.11	14.74	15.79	16.30	15.88	15.79	15.43	15.98	15.76	16.16	15.96	16.32	16.26	16.45
Sum	100	100	100	100	100	100	100	100	100	100	100	100	100	100	100

Table 5.2 Summary of the Experimental Ti, Ti/Al and Fe2+/Mg Partitioning Data in the Spinel Lherzolite Systems

P(kbar)	T°C	Mg#(Ol)	Mg#(Opx)	Mg#(Cpx)	Mg#(Gt)	X(Ca)Gt	Mg#(Sp)	Cr#(Sp)	X(Ti)Sp	X(Fe3+)Sp	lnKd1	lnKd2	lnKd3	lnKd4	lnKd5	lnKd6	lnKd7	lnKd8
20	1200	89.56	89.71	88.89			81.46	21.22	0.0038	0.0245	0.2036	-1.6770	-0.6530	-2.2960	0.6696	0.6857	0.6007	
22	1200	88.98	89.59	89.68			79.25	14.27	0.0052	0.0171	0.2877	-1.6560	-0.3530	-2.2080	0.7486	0.8117	0.8201	
23	1200	89.23	90.15	89.36			79.01	15.57	0.0046	0.0058	0.4613	-1.3760	-0.2980	-2.0230	0.7892	0.8883	0.8020	
25	1200	89.21	89.80	89.06	82.71	0.1589	77.90	20.24	0.0051	0.0235	0.4055	-1.6220	-0.5790	-2.3780	0.8530	0.9161	0.8358	0.3054
25	1200	89.48	90.16	89.96	83.91	0.1601	78.31	21.30	0.0065	0.0258	0.8071	-1.3210	-0.2080	-1.9710	0.8570	0.9310	0.9084	0.3676
27	1200	88.83	89.63	88.86	83.08	0.1507	77.41	23.93	0.0066	0.0276	0.6633	-1.2370	-0.2170	-1.9190	0.8420	0.9260	0.8447	0.3595
28	1200	89.49	90.19	90.41	83.32	0.1528	73.59	32.36	0.0136	0.0285	1.5454	-0.6020	0.3588	-1.3670	1.1167	1.1938	1.2189	0.5838
20	1300	89.13	89.59	89.05			79.50	23.97	0.0040	0.0250	0.1625	-1.6530	-0.1400	-1.8550	0.7487	0.7972	0.7407	
20	1300	89.70	89.94	89.21			79.50	19.58	0.0041	0.0112	0.2796	-1.5340	-0.3290	-2.0530	0.8087	0.8357	0.7560	
23	1300	89.22	89.96	89.31			79.71	19.93	0.0035	0.0168	-0.1080	-1.9060	-0.6040	-2.3060	0.7446	0.8245	0.7543	
25	1300	89.10	89.67	89.15			78.31	20.03	0.0056	0.0200	0.6581	-1.1700	-0.4410	-2.0860	0.8175	0.7062	0.6509	
26	1300	90.37	89.52	88.90			82.88	19.78	0.0031	0.0181	-0.35	-2.077	-0.1210	-1.7770	0.6622	0.5678	0.5041	
26	1300	89.34	89.80	89.69	84.16	0.1503	78.45	19.43	0.0065	0.0167	0.4367	-1.6130	0.0000	-1.8190	0.8332	0.8834	0.8707	0.3782
27	1300	89.23	89.78	89.01	83.72	0.1539	78.44	23.69	0.0076	0.0246	0.7472	-1.1650	0.0822	-1.5980	0.8228	0.8814	0.8003	0.3461
27	1300	88.69	90.20	88.88	84.17	0.1468	76.17	26.77	0.0100	0.0274	1.0217	-0.7460	0.1508	-1.5790	0.8969	1.0576	0.9153	0.5089
28	1300	89.32	89.91	89.63	83.20	0.1535	76.49	26.72	0.0123	0.0311	1.2858	-0.7470	0.5217	-1.3420	0.9440	1.0079	0.9771	0.4200
30	1300	90.09	90.67	90.26	86.16	0.1494	77.70	23.23	0.0086	0.0106	1.3189	-0.6590	0.5225	-1.3670	0.9591	1.0247	0.9788	0.5807
20	1400	89.52	89.72	88.89			82.38	20.02	0.0042	0.0244	0.2113	-1.5360	-0.2510	-1.8850	0.6027	0.6237	0.5377	
22.5	1400	89.58	89.98	88.95			81.23	16.40	0.0031	0.0113	-0.0320	-1.7660	-0.8290	-2.4940	0.6862	0.7302	0.6209	
25	1400	89.38	89.78	89.15			80.91	21.35	0.0049	0.0179	0.5596	-1.2200	-0.0780	-1.7060	0.6856	0.7272	0.6622	
26	1400	89.65	90.19	89.25			83.34	18.92	0.0047	0.0332	1.0776	-0.7290	-0.0210	-1.6400	0.5491	0.6083	0.5061	
27	1400	89.03	89.49	88.29	84.28	0.1494	78.29	26.32	0.0060	0.0233	0.9589	-0.6530	0.4568	-1.0670	0.8114	0.8595	0.7375	0.3969
28	1400	89.24	90.27	88.65	85.94	0.1503	79.79	23.98	0.0063	0.0262	1.0076	-0.8530	0.2113	-1.2990	0.7424	0.8542	0.7078	0.4372
29	1400	89.32	89.65	89.03	85.22	0.1430	81.51	22.42	0.0069	0.0315	0.7077	-1.1900	0.3423	-1.4560	0.6411	0.6758	0.6102	0.2684
30	1400	89.32	90.15	88.72	85.05	0.1527	79.77	19.93	0.0049	0.0155	0.5245	-1.2330	0.0000	-1.7110	0.7513	0.8418	0.6904	0.3666
25	1500	90.69	91.61	90.06			83.83	22.40	0.0031	0.0222	0.6614	-1.2460	0.2559	-1.4720	0.6306	0.7451	0.5580	
28	1500	90.03	90.43	89.17	86.05	0.1455	78.90	30.63	0.0046	0.0078	0.6506	-0.9600	-0.0430	-1.5690	0.8817	0.9265	0.7902	0.5009
30	1500	89.82	90.44	89.72	87.07	0.1468	85.39	23.29	0.0042	0.0232	1.6582	-0.1630	0.2719	-1.4330	0.4125	0.6109	0.4871	0.1418
30	1500	89.84	90.35	89.20	86.53	0.1530	82.23	17.23	0.0034	0.016005	-0.0846	-1.8530	0.2305	-1.6310	0.6476	0.7046	0.5801	0.3280

*) Definitions of mineral composition parameters are given in previous chapters. Definitions of Kds are given in the text.

Table 5.2 Summary of the Experimental Ti, Ti/Al and Fe2+/Mg Partitioning Data in the Spinel Lherzolite Systems (Cont'd)

P(kbar)	T°C	Mg#(Ol)	Mg#(Opx)	Mg#(Cpx)	Mg#(Gt)	X(Ca)Gt	Mg#(Sp)	Cr#(Sp)	X(Ti)Sp	X(Fe3+)Sp	lnKd1	lnKd2	lnKd3	lnKd4	lnKd5	lnKd6	lnKd7	lnKd8
20	1200	89.51	89.54	89.49			70.57	42.98	0.0107	0.0238	1.3055	-0.7647	0.4387	-1.2780	1.2698	1.2726	1.2667	
25	1200	88.89	89.71	89.23			71.31	39.18	0.0112	0.0265	1.1076	-0.7430	0.6242	-1.1110	1.1692	1.2553	1.2039	
26.5	1200	88.78	89.45	89.12			71.20	41.52	0.0117	0.0269	1.1513	-0.7280	0.4995	-1.2040	1.1639	1.2330	1.1993	
27.5	1200	89.04	89.34	89.86	81.68	0.1725	71.87	49.83	0.0105	0.0375	1.1882	-0.5140	0.4643	-1.1550	1.1567	1.1879	1.2431	0.5567
30	1200	89.19	89.85	90.02	81.89	0.1679	68.34	46.89	0.0176	0.0417	1.6441	-0.2960	0.8398	-0.9280	1.3407	1.4106	1.4303	0.7394
32	1200	89.49	90.19	90.01	82.02	0.1744	68.03	48.99	0.0180	0.0409	1.5820	-0.1640	1.3428	-0.3900	1.3864	1.4628	1.4435	0.7627
35	1200	89.30	90.41	90.04	82.38	0.1741	62.25	63.02	0.0253	0.0413	2.9684	1.0802	1.5261	-0.0340	1.6218	1.7434	1.7022	1.0424
25	1300	88.78	89.99	89.28			69.91	44.48	0.0141	0.0259	1.4830	-0.2990	0.7293	-0.9320	1.2253	1.3534	1.2781	
27	1300	89.00	89.61	89.20			69.43	49.54	0.0126	0.0347	1.3099	-0.4620	1.1227	-0.3890	1.2697	1.3342	1.2921	
28	1300	89.10	89.73	89.48	82.78	0.1727	71.48	44.30	0.0124	0.0319	1.2368	-0.4620	0.7772	-0.8220	1.1818	1.2490	1.2212	0.6514
30	1300	89.20	89.95	89.26	83.27	0.1789	69.08	52.07	0.0145	0.0422	1.7186	-0.1250	1.0849	-0.4860	1.3069	1.3885	1.3129	0.8008
32	1300	89.43	90.32	90.23	82.90	0.1821	64.50	60.47	0.0153	0.0317	2.4655	0.7013	1.3169	-0.3030	1.5384	1.6366	1.6259	0.9813
35	1300	88.93	89.91	89.71	82.13	0.1748	64.10	60.46	0.0197	0.0357	2.8853	1.0803	1.3712	-0.2480	1.5043	1.6073	1.5872	0.9452
25	1400	89.80	90.25	89.76			73.56	48.28	0.0070	0.0237	1.0704	-0.6110	0.6109	-1.0240	1.1516	1.2019	1.1473	
27	1400	89.21	90.08	89.14			73.33	47.98	0.0096	0.0333	1.3063	-0.3660	1.0090	-0.5720	1.1003	1.1938	1.0938	
29	1400	89.04	89.90	88.49			70.73	50.16	0.0120	0.0361	1.3218	-0.1910	0.7985	-0.6510	1.2123	1.3036	1.1572	
30	1400	89.24	90.05	89.82			71.84	48.99	0.0115	0.0343	1.3776	-0.2900	0.8948	-0.6340	1.1788	1.2657	1.2408	
30	1400	89.25	89.74	88.18			73.31	48.03	0.0130	0.0444	1.4018	-0.1500	0.7244	-0.7710	1.1058	1.1583	0.9992	
31	1400	89.50	89.79	89.56			71.99	48.89	0.0083	0.0215	1.5285	-0.1990	0.9223	-0.6900	1.1991	1.2298	1.2056	
31	1400	89.27	89.84	89.14			72.01	48.44	0.0112	0.0298	1.2845	-0.3480	0.6754	-0.8670	1.1735	1.2359	1.1602	
32	1400	89.30	90.26	89.28	84.14	0.1661	72.84	48.80	0.0128	0.0408			1.2967	-0.2940	1.1353	1.2396	1.1334	0.6821
35	1400	89.66	90.48	89.90	84.26	0.1789	70.68	58.88	0.0097	0.0236	1.1407	-0.6590	0.9371	-0.7570	1.2801	1.3718	1.3073	0.7980
25	1500	90.87	91.78	89.70			74.47	59.52	0.0049	0.0221	2.7932	1.1377	0.8473	-0.4810	1.2275	1.3416	1.0942	
27	1500	89.56	90.41	89.30			73.22	57.76	0.0051	0.0289	0.7538	-0.6390	0.6360	-0.7730	1.1440	1.2372	1.1160	
30	1500	90.52	90.85	89.67			74.73	55.89	0.0050	0.0218	1.0217	-0.4590	1.3471	-0.1740	1.1719	1.2111	1.0778	
31	1500	90.04	90.91	89.97			74.91	54.30	0.0065	0.0373	1.2840	-0.2510	1.2299	-0.2300	1.1073	1.2094	1.0994	
32	1500	89.94	90.57	89.64	85.73	0.1705	73.96	56.08	0.0056	0.0300	1.2528	-0.1990	1.6275	0.2388	1.1469	1.2182	1.1145	0.7492
32.5	1500	89.34	90.12	89.14			74.29	47.31	0.0094	0.0333	1.0776	-0.5480	1.0776	-0.8730	1.0647	1.1488	1.0438	
33	1500	90.04	90.69				74.16	54.39	0.0063	0.0293	1.8405	0.3580			1.1471	1.2211	1.1689	
34	1500	89.86	90.22	89.32	85.88	0.1622	74.47	53.10	0.0078	0.0438	0.9894	-0.4840	0.7191	-0.8160	1.1115	1.1557	1.0797	0.7345
35	1500	90.09	90.63	89.79	84.62	0.1682	73.43	59.00	0.0076	0.0360	1.4404	0.0346	1.3863	-0.0100	1.1905	1.2518	1.1577	0.6883
28	1200	89.07	89.86	89.94			66.81	49.79	0.0204	0.0284	1.6292	-0.1830	0.9114	-0.8090	1.3982	1.4814	1.4913	

Table 5.2 Summary of the Experimental Ti, Ti/Al and Fe2+/Mg Partitioning Data in the Spinel Lherzolite Systems (Cont'd)

P(kbar)	T°C	Mg#(Ol)	Mg#(Opx)	Mg#(Cpx)	Mg#(Gt)	X(Ca)Gt	Mg#(Sp)	Cr#(Sp)	X(Ti)Sp	X(Fe3+)Sp	lnKd1	lnKd2	lnKd3	lnKd4	lnKd5	lnKd6	lnKd7	lnKd8
30	1200	88.93	89.67	89.45			68.14	53.18	0.0142	0.0340	1.3449	-0.2950	0.7814	-0.7320	1.3231	1.4012	1.3771	
32	1200	89.06	90.15	89.77	81.40	0.1664	63.15	55.89	0.0332	0.0381	2.0675	0.0360	1.5011	-0.2030	1.5583	1.6745	1.6335	0.9373
35	1200	89.46	90.44	90.01	81.34	0.1795	63.81	61.19	0.0356	0.0510	2.3486	0.4282	1.6554	0.0471	1.5717	1.6793	1.6321	0.9049
25	1300	88.57	89.53	89.04			67.54	56.26	0.0178	0.0374	1.5709	-0.0500	1.0386	-0.4150	1.3142	1.4135	1.3612	
31	1300	89.01	89.86	88.99			70.08	48.87	0.0163	0.0292	1.8357	0.0805	1.0864	-0.5650	1.2409	1.3304	1.2381	
32	1300	88.84	89.55	89.16	81.96	0.1731	67.51	53.09	0.0248	0.0424	1.8245	0.0146	1.3238	-0.2950	1.3431	1.4167	1.3752	0.7826
35	1300	88.52	89.97	89.37	81.67	0.1742	63.64	59.68	0.0341	0.0515	2.2484	0.4232	1.7543	0.0712	1.4830	1.6341	1.5698	0.9341
38	1300	89.14	90.20	89.73	81.66	0.1861	63.08	66.59	0.0364	0.0526	2.1595	0.4297	1.8541	0.3141	1.5693	1.6844	1.6318	0.9581
25	1400	89.94	90.92	89.22			73.46	55.10	0.0081	0.0292	0.9605	-0.7870	0.6332	-0.9220	1.1728	1.2858	1.0955	
28	1400	89.54	90.14	88.95			71.10	52.97	0.0127	0.0307	1.4769	-0.1900	1.0155	-0.5120	1.2465	1.3135	1.1857	
31	1400	89.61	90.55	89.28			70.52	52.63	0.0115	0.0266			0.9837	-0.6590	1.2823	1.3879	1.2488	
32	1400	88.96	89.50	88.84	83.20	0.1755	68.34	52.12	0.0189	0.0349	1.6582	-0.0750	0.9933	-0.5360	1.3175	1.3736	1.3053	0.8301
32.5	1400	88.97	89.97	89.14			69.63	54.66	0.0147	0.0287	1.5564	-0.0890	1.1618	-0.3900	1.2586	1.3643	1.2746	
33.5	1400	89.06	89.88	88.82	83.30	0.1722	70.08	51.61	0.0160	0.029014	1.7079	-0.0200	1.1433	-0.4460	1.2461	1.3325	1.2216	0.7562
35	1400	89.30	89.93	88.77	83.40	0.1729	68.41	56.43	0.0269	0.0435	2.1607	0.5005	1.5517	-0.0590	1.3491	1.4167	1.2956	0.8417
32	1500	90.08	90.74	90.03			72.01	58.13	0.0097	0.0250	1.4392	-0.1510	1.1735	-0.5110	1.2614	1.3370	1.2561	
33	1500	90.43	90.98	89.99			73.47	57.98	0.0090	0.0302	2.4204	0.7834	1.2040	-0.3960	1.2280	1.2930	1.1780	
34	1500	89.57	90.47	88.91			71.68	53.21	0.0140	0.0312	1.5743	-0.0850	1.1130	-0.4270	1.2217	1.3217	1.1529	
35	1500	89.38	89.90	88.63	84.69	0.1623	72.70	52.22	0.0144	0.0374	1.6025	0.0009	1.4733	-0.0700	1.1510	1.2062	1.0739	0.7311
38	1500	89.72	90.55	89.31	84.50	0.1740	70.50	60.83	0.0122	0.0310	1.5459	-0.0790	1.7130	0.0841	1.2951	1.3888	1.2513	0.8249
35	1600	91.60	92.23	87.67			75.79	66.28	0.0051	0.0251	1.8524	0.1729	0.6360	-0.5050	1.2488	1.3319	1.0728	
38	1600	90.46	90.93	90.47			74.26	58.40	0.0082	0.0296	1.3622	-0.3210	1.8418	0.1824	1.1899	1.2458	1.1911	
38	1600	90.03	90.86	89.67			74.28	55.71	0.0102	0.0308	1.5805	-0.0090	1.4469	-0.1250	1.1398	1.2351	1.0998	

$$\ln K = \frac{(\Delta H_{P,T} - T\Delta S_{P,T} + P\Delta V)}{- RT}$$

Omitting the thermodynamic significance of $\Delta H_{P,T}$ $\Delta S_{P,T}$ and ΔV, the above relation can be simplified as

$$\ln K = \frac{(A' + BT + CP)}{- T},$$

where A', B, and C are constants. When replacing the equilibrium constant K by the empirical constant K_d (partition coefficient), additional terms representing contributions from the internal compositions should be included, thus A' becomes A, which varies according to the exact element partitioning concerned.

For the Ti-partitioning between spinel and pyroxenes, relevant composition terms are $Mg\#^{(Sp)}$, $Cr\#^{(Sp)}$, X_{Ti}^{Sp}, $X_{Fe^{3+}}^{Sp}$, Mg# and Cr# of the pyroxenes. Taking these terms into account, for $K_d1 = (Ti)^{Sp}/(Ti)^{Opx}$, the above relation can be expressed as:

$$T(°K)\ln K_d1 = a[Mg\#^{(Sp)}]^2 + b[Mg\#^{(Sp)}] + c[Mg\#^{(Opx)}]^2 + d[Mg\#^{(Opx)}] + e[Cr\#^{(Sp)}]^2 + f[Cr\#^{(Sp)}] + g[Cr\#^{(Opx)}] + h[X_{Ti}^{Sp}] + i[X_{Fe^{3+}}^{Sp}] + jT + m + nP.$$

A multiple linear regression analysis was carried out to fit the experimental data listed in Table 5.2 into this expression (similar to what has been used to obtain the spinel-lherzolite to garnet-lherzolite transition barometer described in Chapter Four). The analysis suggests that some of the terms are not significant and can be omitted. As a result, a relation which best fits the experimental data and yet takes the least number of parameters is found:

$$\ln K_d1 = 1.1116 + \frac{(3.8168[Mg\#^{(Sp)}]^2 - 2667.047[Mg\#^{(Sp)}] + 288.732[Mg\#^{(Opx)}] + 86.79P(kbar))}{T(K)},$$

($r^2 = 0.8067$)

This transforms into a barometric expression:

$$P1(kbar) = 0.0115(\ln K_d1 - 1.1116)T - 0.044[Mg\#^{(Sp)}]^2 + 30.73[Mg\#^{(Sp)}] - 3.33[Mg\#^{(Opx)}].$$

The same procedure is followed for analysis of partitioning data of (Ti/Al) between spinel and orthopyroxene (K_d2), of Ti and (Ti/Al) between spinel and clinopyroxene (K_d3 & K_d4); and of Fe^{2+}/Mg between spinel and olivine (K_d5), between spinel and orthopyroxene (K_d6), between spinel and clinopyroxene (K_d7), between spinel and garnet (K_d8). Additional experimental data for Fe^{2+}/Mg partitioning between spinel and olivine from Fujii (1977), Engi (1983), Sack et al. (1987), Hill & Sack (1987), Gee & Sack (1988), Grove & Juster (1989) and Ballhaus et al. (1991) are included, which bring the total number of spinel - olivine pairs considered to 208. Additional experimental data for Fe^{2+}/Mg partitioning between spinel and orthopyroxene come from Engi (1983), Barnes (1986) and Ballhaus et al. (1991). These data together with those listed in Table 5.2 make a total of 144 spinel - orthopyroxene pairs. For spinel - clinopyroxene and spinel - garnet pairs, only the data presented in Table 5.2 are used. These regression analyses give the following results (in the form of barometers and thermometers):

$$P2(kbar) = 0.0111(\ln K_d2 - 0.2188)T - 0.001[Mg\#^{(Sp)}]^2 + 0.68[Mg\#^{(Sp)}] - 0.28[Cr\#^{(Sp)}],$$

$(r^2 = 0.8238)$;

$$P3_{(kbar)} = 0.0167(\ln K_d 3 - 2.3316)T - 0.008[Mg\#^{(Sp)}]^2 + 1.89[Mg\#^{(Sp)}] - 0.46[Cr\#^{(Sp)}] - 303[X_{Ti}^{Sp}], \quad (r^2 = 0.8877);$$

$$P4_{(kbar)} = 0.0203(\ln K_d 4 - 0.6546)T + 0.031[Mg\#^{(Sp)}]^2 + 295.4 + 4.56[Mg\#^{(Sp)}] - 0.91[Cr\#^{(Sp)}] - 649[X_{Ti}^{Sp}], \quad (r^2 = 0.9158);$$

$$T1(^{\circ}k) = \frac{1.15[Mg\#^{(ol)}]^2 - 70.4[Mg\#^{(ol)}] + 0.28[Mg\#^{(sp)}]^2 - 93.5[Mg\#^{(sp)}] + 7.06[Cr\#^{(sp)}] + 1024[X_{Ti}^{sp}] + 2844}{\ln K_d 5 - 0.655}$$

$(r^2 = 0.9448)$;

$$T2(^{\circ}k) = \frac{3.83[Mg\#^{(Opx)}]^2 - 515.7[Mg\#^{(Opx)}] - 69.6[Mg\#^{(Sp)}] - 0.06[Cr\#^{(Sp)}]^2 + 9.2[Cr\#^{(Sp)}] + 20133}{\ln K_d 6 - 1.2034}$$

$(r^2 = 0.9791)$;

$$T3(^{\circ}k) = \frac{156.4[Mg\#^{(Cpx)}] - 1.9[Mg\#^{(Sp)}]^2 + 195.1[Mg\#^{(Sp)}] + 0.12[Cr\#^{(Sp)}]^2 - 9.2[Cr\#^{(Sp)}] - 17728}{\ln K_d 7 - 1.004}$$

$(r^2 = 0.9982)$

$$T4(^{\circ}k) = \frac{117[Mg\#^{(Gt)}] - 1.72[Mg\#^{(Sp)}]^2 + 166.6[Mg\#^{(Sp)}] + 0.1[Cr\#^{(Sp)}]^2 - 8.2[Cr\#^{(Sp)}] - 12564}{\ln K_d 8 - 0.5989}$$

$(r^2 = 0.9988)$.

5.4 Discussion

The barometers and thermometers derived above have been used to derive the experimental pressures and temperatures respectively by incorporating the data presented in Table 5.2 and the additional experimental Fe^{2+}/Mg partitioning data mentioned above. The results are plotted in Figures 5.1 and 5.2. These plots suggest poor accuracies of these barometers (±10 kbar) and particularly the thermometers(upto ±500°C). In view of the good correlation coefficients (r^2) for the thermometric expressions, such a poor reproduction of the experimental temperatures is hardly expected. One possible explanation is that the experimental data themselves are not of high quality, particularly the spinel compositions. The relations between $\ln K_d 5$ and temperature, $\ln K_d 6$ and temperature are shown in Figure 5.3; both imply only moderate correlation. The application of existing spinel-olivine thermometers (Fabries, 1979; O'Neill & Wall, 1987 and its modification by Ballhaus et al., 1991) to the experimental data also demonstrates poor agreement between the calculated and the experimental temperatures (Fig.5.4). This suggests that the $\ln K_d(Fe^{2+}/Mg)$ - T relationship may be obscured by the strong composition effect (Fig.5.5, and also Fig.1.9). Another possibility is that the amount of experimental data-points is insufficient to carry out a meaningful statistical regression analysis. This is

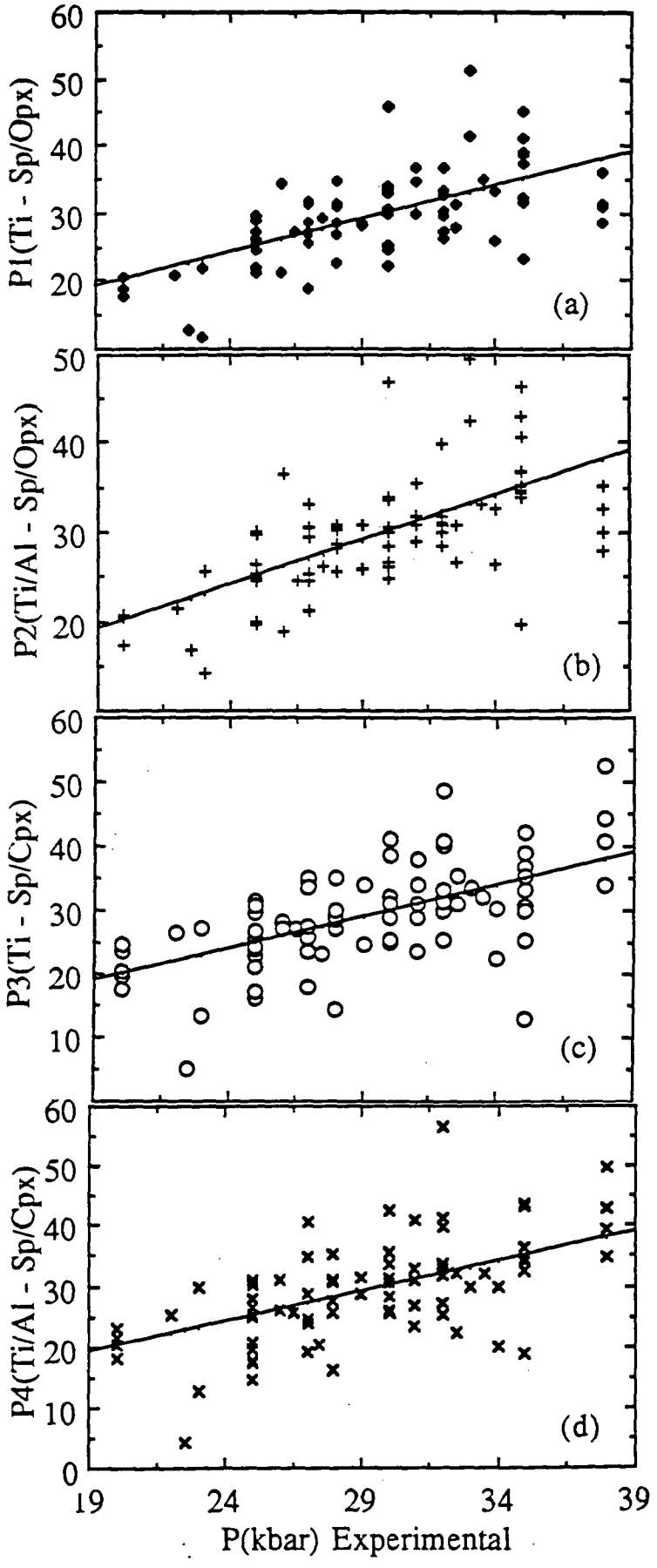

Figure 5.1. A test of the empirical barometers:
calculated pressures versus experimental run pressures.

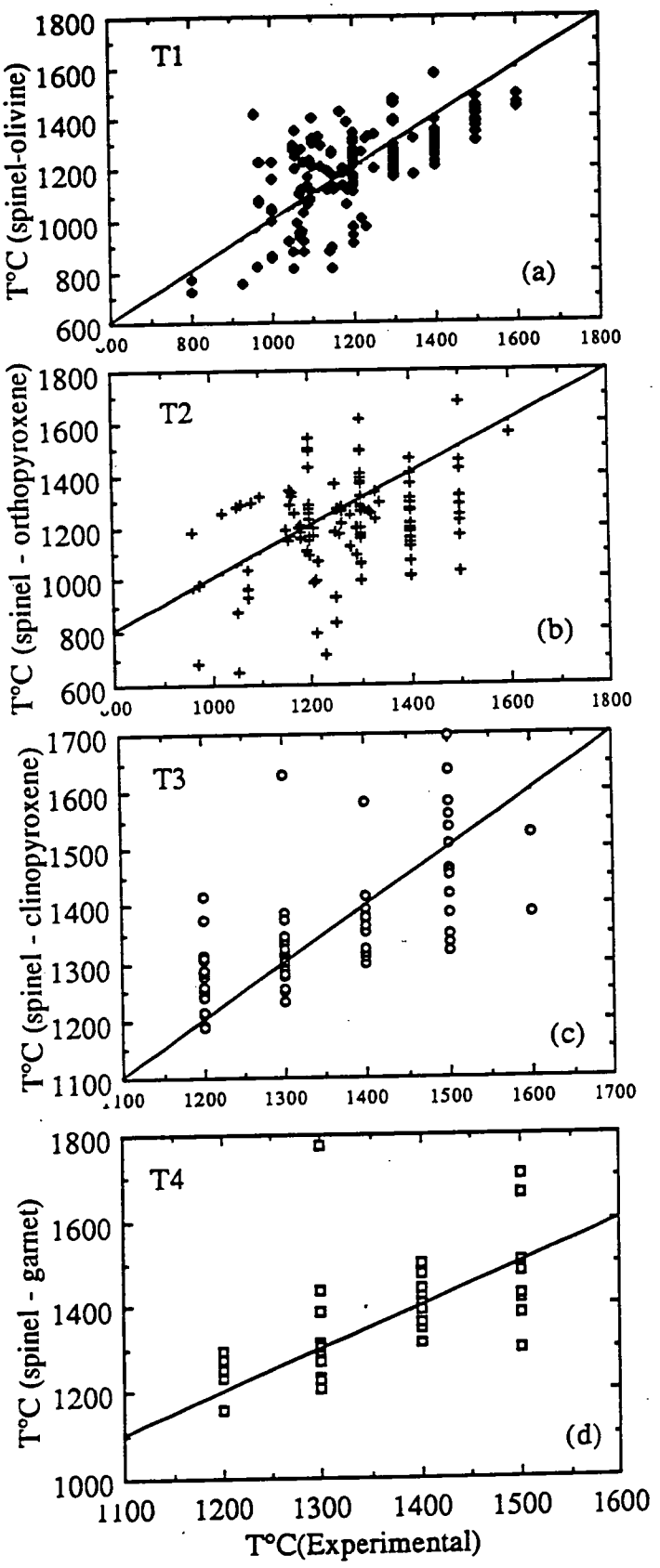

Figure 5.2. A test of the empirical thermometers:
calculated temperatures versus experimental run temperatures.

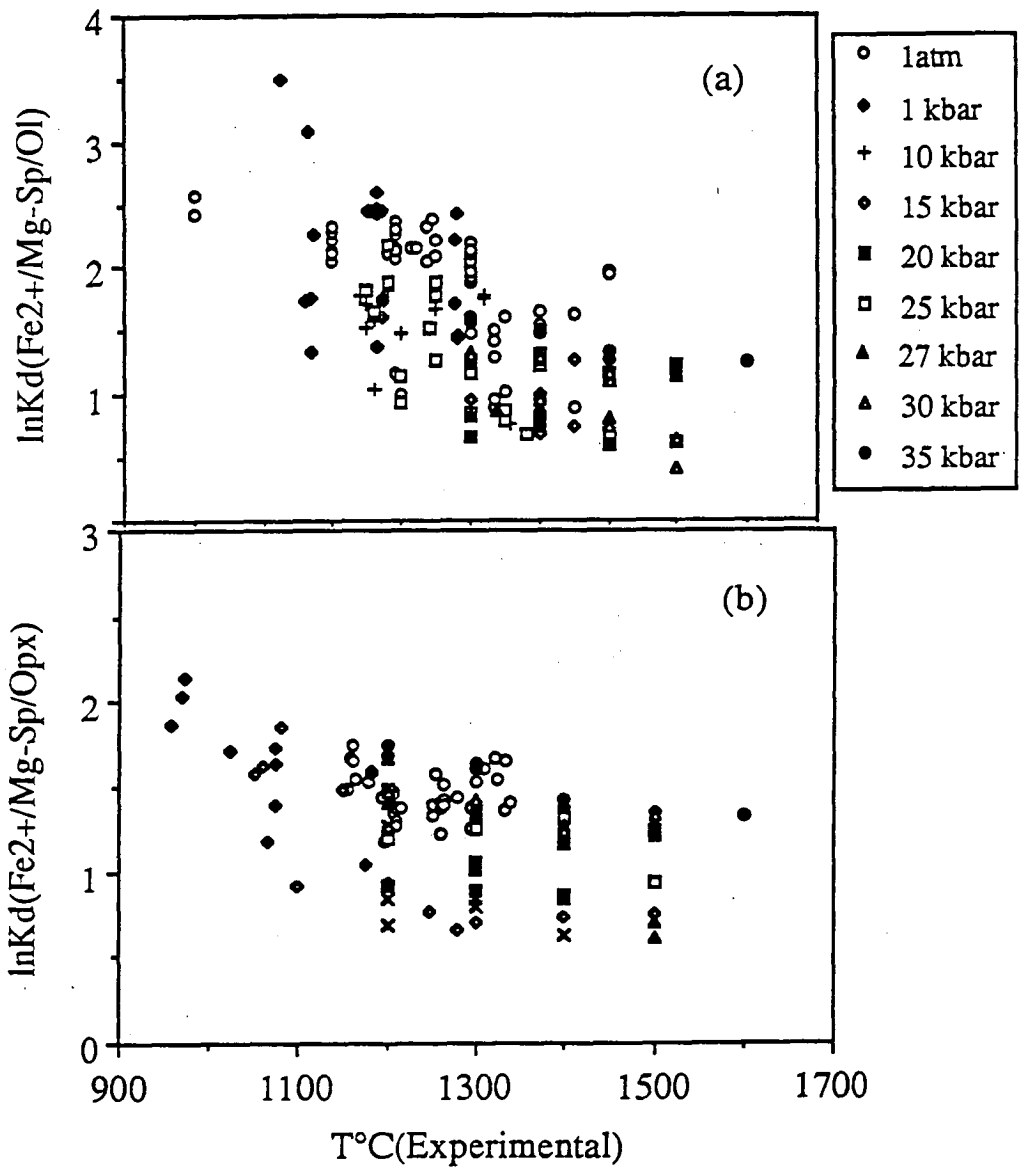

Figure 5.3. Moderate correlation between $\ln K_d$ and temperature from the experimental Fe^{2+}/Mg partitioning data.

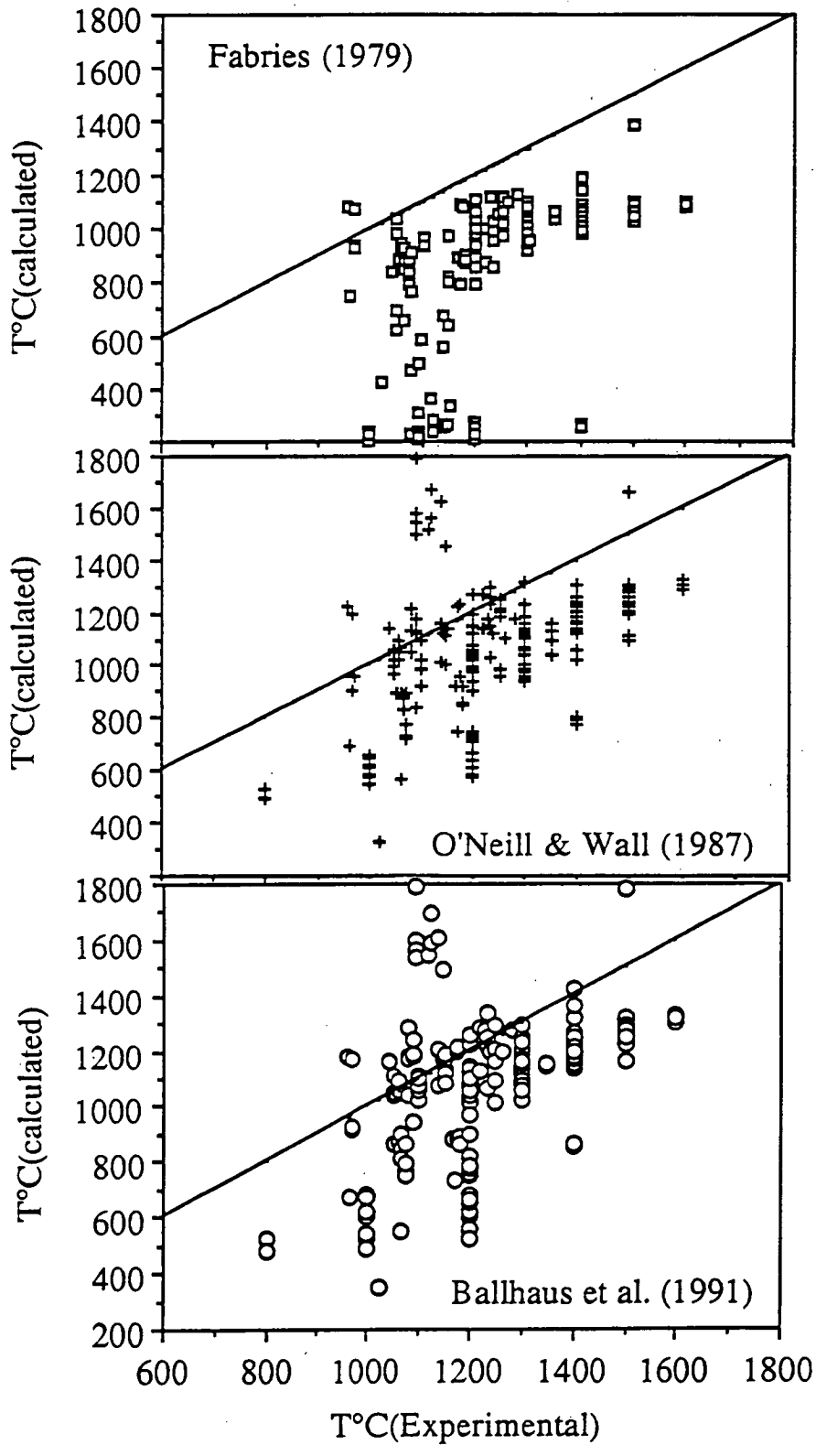

Figure 5.4. A test of the existing spinel - olivine Fe^{2+}/Mg exchange thermometers.

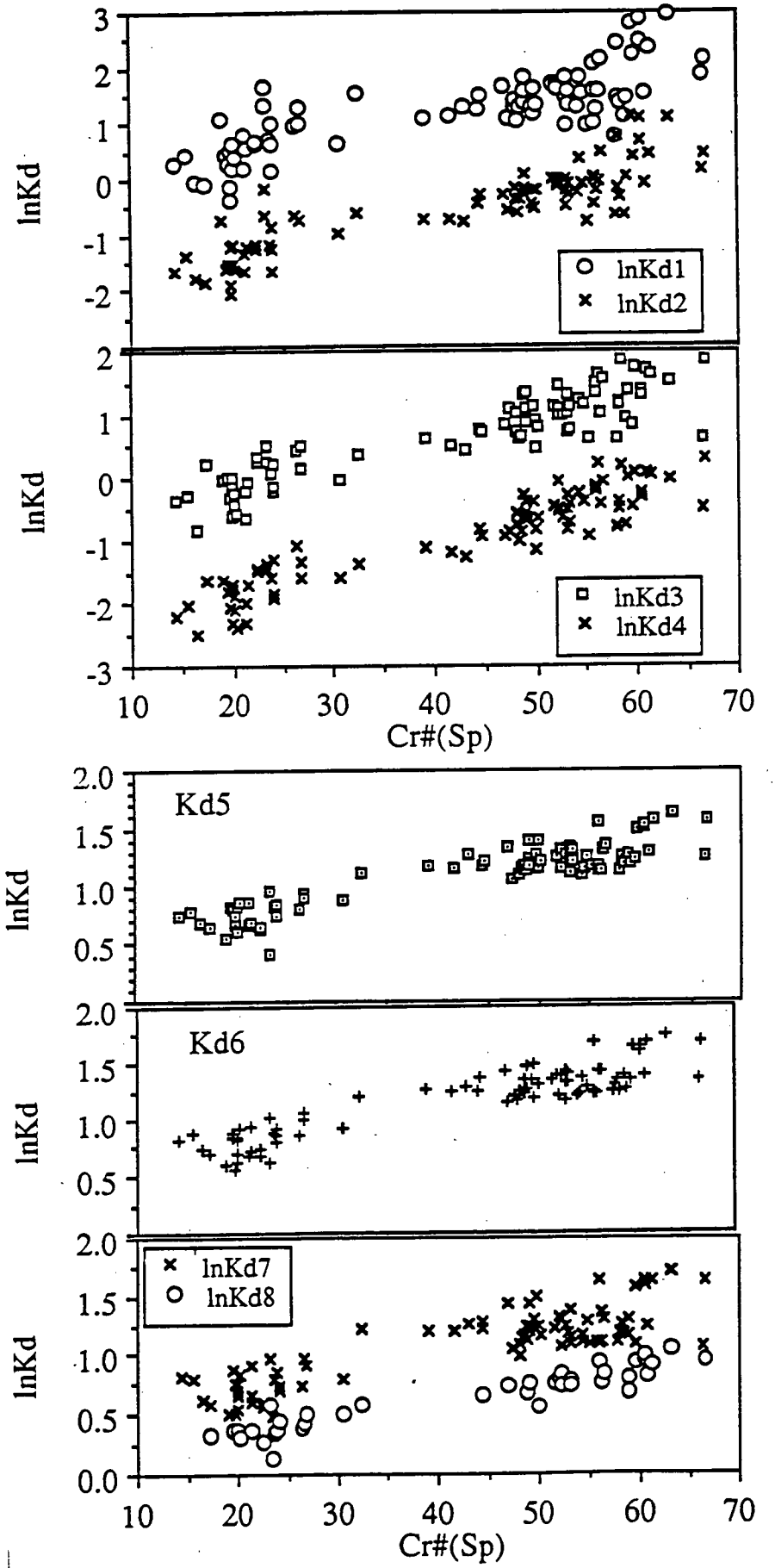

Figure 5.5. Strong composition dependence of $\ln K_d(Fe^{2+}/Mg)$s.

especially true for the spinel - garnet and spinel - clinopyroxene pairs. Therefore, in order to improve these barometers and thermometers, more and better quality experimental data are needed.

These empirical barometers and thermometers have also been employed to calculate the equilibrium pressures and temperatures of a number of natural coexisting garnet and spinel lherzolites. The choice of the garnet and spinel lherzolites is to enable independent estimation of pressure by the above barometers and by the Nickel & Green (1985) barometer; and independent estimation of temperature by the above thermometers and by the two-pyroxene thermometer of Bertrand and Mercier (1985); and to facilitate comparison of the results by these independent methods. When the spinel barometers were used to compute an equilibrium pressure, the temperature calculated from the Bertrand - Mercier thermometer was incorporated so that the uncertainty associated with the temperature term was minimised. The results (Table 5.3) indicate that there is a reasonable agreement between the calculated pressures from the two spinel-clinopyroxene barometers and the Nickel - Green barometer, whereas agreement between the calculated pressures from the two spinel - orthopyroxene barometers and from the Nickel - Green barometer is rather poor, especially for the xenoliths in kimberlites. This poor agreement is probably a consequence of unreliable analysis of the low-Ti in the orthopyroxenes, in addition to the less well-constrained barometers themselves (due to limited data). The TiO_2 concentrations in spinel and clinopyroxene are generally higher than in orthopyroxene, and thus more accurately determined by routine microprobe analysis.

The spinel thermometers generally yield higher temperatures than the two-pyroxene thermometer and sometimes produce unreasonable results (Table 5.3). Correlation between the calculated temperatures by the spinel thermometers and by the Bertrand - Mercier thermometer is very poor. Correlation between temperature estimates by the thermometers of Fabries (1979), Ballhaus et al. (1991) and that of Bertrand & Mercier (1985) is better than by the T1 thermometer of this study and that of Bertrand & Mercier (1985), but is of high order in neither case. This may be attributed to the difference in blocking temperature between Fe^{2+}/Mg exchange between spinel and silicates, and Ca exchange between the two pyroxenes. It may also indicate that the thermometers based on Fe^{2+}/Mg exchange between spinel and silicates are not reliable because of the strong composition effect.

5.5 Conclusions

A strong pressure dependency of Ti-partitioning between spinel and pyroxenes has been found in experimental studies of systematic variation in mineral composition with changing temperature and pressure in three model lherzolite systems. Four empirical

Table 5.3 Calculated Equilibration Temperatures and Pressures for Some Natural Garnet and Spinel Lherzolites

Data source	Sample#	T°C(BM)	T(F)	T(BBG)	T1	T2	T3	T4	P(NG)kbar	P1	P2	P3	P4
	xenoliths in alkali-basalts												
1	M3	1098	1075	1121	1610	1331	1402	1311	27.69	22.1	17.1	19.2	17.4
1	N3	1193	1226	1218	-222	1335	1248	1235	22.25	18.9	18.5	11.1	13.3
2	MD10-10	1022	952	999	-373	1348	1177	1294	20.97				
3	HT-28	1074	1083	1106	16773	1196	1360	1285	19.59	14.9	22.5	14.3	15.0
3	MD-4	1043	1001	1019	1278	1427	435	1357	20.62				
4	76210	1072	1014	1048	727	1942	-260	923	21.53			25.6	24.3
4	76211	1068	1016	1047	700	1952	391	910	22.38	18.9	20.2	21.4	21.1
4	76213	1143	1046	1082	850	1775	771	932	22.78			25.0	23.8
4	76217	1151	998	1023	648	1986	543	724	22.72	17.5	19.2	18.1	19.0
4	76218	1120	1046	1088	812	1830	574	919	22.52			24.8	22.3
4	76222	1135	1064	1109	962	1723	865	982	22.66			24.8	22.2
4	76224	1136	1060	1113	907	1761	784	957	23.35	15.7	19.0	25.6	24.6
5	H077	1096	995	1097	1201	1239	1185	1318	41.49	28.8	32.7	34.4	25.4
6	Causses	1227	909	944	1273	1444	1218	1201	21.94	17.4	21.5	14.9	16.7
6	Ardeche	1252	979	1010	1584	1411	1244	1228	22.45	10.2	16.6	13.2	14.4
7	EGL7501	1229	979	1009	1662	1382	1235	1222	21.33	19.8	23.9	19.8	22.7
8	BN-4	1032	1035	1067	1061	-7159	1273	830	25.37	27.3	25.8	24.9	24.4
10	3567	861	914	904	948	556	1226	1513	20.87	14.9	14.9	18.5	17.3
10	3539	1165				1217	1074	1331	30.55	33.7	33.0		
	xenoliths in kimberlites												
11	GSL3	949	923	997	1272	1276	1007	1087	42.16			27.1	53.4
12	SD2-L11	861	1034	1068	1806	1381	71	1403	26.49	10.2	4.2	17.4	15.7
12	SD2-L189	997	822	874	1106	1219	1111	404	41.02	13.9	10.5	12.2	13.3
13	SIL102	1056	918	1005	1213	1242	1139	1285	50.65	23.5	24.3	46.4	51.5
14	14	947	1169	1249	1233	1178	1158	2144	39.89	31.9	26.2	42.5	32.5
14	32	843	1171	1265	1269	1207	1121	1786	32.26	55.1	51.3	89.7	87.5
15	PTH207	994	784	882	970	778	1036	1182	57.50	14.2	-2.5	45.5	25.6
15		994	1022	1157	1235	1208	1287	1661	57.50	21.6	13.5	41.2	38.2
15	PTH403	995	891	988	1095	1122	1176	1366	48.73	40.2	29.7	53.1	42.6
15		995	911	1005	1174	1238	1148	1221	48.73	30.9	34.1	42.3	45.3
15	PTH404	981	729	812	927	742	1063	500	44.63	43.4	30.4	73.0	57.8
15	PTH405	996	968	1064	1333	1618	-13933	1389	43.02	36.7	22.6	60.8	48.4
15		996	825	923	1047	1031	1098	1357	43.02	56.5	44.9	78.8	68.1
15	PTH407	957	885	967	1185	-2653	166	1474	40.57	22.2	9.0	73.9	59.8
15	PTH409	961	892	941	1186	1247	1174	1258	42.22	6.9	16.4	26.6	49.4
15	PTH410	1021	803	889	1024	271	660	-387	42.60	42.4	29.0	70.8	60.3
16	FRB1008	847	858	881	1093	1170	892	1367	35.05				
16	FRB1009	816	859	879	1181	1266	976	1022	35.12			35.2	55.6
17	1595	879	954	1007	1150	1159	991	1598	35.90			42.9	36.2
17	1567	926	931	966	1119	1173	1028	1430	36.75			48.5	46.8
17	1592	945	931	966	1112	1168	1084	1433	38.27			34.4	37.3
17	1570	949	924	971	1151	1191	1009	1442	38.76			38.1	32.4
17	1573	965	919	957	1118	1173	1046	1429	40.37			39.8	38.3
17	1572	992	919	960	1148	1207	1143	1327	41.58			33.1	47.6
18	K2	725	850	870	1120	1206	975	1214	24.51				
18	K18	1035	863	949	1139	1204	1159	1281	70.95				

*). thermometers: BM - Bertrand & Mercier (1985); F - Fabries (1979); BBG - Ballhaus et al. (1991).
barometer: NG - Nickel & Green (1985)
T1, T2, T3, T4, P1, P2, P3, P4 - this study (see text).
mineral data sources are given Table 5.4.

Table 5.4 Data Sources for Table 5.3

1	Jin et al. (1991)
2	Cao & Zhu (1987)
3	Fan & Hooper (1989)
4	Chapter One
5	Eherenberg (1982)
6	Berger (1979)
7	Berger & Vannier (1984)
8	Skewes & Stern (1979)
9	Ferguson et al. (1977)
10	Nixon & Boyd (1979)
11	Hearn & McGee (1984)
12	Kirkly et al. (1984)
13	McCallum & Eggler (1976)
14	Mitchell (1984)
15	Carswell et al. (1979)
16	Boyd & Mertzman (1987)
17	Nixon & Boyd (1973)
18	Mori (1976)

geobarometers have been formulated on the basis of these experimental data. When tested against these experimental data and some natural mineral data, these barometers give reasonable, but not very accurate results. Four empirical geothermometers have also been constructed on the basis of these experimental data and some existing experimental Fe^{2+}/Mg partitioning data in the literature. Applications of these thermometers are, however, not very successful. It appears that the quality of these thermometers is probably limited by their strong composition dependency, and that the two-pyroxene thermometer remains the best method currently available for equilibrium temperature evaluation of spinel lherzolites. On the other hand, these barometers may be improved with more and better quality experimental data.

Chapter Six

A Revision of the Garnet - Clinopyroxene Fe^{2+} - Mg Exchange Geothermometer

Chapter Six

A Revision of the Garnet - Clinopyroxene Fe^{2+} - Mg Exchange Geothermometer

6.1 Introduction

Several experimental studies have shown that the partitioning behaviour of Fe^{2+}/Mg between garnet and clinopyroxene is sensitively governed by external physical conditions and strongly affected by internal composition variations (e.g. Råheim & Green, 1974a, Ellis & Green, 1979; Pattison & Newton, 1989). The relationship between K_d ($=\frac{(Fe^{2+}/Mg)^{Gt}}{(Fe^{2+}/Mg)^{Cpx}}$) and equilibrium temperature (T) and pressure (P) was first calibrated by Råheim & Green (1974a) to form a geothermometer. A significant effect of Ca-content was recognised by Ellis & Green (1979) and this was quantified and included into the formulation. The result was an improved version of the thermometer, which found a broad application in the field of petrology. Krogh (1988) further improved this thermometer by replacing the simple rectilinear $\ln K_d$ - X_{Ca}^{Gt} ($=\frac{Ca}{Ca + Mg + Fe^{2+} + Mn}$) relationship established by Ellis & Green (1979) with a curvilinear relationship. This was shown to be in the right direction towards perfecting this empirical thermometer (Brey & Köhler, 1990). However, this improvement is limited by the amount of experimental data used and by the exact mathematical model chosen to formulate the thermometer. A recent experimental study by Pattison & Newton (1989) demonstrates that the Mg# ($=\frac{100Mg}{Mg + Fe^{2+}}$) of garnet also has an important effect on the K_d, in addition to the effect of X_{Ca}^{Gt}. Pattison & Newton (1989) fitted their experimental data in the form of a third order polynomial equation to account for this effect. They derived a new version of the thermometer that is applicable to rocks with Mg#(Gt) ranging from 12.5 to 60. Apparent disagreement exists when this and other forms of the garnet - clinopyroxene Fe^{2+}/Mg exchange thermometer (e.g. Ellis & Green, 1979; Ganguly, 1979; Powell, 1985) are applied to the same rocks for equilibrium temperature estimation, indicating the presence of problems in these thermometers. Results of a new set of experiments, specifically designed to test various versions of this thermometer, suggest that none of the existing formulations can be safely applied to rocks of wide origin in terms of P, T, and composition (Green & Adam, 1991). In particular, Green & Adam (1991) found that the popular Ellis - Green thermometer reproduced run temperatures for experiments at 30 kbar, 1150° - 1200°C but increasingly overestimated equilibrium temperature at lower pressure and lower temperature. They also found that the Pattison-Newton graphic

thermometer consistently underestimated experimental temperature but their mathematical formulation overestimated equilibrium temperature with two exceptions. It is clear that additional experimental data are needed for evaluation and improvement of this important geothermometer.

A large amount of experimental data over a wide range of P, T and composition is now available to reformulate this thermometer. In this chapter, I present a comprehensive set of experimental data and obtain a new mathematical model to describe the partitioning behaviour of Fe^{2+}/Mg between garnet and clinopyroxene.

6.2 The Dataset

Fifteen publications containing mineral equilibrium data on the Fe^{2+}/Mg exchange between garnet and clinopyroxene were selected from the literature (Table 6.1). These were combined with a new set of experimental data (Table 6.2) to constitute the whole dataset. Most of the studies in the dataset were made on ultramafic compositions; five series of experiments specifically addressed garnet - clinopyroxene equilibria; and two series of experiments were in the mafic system. These cover a wide range of "bulk rock" compositions. The experimental conditions range from 10 to 60 kbar in pressure and from 600°C to 1500°C in temperature, encompassing almost the entire upper mantle - lower crust region where garnet and clinopyroxene-bearing rocks originate. This makes the dataset reasonably comprehensive, enabling a meaningful statistical analysis.

6.3 Data Analysis

Krogh (1988) proposed a general mathematical equation that governs the partitioning behaviour of Fe^{2+}/Mg between garnet and clinopyroxene:

$$\ln K_d = \frac{(a[X_{Ca}^{Gt}]^2 + b[X_{Ca}^{Gt}] + c + dP(kbar))}{T(K)} + e \qquad \text{..... (6.1)}$$

where a, b, c, d, e are constants. This agrees in principle with the forms of all previous derivations (Råheim & Green, 1974a; Ellis & Green, 1979; Ganguly, 1979; Saxena, 1979; Wells, 1979; Dahl, 1980; Powell, 1985), except that of Pattison & Newton (1989) where the $\ln K_d$ - pressure relationship is unnecessarily complicated and is in apparent contradiction with the experimental observation that K_d increases with increasing pressure (Råheim & Green, 1974a; Green & Adam, 1991). Evaluation of these thermometers showed that the thermometer derived from this general equation (Krogh, 1988) gave better temperature estimates than the other thermometers (Brey & Köhler, 1990). This indicates the validity of this approach. However, to account for the composition effect on K_d by introducing the term X_{Ca}^{Gt} alone is not sufficient. The experimental results of

Table 6.1 Reference Sources for the Experimental Dataset

Ref #	Source	Type of Experiment	P(kbar)	T°C	# of Gt-Cpx Pairs
1	Råheim & Green (1974a)	Gt - Cpx equilibria	20 - 40	600 - 1500	39
2	Råheim & Green (1974b)	Gt - Cpx equilibria	12 - 30.	1100 - 1300	6
3	Wood (1976)	Gt - Cpx equilibria	20 - 45	1100 - 1400	8
4	Ellis & Green (1979)	Gt - Cpx equilibria	15 - 30	750 - 1300	45
5	Pattison & Newton (1989)	Gt - Cpx equilibria	15 - 29	700 - 1200	123
6	Johnston (1986)	mafic system	23 - 30	1275 - 1455	7
7	Green & Adam (1991)	mafic system	10 - 30.	950 - 1200	17
8	Hensen (1973)	ultramafic system	22.5 - 40.5	1110 - 1410	3
9	Akella & Boyd (1973)	ultramafic system	30 - 45	1100	5
10	Akella (1976)	ultramafic system	31 - 44	1100 - 1300	3
11	Mori & Green (1978)	ultramafic system	30 - 40	950 - 1300	20
12	Nickel (1983)	ultramafic system	35	1000 - 1400	10
13	Mengel & Green (1989)	ultramafic system	25 - 28	975 - 1250	11
14	Brey et al. (1990)	ultramafic system	28 - 60	900 - 1400	21
15	Wallace & Green (1991)	ultramafic system	20 - 30	950 - 1100	15
16	Table 2	ultramafic system	25 - 38	1200 - 1500	47

Table 6.2 Additional Experimental Data on the Fe2+/Mg Exchange between Garnet and Clinopyroxene

Run #	P(kbar)	T°C	X(Al)Cpx	Ca*(Cpx)	Mg#(Cpx)	Mg#(Gt)	X(Ca)Gt	ln(Kd)
T3239	20	1200	0.2233	0.7708	89.68	82.79	0.1546	0.5908
T3101	25	1200	0.2549	0.7883	89.05	82.71	0.1589	0.5312
T3168	25	1200	0.2594	0.7242	89.95	83.91	0.1601	0.5409
T3126	27	1200	0.2656	0.7331	88.86	83.08	0.1507	0.4856
T3454	28	1200	0.2275	0.8144	90.41	83.32	0.1528	0.6351
T3151	30	1200	0.1918	0.7700	89.36	82.01	0.1466	0.6106
T3306	35	1200	0.1491	0.7972	90.38	82.51	0.1377	0.6883
T3355	26	1300	0.2542	0.7576	89.69	84.16	0.1503	0.4926
T3136	27	1300	0.2731	0.7250	89.01	83.72	0.1539	0.4543
T3247	27	1300	0.2475	0.6423	88.88	84.17	0.1468	0.4071
T3364	28	1300	0.2150	0.7492	89.63	83.20	0.1535	0.5571
T3160	30	1300	0.2268	0.6432	90.26	86.16	0.1494	0.3981
T3345	35	1300	0.1624	0.7156	89.56	83.65	0.1416	0.5174
T3167	27	1400	0.3090	0.6377	88.29	84.28	0.1494	0.3406
T3453	28	1400	0.3223	0.5393	88.64	85.94	0.1503	0.2444
T3526	29	1400	0.2449	0.6431	89.03	85.22	0.1430	0.3418
T3163	30	1400	0.2823	0.6120	88.72	85.05	0.1527	0.3239
T3342	35	1400	0.1880	0.6224	89.02	83.59	0.1386	0.4648
T3299	35	1400	0.1889	0.5989	89.49	85.86	0.1450	0.3383
T3378	28	1500	0.2966	0.4486	89.17	86.05	0.1455	0.2885
T3249	30	1500	0.2626	0.5251	89.72	87.07	0.1468	0.2594
T3430	30	1500	0.2515	0.4908	89.20	86.53	0.1530	0.2521
T3527	33	1500	0.2581	0.4665	89.20	86.25	0.1406	0.2752
T3302	35	1500	0.1954	0.4961	90.36	86.92	0.1414	0.3441
T3275	27.5	1200	0.1820	0.7908	89.86	81.68	0.1725	0.6873
T3261	30	1200	0.1641	0.8081	90.02	81.89	0.1679	0.6909
T3548	32	1200	0.1630	0.7840	90.01	82.02	0.1744	0.6808
T3269	35	1200	0.1346	0.8113	90.03	82.38	0.1741	0.6586
T3446	28	1300	0.2095	0.7357	89.48	82.78	0.1727	0.5702
T3423	30	1300	0.1791	0.7223	89.26	83.27	0.1789	0.5126
T3556	32	1300	0.1418	0.7519	90.23	82.90	0.1821	0.6445
T3402	35	1300	0.1397	0.7567	89.71	82.13	0.1748	0.6408
T3451	32	1400	0.1896	0.6101	89.27	84.14	0.1661	0.4504
T3417	35	1400	0.1411	0.6531	89.90	84.26	0.1789	0.5080
T3517	32	1500	0.2030	0.5211	89.64	85.73	0.1705	0.3652
T3429	34	1500	0.1817	0.5114	89.32	85.88	0.1622	0.3183
T3268	35	1500	0.1838	0.4802	89.79	84.62	0.1682	0.4695
T3573	32	1200	0.1418	0.7982	89.76	81.40	0.1664	0.6953
T3528	35	1200	0.1302	0.8094	90.01	81.34	0.1795	0.7263
T3583	32	1300	0.1649	0.7431	89.16	81.96	0.1731	0.5935
T3562	35	1300	0.1262	0.7260	89.37	81.67	0.1742	0.6357
T3593	38	1300	0.1163	0.7157	89.73	81.66	0.1861	0.6737
T3568	32	1400	0.1888	0.6331	88.84	83.20	0.1755	0.4751
T3604	33.5	1400	0.1826	0.6212	88.82	83.30	0.1722	0.4654
T3536	35	1400	0.1525	0.6058	88.77	83.40	0.1729	0.4529
T3534	35	1500	0.1856	0.4643	88.63	84.69	0.1623	0.3428
T3598	38	1500	0.1398	0.4635	89.31	84.50	0.1740	0.4264

Pattison & Newton (1989) indicate clear dependence of $\ln K_d$ on Mg#(Gt), particularly in the low Mg#(Gt) region. This is demonstrated further in Figure 6.1, where a negative correlation between $\ln K_d$ and Mg#(Gt) is shown. The effect of X_{Al}^{Cpx}(the number of Al-ions per 6-oxygens in the clinopyroxene structure) on K_d is very subtle, and is perhaps more dependent on bulk rock composition than temperature. Significant correlation between $\ln K_d$ and Ca*(Cpx) ($=\frac{Ca}{1-Na}$) is illustrated in Figure 6.2. Although Ellis & Green (1979) implied that correction of this effect is accomplished by X_{Ca}^{Gt}, there doesn't seem to be a simple relationship between X_{Ca}^{Gt} and Ca*(Cpx) (Fig.6.3). It is known that the term Ca*(Cpx) is closely related to temperature in the assemblage orthopyroxene + clinopyroxene + garnet (Bertrand & Mercier, 1985; Brey & Köhler, 1990). Therefore the dependence of K_d on Ca*(Cpx) may be effectively taken into account by the temperature term. It follows that the composition terms which should be included in modelling the $\ln K_d$ - T relation are X_{Ca}^{Gt} and Mg#(Gt). Presence of Fe^{3+} in both garnet and clinopyroxene imposes an additional problem (Luth et al., 1990), which at present cannot be evaluated from the available experimental data.

Following Krogh (1988) and adding the Mg#(Gt) term in addition to X_{Ca}^{Gt}, I have obtained a general model to describe the partitioning behaviour of Fe^{2+}/Mg between garnet and clinopyroxene:

$$\ln K_d = \frac{(a[X_{Ca}^{Gt}]^2 + b[X_{Ca}^{Gt}] + c[Mg\#(Gt)] + d + eP(kbar))}{T(K)} + f \quad \ldots\ldots (6.2)$$

where a, b, c, d, e, f are constants. A multiple linear regression analysis of 380 pairs of coexisting garnet and clinopyroxene (Table 6.1) to fit this model gives the value for each of these parameters: a=-1523.257, b=2759.182, c=-8.919, d=1974.011, e=17.35, f=-0.849 ($r^2 = 0.926$). Regression with the $[Mg\#(Gt)]^2$ term present does not give a better fit, so that this term is excluded. Consequently the revised garnet - clinopyroxene geothermometer is derived:

$$T(K) = \frac{(-1523.257[X_{Ca}^{Gt}]^2 + 2759.182[X_{Ca}^{Gt}] - 8.919[Mg\#(Gt)] + 1974.011 + 17.35P(kbar))}{\ln K_d + 0.849} \quad \ldots\ldots (6.3)$$

Figure 6.4(a) compares the calculated temperatures from equation (6.3) with the experimental temperatures. Although there is a scatter, which is caused by uncertainties in the experimental data and uncertainties associated with the equation (6.3), the overall agreement is apparent. Similar comparisons made for the Ellis-Green thermometer and that of Krogh (1988) suggest that these two thermometers generally overestimate the experimental temperatures; and they produce larger scatter in temperature estimates than the equation (6.3) [Figs.6.4(b) & (c)].

Figure 6.1. the Effect of Mg#(Gt) on $\ln(K_d)$. The correlation trends for most of the data at constant pressure and temperature are negative. The higher the temperature is, the steeper the slope of the trend becomes.

Figure 6.2. the $\ln(K_d)$ - Ca*(Cpx) Relationship. The parameter Ca*(Cpx) essentially represents temperature. The three, $\ln(K_d)$, Ca*(Cpx) and the reciprocal of temperature, are positively correlated.

Figure 6.3. the X_{Ca}^{Gt} - Ca*(Cpx) Correlation Diagram. There is no clear, straight-forward relation between X_{Ca}^{Gt} and Ca*(Cpx)

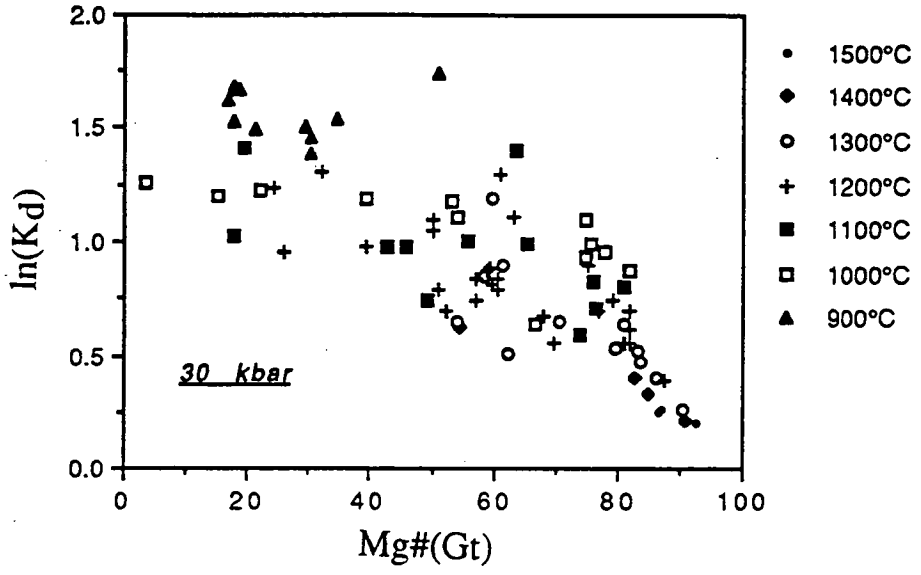
2.0
1.5
1.0
0.5
0.0
ln(Kd)
30 kbar
0
20
40
60
80
100
Mg#(Gt)
1500°C
1400°C
1300°C
1200°C
1100°C
1000°C
900°C

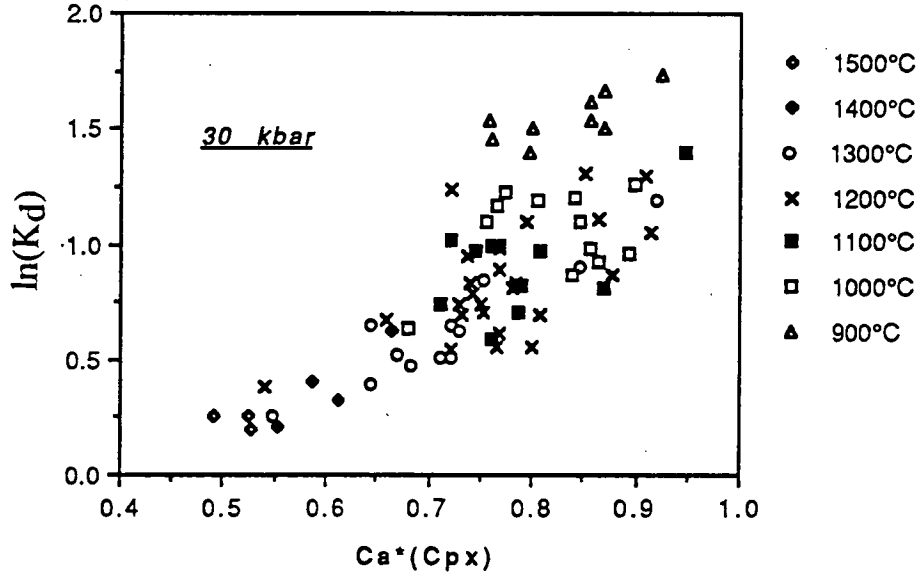
2.0
1.5
1.0
0.5
0.0
ln(Kd)
30 kbar
0.4
0.5
0.6
0.7
0.8
0.9
1.0
Ca*(Cpx)
1500°C
1400°C
1300°C
1200°C
1100°C
1000°C
900°C

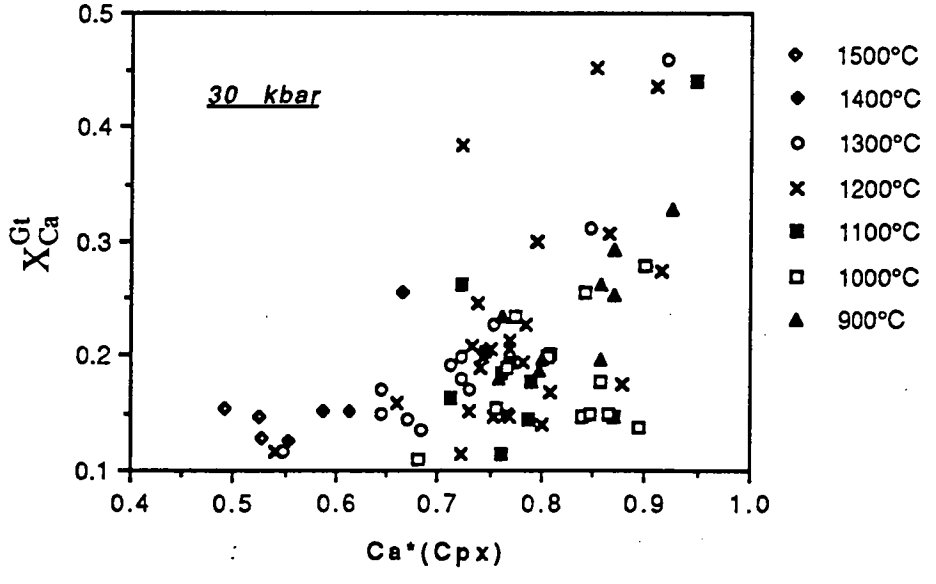
0.5
0.4
0.3
0.2
0.1
X_{Ca}^{Gt}
30 kbar
0.4
0.5
0.6
0.7
0.8
0.9
1.0
Ca*(Cpx)
1500°C
1400°C
1300°C
1200°C
1100°C
1000°C
900°C

Figure 6.4. (a) the Predicted Temperatures according to the Equation (6.3)
Compared with the Experimental Run Temperatures
(b) the Predicted Temperatures by the Krogh (1988) Thermometer
Compared with the Experimental Run Temperatures
(c) the Predicted Temperatures by the Ellis-Green (1979) Thermometer
Compared with the Experimental Run Temperatures

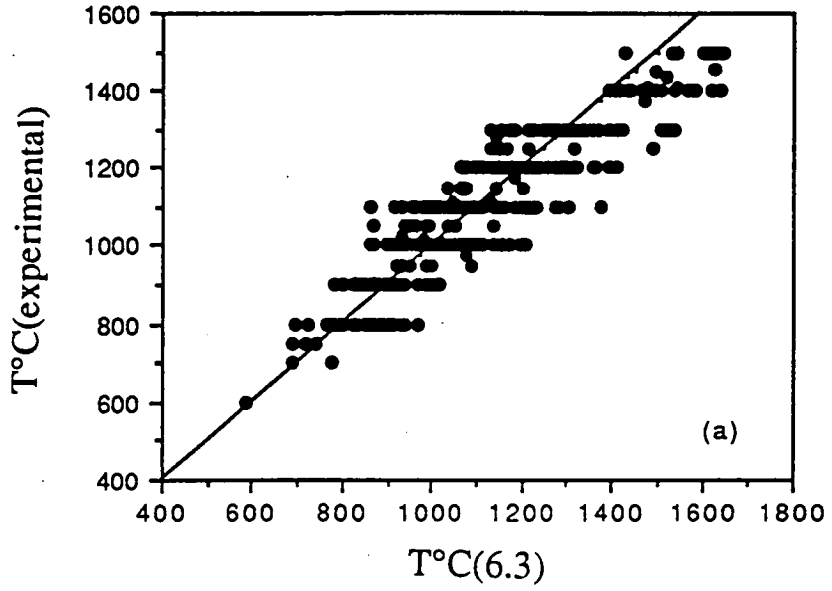
T°C(experimental)
1600
1400
1200
1000
800
600
400
400 600 800 1000 1200 1400 1600 1800
T°C(6.3)
(a)

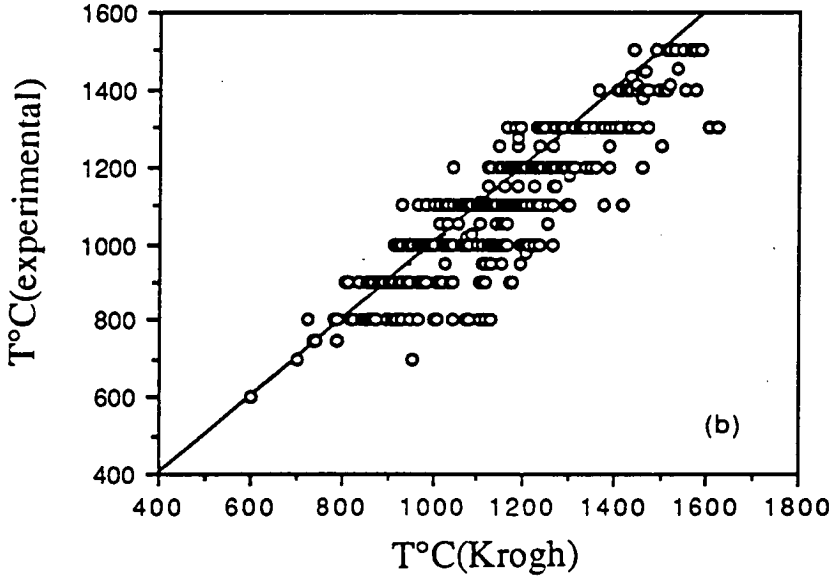
T°C(experimental)
1600
1400
1200
1000
800
600
400
400 600 800 1000 1200 1400 1600 1800
T°C(Krogh)
(b)

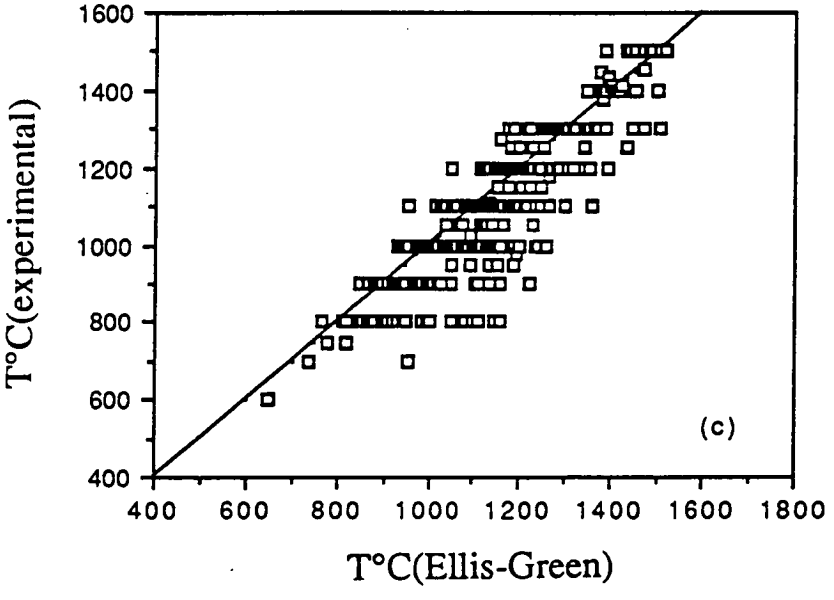
T°C(experimental)
1600
1400
1200
1000
800
600
400
400 600 800 1000 1200 1400 1600 1800
T°C(Ellis-Green)
(c)

6.4 Applications

Equation (6.3) is constructed on the basis of a large amount of experimental data over a wide range of P, T, and composition; therefore it should be applicable to rocks of wide origins. This is tested by calculation of equilibrium temperatures for rocks from the lower crust (amphibolites, granulites, crustal eclogites) and the upper mantle (mantle eclogites, lherzolite xenoliths in kimberlite, mineral inclusions in diamonds) (Table 6.3). A general impression of this revised thermometer is that it gives more realistic temperature estimates than other previously published garnet -clinopyroxene thermometers. For instance, when applied to the metamorphic suites listed by Pattison & Newton (1989) this thermometer not only produces reasonable temperatures, but also gives narrower range of the estimated temperatures for each suite than the Pattison-Newton formulation. Other thermometers (e.g. Krogh, 1988; Powell, 1985; Ellis & Green, 1979) tend to yield temperatures outside the range expected for the corresponding metamorphic grade.

Krogh (1988) estimated the equilibrium temperatures of a suite of eclogitic rocks from the Tromsø nappe complex within the northern Scandinavian Caledonides to be in the range of 690° - 790°C. Equation (6.3) suggests a relatively lower equilibrium temperature range of 561° - 712°C, which may be more appropriate for these rocks (eclogites and gneisses).

Koons (1984) applied the Ellis-Green thermometer to a suite of eclogites from the Sesia zone of the western Alps, Italy and found the calculated temperatures ranging from 400°C to 1040°C. He suggested that the inconsistency was caused by the high-jadeite pyroxene solid solutions. A even larger range (305° - 1132°C) is obtained if equation (6.3) is used for these rocks. However, if no Fe^{3+} is allowed for in both garnets and clinopyroxenes, the calculated temperatures for half of these rocks reported by Koons (1984) fall in the range of 568° - 635°C. (The clinopyroxenes in this half of the rocks contain 7.11 - 11.99 wt% Na_2O). Within the other half, two have relatively low calculated temperatures (453° & 375°C) and two have relatively high calculated temperatures (1154° & 849°C, Table 3). The clinopyroxenes in the low-T rocks contain 8.17 & 9.5 wt% Na_2O; and in the high-T rocks, 14.4 & 12.99 wt% (Koons, 1984). There is no apparent relation between the calculated temperatures and the Na_2O content of the clinopyroxenes. It was mentioned by Koons (1984) that these garnets are usually zoned. The anomalous temperature estimates may be a result of non-equilibrium between the garnet - clinopyroxene pairs. This is further demonstrated by another suite of eclogite from Cima di Gagnone, Switzerland (Evans et al., 1979). The garnets in this suite are zoned, but the clinopyroxenes are not, except for one metarodingite (163-M). If the unzoned clinopyroxene compositons and the garnet rim compositions in samples other

Table 6.3 Results of Calculated Equilibrium Temperatures for a Range of Natural Rocks

Sample	ln(Kd)	X(Ca)Gt	Mg#(Gt)	# of samples	P(kbar)	T6.3(°C)	Tk(°C)	Tp(°C)	T(EG)	T(PN)
amphibolite & granulite (Pattison & Newton, 1989)										
Mica Creek	2.13-2.30	0.29-0.37	12.07-18.97	5	6.00	564-640	645-744	664-765	682-779	521-654
Eastern Dalradian	1.63-2.26	0.24-0.32	15.38-18.84	6	8.00	590-742	680-799	697-806	714-821	583-752
Kapuskasing	1.25-2.13	0.18-0.30	13.64-42.86	11	6.50	542-783	571-894	683-1379	657-917	517-758
Central Gneiss Belt	1.50-1.73	0.17-0.22	16.22-32.05	8	10.00	689-897	727-986	752-1027	754-841	625-777
Adirondack	1.12-2.00	0.19-0.21	13.51-36.99	11	8.00	577-886	638-951	670-957	691-967	568-916
Eclogite (Tromsø, North Norway; Krogh 1988)										
	1.50-2.26	0.15-0.44	17-55	17	15.00	561-712	688-791	705-832	725-844	428-783
Eclogite (Sesia Zone of the Western Alps, Italy; Koons 1984)										
(with Fe3+)	0.87-3.51	0.13-0.30	12.12-28.15	8	15.00	305-1132	325-987	381-1025	406-1035	220-1330
(without Fe3+)	0.85-3.04	0.13-0.30	12.06-28.13	8	15.00	375-1154	388-1002	445-1038	471-1047	287-1362
Eclogite (Cima di Gagnone, Ticino, Switzerland; Evans et al. 1979)										
(Ga.core)	1.88-2.90	0.25-0.43	25.25-46.68	4	25.00	527-781	608-900	636-929	655-941	
(Ga.rim)	1.82-2.49	0.17-0.42	37.56-53.61	4	25.00	571-655	694-766	734-779	757-796	
163-M.Cpx.rim	1.34	0.77	56.02	1	25.00	1158	1066	1501	1481	
163-M.Cpx.core	2.02	0.77	56.02	1	25.00	817	798	1178	1176	
No Fe3+ in Ga										
163-M.Cpx.rim	2.62	0.71	40.98	1	25.00	659	670	938	944	
163-M.Cpx.core	1.95	0.71	40.98	1	25.00	882	862	1161	1159	
Eclogite (Bellsbank, South Africa; Taylor & Neal 1989)										
Group A	1.39-1.44	0.11	77.50-81.85	2	40.00	694-734	761-772	837-850	862-874	
Group B	1.26-1.43	0.23-0.26	56.19-59.83	4	40.00	920-1033	968-1093	964-1068	982-1080	
Group C	1.65-1.81	0.36-0.48	66.34-71.92	3	40.00	866-916	1002-1059	1005-1107	1018-1114	
Diamondiferous Eclogite (southern Africa; Smith et al. 1989)										
EX2	1.09	0.24	59.08	1	50.00	1220	1196	1161	1172	
EX10	1.14	0.27	55.45	1	50.00	1225	1204	1165	1175	
JJG144	1.25	0.19	51.67	1	50.00	1086	1027	1030	1048	
XM23	1.19	0.23	52.74	1	50.00	1168	1129	1105	1119	

Table 6.3 Results of Calculated Equilibrium Temperatures for a Range of Natural Rocks (cont'd)

Sample	ln(Kd)	X(Ca)Gt	Mg#(Gt)	# of samples	P(kbar)	T6.3(°C)	Tk(°C)	Tp(°C)	T(EG)	T(BM)
	Lherzolite (Lesothe; Nixon & Boyd 1973)									
sheared	0.43-0.61	0.10-0.12	80.92-85.94	8	45.6-52.5*	1388-1571	1290-1388	1302-1402	1308-1401	1388-1454
granular	0.97-1.41	0.14-0.20	82.95-85.93	10	35.2-46.1*	743-997	874-1063	909-1097	929-1097	903-1080
	Lherzolite (southern Africa; Cox et al. 1987)									
	0.68-1.10	0.12-0.15	82.97-85.45	13	41.0-54.9*	892-1316	971-1242	1008-1256	1026-1265	926-1281
	Diamondiferous Lherzolite (Sloan, Wyoming, USA; McCallum & Eggler 1976)									
S1L102	0.96	0.13	83.67	1	50.65*	1063	1063	1097	1113	1056
	Diamondiferous Lherzolite (Finsch, South Africa; Shee et al. 1982)									
XM46	1.02	0.15	83.94	1	63.39*	1163	1122	1135	1153	1173
XM48	1.06	0.16	82.83	1	56.51*	1095	1101	1107	1124	1089
	Diamond-inclusions (Sloan, Wyoming, USA; Otter & Gurney 1989)									
A37	1.28	0.26	44.33	1	50.00	1163	1113	1087	1101	
A73	1.16	0.19	65.02	1	50.00	1088	1077	1072	1088	
1-10	1.03	0.16	55.84	1	50.00	1186	1086	1097	1113	
1-15(1)	0.61	0.09	66.23	1	50.00	1430	1192	1250	1259	
1-15(2)	1.15	0.09	78.34	1	50.00	919	884	967	990	
	Diamond-inclusions (Koffiefontein, South Africa; Rickard et al. 1989)									
K2a	0.79	0.10	87.41	1	50.00	1142	1093	1152	1167	
K8a	1.39	0.22	62.56	1	50.00	982	1001	997	1015	
K16a	1.72	0.21	36.41	1	50.00	911	864	875	897	
K41a	0.67	0.09	49.09	1	50.00	1460	1142	1209	1221	
K42a	0.74	0.12	45.87	1	50.00	1454	1177	1209	1219	
K43a	0.65	0.09	63.21	1	50.00	1399	1153	1220	1231	
K56a	0.97	0.17	68.14	1	50.00	1195	1152	1147	1160	
	Diamond-inclusions (Western Australia; Jaques et al. 1989)									
Argyle	0.69-1.30	0.28-0.36	34.86-66.11	6	50.00	1259-1681	1214-1621	1184-1520	1192-1508	
E4/17	1.17	0.22	52.40	1	50.00	1168	1116	1097	1112	
	Green-Garnets (South Africa, Schulze 1989)									
	0.99-1.51	0.29-0.50	61.11-84.84	5	50.00	991-1339	1048-1429	1028-1378	1044-1375	
wehrlite	0.75-1.00	0.12-0.18	81.97-83.43	2	50.00	1117-1229	1153-1169	1143-1200	1155-1212	

1). * pressure calculated by using the Nickel & Green (1985) barometer; otherwise assumed.

2). T6.3 - equation (6.3) of this study; Tk - Krogh (1988); Tp - Powell (1985); T(EG)- Ellis & Green (1979); T(PN) - Pattison & Newton (1989); T(BM) - two-pyroxene thermometer of Bertrand & Mercier (1985).

than 163-M are used to calculate the equilibrium temperature, a range of 571° - 655°C is obtained. If the garnet core compositions are used, the calculated temperatures range from 527°C to 781°C. For the metarodingite (163-M) the garnet is not zoned but the clinopyroxene is. The clinopyroxene rim composition corresponds to a calculated temperature of 1158°C; and the core composition, 817°C. Both are significantly higher than the estimates for other samples, a direct consequence of the high-Fe^{3+} given to the garnet by Evans et al. (1979). Assuming no Fe^{3+} in the garnet, the calculated temperatures for the corresponding clinopyroxene rim and core compositions are 659°C & 882°C. The rim temperature agrees with the rim temperatures of other samples (Table 6.3). It is noted that the garnet in 163-M contains exceptionally high Fe^{3+} compared with other samples from the same locality and that the given cation total per 12 oxygens for this garnet is 8.0525.

A suite of mantle eclogites from Bellsbank, South Africa were designated as groups A, B, and C by Taylor & Neal (1989). The calculated equilibrium temperatures for the group A eclogites are the lowest (694° & 734°C, only two samples); followed by the group C eclogites (866° - 916°C). The group B eclogites have the highest equilibrium temperatures (920° - 1033°C). If the Ellis-Green thermometer is used, the calculated temperatures for groups B and C overlap and group B yields lower temperatures than group C, as reported by Taylor & Neal (1989).

Four diamondiferous eclogites from southern Africa (Smith et al., 1989) generate equilibrium temperatures in the range of 1086° - 1225°C, similar to the temperature range of the Bellsbank group B eclogites (Table 6.3). This is not surprising because the garnets and clinopyroxenes in these diamondiferous eclogites are intermediate in Ca and rich in Fe, within the composition range of the Bellsbank group B eclogites.

Application of the garnet - clinopyroxene thermometer to lherzolite xenoliths included in southern Africa kimberlites produces equilibrium temperatures comparable to those of the two-pyroxene thermometer (Table 6.3). The granular lherzolites yield temperatures in the range of 743° - 997°C, and the sheared ones, 1388° - 1571°C. These are lower than the two-pyroxene temperatures and the ranges are wider than those given by the two-pyroxene thermometer. This observation is also true for a number of garnet lherzolites reported by Cox et al. (1987). It is interesting to note that the equilibrium temperatures of these lherzolites fall between the above granular and sheared types. Three diamondiferous lherzolites from Sloan, USA (McCallum & Eggler, 1976) and Finsch, South Africa (Shee et al., 1982) give equilibrium temperatures in the range of 1063° - 1163°C, similar to the granular type.

Mineral inclusions in single diamonds may not necessarily be in mutual chemical equilibrium. If not, the calculated temperatures may be abnormal. This is best illustrated by Otter & Gurney (1989) and Rickard et al. (1989) and further elaborated by Gurney

(1989). The thermometer is employed to estimate equilibrium temperatures for eclogitic inclusions in diamonds from three localities (Sloan, USA, Otter & Gurney, 1989; Koffiefontein, South Africa, Rickard et al., 1989; and Western Australia, Jaques et al., 1989). Most of these calculated temperatures are within the range of 982° - 1460°C, with two exceptionally low (one in the Sloan diamond, one in the Koffiefontein diamonds) and one extremely high (in the Western Australia diamond) values (Table 6.3), probably a result of disequilibrium.

Finally our attention is turned to a special type of "rocks" -- the so-called green garnets (garnet xenocrysts with clinopyroxene and/or spinel as inclusions or intergrowths; Schulze, 1989). A range of 993° - 1339°C is produced for four samples from Kampfersdam, 991°C is given for the sample from Bobbejaan; and 1229° & 1117°C for the two wehrlites from the Boshof Road dump in Kimberley (all analyses are from Schulze, 1989) by using equation (6.3). These are consistently (about 50°C) lower than the estimates obtained by using the Ellis-Green thermometer (Table 6.3).

The above calculation (Table 6.3) attests to the possible temperature range recorded by rocks from the lower crust and the upper mantle. Most of the calculated temperatures from the equation (6.3) are in accordance with estimates from other constraints [e.g (1) phase relations such as the metamorphic grade and the presence of kyanite; (2) other thermometers based on different reaction schemes such as the two-pyroxene thermometer]. Unusual temperatures given by the thermometer are often indicative of disequilibrium between the garnet - clinopyroxene pairs (typical examples are the eclogitic inclusions in diamonds reported by Otter & Gurney, 1989 and Rickard et al., 1989). More reliable temperature estimates can be obtained if the equilibrium pressure can be determined with confidence and precision; and more importantly only if the garnet - clinopyroxene pair in question is in mutual chemical equilibrium.

6.5 Conclusions

A comprehensive experimental dataset is used to analyse the compositional dependence of the garnet - clinopyroxene Fe^{2+}/Mg partitioning K_d. It is found that in addition to X_{Ca}^{Gt}, Mg#(Gt) also has a significant effect on the K_d. An empirical model is developed to take into account these compositional effects. This model, in the form of a geothermometer,

$$T°K = \frac{(-1523.257[X_{Ca}^{Gt}]^2 + 2759.182[X_{Ca}^{Gt}] - 8.919[Mg\#(Gt)] + 1974.011 + 17.35P(kbar))}{\ln K_d + 0.849}$$

gives reasonable temperature estimates for rocks from the lower crust (garnet amphibolites, granulites and eclogites) and the upper mantle (mineral inclusions in diamonds, xenoliths in kimberlites).

References

Adams GE, Bishop FC (1986) The olivine-clinopyroxene geobarometer: experimental results in the CaO-FeO-MgO-SiO_2 system. Contrib Mineral Pertrol 94: 230-237

Akella J (1974) Solubility of Al_2O_3 in orthopyroxene coexisting with garnet and clinopyroxene for compositions on the diopside-pyrope join in the system $CaSiO_3$-$MgSiO_3$-Al_2O_3. Carnegie Inst Washington Yearb 73: 273-278

Akella J (1976) Garnet pyroxene equilibria in the system $CaSiO_3$-MgSiO-Al_2O_3 and in a natural mineral mixture. Am Mineral 61: 589-598

Akella J, Boyd FR (1973) Effect of pressure on the composition of coexisting pyroxene and garnet in the system $CaSiO_3$-$MgSiO_3$-$FeSiO_3$-$CaAlTi_2O_6$. Carnegie Inst Washington Yearb 72: 523-526

Bailey DK (1982) Mantle metasomatism -- continuing chemical change within the Earth. Nature 296: 525-350

Ballhaus C, Berry RF, Green DH (1991) High pressure experimental calibration of the olivine-orthopyroxene-spinel oxygen geobarometer: implications for oxidation state of the upper mantle. Contrib Mineral Pertrol 107: 27-40

Barnes SJ (1986) The distribution of chromium among orthopyroxene, spinel and silicate liquid at atmospheric pressure. Geochim Cosmochim Acta 50: 1889-1909

Berg W, O'Hara MJ (1973) Source mantle, residuum and partial melt compositions deduced from the kimberlite record. First Int Kimberlite Conf (Capetown), Extended Abs: 31-34

Berger E (1979) The role on partial melting of mantle diapirism, CO_2 and H_2O from the study of herzolite nodules of the French Massif Central. In: Ahrens LH & Protas MG (eds) Origin and distribution of the elements (2nd symposium). Phys Chem Earth 11: 619-629

Berger E, Vannier M (1978) Un géothermomètre reposant sur le partage du nickel et du magnésium entre olivine et orthopyroxène: application à l'étude des péridotites. Comptes Rendus à l'Académie des Sciences, Paris, D 286: 733-736

Berger E, Vannier M (1984) Petrology of megacrysts, mafic and ultramafic xeoliths from the pipe of Eglazines, Causses, France. In: Kornprobst J (ed) Kimberlites II: The Mantle and Crust - Mantle Relationships. Proc Third Int Kimb Conf 2:155-168. Elsevier, Amsterdam

Bertrand P, Mercier J-CC (1985) The mutual solubility of coexisting ortho- and clinopyroxene: toward an absolute geothermometer for the natural system? Earth Planet Sci Lett 76: 109-122

Boyd FR, Mertzman SA (1987) Composition and structure of the Kaapvaal lithosphere, southern Africa. In: Mysen BO (ed) Magmatic Processes: Physicochemical Principles. The Geochemical Society Special Publication No.1: 13-24

Brey GP, Köhler T (1990) Geothermobarometry in four-phase lherzolites II. New thermometers, and practical assessment of existing thermometers. J Petrol 31: 1353-1378

Brey GP, Köhler T, Nickel KG (1990) Geothermobarometry in four-phase lherzolites I. experimental results from 10 to 60 kb. J Petrol 31: 1313-1352

Cao RL, Zhu SH (1983) Correlation of mantle xenolith occurrences with earth's internal zoning and tectonics in Eastern China. Acta Geophysica Sinica 26(2): 158-167 (in Chinese with English abstract)

Cao RL, Zhu SH (1987) Mantle xenoliths and alkali-rich host rocks in eastern China. In: Nixon PH (ed) Mantle Xenoliths. 167-180. John Wiley, Chichester

Carswell DA (1974) Comparative equilibration temperatures and pressures of garnet lherzolites in Norwegian gneisses and in kimberlite. Lithos 7: 113-121

Carswell DA (1975) Primary and secondary phlogopites and clinopyroxenes in garnet lherzolite xenoliths. Phys Chem Earth 9: 417-429

Carswell DA (1980) Mantle-derived lherzolite nodules associated with kimberlite, carbonatite and basalt magmatism: a review. Lithos 13: 121-138

Carswell DA, Gibb FGF (1987) Evaluation of mineral thermometers and barometers applicable to garnet lherzolite assemblages. Contrib Mineral Pertrol 95: 499-511

Carswell DA, Harley SL (1989) Mineral barometry and thermometry. In: Carswell DA (ed) Eclogite Facies Rocks. Blackie, 83-110, New York

Carswell DA, Clarke DB, Mitchell RH (1979) The petrology and geochemstry of ultramafic nodules from pipe 200, northern Lesotho. In: Boyd FR, Meyer HOA (eds) Kimberlites, Diatremes, and Diamonds: Their Geology, Petrology and Geochemistry. Proc Second Int Kimb Conf : 127-144. Am Geophys Union, Washington DC

Carter JL (1970) Mineralogy and chemistry of the Earth's upper mantle based on the partial fusion -- partial crystallisation model. Geological Society of America Bulletin 81: 2021-2034

Chapman DS, Pollack HN (1977) Regional geotherm and lithospheric thickness. Geol 5: 265-268

Chen CY, Frey FA, Song Y (1989) Evolution of the upper mantle beneath southeast Australia: geochemical evidence from peridotitic xenoliths in Mount Leura basanite. Earth Planet Sci Lett 93: 195-209

Cox KG, Smith MR, Beswetherick S (1987) Textural studies of garnet lherzolites: evidence of exsolution origin from high-termperature harzburgites. In: Nixon PH (ed) Mantle Xenoliths. 537-550. John Wiley, Chichester

Dahl PS (1980) The thermal-compositional dependence of Fe^{2+}-Mg distributions between coexisting garnet and pyroxene: applications to geothermometry. Am Mineral 65: 852-866

Danchin RV, Boyd FR (1976) Ultramafic nodules from the Premier kimberlite pipe, South Africa. Carnegie Inst Washington Yearb 75: 531-538

Danckwerth PA, Newton RC (1978) Experimental determination of the spinel peridotite to garnet peridotite reaction in the system MgO-Al_2O_3-SiO_2 in the range 900° - 1100°C and Al_2O_3 isopleths of enstatite in the spinel field. Contrib Mineral Pertrol 66: 189-201

Davis BTC, Boyd FR (1966) The join $Mg_2Si_2O_6$-$CaMgSi_2O_6$ at 30 kilobars pressure and its application to pyroxenes from kimberlites. J Geophys Res 71: 3567-3576

Dawson JB, Smith JV (1975) Chemistry and origin of phlogopite megacrysts in kimberlites. Nature 253: 336-338

Dawson JB, Stephens WE (1975) Statistical analysis of garnets from kimberlites and associated xenoliths. J Geol 83: 589-607

Delaney JS, Smith JV, Dawson JB, Nixon PH (1979) Manganese thermometer for mantle peridotites. Contrib Mineral Pertrol 71: 157-169

Ehrenberg SN (1982) Petrogenesis of garnet lherzolite and megacrystalline nodules from the Thumb, Navajo volcanic field. J Petrol 23: 507-547

Ellis DJ, Green DH (1979) An experimental study of the effect of Ca upon garnet - clinopyroxene Fe-Mg exchange equilibria. Contrib Mineral Pertrol 71: 13-22

Engi M (1983) Equilibria involving Al-Cr spinel: Mg-Fe exchange with olivine: experiments, thermodynamic analysis, and consequences for geothermometry. Am J Sci 283A: 29-71

Evans BW, Trommsdorff V, Richter W (1979) Petrology of an eclogite-metarodingite suite at Cima di Gagnone, Ticino, Switzerland. Am Mineral 64: 15-31

Exley RA, Smith JV, Hervig RL (1982) Cr-rich spinel and garnet in two peridotite xenoliths from the Frank Smith mine South Afria: Significance of Al and Cr distribution between spinel and garnet. Min Mag 45: 129-134

Fabries J (1979) Spinel-olivine geothermometry in peridotites from ultramafic complexes. Contrib Mineral Pertrol 69: 329-336

Falloon TJ, Green DH (1988) Anhydrous partial melting of peridotite from 8 to 35 kb and the petrogenesis of MORB. J Petrol Special Lithosphere Issue: 379-414

Falloon TJ, Green DH, Hatton CJ, Harris KL (1988) Anhydrous partial melting of a fertiile and depleted peridotite from 2 to 30 kb and application to basalt petrogenesis. J Petrol 29: 1257-1282

Fan QC, Hooper PR (1989) The mineral chemistry of ultramafic xenoliths of eastern China: implications for upper mantle composition and the paleogeotherm. J Petrol 30: 1117-1158

Ferguson J, Sheraton JW (1979) Petrogenesis of kimberlitic rocks and associated xenoliths of southeastern Australia. In: Boyd FR, Meyer HOA (eds) Kimberlites, Diatremes, and Diamonds: Their Geology, Petrology and Geochemistry. Proc Second Int Kimb Conf: 140-160. Am Geophys Union, Washington DC

Ferguson J, Ellis DJ, England RN (1977) Unique spinel-garnet lherzolite inclusion in kimberlite from Australia. Geology 5: 278-280

Finnerty AA, Boyd FR (1984) Evaluation of thermobarometers for garnet peridotites. Geochim Cosmochim Acta 48: 15-27

Finnerty AA, Boyd FR (1987) Thermobarometry for garnet peridotite xenoithes: the basis for the determination. In: Nixon PH (ed) Mantle Xenoliths. 381-402. John Wiley, Chichester

Forbes RB, Kuno H (1967) Peridotite inclusions and basaltic host rocks. In: Wyllie PJ (ed) Ultramafic and Related Rocks. John Wily & Sons, New York

Francis D (1987) Mantle -- melt interaction recorded in spinel lherzolite xenoliths from the Alligator Lake volcanic complex, Yukon, Canada. J Petrol 28: 569-597

Frey FA, Green DH (1974) The mineralogy, geochemistry and origin of lherzolite inclusions in Victorian basanites. Geochim Cosmochim Acta 38: 1023-1059

Frey FA, Prinz M (1978) Ultramafic inclusions from San Carlos, Arizona: petrologic and geochemical data bearing on their petrogenesis. Earth Planet Sci Lett 38: 129-176

Frey FA , Suen CJ, Stockman HW (1985) The Ronda high-temperature peridotite: geochemistry and petrogenesis. Geochim Cosmochim Acta 49: 2469-2491

Fujii T (1977) Fe-Mg partitioning between olivine and spinel. Carnegie Inst Wash Yearb 76: 563-569

Galer SJG, O'Nions RK (1989) Chemical and isotopic studies of ultramafic inclusions from the San Carlos volcanic field, Arizona: a bearing on their petrogenesis. J Petrol 30: 1033-1064

Ganguly J (1979) Garnet and clinopyroxene solid solutions, and geothermometry based on Fe-Mg distribution coefficients. Geochim Cosmochim Acta 43: 1021-1029

Gasparik T (1984) Two-pyroxene thermobarometry with new experimental data in the system CaO-MgO-Al_2O_3-SiO_2. Contrib Mineral Petrol 87: 87-98

Gasparik T (1987) Orthopyroxene thermobarometry in simple and complex systems. Contrib Mineral Petrol 96: 357-370

Gasparik T, Newton RC (1984) The reversed Al-contents of orthopyroxene in equilibrium with spinel and forsterite in the system MgO-Al_2O_3-SiO_2. Contrib Mineral Pertrol 85: 186-196

Gee LL, Sack RO (1988) Experimetnal petrology of melilite nephelinites. J Petrol 29: 1233-1255

Green DH (1963) Alumina content of enstatite in a Venezuelan high temperature peridotite. Geol Soc Am Bull 74: 1397-1402

Green DH, Liebermann RC (1976) Phase equilibria and elastic properties of a pyrolite model for the oceanic upper mantle. Tectonophysics 32: 61-92

Green DH, Ringwood AE (1963) Mineral assemblages in a model mantle composition. J Geophys Res 68: 937-945

Green DH, Ringwood AE (1967a) The stability fields of aluminous pyroxene peridotite and garnet peridotite and their relevance in upper mantle structure. Earth Planet Sci Lett 3: 151-160

Green DH, Ringwood AE (1967b) Genesis of basaltic magmas. Contrib Mineral Pertrol 15: 103-190

Green TH, Adam J (1991) Assessment of the garnet-clinopyroxene Fe-Mg exchange thermometer using new experimental data. J Metamorphic Geol 9: 341-347

Grove TL, Juster TC (1989) Experimental investigations of low-Ca pyroxene stability and olivine-pyroxene-liquid equilibria at 1-atm in natural basaltic and andesitic liquids. Contrib Mineral Pertrol 103: 287-305

Gurney JJ (1989) Diamonds. In: Ross J, et al. (eds) Kimberlites and Related Rocks, Geol Soc Aust Special Pub 14, Vol 2: 936-965

Hanson GN, Langmuir CH (1978) Modelling of major elements in mantle-melt systems using trace element approaches. Geochim Cosmochim Acta 42: 725-741

Harley SL (1984a) An experimetal study of the partitioning of Fe and Mg between garnet and orthopyroxene. Contrib Mineral Pertrol 86: 359-373

Harley SL (1984b) The solubility of alumina in orthopyroxene coexisting with garnet in FeO-MgO-Al_2O_3-SiO_2 and CaO-FeO-MgO-Al_2O_3-SiO_2. J Petrol 25: 665-696

Harley SL, Green DH (1982) Garnet-orthopyroxene barometry for granulites and peridotites. Nature 300: 697-701

Harte B (1977) Rock nomanculture with particular relation to deformation and recrystallisation textures in olivine-bearing xenoliths. J Geol 85: 279-288

Hearn Jr. BC, McGee ES (1984) Garnet peridotites from Williams kimberlites, north-central Montana, USA. In: Kornprobst J (ed) Kimberlites II: the Mantle- and Crust-Mantle Relations. Proc Third Int Kimb Conf; Developments in Petrology 11B: 57-70. Elsevier, Amsterdam

Hensen BJ (1973) Pyroxenes and garnets as geothermometers and barometers: Carnegie Inst Washington Yearb 72: 527-534

Hervig RL, Smith JV (1980) Sodium thermometer for pyroxenes in garnet and spinel lherzolites. J Geol 88: 337-342

Hervig RL, Smith JV, Dawson JB (1986) Lherzolite xenoliths in kimberlites and basaltis: petrologenetic and crystallochemical significance of some minor and trace elements in olivine, pyroxenes, garnet and spinel. Trans Roy Soc Edinb Earth Sci 77: 181-201

Hill RL, Sack RO (1987) Thermodynamic properties of Fe-Mg titaniferous magnetite spinels. Candian Mineral 25: 443-464

Hunter RH, Taylor LA (1982) Instability of garnet from the mantle: glass as evidence of metasomatic melting. Geology 10: 617-620

Hutchison R, Chambers AL, Paul DK, Harris PG (1975) Chemical variation among French ultrabasic xenoliths -- evidence for a heterogeneous upper mantle. Min Mag 40: 153-170

Irving AJ, Green DH (1976) Geochemistry and petrogenesis of the Newer basalts of Victoria and South Australia. J Geol Soc Aust 23: 45-66

Jackson ED, Wright TL (1970) Xenoliths in the Honolulu volcanic series, Hawaii. J Petrol 11: 405-433

Jagoutz E, Palme H, Baddenhausen H, Blum K, Cendales M, Dreibus G, Spettel B, Lorenz V, Wanke H (1979) The abundances of major, minor and trace elements in the earth's mantle as derived from primitive ultramafic nodules. Proc Lunar Planet Sci Conf 10th: 2031-2050

Jaques AL, Green DH (1980) Anhydrous melting of peridotite at 0-15 kb pressure and the genesis of tholeiitic basalts. Contrib Mineral Pertrol 73: 287-310

Jaques AL, Hall AE, Sheraton JW, Smith CB, Sun SS, Drew RM, Foudoulis C, Ellingsen K (1989) Composition of crystalline inclusions and C-isotopic composition of Argyle and Ellendale diamonds. In: Ross J, et al. (eds) Kimberlites and Related Rocks, Geol Soc Aust Special Pub 14, Vol 2: 966-989

Jenkins DM, Newton RC (1979) Experiemntal determination of the spinel peridotite to garnet peridotite inversion at 900°C and 1000°C in the system CaO-MgO-Al_2O_3-SiO_2, and at 900°C with natural garnet and olivine. Contrib Mineral Petrol 68: 407-419

Jarosewich E, Nelen JA, Norberg JA (1980) Reference samples for electron microprobe analysis. Geostandards Newsletter 4 (1): 43-47

Jin ZM, Green II HW, Borch RS, Tingle TN (1991) Unusual spinel -- garnet lherzolite xenoliths from basalt in eastern China: constraints on the late-tertiary thermal structure of the upper mantle. Fifth Int Kimberlite Conf (Brazil), Extended Abs: 212-213

Johnston AD (1986) Anhydrous P-T phase relations of near-primary high-alumina basalt from the South Sandwich Islands. Contrib Mineral Petrol 92: 368-382

Kawasaki T (1979) Thermodynamic analyses on the Mg-Fe exchange equilibrium between olivine and garnet: an application to the estimation of P-T relations of ultramafic rocks. J Jap Ass Mineral Petrol Econ Geol 74: 395-405

Kirkley MB, MacCallum ME, Eggler DH (1984) Coexisting garnet and spinel in upper mantle xenoliths from Colorado-Wyoming kimberlites. In: Kornprobst J (ed) Kimberlites II: the mantle- and crust-mantle relations. Proc Third Int Kimb Conf; Developments in Petrology 11B: 85-96. Elsevier, Amsterdam

Köhler TP, Brey GP (1990) Calcium exchange between olivine and clinopyroxene calibrated as a geothermobarometer for natural peridotites from 2 to 60 kb with applications. Geochim Cosmochim Acta 54: 2375-2388

Koons PO (1984) Implications to garnet-clinopyroxene geothermometry of non-ideal solid solution in jadeiitic pyroxenes. Contrib Mineral Petrol 88: 340-347

Kretz R (1982) Transfer and exchange equilibria in a portion of the pyroxene quadrilateral as deduced from natural and experimental data. Geochim Cosmochim Acta 46: 411-421

Krogh EJ (1988) The garnet - clinopyroxene Fe-Mg-geothermometer -- a reinterpretation of existing experimental data. Contrib Mineral Pertrol 99: 44-48

Kushiro I (1990) Partial melting of mantle wedge and evolution of island arc crust. J Geophy Res 95 (B10): 15929-15939

Lane DL, Ganguly J (1980) Al_2O_3 solubilty in orthopyroxene in the system MgO-Al_2O_3-SiO_2: a re-evaluation, and mantle geotherm. J Geophys Rev 85: 6963-6972

Le Maitre RW (1979) A new generalised petrological mixing model. Contrib Mineral Pertrol 71: 133-137

Liang Y, Elthon D (1990) Geochemistry and petrology of spinel lherzolite xenoliths from Xalapasco de La Joya, San Luis Potosi, Mexico: partial melting and mantle metasomatism. J Geophys Res 95 (B10): 15859-15877

Lindsley DH, Dixon SA (1976) Coexisting diopside and enstatite at 20 kbar and 900°-1200°C. Am J Sci 276: 1285-1301

Lock NP, Dawson JB (1980) Garnet-olivine reaction in the upper mantle: evidence from peridotite xenoliths in the Letseng-la-Terae kimberlites, Lesotho. Trans R Soc Edinburgh Earth Sci 71: 47-53

Luth RW, Virgo D, Boyd FR, Wood BJ (1990) Ferric iron in mantle-derived garnets. Contrib Mineral Petrol 104: 56-72

Maaløe S, Aoki K (1977) The major element composition of the upper mantle estimated from the composition of lherzolites. Contrib Mineral Pertrol 63: 161-173

MacGregor ID (1970) The effect of CaO, Cr_2O_3, Fe_2O_3 and Al_2O_3 on the stability of spinel and garnet peridotites. Phys Earth Planet Interior 3: 372-377

MacGregor ID (1974) The system MgO-Al_2O_3-SiO_2: solubility of Al_2O_3 in enstatite for spinel and garnet peridotite compositions. Am Mineral 59: 110-119

MacGregor ID (1979) Mafic and ultramafic xenoliths from the Kao kimberlite pipe. In: Boyd FR, Meyer HOA (eds) Kimberlites, Diatremes, and Diamonds: Their Geology,

Petrology and Geochemistry. Proc Second Int Kimb Conf : 156-172. Am Geophys Union, Washington DC

McCallum ME, Eggler DH (1976) Diamonds in an upper mantle peridotite nodule from kimberlite in southern Wyoming. Science192: 253-256

McKenzie DP (1984) The generation and compaction of partially molten rock. J Petrol 25: 713-765

Mengel K, Green DH (1989) Stability of amphibole and phlogopite in metasomatized peridotite under water-saturated and water-undersatureated conditions. In: Ross J, et al. (eds) Kimberlites and Related Rocks, Geol Soc Aust Special Pub 14, Vol 1: 571-581

Menzies MA (1990) Continental Mantle. Oxford Unversity Press

Mercier J-C C, Nicolas A (1975) Texture and fabrics of upper mantle peridotites as illustrated by xenoliths from basalts. J Petrol 16: 454-487

Mitchell RH (1984) Garnet lherzolites from the Hanaus-I and Louwrensia kimberlites of Namibia. Contrib Mineral Pertrol 86: 178-188

Mori T (1976) Pyroxene equilibria in ultramafic rocks. Unpubl PhD thesis, Australian National University

Mori T, Green DH (1975) Pyroxenes in the system $CaMgSi_2O_6$-$Mg_2Si_2O_6$ at high pressure. Earth Planet Sci Lett 26: 277-286

Mori T, Green DH (1978) Laboratory duplication of phase equilibria observed in natural garnet lherzolites. J Geol 86: 83-97

Neal CR (1988) The origin and composition of metasomatic fluids and amphiboles beneath Malaita, Solomon Islands. J Petrol 29: 149-179

Neal CR, Nixon PH (1985) Spinel - garnet relationships in mantle xenoliths from the Malaita alnoites, Solomon Islands, South-western Pacific. Trans geol Soc S Afr 88: 347-354

Newton RC (1989) Thermodynamic analysis of phase equilibria in simple mineral systems. In: Carmichael ISE, Eugster HP (eds) Thermodynamic Modelling of Geological Materials: Minerals, Fluids and Melts. Reviews in Mineralogy 17: 1-33

Nickel KG (1983) Petrogenesis of garnet and spinel peridotites. Unpubl PhD thesis, University of Tasmania

Nickel KG (1986) Phase equilibria in the system SiO_2-MgO-Al_2O_3-CaO-Cr_2O_3 (SMACCR) and their bearing on spinel/garnet lherzolite relationships. N Jb Min Abh 155: 259-287

Nickel KG (1989) Garnet - pyroxene equilibria in the system SMACCR (SiO_2-MgO-Al_2O_3-CaO-Cr_2O_3): the Cr-geobarometer. In: Ross J, et al. (eds) Kimberlites and Related Rocks, Geol Soc Aust Special Pub 14, Vol 2: 901-912

Nickel KG, Green DH (1984) The nature of the uppermost mantle beneath Victoria, Australia as deduced from ultramafic xenoliths. In: Kornprobst J (ed) Kimberlites II: the

Mantle- and Crust-Mantle Relations. Proc Third Int Kimb Conf; Developments in Petrology 11B: 161-178. Elsevier, Amsterdam

Nickel KG, Green DH (1985) Empirical geothermobarometry for garnet peridotites and implications for the nature of the lithosphere Kimberilites and diamonds. Earth Planet Sci Lett 73:158-170

Niida K, Green DH (in prep) Stability and chemical composition of pargasitic amphibole in MORB pyrolite under water-undersaturated conditions.

Niu YL, Batiza R (1991) DENSCAL: a program for calculating densities of silicate melts and mantle minerals in melting range. Computers and Geosciences, in press

Nixon PH (1987) Mantle Xenoliths. John Wiley, Chichester

Nixon PH, Von Knorring O, Rooke JM (1963) Kimberlites and associated inclusion of Basutoland: a mineralogical and geochemical study. Am Mineral 48: 1090-1132

Nixon PH, Boyd FR (1973) Petrogenesis of the granular and sheared ultabasic nodule suite in kimberlites. In: Nixon PH (ed) Lesotho Kimberlites. Lesotho National Development Corporation, Maseru, Lesotho: 48-56

Nixon PH, Boyd FR (1979) Garnet bearing lherzolite nodule suites from the Malaita alnoite, Solomon Island, SW Pacific, and their bearing on oceanic mantle composition and geotherm. In: Boyd FR, Meyer HOA (eds) The Manlte Sample: Inclusions in Kimberlites and Other Volcanics. Proc Second Int Kimb Conf 2: 400-423. Am Geophys Union, Washington DC

O'Hara MJ, Richardson SW, Wilson G (1971) Garnet-peridotite stability and occurrance in crust and mantle. Contrib Mineral Pertrol 32: 48-68

O'Hara MJ, Sunders MJ, Mercy ELP (1975) Garnet peridotite, primary ultrabasic magma and eclogites: interpretation of upper mantle processes in kimberlite. Phys Chem Earth 9: 571-604

O'Neill HStC (1980) An experimental study of Fe-Mg partitioning between garnet and olivine and its calibration as a geothermometer: corrections. Contrib Mineral Pertrol 72: 337

O'Neill HStC (1981) The transition between spinel lherzolite and garnet lherzolite, and its use as a geobarometer. Contrib Mineral Pertrol 77: 185-194

O'Neill HStC, Wall VJ (1987) The olivine-orthopyroxene-spinel oxygen geobarometer, the nickel precipitation curve, and the oxygen fugacity of the Earth's upper mantle. J Petrol 28: 1169-1191

O'Neill HStC, Wood BJ (1979) An experimental study of Fe-Mg partitioning between garnet and olivine and its calibration as a geothermometer. Contrib Mineral Pertrol 70: 59-70

O'Reilley SY, Griffin WL (1988) Mantle metasomatism beneath western Victoria, Australia: I. Metasomatic processes in Cr-diopside lherxzolites. Geochim Cosmochim Acta 52: 433-447

O'Reilly SY, Griffin WL (1985) A xenolith-derived geotherm for southeastern Australia and its geophysical implications. Tectonophysics 111: 41-63

O'Reilly SY, Griffin WL (1987) Eastern Australia -- 4000 kliometres of mantle samples. In: Nixon PH (ed) Mantle Xenoliths. 267-280. John Wiley, Chichester

Otter ML, Gurney JJ (1989) Mineral inclusions in diamonds from the Sloan diatremes, Colorado-Wyoming state line kimberlite district, North America. In: Ross J, et al. (eds) Kimberlites and Related Rocks, Geol Soc Aust Special Pub 14, Vol 2: 1042-1053

Padovani ER, Carter JL (1973) Aspects of the deep crustal evolution beneath south-central New Mexico. American Geophysical Union Geophysical Monograph 14: 19-55

Parsons B, Sclater JG (1977) An analysis of the variation of ocean floor bathymetry and heat flow with age. J Geophy Res 82: 803-827

Pattison DRM, Newton RC (1989) Reversed experimental calibration of the garnet-clinopyroxene Fe-Mg exchange thermometer. Contrib Mineral Pertrol 101: 87-103

Pearson NJ, O'Reilly SY, Griffin WL (1991) The thermal evolution of cratonic lower crust/upper mantle: examples from eastern Australia and southern Africa. Fifth Int Kimberlite Conf (Brazil), Extended Abs: 332-333

Perkins III D, Newton RC (1980) The compositions of coexisting pyroxenes and garnets in the system CaO-MgO-Al_2O_3-SiO_2 at 900°-1100°C and high pressures. Contrib Mineral Pertrol 75: 291-300

Perkins III D, Holland TJB, Newton RC (1981) The Al_2O_3 contents of enstatite in equilibrium with garnet in the system MgO-Al_2O_3-SiO_2 at 15-40 kbar and 900°-1600°C. Contrib Mineral Pertrol 78: 99-109

Podvin P (1988) Ni-Mg partitioning between synthetic olivines and orthopyroxenes: application to geothermometry. Am Mineral 73: 274-280

Powell R (1985) Regression diagnostics and robust regression in geothermometer/ geobarometer calibration: the Fe-Mg exchange thermometer revisited. J Metamorphic Geol 3: 231-243

Preß S, Witt G, Seck HA, Eonov D, Kovalenko VI (1986) Spinel peridotite xenoliths from the Tariat Depression, Mongolia I: major element chemistry and mineralogy of a primitive mantle xenolith suite. Geochim Cosmochim Acta 50: 2587-2599

Raheim A, Green DH (1974a) Experimental determination of the temperature and pressure dependence of the Fe-Mg partition coefficient for coexisting garnet and clinopyroxene. Contrib Mineral Pertrol 48: 179-203

Råheim A, Green DH (1974b) Experimental petrology of lunar highland basalt composition and application to models for the lunar interior. J Geol 82: 607-622

Reid AM, Dawson JB (1972) Olivine-garnet reaction in peridotites from Tanzania. Lithos 5: 115-124

Reid JB, Woods GA (1978) Oceanic mantle beneath the southern Rio Grande rift. Earth Plant Sci Lett 41: 303-316

Rickard RS, Harris JW, Gurney JJ, Cardoso P (1989) Mineral inclusions in diamonds from Koffiefontein Mine. In: Ross J, et al. (eds) Kimberlites and Related Rocks, Geol Soc Aust Special Pub 14, Vol 2:1054-1062

Ringwood AE (1975) Composition and Petrology of the Earth's Mantle. McGraw-Hill, New York

Roden MF, Murthy VR (1985) Mantle metasomatism. Ann Rev Earth Planet Sci 13: 269-296

Sachtleben Th, Seck HA (1981) Chemical control of Al-solubility in orthopyroxene and its implications for pyroxene geothermometry. Contrib Mineral Pertrol 78: 157-165

Sack RO, Walker D, Carmichael ISE (1987) Experimental petrology of alkalic lavas: constraints on cotectics os multiple saturation in natural basic liquids. Contrib Mineral Pertrol 96: 1-23

Saxena SK (1979) Garnet-clinopyroxene geothermometer. Contrib Mineral Pertrol 70: 229-235

Schulze DJ (1989) Green garnets from South African kimberlites and their relationship to wehrlites and crustal uvarovites. In: Ross J, et al. (eds) Kimberlites and Related Rocks, Geol Soc Aust Special Pub 14, Vol 2: 820-826

Scott DR, Stevenson DJ (1989) A self-consistent model of melting, magma migration, and buoyancy-driven circulation beneath mid-ocean ridges. J Geophys Res 94 (B3): 2973-2988

Sen SK, Bhattacharya A (1984) An orthopyroxene-garnet thermometer and its application to the Madras charnockites. Contrib Mineral Pertrol 88: 64-71

Shee SR, Gurney JJ, Robinson DN (1982) Two diamond-bearing peridotite xenoliths from the Finsch kimberlite, South Africa. Contrib Mineral Petrol 81: 79-87

Shibata T, Thompson G (1986) peridotites from the Mid-Atlantic Ridge at 43° N and their petrogenetic relation to abyssal tholeiites. Contrib Mineral Pertrol 93: 144-159

Skews MA, Stern CR (1979) Petrology and geochemistry of alkali basalts and ultramafic inclusions from the Palei-Aike Volcanic field in Southern Chile and the origin of the Patagonian Plateau lavas. J Volcanic Geotherm Res 6: 3-25

Smith CB, Gurney JJ, Harris JW, Robinson DN, Shee SR, Jaqoutz E (1989) Sr and Nd isotopic systematics of diamond-bearing eclogite xenoliths and eclogitic inclusions in diamond from southern Africa. In: Ross J, et al. (eds) Kimberlites and Related Rocks, Geol Soc Aust Special Pub 14, Vol 2: 853-863

Stern CR, Saul S, Skewes MA, Futa K (1989) Garnet peridotite xenoliths from the Pali-Aike alkali basalts of southernmost South America. In: Ross J, et al. (eds) Kimberlites and Related Rocks, Geol Soc Aust Special Pub 14, Vol 2: 735-744

Stolper E (1980) A phase diagram for mid-ocean ridge basalts: prelimary results and implications for petrogenesis. Contrib Mineral Petrol 74: 3-27

Stolper E, Walker D, Hager BH, Hays JF (1981) Melt segregation from partially molten source regions: the importance of melt density and source region size. J Geophys Res 86: 6261-6271

Stolz AJ, Davies GR (1988) Chemical and isotopic evidence from spinel lherzolite xenoliths for episodic metasomatism of the upper mantle beneath southeast Australia. J Petrol Special Lithosphere Issue: 303-330

Sun SS, McDonough WF (1989) Chemical and isotopic systematics of oceani basaltis: implications for mantle composition and processes. In Saunders AD, Norry MJ (eds) Magmatism in the Ocean Basains. Geological Society Special Publication No.42: 313-345

Sun WH, Lai ZM (1980) Petrochemical characteristics of Cenozoic volcanic rocks in Fu-jian Province and its relationship to tectonics. Geochimica 2: 134-147 (in Chinese with English absttact)

Sutherland FL, Hollis JD, Barron LM (1984) Garnet lherzolite and other inclusions from a basalt flow, Bow Hill, Tasmania. In: Kornprobst J (ed) Kimberlites II: the Mantle- and Crust-Mantle Relations. Proc Third Int Kimb Conf; Developments in Petrology 11B: 257-264. Elsevier, Amsterdam

Takahashi E (1986) Melting of a dry peridotite KLB-1 upto 14 GPa: implications on the origin of peridotitic upper mantle. J Geophys Res 91: 9367-9382

Takahashi E, Kushiro I (1983) Melting of a dry peridotite at high pressures and basalt magma genesis. Am Mineral 68: 859-879

Taylor LA, Neal CR (1989) Eclogites with oceanic crustal and mantle signatures from the Bellsbank kimberlite, South Africa, Part I: Mineralogy, petrology, and whole rock chemistry. J Geol 97: 551-567

Taylor WR (1985) The role of C-O-H fluids in upper mantle processes - a theoretical, experimental and spectroscopic study. Unpubl PhD thesis, University of Tasmania

Taylor WR, Green DH (1988) Measurement of reduced peridotite-C-O-H solidus and implications for redox melting of the mantle. Nature 332: 349-352

Taylor WR, Green DH (1991) Mineral chemistry of silicate and oxide phases from fertile peridotite equilibrated with a C-O-H fluid phase -- a low fo_2 dataset for the evaluation of mineral barometers, thermometers, and oxygen sensors. Fifth Int kimberlite Conf (Brazil), Extende Abstracts: 417-419

Varne R (1977) On the origin of spinel lherzolite inclusions in basaltic rocks from Tasmania and elsewhere. J Petrol 18: 1-23

Waff HS (1980) Effects of the gravitational field on liquid distribution in partial melts within the upper mantle. J Geophys Res 85: 1815-1825

Wallace ME, Green DH (1988) An experimental determination of primary carbonatite magma composition. Nature 335: 343-346

Wallace ME, Green DH (1991) The effect of bulk rock composition on the stability of amphibole in the upper mantle: implications for solidus positions and mantle metasomatism. Mineral Petrol 44: 1-19

Wass SY, Rogers NW (1980) Mantle metasomatism -- precursor to continental alkaline volcanism. Geochim Cosmochim Acta 44: 1811-1823

Webb SAC, Wood BJ (1986) Spinel-pyroxene-garnet relationships and their dependence on Cr/Al ratio. Contrib Mineral Pertrol 92: 471-480

Wells PRA (1977) Pyroxene thermometry in simple and complex systems. Contrib Mineral Pertrol 62: 129-139

Wells PRA (1979) Chemical and thermal evolution of Archaean sialic crust, southern West Greenland. J Pertrol 20: 187-226

Wilshire HG, Shervais JW (1975) Al-augite and Cr-diopside ultramafic xenoliths in basaltic rocks from the western United States. Phys Chem Earth 9: 257-272

Wilshire HG, Meyer CE, Nakata JK, Calk LC, Shervais JW, Nielson JE, Schwazman EC (1988) Mafic and ultramafic xenoliths from volcanic rocks of the western United States. US Geol Survey Professional Paper 1443.

Witt-Eickschen G, Seck HA (1991) Solubility of Ca and Al in orthopyroxene from spinel peridotite: an improved version of an empirical geothermometer. Contrib Mineral Pertrol 106: 431-439

Wood BJ (1974) Solubility of alumina in orthopyroxene coexisting with garnet. Contrib Mineral Pertrol 46: 1-15

Wood BJ (1976) The partitioning of iron and magnesium between garnet and clinopyroxene. Carnegie Inst Washington Yearb 75: 571-574

Wood BJ, Banno S (1973) Garnet-orthopyroxene and orthopyroxene-clinopyroxene relationships in simple and complex systems. Contrib Mineral Pertrol 42: 109-124

Wood BJ, Bryndzia LT, Johnson KE (1990) Mantle oxidation state and its relations to tectonic environment and fluid speciation. Sicence 248: 337-345

Wood BJ, Yuen DA (1983) The role of lithospheric phase transitions on seafloor flattening at old ages. Earth Plant Sci Lett 66: 303-314

Wu LR, Zhai MZ, Zheng XS, Yang RY, Huang ZX (1985) Cenozoic volcanic rocks in eastern China. Acta Petrologica Sinica 1 (4): 1-23 (in Chinese with English abstract)

Zhang DQ (1982) Study of the Cenozoic volcanics and upper-mantle xenoliths from Da-Yang-Ke, Ming-xi county, Fu-jian Province, China. Unpub M Sc thesis. China University of Geosciences, Bei-jing (in Chinese)

Zhang RY, Cong BL (1987) Cenozoic volcanic rock series and their ultramafic xenoliths in southeastern China. In: E ML, Zhao DS (eds) Cenozoic Basalts and Deep Seated

Xenoliths from Eastern China. Science Publishing House, Bei-jing: 349-475 (in Chinese)

Zhou XM, Chen TH (1984) Petrogenetic aspects of Cr-clinopyroxene- and Al-clinopyroxene-bearing ultramafic inclusions in basaltic rocks from southeastern coastal provinces of China. Acta Geologica Sinica 3: 238-252 (in Chinese with English abstract)